EFFECTIVE CONTROL STRATEGIES FOR HIGHWAY NONPOINT POLLUTION

Authors:

John J. Sansalone, Research Assistant Professor
Steven G. Buchberger, Associate Professor

Research Agency:

University of Cincinnati
Department of Civil and Environmental Engineering

Report Date:

1 October 1997

Sponsoring Agencies:

Ohio Department of Transportation (ODOT)
Federal Highway Administration (FHWA)
National Science Foundation (NSF)

Credit Reference

Preparation in cooperation with the Ohio Department of Transportation and the U.S. Department of Transportation, Federal Highway Administration.

EFFECTIVE CONTROL STRATEGIES FOR HIGHWAY NONPOINT POLLUTION

Authors:

John J. Sansalone, Research Assistant Professor
Steven G. Buchberger, Associate Professor

Research Agency:

University of Cincinnati
Department of Civil and Environmental Engineering

Report Date:

1 October 1997

Sponsoring Agencies:

Ohio Department of Transportation (ODOT)
Federal Highway Administration (FHWA)
National Science Foundation (NSF)

Credit Reference

Preparation in cooperation with the Ohio Department of Transportation and the U.S. Department of Transportation, Federal Highway Administration.

Disclaimer Statement

The contents of this report reflect the views of the authors who are responsible for the facts and accuracy of the data presented herein. The contents do not necessarily reflect the official views or policies of the Ohio Department of Transportation or the Federal Highway Administration. This report does not constitute a standard, specification or regulation.

1. Report No.	2.	3. Recipient's Catalog No.
FHWA/OH-98/002	PB99-109746	

4. Title and Subtitle	5. Report Date
EFFECTIVE CONTROL STRATEGIES FOR HIGHWAY NONPOINT POLLUTION	October 1, 1997
	6. Performing Organization Code
7. Author(s)	8. Performing Organization Report No.
John J. Sansalone Steven G. Buchberger	10. Work Unit No. (TRAIS)
9. Performing Organization Name and Address	11. Contract or Grant No.
The University of Cincinnati Department of Civil and Environmental Engineering Cincinnati, OH 45221-0071	State Job No. 14562(0)
	13. Type of Report and Period Covered
	Final Report
12. Sponsoring Agency Name and Address	14. Sponsoring Agency Code
Ohio Department of Transportation 25 S. Front St. Columbus, OH 43215	

15. Supplementary Notes

Prepared in cooperation with the U.S. Department of Transportation, Federal Highway Administration

16. Abstract

Storm water drainage from urban highways often transports elevated levels of metal elements, solids and dissolved constituents. The goals of this research were the characterization of lateral pavement sheet flow and based on characterization results, development of passive in-situ treatment for metal elements and solids transported in storm water drainage. Characterization results were obtained from a highway experimental site which intercepted lateral pavement sheet flow directly from Inter State Route 75 (I-75) in Cincinnati, Ohio. The site was located in a heavily traveled urban section of I-75 with an ADT of 150,000. The drainage area to the sampling device was 300 m^2 of asphalt pavement. Measurements at the site included rainfall, flow and water quality parameters for 12 storm events over 3 years. Laboratory analysis included metal element concentrations and partitioning. Solids analysis included fractionation, particle size distributions (PSD) and specific surface area (SSA). Results indicated that Zn, Cd and Cu were mainly in dissolved form, and on an event basis exceeded USEPA and OEPA surface water quality standards. SSA results demonstrated that particle size cannot be used as a SSA surrogate and the assumption of spherical particles grossly underestimates actual SSA. Based on characterization results an in-situ treatment strategy called a partial exfiltration trench (PET) was developed. The PET was designed as a water quality upgrade to the current practice of underdrainage along Ohio highways. The PET functions by intercepting and infiltrating lateral pavement sheet flow influent while exfiltrating treated effluent to surrounding soils or to a perforated underdrain at the base of the trench. The body of the trench was filled with iron oxide coated sand (OCS) for adsorptive filtration of metal elements in the percolating stormwater. Bench scale PET columns loaded with metal element-spiked DI water and stormwater were utilized to simulate breakthrough capacity. Results indicated that breakthrough capacity was controlled by particulate-bound metal element breakthrough. Using breakthrough results, calculations indicated the PET design life could exceed 10 years. A prototype PET was constructed on I-75. After one year of storm water loadings, PET removal efficiency exceeded 80 percent for dissolved and 70 percent for particulate-bound metal elements, respectively.

17. Key Words	18. Distribution Statement
Adsorptive-filtration, Breakthrough, First flush, Metal Elements, Oxide coated sand, Partial exfiltration trench, Particle size Distribution, Specific surface area, Storm water, Urban highway drainage.	No Restrictions. This document is available to the public through the National Technical Information Service, Springfield, Virginia 22161

19. Security Classif. (of this report)	20. Security Classif. (of this page)	21. No. of Pages	22. Price
Unclassified	Unclassified		

EFFECTIVE CONTROL STRATEGIES FOR HIGHWAY NONPOINT POLLUTION

Authors:

John J. Sansalone, Research Assistant Professor
Steven G. Buchberger, Associate Professor

Research Agency:

University of Cincinnati
Department of Civil and Environmental Engineering

Report Date:

1 October 1997

Sponsoring Agencies:

Ohio Department of Transportation (ODOT)
Federal Highway Administration (FHWA)
National Science Foundation (NSF)

Credit Reference

Preparation in cooperation with the Ohio Department of Transportation and the U.S. Department of Transportation, Federal Highway Administration.

EXECUTIVE SUMMARY

By the year 2000 approximately 50% of the world population will live in urban areas. With this growth is an increase in vehicular traffic, urban infrastructure, waste generation and non-point anthropogenic pollutants. Urban waters often contain high concentrations of metal elements and solids. These pollutants pose acute and chronic threats to receiving water bodies and soils.

The goal of this research was to develop and demonstrate an effective passive treatment strategy for metal elements transported in urban waters. There were four main objectives of this research. The first objective was to characterize metal elements, specifically Zn, Cd, Pb and Cu, and solids sampled throughout rainfall runoff events. The second objective was utilization of this field information and the concept of surface complexation to develop a passive treatment device for immobilizing metal elements and solids in urban waters. The third main objective was laboratory bench scale column simulations to evaluate metal element breakthrough for the proposed treatment device. The final objective was to install and evaluate an in-situ prototype treatment device subject to polluted urban water loadings.

Field experimental methodology required construction of a sampling device for intercepting lateral pavement sheet flow directly from Interstate 75 in Cincinnati. The site is located in a heavily traveled urban section of I-75 with an average daily traffic (ADT) count of 150,000 vehicles. The drainage area to the sampling device is 300 m^2 of asphalt pavement. Site measurements included rainfall, flow and water quality parameters for 12 rainfall and 2 snow events from 1995 through 1996. Laboratory analysis included metal element concentrations and partitioning, while solids analyses included fractionation, particle size distributions (PSD) and specific surface area (SSA) in addition to a wide range of water quality analysis. Results indicated that Zn, Cd and Cu, mainly dissolved, exhibited a strong first flush and exceeded USEPA and OEPA surface water quality standards. Pb exhibited a weak first flush.

The geochemical transport and eventual fate of a majority of reactive substances, including infiltrated metal elements, is controlled by the reaction of these substances with solid surfaces. The solid-liquid interface of these solids, which include natural iron oxides and synthetic iron oxide coated media are a reservoir for reactive substances, and are characterized by large surface area to solid volume ratios. In the presence of water these oxide surfaces are generally covered with surface hydroxyl groups, protons and coordinated water molecules. The formation of surface complexes of metal ions by hydrated iron oxides involves the coordination of the metal ions with surface hydroxyl atoms.

The net surface charge of the hydrous iron oxide is strongly pH dependent and therefore the sorption of a metal ion to the hydrous iron oxide surface is strongly pH dependent. These mineral surfaces are amphoteric. The surface point of zero charge (PZC) in its most simple definition is the pH at which the net surface charge is zero. Therefore for iron oxides, which have

a PZC between 7 and 8, a solution pH of 8 or greater would indicate the predominance of surface bonding sites would be negatively charged and available as metal ion bonding sites. Under conditions where a number of metal elements are present in solution the competitive order of sorption can be explained by the tendency of a metal element to undergo hydrolysis followed by sorption. Based on the tendency to hydrolyze, the bonding preference of metal ions to iron oxides would be : Pb > Cu > Zn > Co > Ni > Cd > Mn. Bench scale results confirm this bonding preference.

The concept of surface complexation for metal elements onto iron oxide surfaces was applied to develop a novel passive treatment strategy called a partial exfiltration trench (PET). The PET has four critical components. The upper surface is porous pavement to intercept and elevate the pH of infiltrating urban waters while straining solids at the pavement surface. The body of the trench is filled with iron oxide coated sand (IOCS) for adsorptive filtration of metal elements in the percolating urban waters. Geosynthetic liners at the porous pavement-IOCS interface and the underdrain are used for control of solids. A geosynthetic lined underdrain conveys infiltrated flow from the PET. The PET is a water quality upgrade to the current practice of underdrainage along highways.

Bench scale PET columns loaded with metal element-spiked DI water and stormwater were utilized to simulate breakthrough capacity at a pH of 6.5 and 8.0. Porous media evaluated included IOCS, silica sand and granular activated carbon. The IOCS capacity for Zn, Cd, Pb and Cu was significantly increased as the pH was raised from 6.5 to 8.0. Additionally, results using actual stormwater indicated that breakthrough capacity is controlled by particulate-bound metal element breakthrough. Using breakthrough results it was determined that the design life of a prototype PET could exceed 10 years in a humid climate. A prototype PET has been recently constructed on I-75 and has been under evaluation for approximately one year. The performance of this full-scale prototype PET indicates metal element and solid mass removal efficiency are generally greater than 80 percent. The PET concepts provides a unique and potentially viable strategy for the integration of water quantity and quality control to urban conditions where constraints preclude other treatment strategies.

TABLE OF CONTENTS

LIST OF FIGURES

LIST OF TABLES

NOTATION

ADT	average daily traffic
A_i	incremental areas for i^{th} hyetograph and resulting i^{th} hydrograph (L^2)
$\overline{APRT}$	mean average pavement residence time (T)
APRT	average pavement residence time (min.)
"C"	average runoff volume coefficient
C_c	coefficient of concavity
c(t)	time variable concentration (ug/L or mg/L)
$\overline{C}1$	flow weighted average concentration
C_s	particulate-bound metal element mass (mg/kg of dry solids as TSS)
COD	chemical oxygen demand [mg O_2/liter] (M/L^3)
C_u	coefficient of uniformity
D	dissolved mass of metal element (ug or mg)
d_{10}	particle size at which 10% of particle size gradation mass is finer (L)
EGME	Ethylene-Glycol-Monoethyl-ether
EMC	event mean concentration (ug/L)
f_d	dissolved fraction of metal element
f_p	particulate-bound fraction of metal element
ICP-AES	Inductively Coupled Plasma-Atomic Emission Spectroscopy
IOCS	Iron oxide coated sand
IPRT	initial pavement residence time (min.)
K_d	partition coefficient [L/kg]
LEMF	ateral event mean flow (L/min-m)
LPF	lateral pavement flow (L/min-m)
m	TSS concentration (mg/L)
m(t)	constituent mass transported up to time, t
m'(t)	dimensionless normalized mass of constituent
M	total event mass of constituent (ug or mg)
M_f	total event mass of constituent fraction (ug or mg)
n	number of hyetographs with a resulting distinct hydrograph
NTS	not to scale
OCS	iron oxide coated sand
OEPA	Ohio Environmental Protection Agency
ORP	oxidation reduction potential (mV)
P	particulate-bound mass of metal element (ug or mg)
PAH	polycyclic aromatic hydrocarbon
pdh	previous dry hours (T)
PEMC	partial event mean concentration (ug/L or mg/L)
q	flow rate (L/min)
q(t)	time variable flow rate (L/min.)
PET	partial exfiltration trench
PSD	particle size distribution

RSD	relative standard deviation
SD	standard deviation
SSA	specific surface area (m^2/g)
t	time
TDS	total dissolved solids
TSS	total suspended solids
t_r	time duration of entire runoff event (min or days)
t_i	distance between incremental area of i^{th} hyetograph & i^{th} hydrograph (T)
UCC	Unconfined compressive strength (lb/in^2)
USEPA	United States Environmental Protection Agency
v(t)	flow volume up to time, t
v'(t)	dimensionless normalized flow volume
V	flow volume [L]
vdr	vehicles during runoff
vprv	vehicles per runoff volume
v(t)	dimensionless normalized flow volume at time, t
Wa	measured weight of EGME retained by sample (M)
VDS	volatile dissolved solids
VSS	volatile suspended solids
W_s	measured weight of dried sample (M)
τ_i	$APRT_i$ for hyetograph and resulting hydrograph i (T)
$\overline{\tau}$	event mean APRT ($\overline{APRT}$) (T)

ACKNOWLEDGMENTS

This work was supported by the Ohio Department of Transportation (ODOT) as a sub-contract from the Federal Highway Administration (FHWA). We would like to express our appreciation to Messrs. William Edwards, Roger Green, John Herl, John Hurd, Tom Linkous, and Kevin White of ODOT for their assistance and interest in this research. This work was also supported in part by the National Science Foundation through National Young Investigators Award BCS-9257608.

A number of individuals were actively involved in the laboratory or field investigations of this research. These individuals include Joseph Koran, Joseph Smithson, Scott Schulte, Karin Ghia, Kitty Sansalone, and Janet Anno.

Tony Manch and Rena Puckett of ODOT provided traffic counting data and advice on traffic data interpretation. At the local level, Chris Hilbert and Dave Spisak of ODOT District 8 provided assistance and plan review for installation of the field experimental facility on I-75. Dirk Gross of ODOT provided permit assistance at the state and federal level. Tom Klug of ODOT District 8 and the City of Cincinnati, Division of Highway Maintenance provided pavement crack sealing as required.

INTRODUCTION

1.1 Problem statement

Stormwater runoff from heavily traveled urban highways, parking and impervious areas may adversely impact the quality of adjacent receiving waters (Hamilton & Harrison, 1991). Urban runoff often contains significant concentrations of soluble, insoluble and speciated fractions of metal elements. Additionally, urban runoff contains suspended, colloidal and volatile fractions of inorganic and organic particulates. Anthropogenic organic compounds of interest are polycyclic (polynuclear) aromatic hydrocarbons, oil and grease. De-icing chemicals also represent an important constituent source for urban runoff in the winter season of northern climates. Typical sources of these anthropogenic constituents include vehicular component wear, fluid leakage and engine exhaust; roadway abrasion and degradation; highway maintenance and roadway re-construction as summarized in Table 1.1.1 (Sansalone & Buchberger, 1997). For example, tire and pavement interaction causes abrasion of solids from both materials (Muschack, 1990). Tire-pavement interaction is a significant source of solids (Muschack, 1990). Pavements account for 40 to 50% and tires for 20 to 30% of solids generated (Kobriger and Geinopolos, 1984).

The potential impacts of highway nonpoint pollution are greatest in urban corridors where Average Daily Traffic (ADT) counts approach 100,000 vehicles. Urban areas of the United States with populations exceeding 500,000 generally have urban traffic corridors with ADT values in the 100,000 range. However, for watersheds with sensitive waters, potential deleterious impacts can occur at ADT counts lower than 30,000 (Wanielista and Yousef, 1993).

Table 1.1.1 Sources of anthropogenic constituent in roadway runoff (Sansalone & Buchberger, 1997).

Legend: ■ Primary source ▨ Secondary source

	Brakes	Tires	Frame & body	Fuels & oil	Concrete pavement	Asphalt pavement	De-icing salts	Litter
Cadmium	▨	■						
Chromium		■						
Copper	■	■						
Iron		■	■					■
Lead	▨	▨		▨			▨	
Nickel		■						
Vanadium				■				
Zinc	■	■	■					
Chlorides							■	
Organic Solids		▨				■		■
Inorganic Solids	▨		▨		▨			■
PAHs				▨		■		
Phenols						■		

Metals and particulates accumulate on the pavement surface between precipitation events or pavement cleaning operations. Metal elements and their cations, unlike micro-organics, cannot be degraded. One example of this persistence is total lead, which even today is measured in highway runoff and in surficial urban soils at concentrations significantly above background levels even though over 90 percent of the vehicular fuels consumed since 1985 have been unleaded (USEPA, 1989). A significant fraction of the soluble, complexed and particulate-bound fractions of these constituents is washed off the pavement surface during the rising limb of the runoff hydrograph. This phenomenon is commonly referred to as the "first-flush" of constituents. Concentrations of metals such as Pb, Cd, Zn, and Cu in urban highway runoff "first-flush" or snowmelt washoff have been measured at several orders of magnitude above background levels (<10 μg/L for Zn, Cu and <1μg/L for Cd, Pb) and significantly above levels found in the contributing precipitation. Metal elements, total solids and suspended solid concentrations in snowmelt washoff samples have been measured at concentrations up to an order of magnitude higher than "first-flush" levels in rainfall-runoff.

From a water quality perspective, solids having reactive sites with large surface to volume ratios can mediate partitioning and transport of metal elements and organic compounds in water. Solids of large surface area transported by urban runoff serve as reservoirs for many reactive constituents. Water quality and drainage considerations require characterization of solid gradation, mass loading and surface area. With respect to drainage design, the transport and accumulation of solids in and around surface and subsurface drainage appurtenances can lead to reduced hydraulic capacity, clogging and additional maintenance. Annual loadings from roads to receiving waters and/or treatment plants are significant for urban metropolitan areas. For example in Cincinnati, with a population of 1.5 million, there are approximately 5200 hectares of interstate and major arterial roadways. Anthropogenic solids transported in runoff from these 5200 hectares generate an annual load of total suspended solids (TSS) and chemical oxygen demand (COD) comparable to untreated domestic wastewater.

The principal factors affecting highway runoff quality include precipitation type (rain or snow), intensity, duration and frequency; vehicular and truck count; highway surface and subsurface drainage design; highway maintenance practices; constituent accumulation and deposition; local land use; geological and geographic characteristics; and pavement type and condition. Drainage conditions in and around urban highways, roadways and parking areas encourage transport of nonpoint constituents into adjacent receiving waters or sewer systems. The highly impervious nature of these areas coupled with the practice of efficient surface drainage results in a corresponding flushing of constituents from these areas during runoff events.

Once in receiving waters, the constituents may accumulate over time in the sediment of the receiving water, may be transported downstream, or remain in the water column posing a potential toxicity threat to aquatic life. The partitioning and distribution of these constituents is a function of the physico-chemical and hydraulic conditions of the receiving water. Nonpoint constituents, specifically metal elements and solids transported by combined sewer flows to treatment plants, may be trapped in the sludge of a wastewater treatment plant and represent a disposal concern especially for land applications (Monteith et al., 1993; McBride 1995).

1.2 Control strategies

The objective of any effective control strategy for highway nonpoint constituents is to contain a diffuse, relatively mobile water constituent before it exerts a toxicity impact on aquatic, terrestrial, animal or human life. For metal elements an effective control strategy can be viewed essentially as a "garbage can". Like any garbage can, it must be emptied and cleaned periodically.

A variety of passive best management practices (BMPs) have already been used as effective control strategies for runoff from urban areas and roads in the United States, Europe and Japan. Table 1.2.1 presents the effectiveness of various urban control strategies (Sansalone et al., 1995). In view of the nonpoint constituent loads that originate in highway corridors and the emerging NPDES stormwater criteria, it is likely that use of BMPs to control urban and highway constituents will grow in the future.

Table 1.2.1 Effectiveness of passive urban runoff control strategies (Sansalone et al., 1995).

Urban Runoff Parameter	Metal Elements	Suspended Solids	Colloidal Solids	PAHs	Chlorides	Peak Flow
Control Strategy	**PERCENT REMOVAL**					
Infiltration Trench	70 - 100	70 - 100	50 - 80	70 - 100	unknown	reduced
Porous Pavement	20 - 100	80 - 100	unknown	unknown	unknown	reduced
PET	70 - 100	70 - 100	50 - 80	80 - 100	unknown	reduced
Detention Basin	40 - 60	40 - 60	0 - 20	unknown	0 - 20	reduced
Retention Basin	60 - 80	60 - 90	20 - 60	unknown	0 - 20	reduced
Vegetated Swale	20 - 100	20 - 90	20 - 60	unknown	0 - 20	reduced
Wetland	60 - 100	70 - 100	60 - 80	unknown	unknown	reduced

Passive control strategies can be nominally classified as "infiltration methods", detention/retention, vegetative, or wetlands. A variety of sub-classifications exist for each of these main classifications. Within infiltration methods, for example, there are specific strategies such as porous pavement, infiltration trenches, partial exfiltration trenches (PET) and infiltration basins. Each of these control strategies will have differing degrees of effectiveness for specific constituents and differing suitability constraints for a given application. Because of constraints such as available land area and issues related to safety these control strategies may not be suitable for all highway conditions. Table 1.2.2 presents the potential suitability of control strategies for highway site conditions (Sansalone et al., 1995). These control strategies can be separated into two basic groups. The first group are infiltration strategies such as porous pavement, infiltration trenches and PETs. The second group are surface water impoundment strategies such as basins and wetlands.

Table 1.2.2 Suitability of Control Strategies for Highway Site Conditions (Sansalone et al., 1995).

Urban Runoff Parameter	Areal Size	Maintenance and Cleaning	Safety and Concerns	Native Soil Conductivity	Cost
Control Strategy					
Infiltration Trench	minimal	periodic	clogging	important	low/moderate
Porous Pavement	minimal	periodic	clogging	some importance	low/moderate
PET	minimal	periodic	clogging	slight importance	low/moderate
Detention Basin	large	periodic	water surface	important	moderate
Retention Basin	large	infrequent	water surface	important	moderate
Vegetated Swale	small	infrequent	none	some importance	low
Wetland	large	infrequent	water surface	important	moderate/high

1.3 The partial exfiltration trench (PET) concept

A novel passive treatment strategy developed herein, a partial exfiltration trench (PET), synthesizes the best attributes of porous pavement and infiltration trenches. The PET serves as a replacement to the practice of underdrain installation along highways. A schematic of a PET is shown in Figure 1.2.1. The primary differences between current underdrain designs and the PET are the installation of porous pavement directly above the trench to promote infiltration and coating of the granular backfill to enhance sorptive capacity. This PET design is based on the use of oxide coated granular backfill as the replacement to uncoated granular backfill.

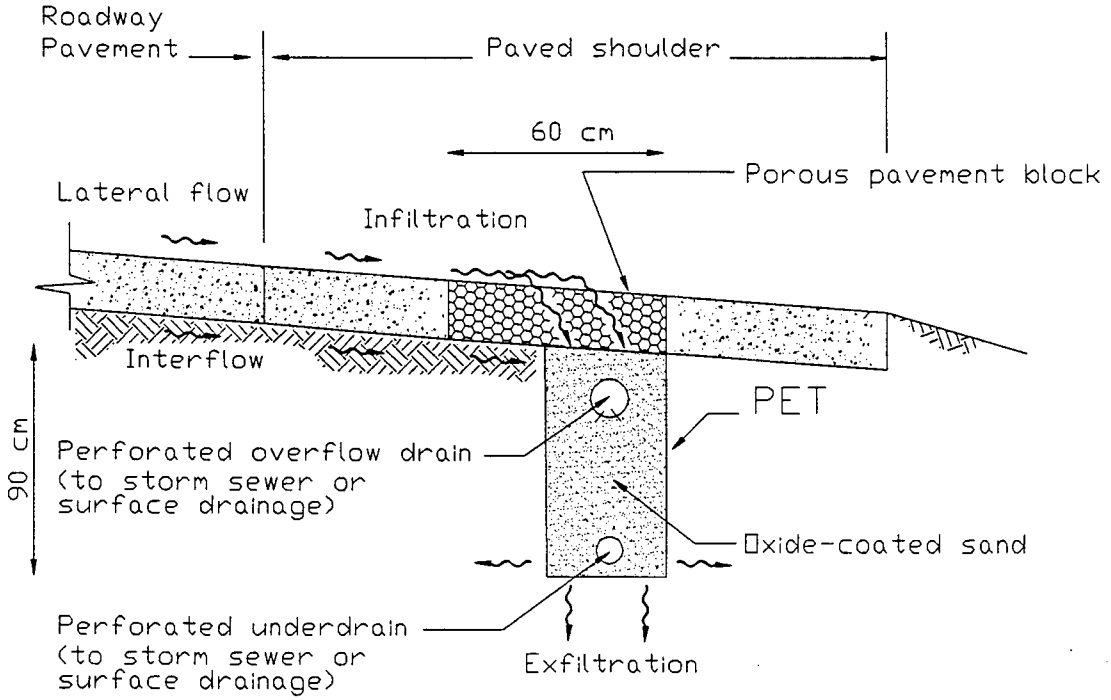

Figure 1.2.1. Schematic of a partial exfiltration trench section (PET).

When the concept of the PET was developed there were three major uncertainties regarding PET performance. The first is the metal element removal capacity of the PET. The PET must have sufficient immobilization capacity to retain and filter targeted constituents such that discharge levels of these constituents do not exceed a chosen discharge criterion for the design life of the PET. The second is the hydraulic capacity of the PET. The PET must be able to infiltrate lateral pavement sheet flow for the design inflow hydrograph. The third is the ability of the PET to buffer low pH runoff. Once the PET immobilizes metal elements, they must be prevented from being desorbed or remobilized.

PETs offer several advantages when compared to other control strategies. The narrow width of a PET allows them to be located along the edge of the paved berm.. These devices are ideally suited to intercept long duration rainfall events and the "first flush" from the pavement. When properly designed, they can surficially strain suspended solids at the porous pavement surface. PETs can function as a multi-purpose replacement to the current practice of underdrain installation. Finally, a PET can intercept subgrade interflow, which is significant for deteriorated pavement or roadways with unsealed joints (Jeffcoat et al., 1992).

PETs can also effectively trap soluble heavy metals through the mechanisms of adsorption, ion-exchange and precipitation. PETs are one of the most effective control options under conditions where the suspended solid gradation approaches the colloidal size and metal elements occur predominantly in soluble form. Wet and dry extended detention basins are not likely to be effective in removing the colloidal size particles or dissolved metal elements. Any device that does effectively trap suspended solids and metal elements must be designed so that periodic cleaning and maintenance is feasible.

Swedish researchers have shown that asphaltic porous pavement, a type of infiltration device, effectively removes constituents in highway runoff. The Swedish porous pavement, known as the Swedish Unit Superstructure, was developed as both a water quantity and quality control device. Simulations using 30 years of exposure to "stormwater rain" indicated the Unit Superstructure performed as effectively as any other control option listed in Table 1.2.1 The simulation produced negligible clogging and these results were confirmed during tests of in-situ porous pavement (Niemczynowicz, 1989).

The porous pavement block functions as a rigid surface finish, allows the infiltration of runoff and acts as a straining layer for the surficial trapping of the larger size suspended solids. The porous pavement block is a critical element of the PET for both the OCS effectiveness and maintenance aspects of the control strategy. In order to be hydraulically effective the porous pavement block must have adequate infiltration capacity yet be designed such that the suspended solid particle sizes responsible for long-term deep bed clogging are strained or captured in the porous pavement. Suspended solids trapped in the porous pavement can be easily removed with modified street cleaning techniques such as water spray injection and subsequent vacuuming (Niemczynowicz, 1989). Such surficial cleaning techniques would be applied to a PET on a periodic basis. Experience indicates that clogging of porous pavements is minimal. Loss of infiltration capacity is readily restored by surficial cleaning. Nonetheless, the potential for clogging of PET's porous pavement requires investigation. Unlike drinking water rapid sand filters which are regularly backwashed to remove suspended solids

and other constituents, a PET cannot be backwashed and therefore deep-bed clogging needs to be minimized. Additionally, PET capacity must be sufficiently long to be feasible.

1.4 Research objectives

There were four objectives of this research.

(1) Carry out a comprehensive characterization of metal elements and solids transported in highway runoff at an urban highway experimental site in Ohio.

(2) Develop and design a passive control strategy for immobilizing metal elements and solids.

(3) Perform bench scale laboratory simulations for the proposed passive control strategy using simulated and actual stormwater, and

(4) Install and evaluate of a prototype control strategy installed at the urban highway experimental site.

1.5 Significance of the research

Urban stormwater contains metals, metal complexes, solids and other contaminants which have a deleterious effect on aquatic ecosystems in receiving waters and represent a disposal problem when trapped in wastewater sludges. Studies have documented that nonpoint sources of contaminants are responsible for a majority of the metal contaminant loading to the United States waters (Wanielista and Yousef, 1993). In western Europe the problems of urban stormwater contamination and receiving water impacts have been recognized and mitigated for over a decade. Potential applications for this research can be found along any heavily traveled urban highway in the USA. State DOTs are beginning to address recent court-directed mandates to treat their highway runoff before discharge to receiving waters or municipal sewer systems.

Passage of the Clean Water Act (CWA) in 1972 established the National Pollutant Discharge Elimination System (NPDES) to regulate industrial and municipal point sources discharging into waters of the United States. By the mid-1980s, it was evident that control of nonpoint source constituents was crucial to meeting CWA objectives (Wanielista & Yousef, 1993). Therefore, in 1987 the CWA was amended to include NPDES permits for stormwater discharges from industrial activities and municipal separate storm water systems. Soon thereafter, the US Environmental Protection Agency promulgated regulations governing permits for stormwater discharges. This evolving regulatory framework has prompted some State Department of Transportations (DOTs) to implement pro-active efforts to characterize highway stormwater discharges and to identify best management practices (BMPs).

Using oxide coated porous media, a PET is a novel passive device, intended to immobilize metal elements, complexes and particulate-bound metals more effectively than other control strategies. However, performance and capacity of OCS to immobilize metal elements in urban runoff has not been considered or quantified until this research.

There are several reasons why this research is unique and important:

1. The PET concept provides a unique and potentially viable strategy for the integration of water quantity and quality control adaptable to urban conditions.

2. The treatment of urban stormwater by adsorptive infiltration through OCS of the PET represents the first attempt at in-situ passive immobilization of nonpoint metal element pollution using OCS.

3. This research provides new knowledge regarding the OCS capacity of a PET for actual stormwater loadings using bench scale column simulations to quantify competitive metal element breakthrough capacity.

4. This research is the first attempt to characterize lateral pavement sheet flow providing new knowledge for the feasibility and design of passive source control strategies.

5. The adaptation of the ethylene glycol monoethyl ether (EGME) method provides new knowledge regarding the specific surface area (SSA) of solids in runoff and snowmelt. The application of this method to measurement of SSA for OCS is unique.

STORMWATER CHARACTERIZATION AT I-75 EXPERIMENTAL SITE

2.1 Introduction

Rainfall runoff from urban roadways often contains significant loads of metal elements, particulate and dissolved solids, organic compounds and inorganic constituents including de-icing salts. Unlike organic compounds, metal elements are not degraded in the environment and constitute an important class of constituents generated by traffic activities. Metal elements partition into dissolved and particulate-bound fractions as a function of pH, pavement residence time and solids concentration. Solids are classified as either dissolved or suspended. As summarized in Table 1.1.1, the deposition and accumulation of these constituents result from traffic activities, vehicular component wear, fluid leakage, pavement degradation and roadway maintenance (Armstrong, 1994; Ball et al., 1991; Lygren et al., 1984; Muschack, 1990). Winter maintenance practices such as de-icing salt application generate chloride anions and associated cations such as sodium or calcium.

Particulate matter, generated from both natural and anthropogenic sources, is ubiquitous in natural waters and urban waters. Urban drainage from paved areas transports dissolved, colloidal and solid constituents in a heterogeneous mixture of metal elements, organic and inorganic compounds (Sansalone and Buchberger, 1997). Tire-pavement interaction is a significant source of solids (Muschack, 1990). For example, tire and pavement interaction causes abrasion of solids from both materials (Muschack, 1990). Pavements account for 40 to 50% and tires for 20 to 30% of solids generated (Kobriger and Geinopolos, 1984).

From a water quality perspective, solids having reactive sites with large surface to volume ratios can mediate partitioning and transport of metal elements and organic compounds in water. Solids of large surface area transported by urban runoff serve as reservoirs for many reactive constituents. Water quality and drainage considerations require characterization of solid gradation, mass loading and surface area. With respect to design, solid accumulation in and around surface/subsurface drainage appurtenances can lead to reduced hydraulic capacity, clogging and additional maintenance.

2.2 Previous Work

Various aspects of urban stormwater degradation related to highway runoff have been investigated by researchers over the last two decades (Morrison, et al., 1984; Harrison and Wilson, 1985; Ellis and Harrop, 1984; Stotz, 1987; Grottker, 1987). During the 1970s and early 1980s the Federal Highway Administration (FHWA) and state agencies carried out a field program to characterize the water quality impacts of highway runoff. Runoff water quality data were collected during 993 storm events at 31 highway sites in 11 states (Driscoll, et al.,1990). The storms included both rainfall and snow events. Most of these water quality constituents were reported as event mean concentrations, EMCs. Although the FHWA database is extensive, the temporal variation of metal element washoff during these events was not published. In addition, metal elements were measured as total recoverable metals, instead of dissolved and particulate-bound metals. Recent policy from USEPA's Office of Water mandates the use of dissolved metal to set and measure compliance with

water quality standards. Dissolved metals more closely approximate the bioavailable metal fraction than total metals (40 CFR Part 131, 1995).

The delivery and characteristics of urban roadway runoff solids have been investigated by researchers for both impairment of drainage and water quality considerations. Indices such as vehicles during storm, VDS have been used to predict solid loadings at highway sites (Chui et al, 1982; Racin et al.,1982). or more commonly some measure of traffic intensity such as average daily traffic, ADT (Yousef, 1985). Because of the uncertainty associated with the occurrence of rainfall and the unique nature of each event, sweeping and flushing techniques are often used to collect solids from roadway pavement. Mechanical sweeping, flushing and sprinkling of the pavement surface using potable water have been used to assess pavement surface particle size distributions (PSDs), loading of solids, metal element mass, biological oxygen demand (BOD) and chemical oxygen demand (COD) of solids (Sartor and Boyd, 1972; Kobriger and Geinopolos, 1984, Irish et al, 1995). Such techniques provide experimental control for otherwise unique and nonreproducible experiments subject to the unpredictable arrival, intensity and duration of natural rainfall runoff events as well as traffic. Although improving experimental control, these techniques may not provide an accurate representation of solid characteristics, constituent partitioning, and the temporal variation of actual rainfall runoff events.

One comparison between roadway sweeping and rainfall washoff at a roadway site in Germany indicated that finer solids are transported from the pavement more effectively in rainfall runoff while sweeping preferentially removed coarse solids (Grottker, 1987). In addition to the difficulty associated with obtaining data for hydrologically generated events, sampling and analysis are expensive. As a consequence, inexpensive surrogates are often measured in place of other parameters such as ionic species, metal elements and nutrients. These measured solids indices include total suspended solids (TSS), total dissolved solids (TDS), and total volatile solids (TVS) (Thomson, et al., 1997).

Particle counting and sizing have been applied to drinking water and wastewater for analysis of solids ("Standard" 1995). Particle counting instrumentation commonly applied employs one of three particle measurement principles. These principles are light scattering, light obscuration or electrical resistance (Coulter Counters). Aside from a study by Roberts et al., 1988, the authors are not aware of published research applying particle counting to urban runoff. Roberts et al., 1988 utilized a Coulter Counter to measure particle sizes, but not particle counts, and employed scanning electron microscopy to characterize the alteration of runoff-entrained pavement solids transported through a pipe sewer during rainfall runoff events.

Other researchers have investigated the influence of precipitation type on correlations for total metal element concentration regressed against particle size (Sansalone et al., 1995). Correlations between particle size and metal elements for highway runoff solids captured in detention basins and roadway drainage structures have generally shown metal elements are primarily associated with the smaller particle sizes (Price and Yonge, 1995; Xanthopoulos and Hahn, 1990). The association of metal elements with various physico-chemical fractions of urban runoff solids has also been investigated (Bourcier and Sharma, 1980). Particle size is commonly utilized as a surrogate measure for solid SSA (Foster and Charlesworth, 1996). A search of the

literature found only one study which measured SSA for urban roadway solids, although the SSA procedure was not presented (Grottker, 1990).

2.3 Characterization objectives

Sampling and laboratory analysis was carried out for thirteen rainfall runoff. As part of the characterization, there were specific objectives for both metal elements and solids.

Metal Elements:

First, using 1995 data collected from an instrumented highway site in urban Cincinnati, the partitioning of metal elements between the dissolved and particulate-bound phases was investigated. Partitioning has implications not only for washoff of metal elements and solids but also can indicate what physico-chemical mechanisms will be most effective for immobilization of dissolved and particulate-bound mass. Second, using event mean concentration (EMC) values from the Cincinnati highway site, dissolved and total metal element EMCs were compared to USEPA and Ohio EPA (OEPA) surface water discharge criteria. Finally, the phenomenon of a first flush for lateral pavement sheet flow, in contrast to concentrated gutter flow, was evaluated for metal elements and solids transported directly from the roadway surface.

Solids:

For a subsequent series of events in 1996 and 1997 the first objective was to characterize the mass delivery and first flush of suspended and dissolved solid fractions as well as particle counts and size. A second objective was to measure and evaluate particle size distributions and specific surface area of transported solids. The final objective was to integrate the SSA results over the PSD to determine the total surface area contribution of various particle sizes. The results presented herein will improve the database for temporal washoff of solids and provide the designer of treatment strategies with physical characteristics and loadings of solids.

2.4 The first-flush concept

Urban nonpoint constituents are transported off roadway pavements during rainfall runoff and snow washoff events. Because nonpoint constituent concentrations often vary by several orders of magnitude during a runoff event, a single index, known as event mean concentration, is often used to characterize nonpoint source constituents (Wanielista & Yousef, 1993). EMC for an individual storm event is defined as the total constituent load (mass) divided by the total runoff volume.

From a practical point of view, EMCs are obtained from a flow-weighted composite of concentration samples taken at intervals throughout the entire storm event. Individual storm events can be either rainfall or snow and the constituent EMC will vary from event to event. Owing to this variability, EMCs are often treated as random variables having a lognormal probability distribution irrespective of the type of runoff generating event (Huber, 1993).

Significant amounts of dissolved and particulate-bound fractions of metal elements and solids can be washed off the roadway surface during the runoff hydrograph. The first flush has been qualitatively defined as the delivery of a disproportionately large load of constituents during the early part of the runoff hydrograph (Schueler, 1987). For the development of a criterion to determine whether the delivery of a disproportionately large load of constituents occurs during the early part of the runoff hydrograph the definition for the event mean concentration is applied. The EMC for an individual storm event is defined as the total pollutant load (mass) divided by the total runoff volume, or

$$EMC = \bar{C} = \frac{M}{V} = \frac{\int_0^{t_r} c(t)q(t)dt}{\int_0^{t_r} q(t)dt} \qquad (2.4.1)$$

where: M = total mass of pollutant
V = total liquid volume of flow or sample
$\bar{C}$ **Error! Switch argument not specified.** = flow-weighted concentration average
c(t) = time-variable concentration
q(t) = time-variable flow
t_r = entire duration of event

The EMC is computed for the entire runoff duration. For any time t, less than the entire runoff duration, a partial event mean concentration (PEMC) can be defined as

$$PEMC(t) = \frac{m(t)}{v(t)} = \frac{\int_0^{t} c(t)q(t)dt}{\int_0^{t} q(t)dt} \qquad (2.4.2)$$

where: m(t) = mass transported up to time t, [M]
v(t) = flow volume up to time t, [L^3]

From equations (2.4.1) and (2.4.2) it follows, $M = m(t_r)$, $V = v(t_r)$ and therefore for time equal to the duration of runoff, t_r,

$$EMC = PEMC\ (t_r). \qquad (2.4.3)$$

Several criteria have been suggested to identify the occurrence of a first-flush. One quantitative criterion of the first flush is when the ratio of cumulative incremental mass load divided by the cumulative incremental flow volume is greater than one for any time (Helsel et al., 1979). This criterion can be stated as

$$\frac{\frac{m(t)}{M}}{\frac{v(t)}{V}} \geq 1.0 \qquad (2.4.4)$$

By rearrangement and substitution, equation (2.4.4) can be represented as

$$PEMC(t) \geq EMC \qquad (2.4.5)$$

Other more restrictive first-flush criteria are when 50% of the constituent mass is transported in the first 25% of the runoff volume (Wanielista and Yousef, 1993) or when the initial 20% of runoff volume contains 80% of transported constituent mass which defines a very strong first flush (Stahre and Urbonas, 1990).

Let $m'(t) = m(t)/M$ and $v'(t) = v(t)/V$ represent dimensionless normalized mass and flow volumes transported from the roadway surface. Three criteria for defining the occurrence of a first flush are summarized below.

Criterion	Condition	Reference
1	$m'(t) \geq v'(t)$	Helsel et al., 1979
2	$m'(t) \geq 0.50$ and $v'(t) \leq 0.25$	Wanielista & Yousef, 1993
3	$m'(t) \geq 0.80$ and $v'(t) \leq 0.20$	Stahre & Urbonas, 1990

Note criterion 1 is equivalent to $PEMC(t) \geq EMC$ or $m'(t)/v'(t) \geq 1$. The conditions for criteria 2 and 3 are more restrictive. However it must be kept in mind that criteria 2 and 3 are "rules of thumb" developed for concentrated gutter flow and not for lateral pavement sheet flow. Criterion 1 was chosen to evaluate a first flush for each constituent for each event.

2.5 Experimental site and local climate

The experimental site is located along the Millcreek Expressway of Inter State Route 75 in Cincinnati Ohio, a major north-south interstate. Average daily traffic counts are 135,000 passenger vehicles and 15,000 commercial vehicles. The site has four southbound lanes, an exit lane and a paved shoulder which all drain towards a wide, grassed v-section median at a transverse cross slope of 0.020. The pavement is asphalt, with an asphalt overlay placed in 1990. The site is located in a relatively flat vertical sag with a well-defined and completely paved catchment area, 15 meters long by 20 meters wide. Longitudinal slopes approaching the sag are less than 0.004. Site stormwater drains via a pipe sewer directly to Mill Creek, designated a modified warmwater habitat. A plan view of the site is presented in the upper half of Figure 2.5.1. Cincinnati receives on average 1020 mm of rainfall and 420 mm of snow per year. The average summer temperature is 23.4°C. The average winter temperature is

0°C. The highest monthly rainfalls are March with 106 mm and July with 104 mm. The highest monthly snowfall is 150 mm in January (USDA, 1982).

2.6 Methodology

Experimental site configuration

In early 1995 the highway stormwater collection and sampling system was constructed. The experimental site was designed to intercept only lateral pavement sheet flow from across the four lanes, exit lane and shoulder. Since the catchment lies in a flat vertical sag there was no concentrated longitudinal gutter flow, or flows from outside the 15 meter by 20 meter pavement catchment. The focus on lateral pavement sheet flow is a departure from the work of other researchers who sampled stormwater runoff as an aggregation of lateral sheet flow, longitudinal gutter flows and occasionally pipe flows (Morrison et al., 1984; Harrison and Wilson, 1985). The characterization of lateral pavement sheet flow as opposed to curb/gutter or concentrated flow is critical since the PET will be loaded by lateral pavement sheet flow. Characterization of gutter flow in urban areas of London reported dissolved fractions for Cd of 69%, Cu of 87%, Pb of 47% Zn of 82% (Revitt et al., 1990).

The edge of the high-speed lane shoulder was saw-cut and excavated to allow construction of a 15 meter wide concrete collector slab. A 15 cm diameter semi-circular PVC interception trough was attached to the saw-cut edge of the paved shoulder and supported by the collection slab. The trough had three, 20 cm orifice openings at the bottom to accommodate low flows. Both the collection slab and interception trough were longitudinally sloped towards the center with a grade of 0.040 to form a v-section. The slope of the collection slab was 0.060 from the saw-cut edge of the shoulder to the entrance of a Parshall flume. The steep slope and smooth epoxy finish of the collection slab ensured solids were not deposited in the experimental facility. Details of the sampling and instrumentation configuration, in plan, are shown in the lower half of Figure 2.5.1. A profile through the experimental facility is shown in Figure 2.5.2.

Sampling and hydrologic data collection

Stormwater runoff was sampled from the center of the interception trough, immediately after runoff left the pavement surface. One liter samples were obtained at regular intervals, using an American Sigma automated 24 bottle sampler with polypropylene bottles. The initial runoff trickling into the trough was sampled using a 25 ml wide-bore pipette. 500 ml was collected for the first sample in this manner. Automatic sampling was initiated when the depth of water in the converging section of the Parshall flume reached 3 mm. Samples were then taken at two minute intervals for the first 48 minutes and thereafter at intervals ranging from 10 minutes to 30 minutes. Sampling continued for the duration of runoff. After discharging from the trough, runoff flowed down an epoxy-coated converging slab and through a 2.54 cm Parshall flume for flow measurements. Flows leaving the flume were transported through a 25.4 cm dia. PVC pipe trough for two meters to a 2000 liter storage tank. Runoff not directed into the tank was discharged to the a swale in the grassed median.

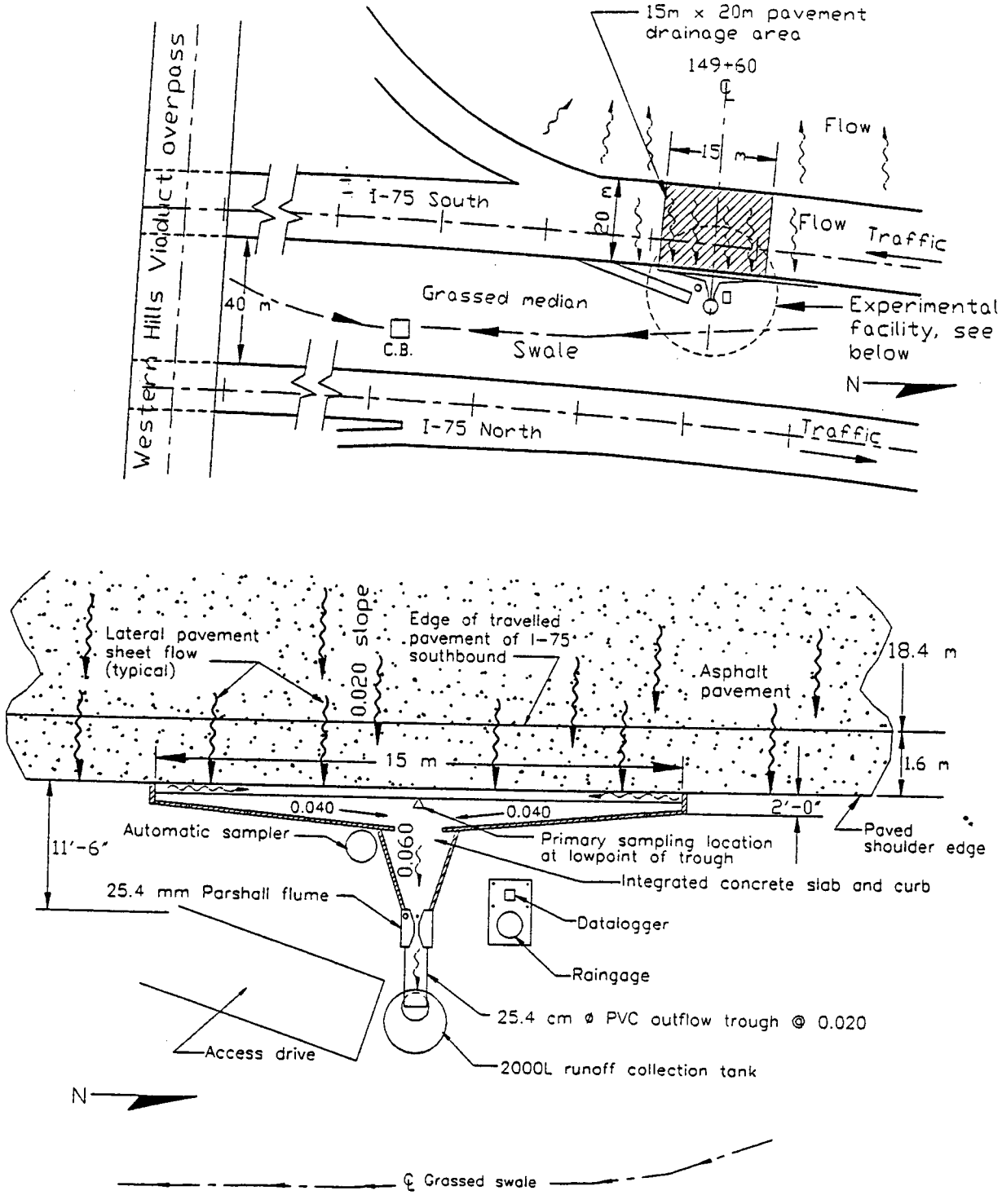

Figure 2.5.1 Plan view of I-75 experimental site and experimental facility (NTS).

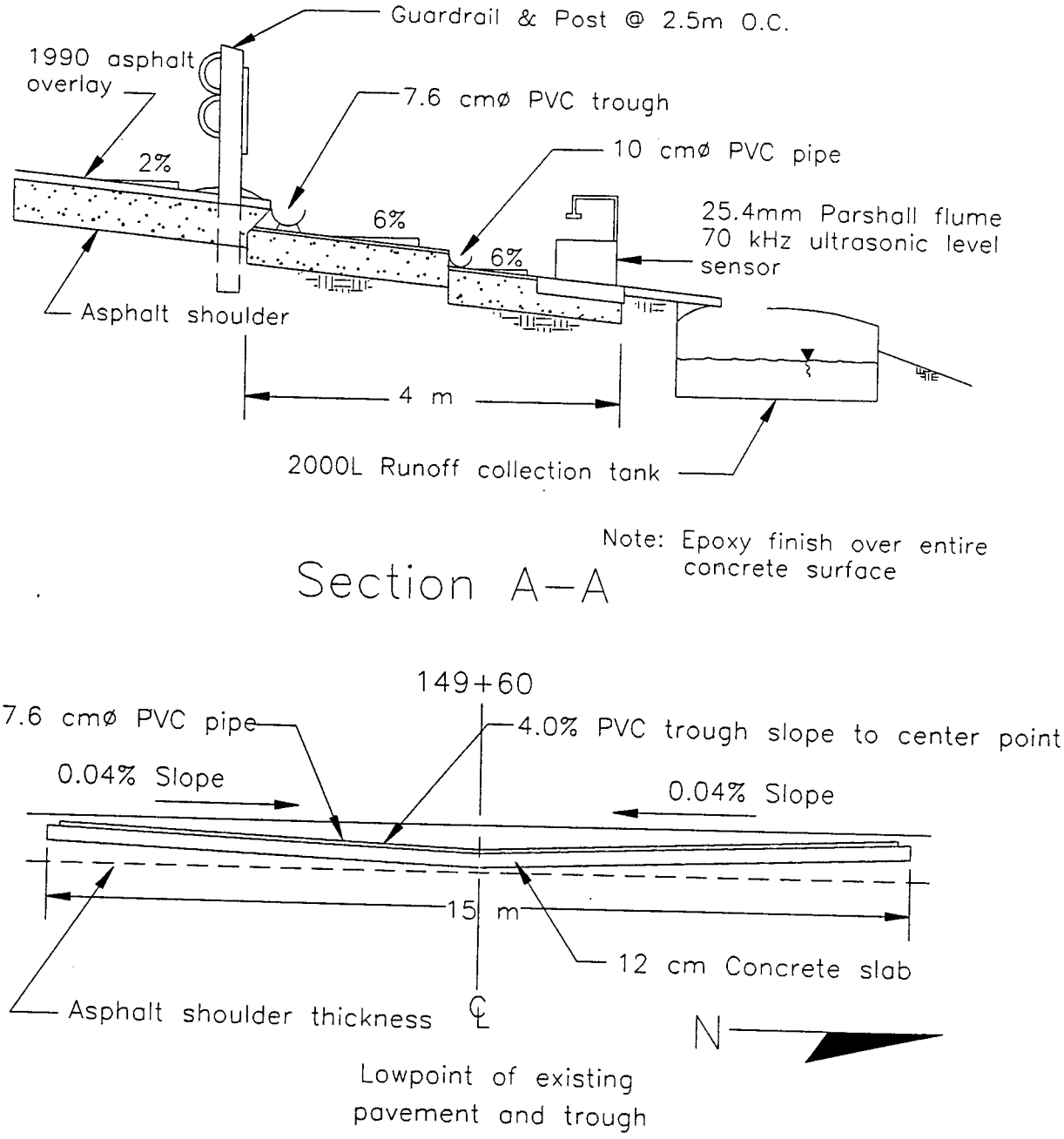

Figure 2.5.2 Sections through experimental facility (NTS).

Field measurements included rainfall, flow depth, pH, oxidation reduction potential (ORP), and temperature. Rainfall was recorded with a tipping bucket gage in increments of 0.254 mm. A 70 kHz ultrasonic level sensor was mounted 26 cm above the top of the Parshall flume to measure flow depths. Flow levels were transmitted to the datalogger every second and averaged over one minute to provide a single average flow level for each minute. The one minute flow level average value was converted to a flow rate using the upstream head-discharge relationship for Parshall flumes, Equation 2.5.1. The flume's low-flow capacity is 2 liters per minute and the high-flow capacity is 400 liters per minute. The

flume's low-flow capacity is 2 liters per minute and the high-flow capacity is 400 liters per minute. The depth readings were recorded by an American Sigma 950 datalogger. In the case of a 2.54 cm flume K is equal to 0.0604 and u is equal to 1.55 (Bos, 1990).

$$Q = Kh^u \tag{2.6.1}$$

where:
- h = the measured level (m)
- Q = the calculated flowrate (m^3/s)
- K = a dimensional factor which is a function of the throat width
- u = a power that varies between 1.522 and 1.60

Hydrologic and water quality data were collected during five rainfall-runoff events at the experimental site. The rain events varied in duration, intensity and interarrival times and generated flows ranging from the low-flow to high-flow capacity of the flume. Samples were analyzed for metals and solids for all events and pH, ORP, and conductivity for selected events. For each rainfall event, runoff and solids were pumped from the storage tank while keeping the tank mixed. A 210 L tank was returned to lab and the solids settled under quiescent conditions for 48 hours. Assuming Stokesian settling, 2 micrometer particles with a specific gravity of 1.4 g/cm^3 (as opposed to inorganic particles) would reach the tank bottom within 48 hours. The clarified stormwater was then poured off and the solids collected for analysis. Solids were dried at 60°C.

During 1995, five rainfall runoff events were sampled at the I-75 site. The analysis focused on the partitioning and first flush of metal elements in lateral pavement sheet flow (Sansalone and Buchberger, 1997). Solids data reported from the 1995 events included only TSS, volatile suspended solids (VSS), TDS and volatile dissolved solids (VDS). During 1996 and 1997, eight rainfall runoff events were sampled and analyzed. During 1996 and 1997 hourly traffic counting data were obtained from an automatic traffic counter operated by the Ohio Department of Transportation.

For each event, the beginning of rainfall was designated as time 0. The initial rainfall would wet the roadway surface, fill pavement depressions and be re-entrained and deflected by traffic resulting in a time lag from initial rainfall to initial runoff. Consistent with sampling protocol employed for 1995 events, once the initial runoff trickled into the trough, a manual sample was taken. One liter samples were automatically taken at two minute intervals while flow continued. After 24 samples, sampling intervals were increased to a range from 10 to 30 minutes for runoff duration. From the hydrologic data and field sampling analysis, pavement residence time and flow indices were computed. Average pavement residence time (APRT) and initial pavement residence time (IPRT) were calculated using the methodology shown in Figure 2.5.3. For each hyetograph and resulting hydrograph, APRT is defined as,

$$\tau_i = APRT_i = \left[\frac{\sum(A_i t_i)}{\sum A_i}\right]_{Hi} - \left[\frac{\sum(A_i t_i)}{\sum A_i}\right]_{hi} \tag{2.6.2}$$

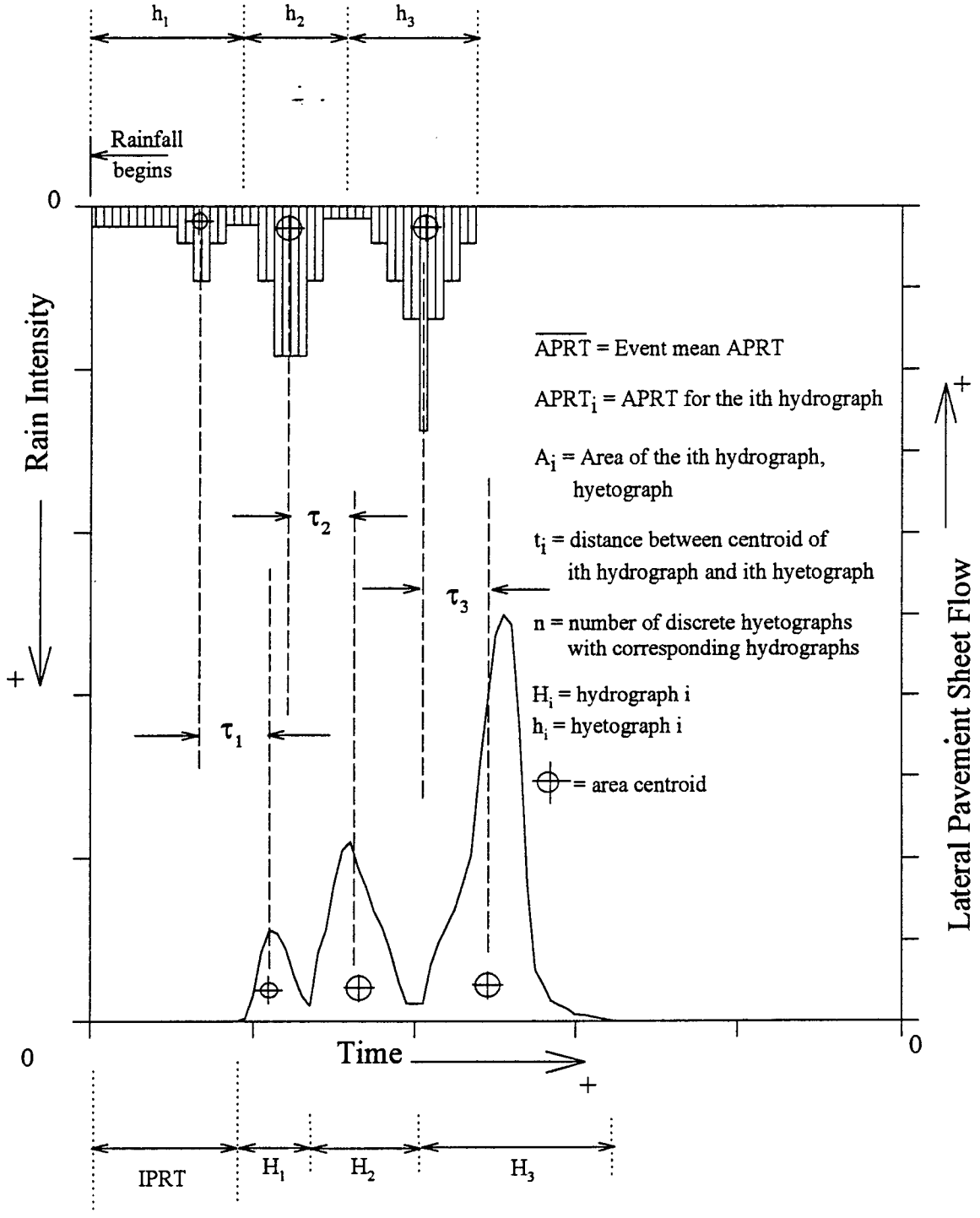

Figure 2.5.3 Methodology for determination of APRT and IPRT.

The mean APRT for an event of multiple hydrographs is defined as follows.

$$\bar{\tau} = \overline{APRT} = \frac{\sum \tau_i}{n} \qquad (2.6.3)$$

where: t_i = $APRT_i$ for hyetograph and resulting hydrograph I (T)
A_i = incremental areas for hyetograph and resulting hydrograph i (L^2)
t_i = incremental area moment arm from origin at time = 0 (L)
H_i = ith hydrograph
h_i = ith hyetograph
$\bar{\tau}$ = event mean APRT ($\overline{APRT}$) (T)
n = number of discrete hyetographs with resulting hydrographs

Metal element fractionation

Once sampling was completed for a runoff event, samples were immediately transported to the nearby laboratory. Metal element partitioning between the dissolved and particulate-bound phases in surface waters is a dynamic process. Therefore, samples were fractionated between dissolved and particulate-bound metal elements and then acidified within hours of being logged in at the laboratory. Samples were stored at 4°C.

The dissolved fraction is defined as metal elements of an unacidified sample that pass through a 0.45 micrometer membrane filter (American Public Health Association, 1992). Each one liter sample was mixed on a magnetic stirrer and a 50 ml sample obtained using a wide-bore pipette. The 50 ml dissolved fraction was immediately acidified with 2.5 ml of trace-metal HNO_3. Particulate-bound metal element fractions, retained on the membrane filter, were digested using a microwave-assisted procedure based on SW-846 Method 3015 (USEPA, 1990). Analysis were conducted on a Perkin-Elmer Optima 3000 Inductively Coupled Plasma Spectrometer, included scans for Na, Mg, Al, Ca, Cr, Mn, Fe, Ni, Cu, Zn, Cd, and Pb. Measurement of the metal element dissolved fraction is important as an indicator of bioavailability and has implications for metal transport and immobilization. The dissolved fraction, f_d and the particulate-bound fraction, f_p are defined as:

$$f_d = \frac{D}{D+P} \qquad (2.6.4)$$

$$f_p = \frac{P}{D+P} \qquad (2.6.5)$$

where: D = dissolved mass of a metal element (mg)
P = particulate-bound mass of a metal element (mg)

The equilibrium partition coefficient, K_d for dilute solutions expresses the ratio of metal element mass normalized to the dry mass of solids to the metal element concentration in solution. Assuming a linear isotherm, a partition coefficient can also be used to evaluate the distribution between dissolved and particulate-bound metal elements. Therefore, the partition coefficient accounts for the

presence of solids in runoff. Sample K_d values were determined using individual sample C_s and C data. K_d values computed from each event were compared to surface water K_d values reported by other researchers. The partition coefficient is defined as:

$$K_d = \frac{C_s}{C} \tag{2.6.6}$$

where : K_d = partition coefficient between particulate-bound mass and dissolved mass [L^3/M]
C_s = particulate-bound metal element mass [M/M of dry solids, TSS]
C = dissolved metal element concentration [M/L^3]

Experimental control - rainfall analysis

For each event, rainfall sampling was also conducted at an urban residential site 3 km from the highway. Rainfall sampling at this site was used to establish background levels for metal elements, solids, pH and ORP. Rainfall was collected in a 20 liter polypropylene container, elevated one meter off the ground to prevent rainfall splash up. Rainfall samples were returned within an hour of collection to the laboratory for analysis and fractionation.

Solids fractionation

Runoff samples were separated into total suspended solids (TSS), volatile suspended solids (VSS), total dissolved solids (TDS), and volatile dissolved solids (VDS) fractions. Each one liter sample was mixed on a magnetic stirrer and a 100 ml sample obtained by a wide-bore pipette. TSS, VSS and TDS were determined using Standard Methods 2540 (American Public Health Association, 1992). The VDS fraction, not covered under Method 2540, was evaluated in a similar manner to VSS, by the ignition of TDS residue at 550 °C for one hour.

Particle Counting

Particle size and number for a discrete size range were measured using a HIAC/ROYCO Model 9064 with a HRLD-400 light obscuration sensor. The operation of this instrument is typical of a displacement technique utilized for both light obscuration and electrical resistance sensors (AWWA 1992). The instrument, designed for batch sample analysis, had capacity to accurately characterize water up to concentrations of 18,000 particles per milliliter (mL) for sizes between 2 and 300 micrometers (mm). For light obscuration, the maximum particle concentration is 20,000 particles per mL and the measurable size range is from 1 mm to 500 mm. Liquids containing higher concentration require dilution with particle free water. The sample collection, handling and counting procedure followed Standard Methods 2560 ("Standard" 1995). Particle counting and size analysis were carried out within six hours of sample collection in the field. Dilutions with particle free water at ratios of up to 100 were required for some samples. A schematic of particle counting components and operation is shown in Figure 2.5.4.

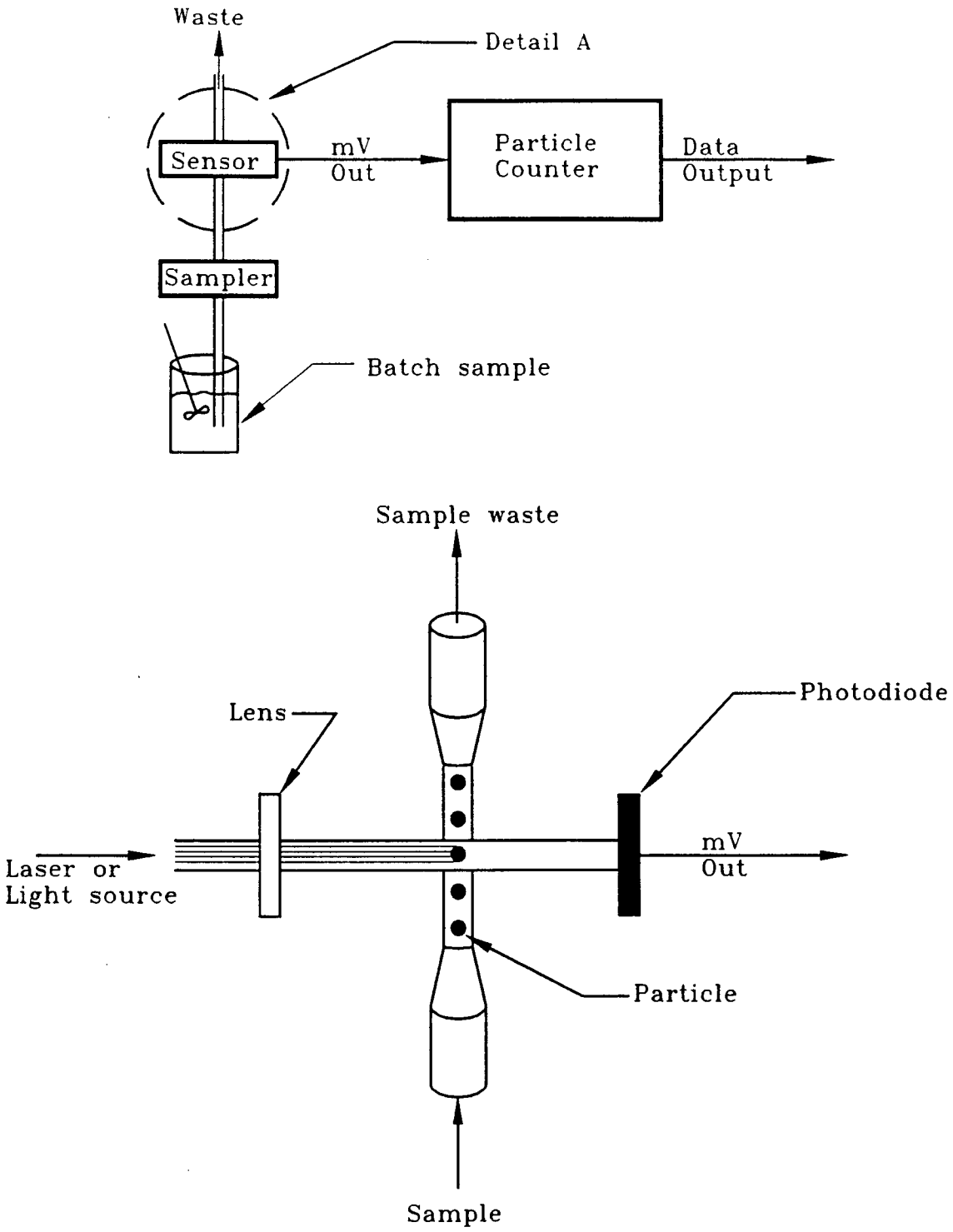

Figure 2.5.4 Schematic of particle counting components and operation of a light obscuration sensor.

Particle size distributions

The determination of the particle size distribution was performed according to ASTM D 421 for the sample preparation (with the exception of air drying) and ASTM D 422 for the sieve analysis (ASTM 1993). Thus, all samples were oven dried. The set of sieves encompassed the 9.5 millimeter (#3/8) through the 25 mm (#500) sieves. Typically, a hydrometer analysis would be performed for particles less than 75 mm (ASTM 1993). However, for sample recovery, SSA determination and chemical composition analysis, mechanical sieve analysis proved the best protocol.

From the particle size analysis, semilog plots of percent finer as a function of particle size were constructed to give large and small diameter particles nearly equal weight (Bowles 1992). The effective size, d_{10} of each gradation was determined from the resulting gradations. This effective size is defined as the size at which ten percent of the material is finer. From each gradation result, a d_{60}, d_{50}, d_{30}, uniformity coefficient, C_u and a coefficient of concavity were determined. C_u is defined as:

$$C_u = \frac{d_{60}}{d_{10}} \qquad (2.6.7)$$

The uniformity coefficient provides an indication of the distribution of particle sizes. A large value of C_u indicates that the d_{10} and d_{60} particles differ significantly. The coefficient of concavity is a measure of the shape of the PSD curve between the d_{60} and the d_{10} particle sizes and is defined as:

$$C_c = \frac{d_{30}^2}{d_{10}d_{60}} \qquad (2.6.8)$$

If C_c varies greatly from 1.0, particle sizes between d_{60} and d_{10} are missing (Das, 1992). Visual observation of each particle size range indicated solids retained on the #200 sieve, particles larger than 75 mm, were inorganic material with a variable organic coating or asphaltic binder. Particles passing the #200 sieve appeared increasingly organic. The organic content of the minus 200 material may be approximated by the ratio of VSS to TSS mass.

Specific surface area (SSA)

Two commonly used methods for the experimental measurement of surface area are the Brunauer-Emmett-Teller (BET) and the Ethylene-Glycol-Monoethyl Ether (EGME) methods (Schwertmann and Cornell, 1991). Both the BET and EGME methods assume a monolayer coverage of the adsorbate. The BET method employs N_2 gas which is physically adsorbed onto the surface of the solid at a series of known gas pressures. The surface area is determined by measuring the adsorbed gas volumes, and applying these volumes, using a cross-sectional area of an N_2 molecule, 0.162 nm^2, to the BET isotherm expression. This method requires sample drying at 150°C to remove all physically adsorbed water which would otherwise interfere with surface area determination. However, drying at 150°C modifies the structure and SSA of many solids and volatilizes organic coatings resulting in a less accurate determination of SSA.

The EGME method determines the amount of Ethylene-Glycol-Monoethyl Ether ($HOCH_2CH_2OCH_2CH_3$), a polar liquid with a relatively high vapor pressure, adsorbed at a constant vapor pressure by measuring the increase in sample weight due to the adsorbed monolayer of EGME. A representative sample of 0.5 to 2.0 grams dry weight was selected for each discrete size range sample. Each sample was placed in a small glass petri dish for drying and EGME addition. All discrete size range samples from a single event were first dried to a constant weight at 60°C and then dried in an evacuated dessicator over phosphorus pentoxide, P_2O_5. Once a constant dry weight was obtained, each solid sample was saturated with EGME, completely wetting all particle surfaces, and placed in an evacuated glass dessicator over 600 grams of an EGME-$CaCl_2$ solvate. A constant vapor pressure was produced from this solvate. The EGME to $CaCl_2$ ratio was 1.5:1. Samples were held in an evacuated dessicator and weighted until a constant weight for each sample was obtained as determined by a weight differential of less than 1 mg across a time interval of at least four hours. Each event generated 15 discrete size samples, all placed in the same dessicator along with control samples. Each dessicator of 18 samples required from 30 to 50 hours of drying time to produce a monolayer coverage.

One EGME molecule has a cross section coverage of 0.52 nm^2 and a molecular weight of 90.12 grams per mole. Therefore, an EGME monolayer of 1 m^2 consists of 0.286 mg of EGME. Carter et al. (1986) present a thorough discussion of the EGME method along with a standard procedure for the method. This method was modified to measure SSA of sieved solids having a specific size in batches of 15 samples per dessicator. Based on monolayer surface coverage and molecular weight of the EGME molecule, SSA was calculated according to the expression:

$$SSA = \frac{W_a}{(0.000286)W_s} \tag{2.6.9}$$

where:
- SSA = specific surface area (m^2/g)
- W_a = measured weight of EGME retained by sample (g)
- W_s = measured weight of dried sample (g)

Three materials of known SSA served as control for the precision and accuracy of the EGME method: research-grade kaolinite, research-grade hectorite and granular activated carbon, GAC. The research-grade kaolinite and hectorite have reported SSA values of 39.5 m^2/g and 461.5 m^2/g, respectively (Carter et al, 1965). The GAC was a F400 with an SSA of 1000-1100 m^2/g (N_2-BET method), a pore volume of 0.85 - 0.95 cm^3/g, an effective size of 0.55 - 0.75 mm and a maximum C_u of 1.9 (Calgon, 1995).

Because of the wide gradation of particle sizes and variation of SSA across the gradation, a measure of total surface area was needed. SSA results were integrated over the PSD to yield a surface area distribution as a function of particle diameter for each event using the following formulation,

$$SA_i = (m_i)(SSA_i) \tag{2.6.10}$$

where:
- SA_i = surface area of solids having particle diameter i (m^2)
- m_i = mass of solids having particle diameter i (g)
- SSA_i = specific surface area of solids having particle diameter i (m^2/g)

2.7 1995 rainfall-runoff events results

Once the experimental sampling facility was completed in March of 1995, five events were captured and analyzed that year. The intent of this work was to determine runoff hydrographs, constituent loading, constituent partitioning, solids fractionation and constituent first flush for the purpose of designing a control strategy which would be effective given the runoff characteristics. This work was also carried out so that loading and flow parameters for bench scale experiments could be chosen. The site hydrology is described for each event by rainfall hyetographs and runoff hydrographs. The hyetographs and hydrographs for each event are plotted in Figure 2.7.1. The hydrographs show lateral pavement sheet flow from the 15 meter long by 20 meter wide pavement watershed.

Time was initialized to zero at the beginning of rainfall. For all events discrete runoff samples were obtained with the exception of the 15 July event which lasted only 20 minutes and generated only 41 L of runoff which was composited as a single sample. Table 2.7.1 presents hydrologic data for each event, including antecedent dry period, runoff and rainfall duration, rainfall depth, runoff volume and indices to describe lateral pavement sheet flow.

Table 2.7.1 Hydrologic indices & pavement residence time data (I-75 site - 300 m^2 drainage area).

Event date (19##) (1)	Previous dry hours (hr.) (2)	Rainfall duration (min.) (3)	Runoff duration (min) (4)	Rain depth (mm) (5)	Runoff volume (L) (6)	"C" (7)	IPRT (min) (8)	APRT (min) (9)	LEMF (L/min-m) (10)	LPF (L/min-m) (11)
8 April 95	120	295	288	25.0	5,439	0.73	8	1.7	1.21	23.7
30 April 95	96	109	100	1.0	211	0.70	10	7.2	0.11	0.6
15 July 95	288	16	11	0.4	41	0.34	10	5.6	0.23	0.6
8 September 95	480	202	207	4.0	401	0.33	13	2.3	0.14	0.7
3 October 95	216	393	386	8.5	1,260	0.49	11	3.3	0.20	16.5

Initial pavement residence time, IPRT is the time from initial rainfall to initial runoff for each event. The IPRT was measured through observation of initiation of rainfall and subsequent initial runoff. The IPRT indicates the time required for rainfall to wet the pavement surface, fill depression storage and overcome airborne re-suspension as a result of traffic wheel suctions. Once these factors were overcome, pavement runoff is generated. Although the IPRT is lowest for the high intensity event of 8 April, in comparing all events IPRT results do not vary by more than a factor of two.

APRT is the average pavement residence time and is a measure of the average time of concentration for each event. APRT was computed by determining the time between each distinct hydrograph centroid and the corresponding hyetograph centroid and then calculating the mean of these times for each event. Comparing all events, the APRT values vary by a factor of four. The lowest APRT value corresponded to the high intensity event of 8 April while the highest APRT value was associated with the low intensity events of 30 April and 15 July.

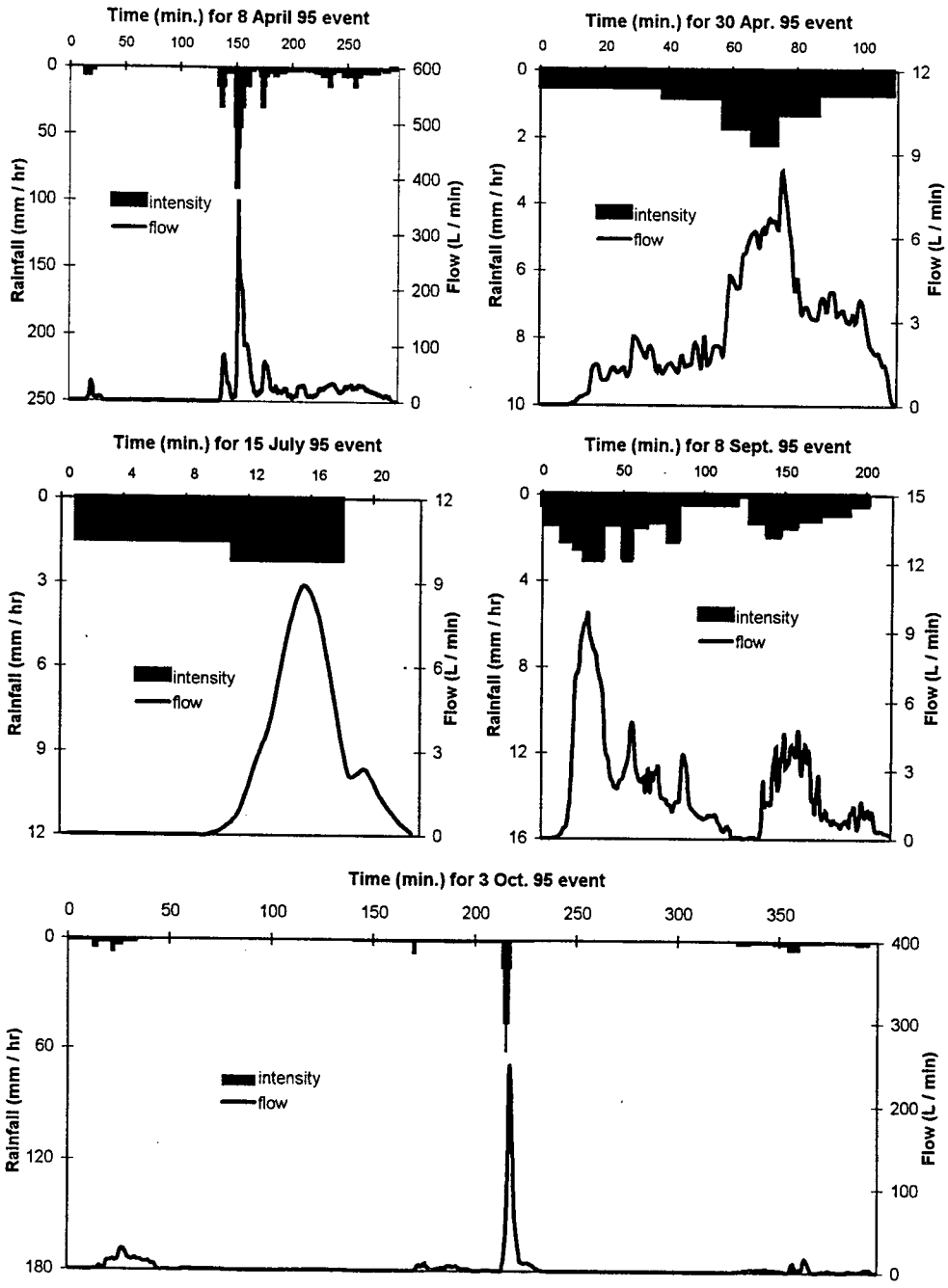

Figure 2.7.1 Hydrographs and hyetographs for 1995 events

Lateral event mean flow (LEMF) is the average flow per unit width of pavement for each event. LEMF was computed by dividing the total runoff volume per meter of pavement width by the runoff duration. Although the LEMF is greatest for the high runoff volume event of 8 April, the LEMF values for all other events did not vary by more than a factor of two. Lateral peak flow (LPF) is the event peak flow per meter of pavement width for drainage from four traveled lanes plus an exit lane (20 meters). The highest LPF values correspond to the high intensity portions of 8 April and 3 October events while the lowest LPF values correspond to the low intensity events of 30 April, 8 September and 15 July. The LPF values for the high intensity events are a factor of 20 or greater than the LPF values of the low intensity events. The peak flow of 370 L/min for the 8 April event was approaching the upper flow capacity of the Parshall flume while the lower flow capacity of the Parshall flume was approximately 2 L/min for the 30 April event.

Partitioning of metal elements and solids

In water, metal elements partition between dissolved and particulate-bound fractions. This partitioning is influenced by pavement residence time, rainfall pH, the nature and quantity of solids present and solubility of the metal element. pH, ORP and conductivity data for each event are presented in Table 2.7.2. Although not reported for these events, alkalinity has been measured for four events in 1996 at this site with EMC $\leq$ 30 mg/L as $CaCO_3$. Metal element partitioning was evaluated using equations (2.6.4), (2.6.5) and (2.6.6). To determine the event mass fraction, incremental values for metal element or solids mass were determined from sample analysis and summed over the entire event using incremental runoff volumes:

$$M_f = \sum c_i v_i \qquad (2.6.11)$$

where: M_f = event mass total of metal element or solids fraction: D,P,TSS,TDS, etc.,
c_i = incremental concentration determined from sample analysis, [M/L^3]
v_i = incremental runoff volume corresponding to c_i, [L^3].

Table 2.7.2 Water quality data from I-75 site.

	pH			ORP (mV)			Conductivity (µS/cm)		
Event date (1995)	Rain[1]	Initial runoff[2]	Final runoff[3]	Rain	Initial runoff	Final runoff	Rain	Initial runoff	Final runoff
8 April 95	4.5	6.4	7.1	----	----	----	----	----	----
30 April 95	4.1	6.3	6.8	----	----	----	----	----	----
15 July 95	3.8	5.8	5.9	----	----	----	----	----	----
8 September 95	3.9	5.6	7.2	320	230	191	----	1397	270
3 October 95	4.2	6.0	6.7	396	212	202	----	984	171

1: Rainfall water quality samples collected from an urban location 3 km from the I-75 site
2: Initial 10 L of runoff
3: Final 10 L of runoff

Metal element mass data are summarized in Table 2.7.3 for each event. For each event a single value of f_d, f_p and K_d was computed from these event totals. Results are presented for Cu, Zn and Cd as well as more particulate-bound metal elements of Al, Fe and Pb in Figure 2.7.2.

Table 2.7.3 Metal element and solids mass data from I-75 site.

Event date	8 April 95	30 April 95	15 July 95	8 September 95	3 October 95
(a) Event dissolved metal fraction mass (mg)					
Zn	1137.0	280.0	564.0	1223.0	1348.0
Cd	15.1	3.9	0.8	0.9	4.0
Cu	73.0	9.3	9.2	41.2	36.5
Ni	26.4	3.3	2.9	14.7	14.9
Pb	70.4	3.0	0.6	6.3	30.8
Cr	51.0	1.3	1.2	2.3	15.7
Mn	332.7	33.9	30.5	95.4	90.9
Fe	235.1	28.9	23.9	81.9	117.2
Al	33.2	4.7	17.7	23.4	288.1
(b) Event dissolved solid fractions (g)					
TDS	235.5	43.9	10.8	132.8	113.3
VDS	135.2	43.1	---	72.3	65.4
(c) Event total metal elements (dissolved + particulate-bound fractions) (mg)					
Zn	2125.0	316.0	590.3	1448.0	2127.0
Cd	29.3	4.6	0.8	2.0	7.4
Cu	235.4	14.8	12.9	66.7	105.0
Ni	46.8	4.8	3.7	33.2	31.6
Pb	334.5	6.6	1.9	35.4	144.2
Cr	191.5	3.0	1.2	5.7	20.9
Mn	654.4	36.9	33.6	135.3	208.6
Fe	18914.0	196.6	191.7	2572.6	6524.5
Al	12098.7	392.3	57.0	650.2	2203.9
(d) Event total solid fractions (suspended + dissolved fractions) (g)					
TS	924.3	61.8	21.4	199.6	285.6
VS	292.1	51.1	---	107.4	130.3

There is an inverse relationship between the dissolved fraction, f_d and the partition coefficient K_d for a given metal element as shown by the following equation, where m = solids concentration as

$$f_d = \frac{1}{1 + K_d\, m} \qquad (2.6.12)$$

TSS, [M/L^3]. Figure 2.7.2 illustrates the inverse relationship between f_d and K_d for the predominately dissolved metals of Cu, Cd and Zn analyzed in stormwater from the I-75 site. For highway sites, reported f_d values ranged from 0.40 to 0.59 for Zn, from 0.40 to 0.75 for Cu, and from 0.10 to 0.24 for Pb (Driscoll et al., 1990; Yousef, 1985). For surface waters, reported K_d values for Zn, Cd, Cu and Pb ranged from 10^4 to 10^5 (L/kg) (Thomann and Mueller, 1987).

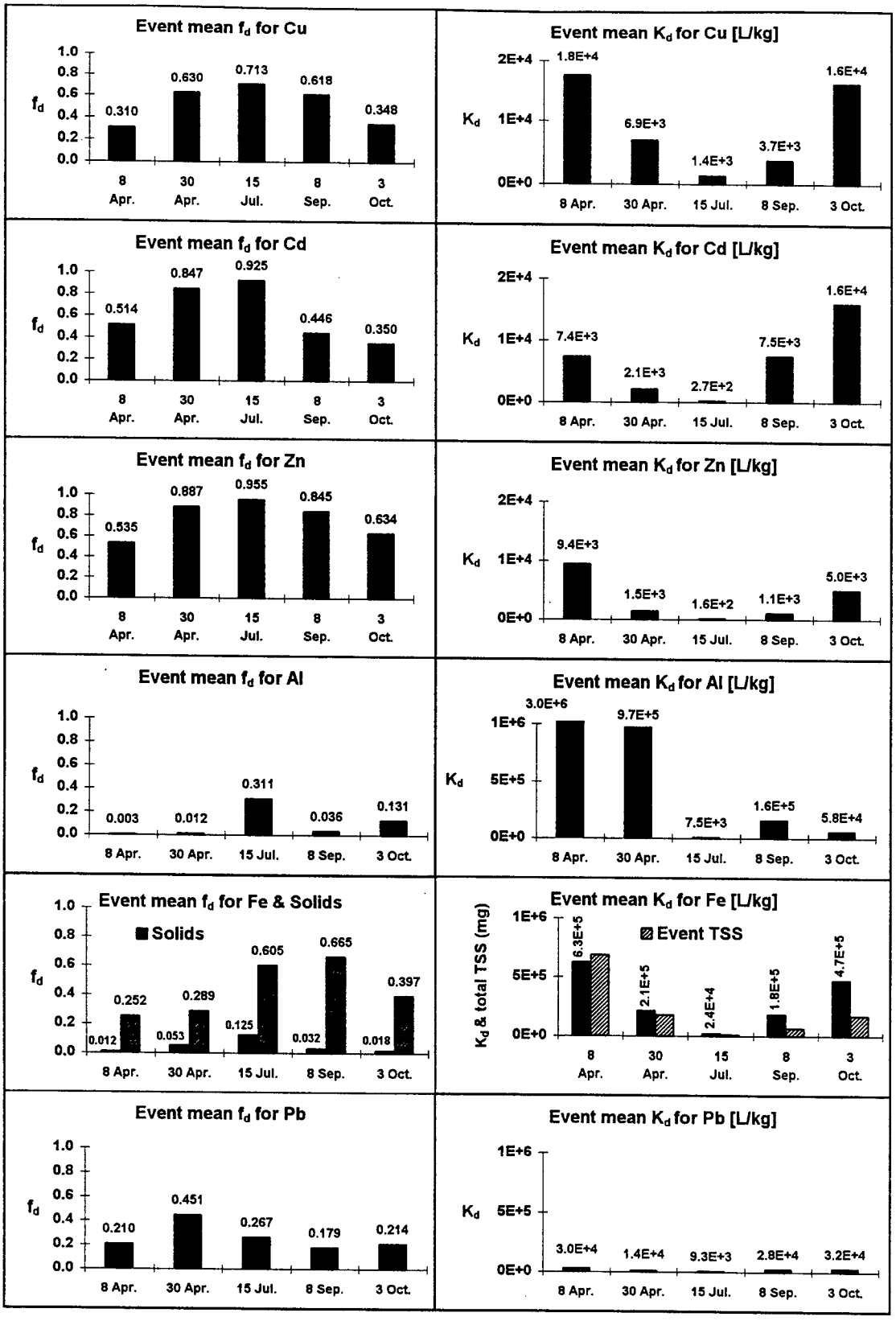

Figure 2.7.2 Event mean f_d and K_d results

The influence of rainfall pH, summarized in Table 2.7.2 and APRT summarized in Table 2.7.1 for each event, can be discerned from the f_d and K_d results presented in Figure 2.7.2. Events where the rainfall pH is lowest and where APRT is highest resulted in significantly larger metal element dissolved fractions. For example, the combination of the lowest rainfall pH (3.8) combined with a relatively long APRT (5.6 min.) resulted in the 15 July event having the highest f_d values for all metal elements except Pb as well as the lowest K_d values for all metals. The influence of APRT on metal element dissolution has been observed by other researchers (Muschack, 1990). The dissolved fraction of total solids follows a trend similar to that of the dissolved fraction of metal elements. This indicates that metal element partitioning in lateral pavement runoff is influenced not only by pH but also by APRT.

Sample holding time

Because partitioning is a dynamic process sample holding time was minimized. To investigate the effect of sample holding time on metal element partitioning, a three liter sample from the 15 July 1995 event was analyzed over a 24 hour period. Time was initialized to zero when samples were collected. Results presented in Figure 2.7.3 indicate that a sample holding time of up to 24 hours had a minor influence on partitioning of metals which were either primarily dissolved (Zn, Mn and Cd) or primarily particulate-bound (Al or Fe). Both dissolved and particulate-bound data were measured separately to generate results, as opposed to measuring f_d and subtracting from 1 to determine f_p.

However, sample holding time is important for metal elements whose partitioning is neither predominately dissolved or predominately particulate-bound. Cu, Pb and to a lesser degree Ni illustrate this point for the 15 July 1995 event. From Table 2.7.3, Cu is 71% dissolved, Pb is 27% dissolved and Ni is 78% dissolved. These values are intermediate to those of Cd and Zn with over 95% dissolved and Fe with 13% dissolved. The variability of the particulate-bound Pb concentrations in Figure 2.7.3 illustrates the difficulty in obtaining aqueous samples with representative solids concentrations as compared to sampling and analyzing the dissolved fraction of a metal element. Flocculation of fine particulate matter observed during the initial 6 to 8 hours of holding time was in part responsible for the difficulty in obtaining representative particulate-bound samples. This difficulty is exhibited by deviations from symmetry between dissolved and particulate-bound curves in each plot of Figure 2.7.3. Cu illustrates reasonably well the symmetry expected as partitioning changes as a function of time between the dissolved and particulate-bound fractions.

First flush of metal elements

The first flush definition from criterion 1 was applied to four events. The 30 April and 8 September storms were grouped and compared as low intensity, low runoff volume events. The 8 April and 3 October storms were grouped and classified as high intensity, high runoff volume events. First-flush evaluations were performed for the dissolved and particulate-bound metal fractions separately as well as for various solid fractions. Zn, Cd, Cu and Pb were used for the analysis of a first flush because Zn and Cd are almost entirely dissolved, Cu is mainly dissolved and Pb is mainly particulate-bound. Additionally, Zn, Cd, and Cu are of interest at this site because, when compared to water quality standards for surface water discharges, their EMCs can exceed such standards as shown in Table 2.7.4. Therefore these metal elements would be primary targets for immobilization by control strategies.

The influence of rainfall pH, summarized in Table 2.7.2 and APRT summarized in Table 2.7.1 for each event, can be discerned from the f_d and K_d results presented in Figure 2.7.2. Events where the rainfall pH is lowest and where APRT is highest resulted in significantly larger metal element dissolved fractions. For example, the combination of the lowest rainfall pH (3.8) combined with a relatively long APRT (5.6 min.) resulted in the 15 July event having the highest f_d values for all metal elements except Pb as well as the lowest K_d values for all metals. The influence of APRT on metal element dissolution has been observed by other researchers (Muschack, 1990). The dissolved fraction of total solids follows a trend similar to that of the dissolved fraction of metal elements. This indicates that metal element partitioning in lateral pavement runoff is influenced not only by pH but also by APRT.

Sample holding time

Because partitioning is a dynamic process sample holding time was minimized. To investigate the effect of sample holding time on metal element partitioning, a three liter sample from the 15 July 1995 event was analyzed over a 24 hour period. Time was initialized to zero when samples were collected. Results presented in Figure 2.7.3 indicate that a sample holding time of up to 24 hours had a minor influence on partitioning of metals which were either primarily dissolved (Zn, Mn and Cd) or primarily particulate-bound (Al or Fe). Both dissolved and particulate-bound data were measured separately to generate results, as opposed to measuring f_d and subtracting from 1 to determine f_p.

However, sample holding time is important for metal elements whose partitioning is neither predominately dissolved or predominately particulate-bound. Cu, Pb and to a lesser degree Ni illustrate this point for the 15 July 1995 event. From Table 2.7.3, Cu is 71% dissolved, Pb is 27% dissolved and Ni is 78% dissolved. These values are intermediate to those of Cd and Zn with over 95% dissolved and Fe with 13% dissolved. The variability of the particulate-bound Pb concentrations in Figure 2.7.3 illustrates the difficulty in obtaining aqueous samples with representative solids concentrations as compared to sampling and analyzing the dissolved fraction of a metal element. Flocculation of fine particulate matter observed during the initial 6 to 8 hours of holding time was in part responsible for the difficulty in obtaining representative particulate-bound samples. This difficulty is exhibited by deviations from symmetry between dissolved and particulate-bound curves in each plot of Figure 2.7.3. Cu illustrates reasonably well the symmetry expected as partitioning changes as a function of time between the dissolved and particulate-bound fractions.

First flush of metal elements

The first flush definition from criterion 1 was applied to four events. The 30 April and 8 September storms were grouped and compared as low intensity, low runoff volume events. The 8 April and 3 October storms were grouped and classified as high intensity, high runoff volume events. First-flush evaluations were performed for the dissolved and particulate-bound metal fractions separately as well as for various solid fractions. Zn, Cd, Cu and Pb were used for the analysis of a first flush because Zn and Cd are almost entirely dissolved, Cu is mainly dissolved and Pb is mainly particulate-bound. Additionally, Zn, Cd, and Cu are of interest at this site because, when compared to water quality standards for surface water discharges, their EMCs can exceed such standards as shown in Table 2.7.4. Therefore these metal elements would be primary targets for immobilization by control strategies.

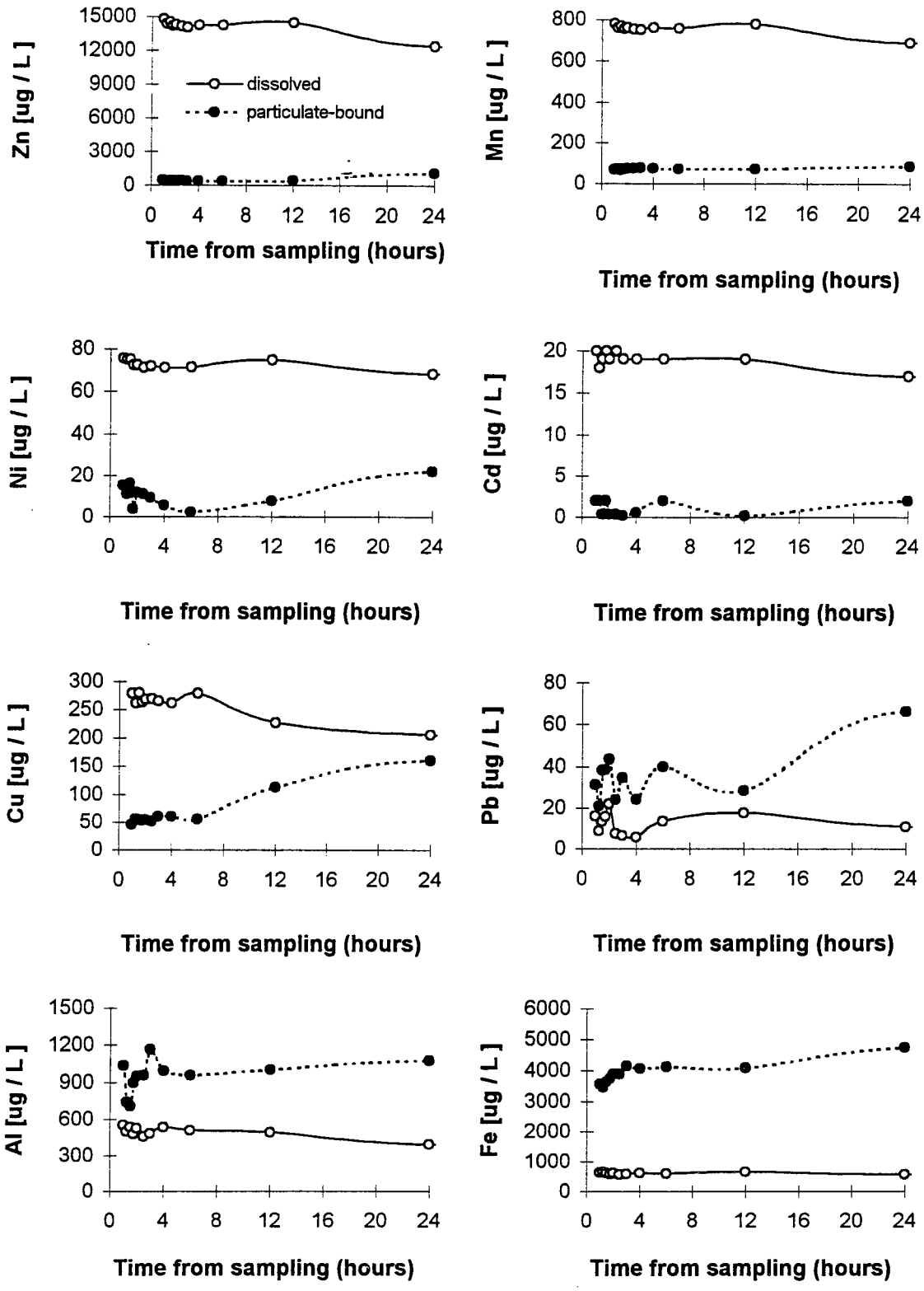

Figure 2.7.3 Comparison of time-dependent metal element partitioning for 15 July 1995 event.

Table 2.7.4 I-75 event mean concentration (EMC) data versus EPA discharge criteria.

	Cincinnati, OH					Milwaukee, WI			
Event date	8 Apr. 95	30 Apr. 95	15 Jul. 95	8 Sept. 95	3 Oct. 95	I-94	I-794	Highway 45	EPA criteria
Total (dissolved + particulate-bound) EMC (µg/L)									
Zn	459	628	15244	2612	1427	465	336	371	120.0
Cd	5	6	11	5	8	11	32	29	5.6
Cu	43	70	325	166	71	155	88	75	18.0
Pb	62	31	44	88	97	817	1457	738	82.0
Ni	9	23	91	83	11	no data	no data	no data	1700.0
Cr	35	14	29	14	14	no data	no data	no data	1400.0
Mn	120	175	820	337	166	no data	no data	no data	none
Fe	3477	932	4676	6415	5178	no data	no data	no data	none
Al	2224	1859	270	1621	5496	no data	no data	no data	none
Hardness	52	70	92	68	56	no data	no data	no data	none
Dissolved EMC (µg/L)									
Zn	209.0	1322.0	14786.0	3051.0	904.0	no data	no data	no data	110.0
Cd	2.0	4.0	9.0	2.0	3.0	no data	no data	no data	3.7
Cu	13.0	44.0	279.0	103.0	25.0	no data	no data	no data	17.0
Pb	13.0	14.0	16.0	16.0	21.0	no data	no data	no data	65.0
Ni	5.0	16.0	76.0	37.0	10.0	no data	no data	no data	1400.0
Cr	9.0	6.0	28.0	6.0	10.5	no data	no data	no data	550.0
Mn	61.0	161.0	744.0	238.0	72.0	no data	no data	no data	none
Fe	43.0	137.0	583.0	204.0	93.0	no data	no data	no data	none
Al	6.0	22.0	84.0	58.0	229.0	no data	no data	no data	none
Selected site characteristics									
# of events	1	1	1	1	1	107	35	29	
ADT/1000	150	150	150	150	150	116	53	85	
Pavm.	asphalt	asphalt	asphalt	asphalt	asphalt	asphalt	concrete	concrete	

: Total metal element discharge criteria are OEPA discharge to modified warmwater criteria.
: Dissolved metal element discharge criteria are USEPA discharge criteria.
: Milwaukee data from Federal Highway Administration (Driscoll et al, 1990) collect from 1976-1981 as EMCs.

Normalized metal element mass and flow volume were plotted as a function of dimensionless time, based on the duration of runoff for each event. A first flush occurs when the metal element mass curve is positioned above the flow volume curve. The ratio of metal element mass curve area to the flow volume curve area is a measure of the strength of the first flush for the event. These area ratios and the actual areas under each curve are tabulated at the bottom of Figure 2.7.4, 2.7.5 and 2.7.6. The slope of the metal element mass curve indicates the rate at which the metal element is mobilized. For the 30 April and 8 September events the dissolved fraction of Cd, Zn and Cu exhibit a pronounced first flush whereas Pb exhibits a weak first flush. For both low intensity, low volume events the relative strength of the dissolved fraction first flush is Cd > Zn > Cu > Pb > runoff volume.

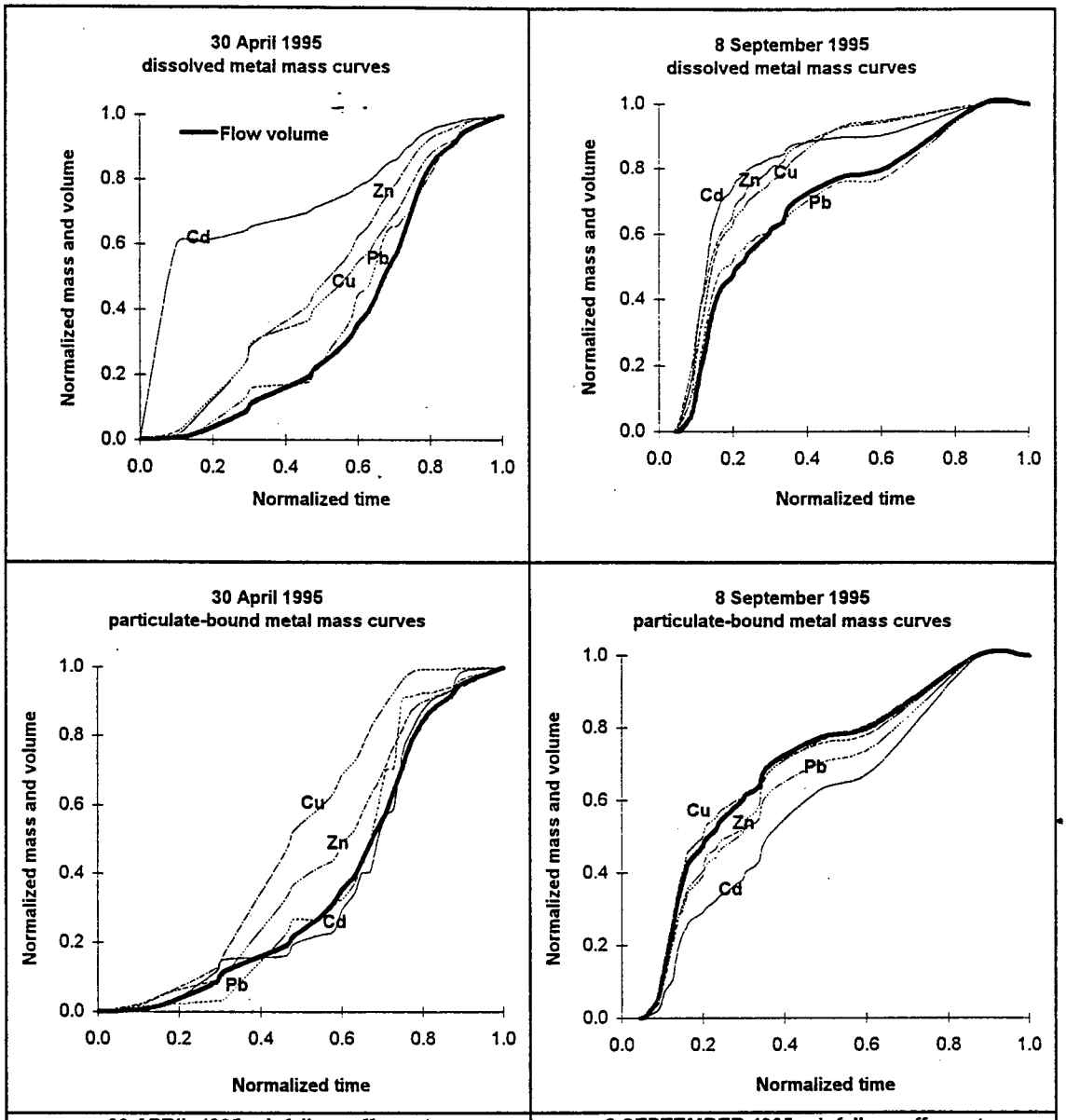

30 APRIL 1995 rainfall runoff event					8 SEPTEMBER 1995 rainfall runoff event				
Curve	*dissolved*		*particulate-bound*		Curve	*dissolved*		*particulate-bound*	
	curve area	area ratio	curve area	area ratio		curve area	area ratio	curve area	area ratio
Volume	0.4611	1.0000	0.4611	1.0000	**Volume**	0.4399	1.0000	0.4399	1.0000
Zn	0.6118	1.3269	0.5407	1.1726	**Zn**	0.5899	1.3411	0.3983	0.9055
Cd	0.7677	1.6650	0.4516	0.9795	**Cd**	0.6253	1.4215	0.3005	0.6832
Cu	0.5634	1.2219	0.6523	1.4148	**Cu**	0.5587	1.2703	0.4544	1.0331
Pb	0.4911	1.0652	0.4914	1.0658	**Pb**	0.4629	1.0523	0.3805	0.8651

Figure 2.7.4 Mass and flow curves for low intensity, low flow events. Area under each curve and the ratios of metal to flow volume are tabulated.

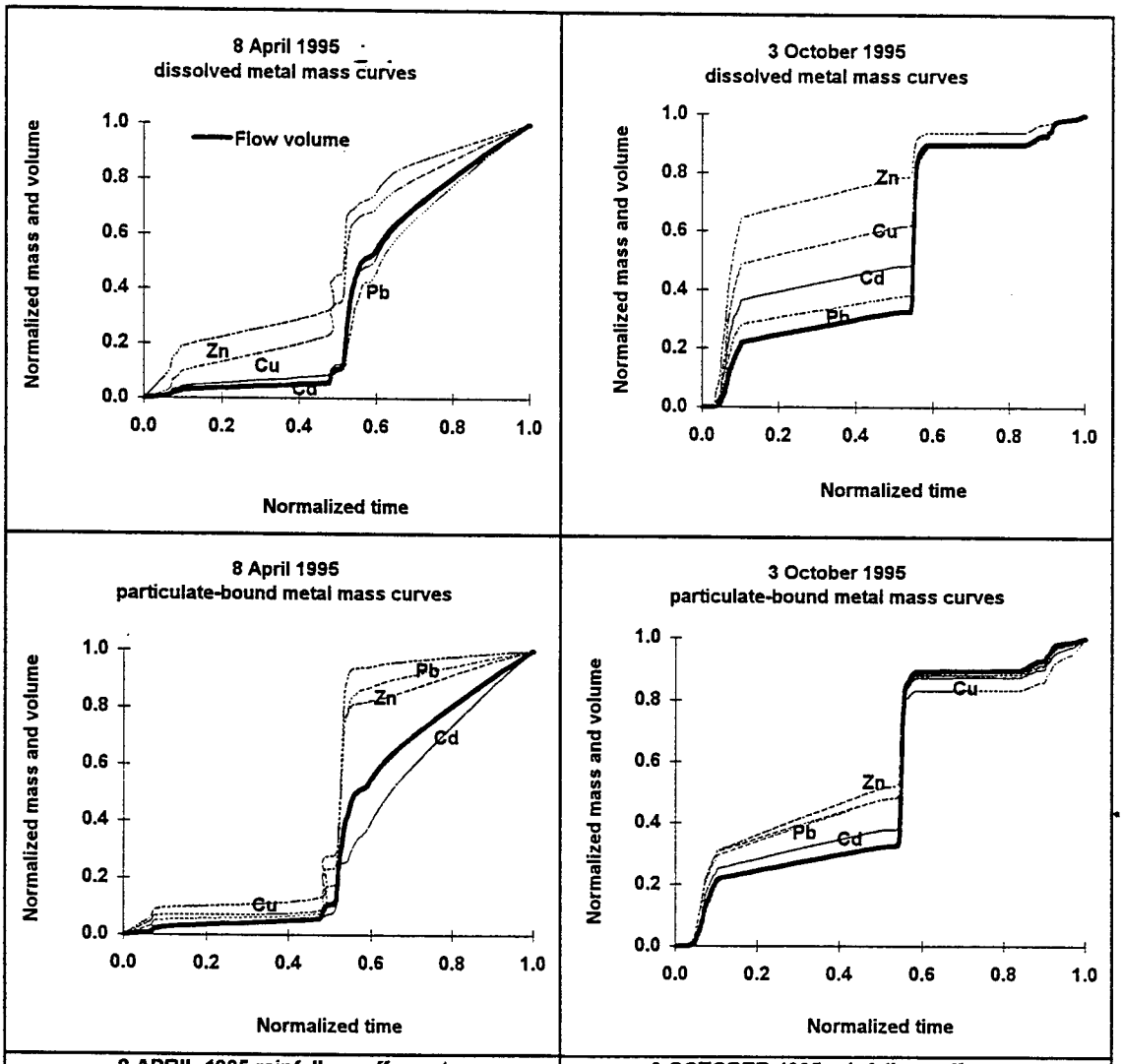

8 APRIL 1995 rainfall runoff event					3 OCTOBER 1995 rainfall runoff event				
Curve	*dissolved*		*particulate-bound*		Curve	*dissolved*		*particulate-bound*	
	curve area	area ratio	curve area	area ratio		curve area	area ratio	curve area	area ratio
Volume	0.27473	1.0000	0.27473	1.0000	**Volume**	0.55977	1.0000	0.55977	1.0000
Zn	0.49746	1.8107	0.43894	1.5977	**Zn**	0.70770	1.2643	0.59218	1.0579
Cd	0.27114	0.9869	0.20701	0.7535	**Cd**	0.60902	1.0880	0.56177	1.0036
Cu	0.42715	1.5548	0.50191	1.8269	**Cu**	0.63658	1.1372	0.56326	1.0062
Pb	0.23163	0.8431	0.43257	1.5745	**Pb**	0.57620	1.0294	0.58442	1.0440

Figure 2.7.5 Mass and flow curves for high intensity, high flow events. Area under each curve and the ratios of metal to flow volume are tabulated.

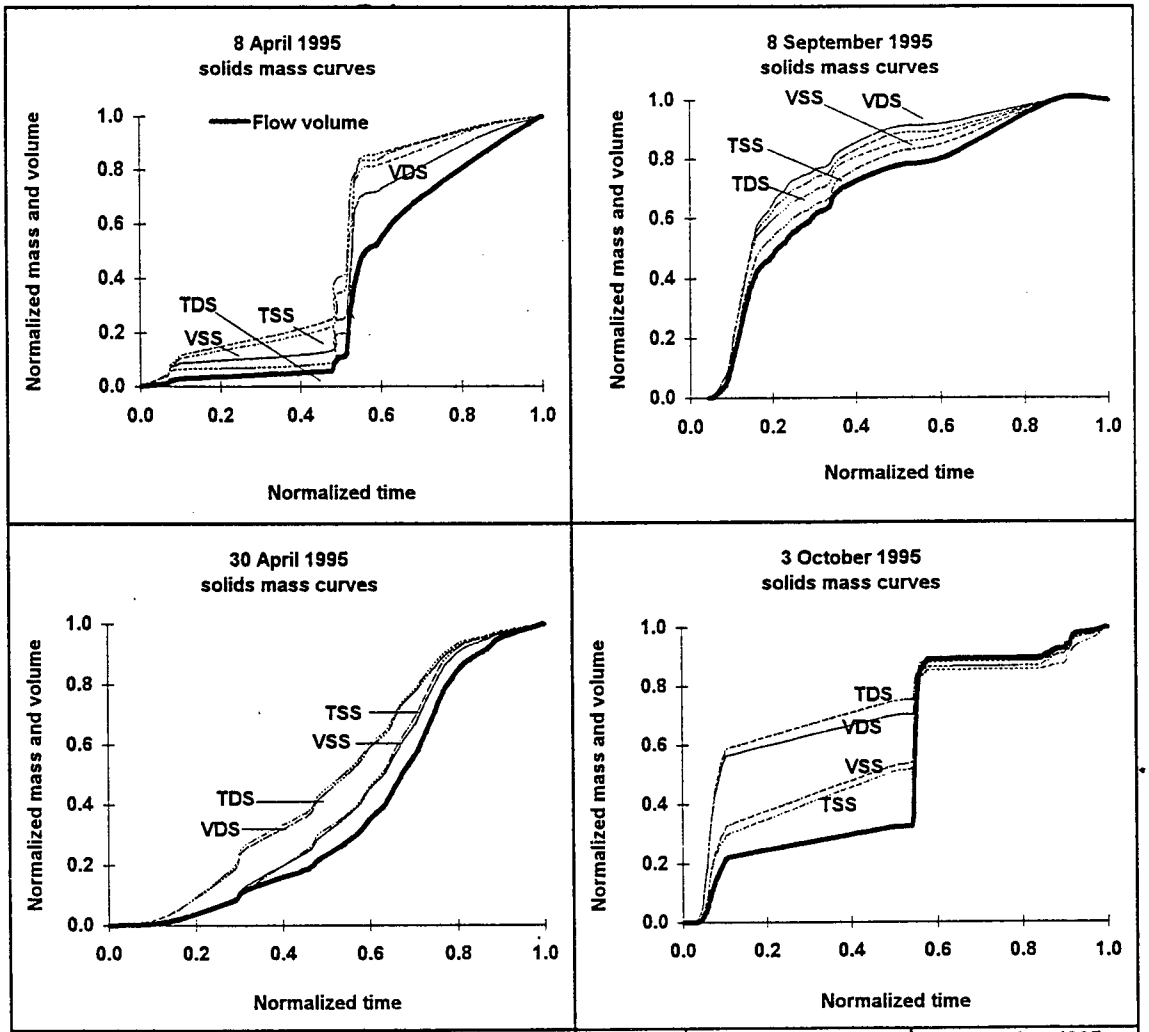

Curve	8 April 1995 curve area	8 April 1995 area ratio	30 April 1995 curve area	30 April 1995 area ratio
Volume	0.2747	1.0000	0.4611	1.6783
TSS	0.4780	1.7400	0.6020	2.1912
VSS	0.5102	1.8570	0.5938	2.1614
TDS	0.4380	1.5941	0.5305	1.9309
VDS	0.4063	1.4790	0.5201	1.8931

Curve	8 September 1995 curve area	8 September 1995 area ratio	3 October 1995 curve area	3 October 1995 area ratio
Volume	0.4399	1.0000	0.5598	1.0000
TSS	0.5174	1.1763	0.5746	1.0264
VSS	0.4749	1.0796	0.5934	1.0600
TDS	0.5381	1.2234	0.6575	1.1746
VDS	0.5536	1.2585	0.6627	1.1839

Figure 2.7.6 Solids fractions mass and flow curves for all events. Area under curve and the ratios of metal to flow volume are tabulated.

The results for the particulate-bound fraction are different. For the 30 April event the relative strength of the particulate-bound fraction first flush is Cu > Zn > Pb > runoff volume > Cd. Particulate-bound Cd did not exhibit a first flush. For the 8 September event the relative strength of the particulate-bound fraction first flush is Cu > runoff volume > Zn > Pb > Cd. Particulate-bound Zn, Pb and Cd did not exhibit a first flush for the 8 September event. The 8 September 1995 event demonstrates a distinct first-flush for dissolved Cd, Zn and Cu. The results for the 8 April and 3 October events are presented in Figure 2.7.5 for the high intensity, high volume events. For both events the dissolved fraction of Zn and Cu exhibit a strong first flush whereas dissolved Pb and Cd exhibits a poor first flush. The strength of the first flush for dissolved Zn and Cu is greater than both low intensity, low volume events of Figure 2.7.5. The strength of the first flush for particulate-bound Zn and Cu is greater than for the 30 April event yet weaker than the 8 September first flush for these particulate-bound metals. Washoff of both fractions during the event results in several clear trends.

While dissolved Zn and Cu exhibit a strong first flush during the initial portion of the 8 April event, all particulate-bound metal elements exhibit a weak first flush during this time. However during the latter half of the event the high intensity of runoff mobilizes both fractions of Zn and Cu and the particulate-bound fraction of Pb. The 3 October event resulted in a strong first flush for all dissolved metal elements except Pb during the first half of the event. Although the particulate-bound fraction exhibited a first flush for all metals, during the first half of the 3 October event, albeit a weaker first flush, there was no first flush during the latter half of the event.

First flush of solids

Figure 2.7.6 presents mass curves for various solids fractions for all events. Surprisingly all solids fractions exhibit a first flush except during the latter half of the 3 October event. TDS and VDS generally exhibit a stronger and more rapid first flush than do TSS and VSS. First flush behavior of TDS and VDS are similar as is the behavior of TSS and VSS. This can be seen clearly for the 3 October and 30 April events. This response may indicate that much of the dissolved and particulate-bound metal element load as well as the solids fraction loads have been exhausted.

EPA surface water discharge criteria

EMC values for the dissolved and particulate-bound fractions were calculated for each metal element, total dissolved mass and particulate-bound mass. Table 3.6.4 compares the EMC values to USEPA criteria, OEPA criteria and to EMC values for other highway sites. The Milwaukee sites were chosen for comparison because they have an urban setting, a similar and comparable traffic volumes. There are two separate results which stand out when comparing the Cincinnati site to the Milwaukee sites. First, the Milwaukee data were collected in the late 1970s and early 1980s as leaded gasolines were being phased out. The significantly lower EMC values for lead in 1995 at the Cincinnati site illustrate the effect of this source reduction. Second, 1995 Zn EMC values for Cincinnati are significantly higher than 1979 Zn values for Milwaukee. The additional source(s) of zinc are not as easily identified. Certainly, the increased use of galvanized and corrosion resistant automobile parts, containing a plating which includes zinc and use of zinc in the manufacture of tires contributes to increased zinc loadings. Additionally, during rain events acidic runoff is onto exposed galvanized vehicular parts potentially generating higher levels of Zn.

In addition to Cd, Cu, Zn, Pb and Fe, analyses for both Ni and Mn were also carried out. Ni was chosen because traffic related activities are a source of Ni and there are discharge criteria established at both the state and federal level. There are no discharge criteria established for either dissolved or total Mn. However, traffic related activities are a source of Mn. Mn and Fe were measured in dissolved and particulate-bound form because both Fe and Mn oxides, whether in solution or bound to solids, have a very high affinity for metal elements. The measurements of these metals may allow a more rigorous analysis of why selected metal elements partition to various solid fractions and sizes.

USEPA discharge criteria are based on the dissolved fraction mass of a metal element while OEPA criteria are based on total extractable metal mass. USEPA and OEPA criteria are based on discharge to modified warmwater surface waters because the Mill Creek, as the receiving water body, fits this category. Results presented in Table 3.6.4 indicate that Zn, Cu and Cd, exceed USEPA and OEPA water quality criteria on an event mean basis for most storms. Pb and Ni do not exceed discharge criteria for either the total or dissolved fractions.

2.8 Discussion and implications of 1995 results

Results from analysis of urban roadway stormwater washoff from a heavily traveled highway site in Cincinnati during 1995 indicate that metal elements in lateral pavement sheet flow can be predominately dissolved. Examples include Zn, Cd and Cu as well as Ni and Mn. Low rainfall pH and average pavement residence time (APRT) appear to have a significant influence on metal dissolution. Even though the pH increases, asphalt pavement does not provide a significant level of alkalinity to neutralize low pH rainfall. The relatively low hardness values from Table 2.7.4 provide an indication of this. The use of concrete pavement would provide the necessary alkalinity to sufficiently raise the runoff pH and alter the metal element partitioning.

Figure 2.7.3 indicates that sample holding time can influence the partitioning of certain metal elements, especially Cu, Pb and Ni, metal elements which have been traditionally monitored in urban and roadway runoff. However, most monitoring programs, including the previous FHWA work reported in this paper, set up sampling systems where samples may not have been retrieved and subsequently fractionated within 24 hours. Additionally, most monitoring programs required under NPDES Stormwater Permitting collect samples from storm sewer junctions or sewer outfalls where residence times and mixing has occurred as compared to lateral pavement sheet flow. The choice of sampling bottle material can also affect the dissolved concentration of a sample. For dissolved metals, polypropylene is preferred over HDPE which is preferred over glass.

Metal elements which are primarily particulate-bound include Pb, Fe and Al as well as Cr. Of the predominately dissolved metal elements, Zn, Cd and Cu exceed surface water discharge concentration limits for the adjacent receiving waters. Metal elements which exceed surface water criteria are those which are predominately dissolved in lateral pavement sheet flow. This is a major concern because dissolved metal elements are readily bioavailable and very mobile. Therefore any control strategy intended to effectively immobilize these metals must provide for adsorption, ion-exchange or precipitation in addition to a mechanism to trap particulate-bound metal elements. A

pronounced first flush for pavement sheet flow occurs for all events for dissolved Zn and Cu but not for Pb. The first flush for the particulate-bound fractions of these metals was not well defined.

A first flush occurred for all events for all solids fractions. As with the metal elements, the solids first flush behavior varied depending whether or not the solids fraction was dissolved or suspended. The characterization of metal element partitioning, mass loadings and association with solids for each rainfall runoff event provides a basis for evaluation of annual loadings from an urban highway site. Such information can be helpful in selecting strategies for controlling the quality of urban runoff. Results also provide estimates of design loadings and long-term capacity for which the efficacy of a partial exfiltration trench can be evaluated.

2.9 1996-1997 rainfall-runoff events results

These events were collected during the time the bench-scale PET and prototype PET were being tested. Analysis of these events continued to collect metal element data while more emphasis was placed on the physical characteristics of solids and the influence of traffic counts. Specific characterization objectives for these events were presented in Section 2.3 and the methodology presented in Section 2.6. Of the eight events analyzed in 1996 and 1997, the last four events served the dual purpose of providing loading to the prototype PET installed at the experimental site. Results of these four events in relationship to the prototype PET performance will be presented in the chapter on the prototype PET.

Washoff of Solid Fractions and Particle Counts

Flow rate is a critical variable for the transport of heterogeneous material. Consequently, the delivery of solids fractions was very dependent on flow and traffic intensity/duration. Hydrologic, sheet flow residence time and runoff volume coefficient "C" data for the 1996 - 1997 events are summarized in Table 2.9.1. Solid fraction mass and corresponding EMCs are summarized in Table 2.9.2. The hydrologic loading and solids response for 21 May and 18 June events are plotted in Figure 2.9.1, 7 July and 8 August plotted in Figure 2.9.2, 17 October and 25 November plotted in Figure 2.9.3, 16 December and 12 June are plotted in Figure 2.9.4. Events are classified based on event lateral peak flow (LPF) summarized in Table 2.9.1. The 21 May, 25 November and 16 December are low flow rate events (LPF $<$ 1 L/min-m); 17 October and 12 June are moderate flow rate events and 18 June, 7 July and 8 August are high flow rate events (LPF $>$ 10 L/min-m). The low flow events had two distinct runoff hydrographs separated by a period of no flow, during which the pavement surface dried. These events were also grouped based on low or high runoff volume and plotted as cumulative mass fractions versus cumulative runoff volume in Figure 2.9.5. Event and traffic data are shown in the table at the bottom of Figure 2.9.5.

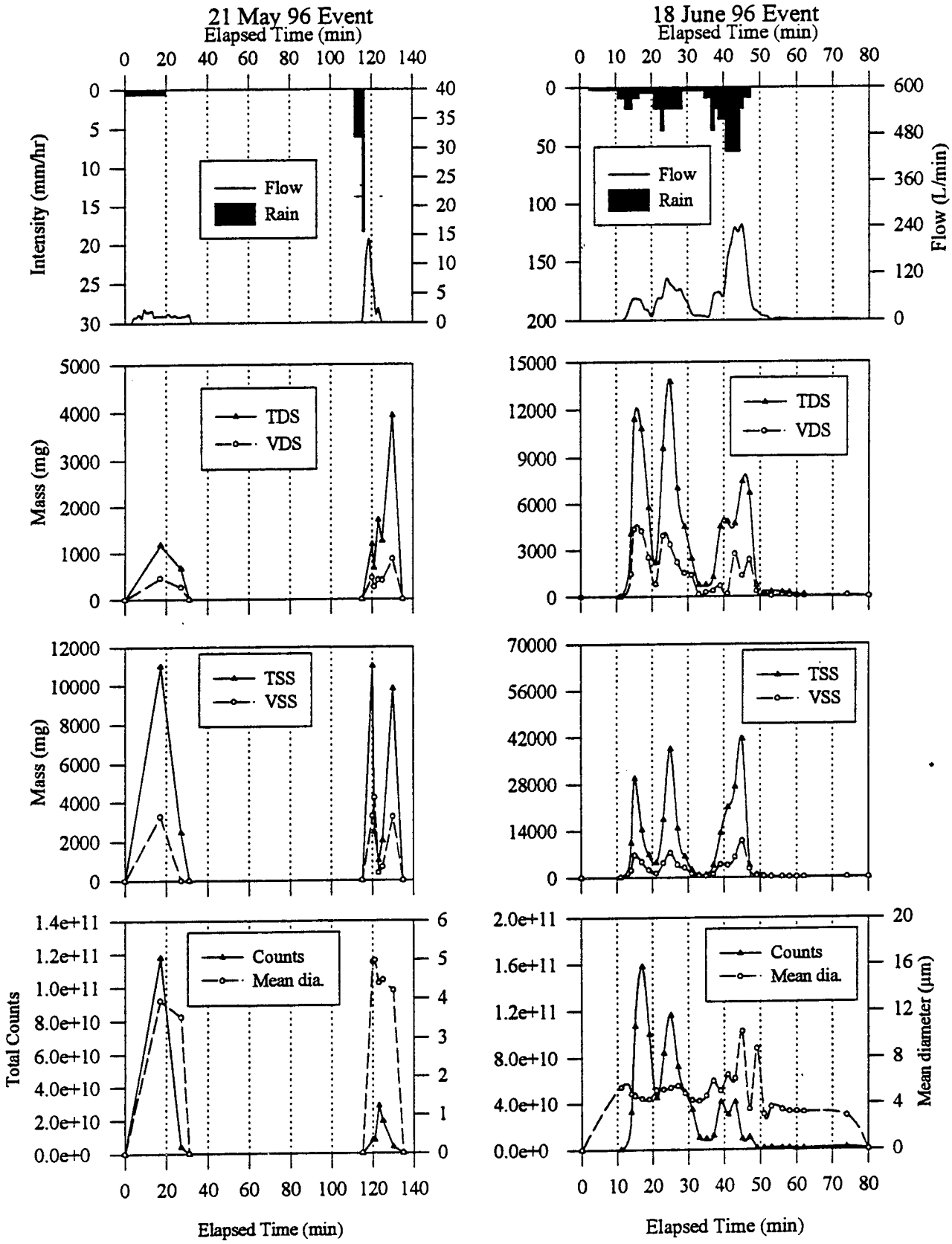

Figure 2.9.1 Hydrologic loading with solids and particle response for 21 May and 18 June events.

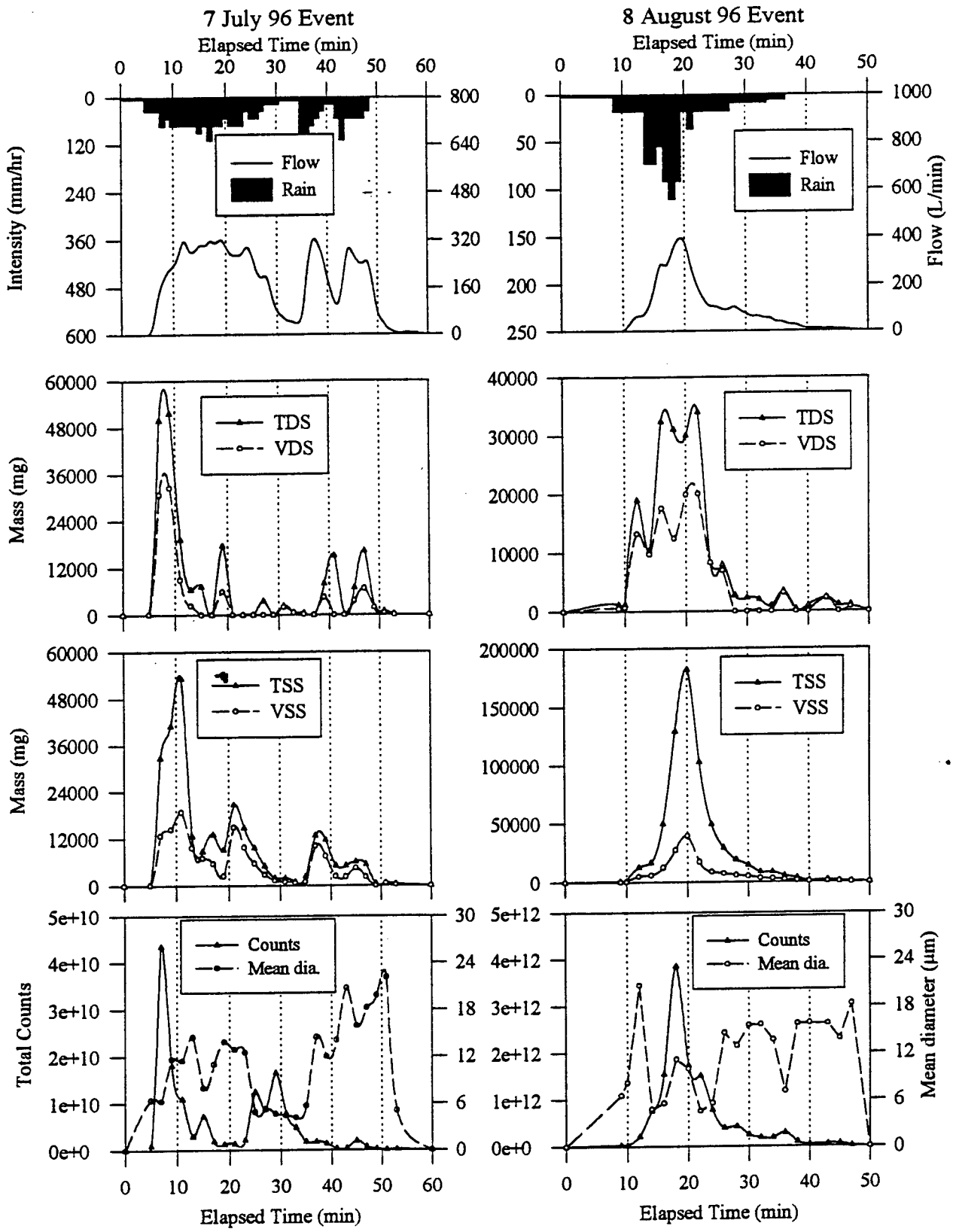

Figure 2.9.2 Hydrologic loading with solids and particle response for 7 July and 8 August events.

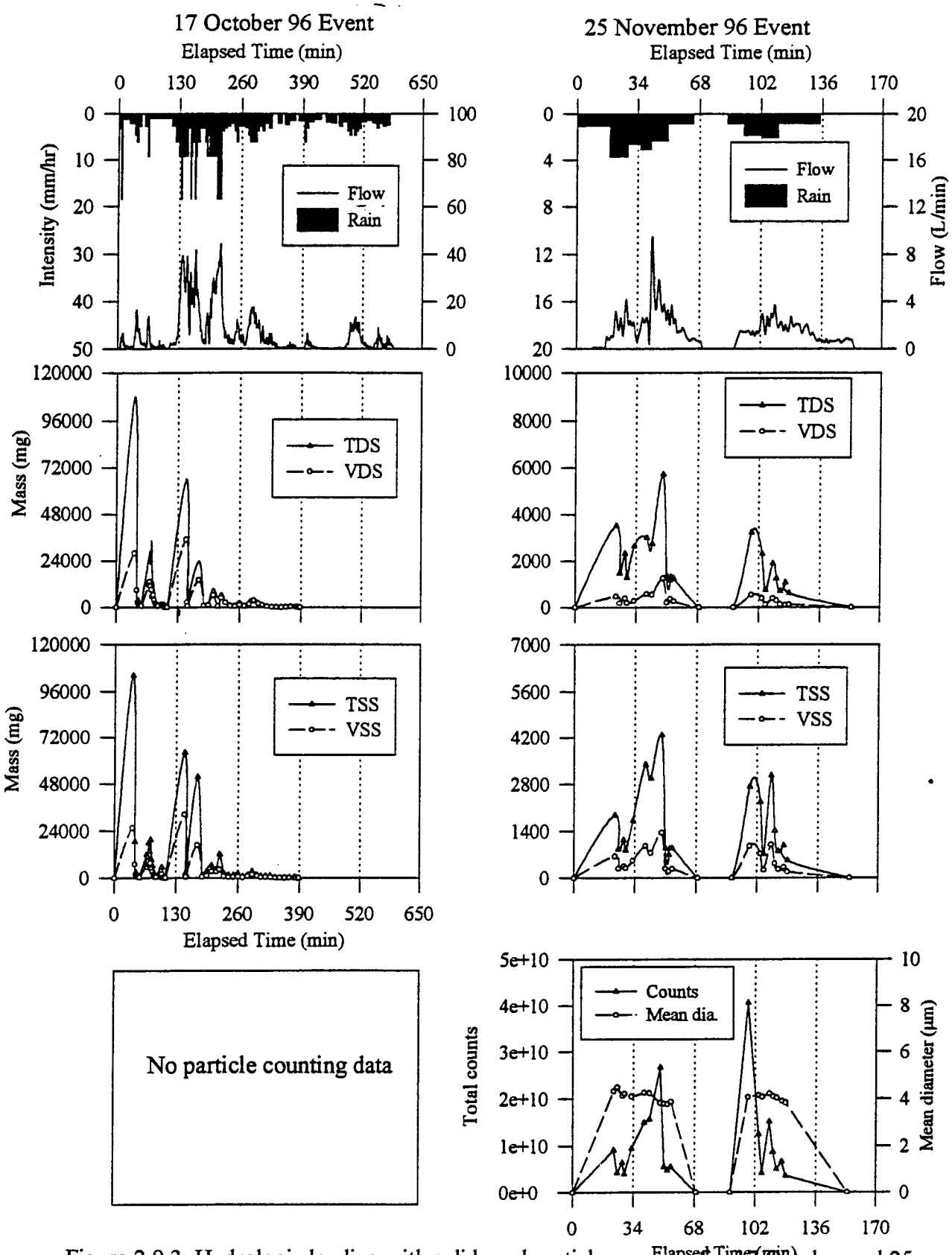

Figure 2.9.3 Hydrologic loading with solids and particle response for 17 October and 25 November events.

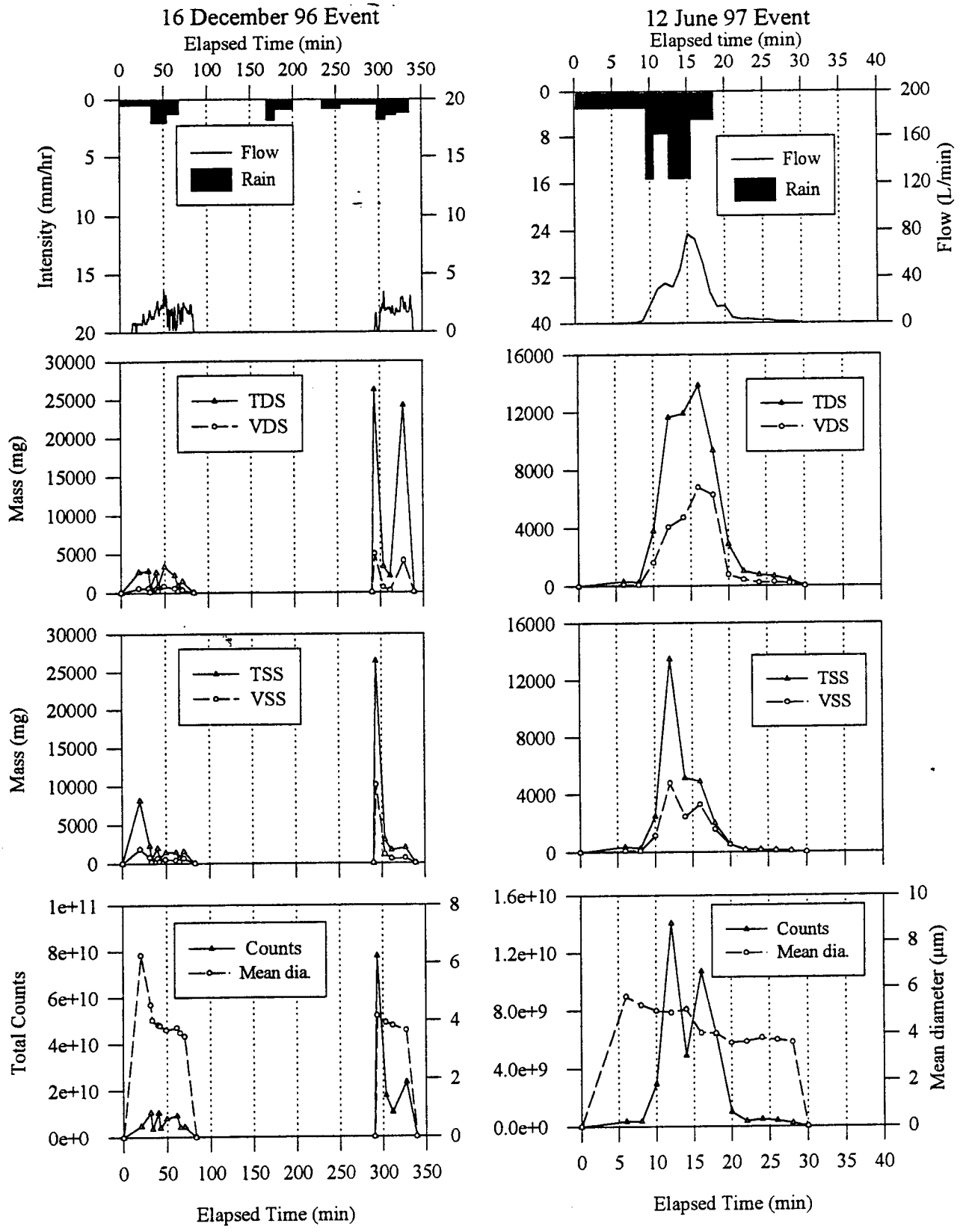

Figure 2.9.4 Hydrologic loading with solids and particle response for 16 December and 12 June.

Table 2.9.1 Hydrologic indices & pavement residence time data (I-75 site-300 m^2 drainage area).

Event date (19##) (1)	Previous dry hours (hr.) (2)	Rainfall duration (min.) (3)	Runoff duration (min) (4)	Rain depth (mm) (5)	Runoff volume (L) (6)	"C" (7)	IPRT (min) (8)	APRT (min) (9)	LEMF (L/min-m) (10)	LPF (L/min-m) (11)
21 May 96	128	35	22	1.0	96.5	0.35	4	6	0.051	0.922
18 June 96	73	63	76	11.3	2779	0.82	5	2	2.29	16.3
7 July 96	117	50	60	40.4	9643	0.79	4	1.5	11.08	21.50
8 August 96	216	51	52	14.1	3877	0.91	7	3	4.32	26.1
17 October 96	182	616	609	29.1	3693	0.42	5	7	0.40	2.95
25 November 96	93	150	146	3.1	216	0.23	10	8	0.09	0.61
16 December 96	96	340	324	3.4	269	0.26	14	15	0.10	0.24
12 June 97	90	20	24	2.0	464.1	0.76	3	5.2	0.52	5.14

Table 2.9.2 Summary of solid fractions total mass, EMCs and runoff water quality parameters.

Event date (19##) (1)	TSS mass (gm.) (2)	VSS mass (gm.) (3)	TDS mass (gm.) (4)	VDS mass (gm.) (6)	TSS EMC [mg/L] (7)	VSS EMC [mg/L] (8)	TDS EMC [mg/L] (9)	VDS EMC [mg/L] (10)	COD EMC [mg/L] (11)	pH EMC (12)	ORP EMC (mV) (13)
21 May 96	13.9	3.8	32.6	15.1	142.3	38.3	333.2	154.5	----	6.86	+161
18 June 96	257.6	66.1	104.8	34.8	93.1	24.2	38.4	13.1	218	7.50	+232
7 July 96	275.6	137.7	210.5	121.6	28.6	14.3	21.8	12.6	115	6.20	+265
8 August 96	637.5	147.1	166.8	148.3	164.7	38.0	43.1	38.3	243	7.29	+197
17 October 96	39.7	12.6	47.5	8.4	177.1	56.0	212.3	37.4	270	7.12	+207
25 November 96	400.5	156.9	454.1	192.1	107.0	42.3	120.8	51.3	332	7.56	+180
16 December 96	37.9	12.7	59.6	11.1	141.0	47.3	221.9	42.4	238	7.54	+158
12 June 97	32.9	15.1	60.2	26.7	71.7	32.8	131.3	58.3	192	6.70	+267

Figures 2.9.1 through 2.9.4 show the delivery of solid fractions, particle counts and sizes in response to the intensity and duration of lateral pavement sheet flow. Although the response varies as a result of traffic levels, previous dry days and runoff volume, these figures demonstrate the pattern of delivery is driven by runoff intensity and duration. In Figure 2.9.5, where events are grouped based on runoff volume, the influence of traffic measured as vehicles during runoff, previous dry hours and runoff duration can be discerned. The low runoff volume events generally have large vehicle to runoff volume ratios, except for the 12 June event. The slope of both the suspended and dissolved curves indicates mass is still available for delivery. Washoff of suspended and dissolved solids from these events is flow limited, with the exception of the suspended solids fraction for 12 June. A flow limited condition is a function of the low runoff volumes and the concurrent high traffic levels as summarized in the table with Figure 2.9.5.

In contrast to the low runoff volume events, the high runoff volume events generally have low vehicle to runoff volume ratios. The flat slope of both the suspended and dissolved curves indicates little remaining mass is available for delivery. Washoff of suspended and dissolved solids from these events is mass limited. The influence of previous dry hours can also be demonstrated from these results. For example, the 18 June 1996 event had the highest vehicle to runoff volume ratios for high volume events. However, it had the lowest previous dry hours and, therefore, the slopes of the suspended and dissolved curves quickly turned flat indicating mass limitations.

For the low flow intensity events, particle counts appear more influenced by traffic intensity and dry period between hydrographs than by flow intensity. Particle mean diameter was strongly influenced by flow intensity. Particle counts, dominated by particles smaller than 8 mm were rapidly washed from the pavement during high flow events as shown in Figure 2.9.6. During short duration events with high flows, particles were not replenished at a sufficient rate, generating a mass limited condition. Particle mean diameter was influenced by flow intensity for all high intensity events.

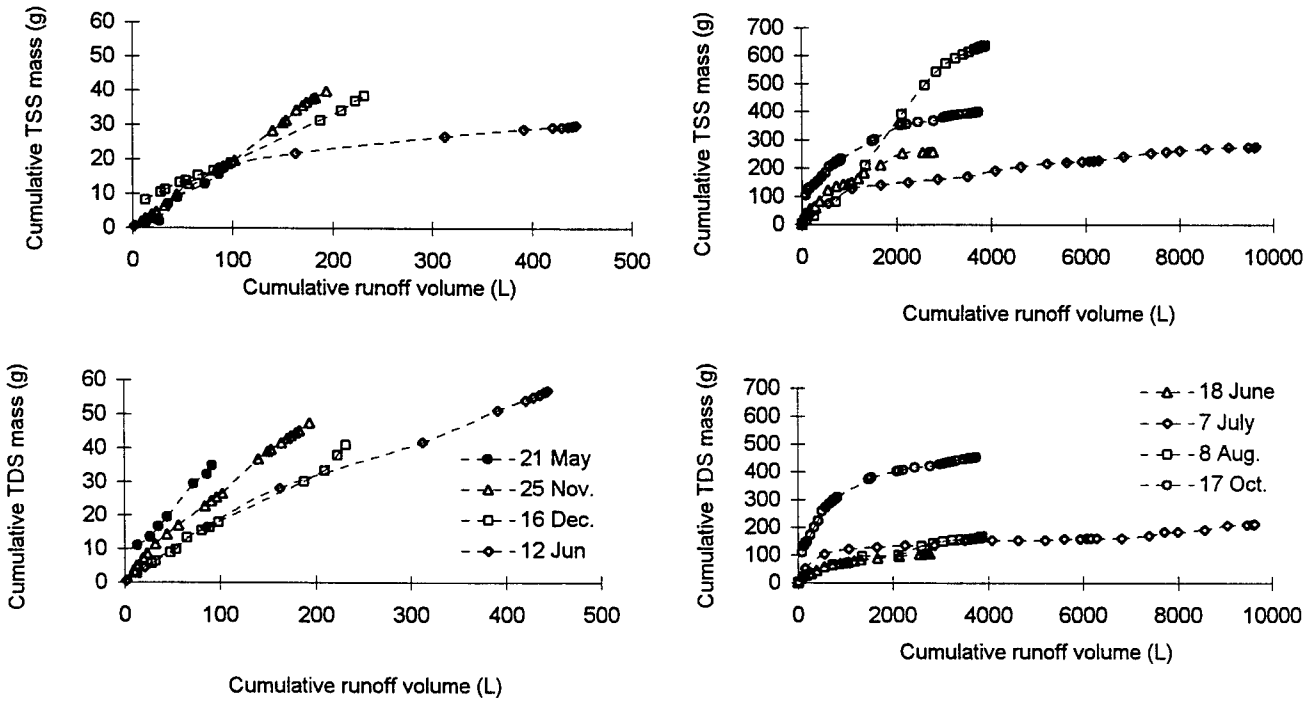

Event:	21 May 96	25 Nov. 96	16 Dec. 96	12 Jun. 97	18 Jun. 96	7 Jul. 96	8 Aug. 96	17 Oct. 96
	flow-limited, low runoff volume events				mass-limited, high runoff volume events			
vehicles during runoff	2,203	10,148	8,970	616	6,496	4,417	1,999	4,772
previous dry hours (hr)	128	93	96	90	73	117	216	182
runoff duration (min.)	22	146	324	24	76	60	52	609
runoff volume (L)	96.5	216	269	464	2,779	9,643	3,897	3,693
vehicles/runoff volume (L)	22.8	47	33.3	1.3	2.3	0.46	0.52	1.3

Figure 2.9.5 Plots of cumulative mass fractions as a function of cumulative runoff volume.

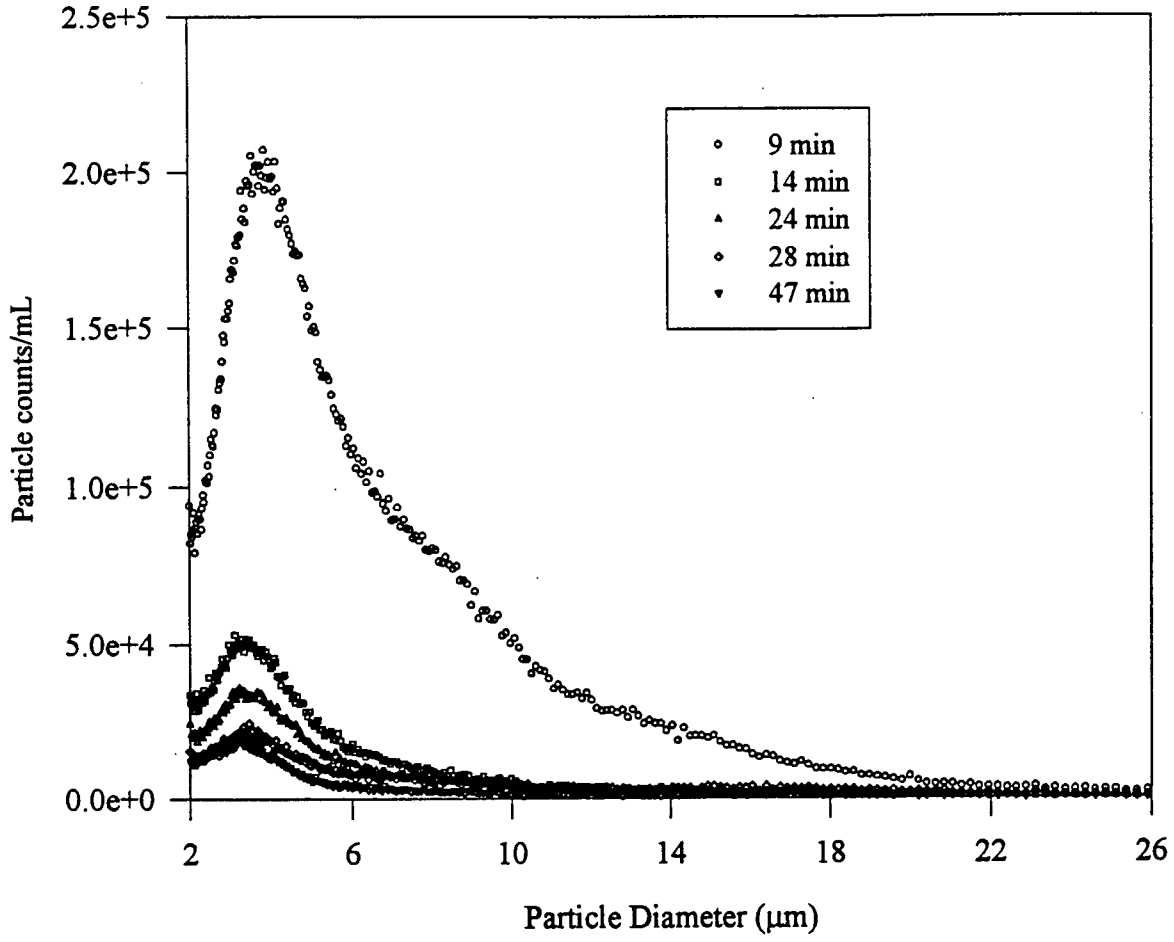

Figure 2.9.6 Temporal variation in particle counts and diameters for selected 8 August samples.

First Flush Behavior of Solids and Particle Counts

First flush results for solid fraction indices and particle counts are presented in Figure 2.9.7. The curve areas and curve area ratios are summarized in Table 2.9.3. These quantities and flow volume were normalized and plotted as a function of dimensionless time, based on event runoff duration. A first flush occurred when the solid fraction or particle count curve was positioned above the flow volume curve. The ratio of the area under these curves to the flow volume curve area is a measure of first flush strength. Ratios that exceed one signal a first flush. Slopes of the curves indicates the rate at which these quantities are delivered from the roadway surface. Consistent with the presentation earlier, first flush results are grouped and compared based on event LPF.

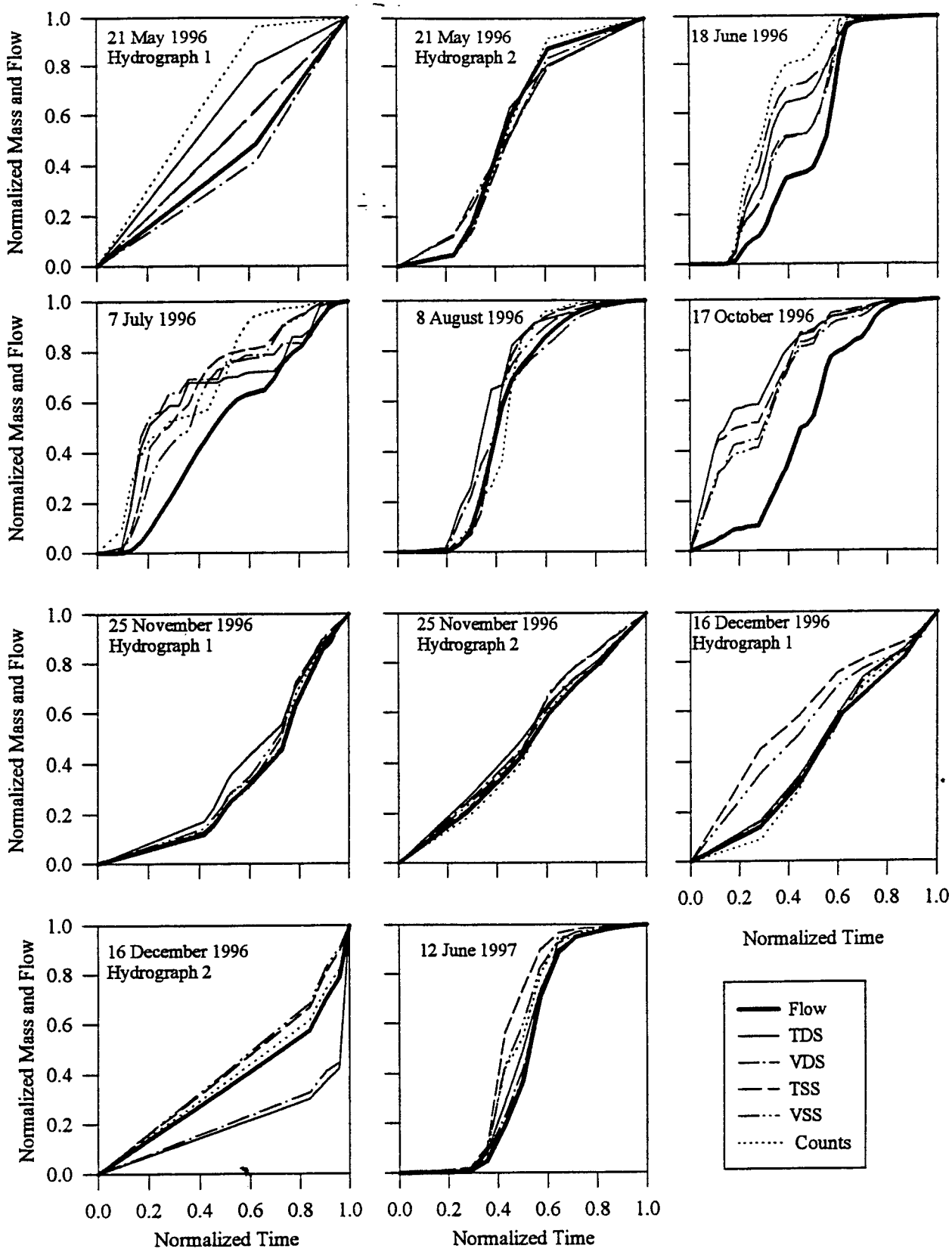

Figure 2.9.7 First flush plots for solid fractions and particle counts for each event.

Because all three low flow events had two distinct runoff hydrographs separated by a period of no flow, a first flush was evaluated separately for each hydrograph. The first hydrograph of each event generally exhibited a stronger first flush than the second hydrograph for most solid indices and particle counts. Exceptions included VDS for 21 May and 25 November as well as suspended fractions for 25 November. Excepting VDS and particle counts for 8 August, all solid indices and particle counts from the three high flow rate events exhibited a first flush. The 18 June and 7 July events produced significantly stronger first flush results than the 8 August event. Particle counts exhibited the strongest first flush and with one exception for TSS, the suspended fractions had the weakest first flush in both the 18 June and 7 July events.

Table 2.9.3 First flush curve areas and area ratios for solid fractions and particle counts.

Event (19##) (1)	Volume (2)	Volume (3)	TDS (4)	VDS (5)	TSS (6)	VSS (7)	Counts (8)
	Curve Area	*Curve area ratios(ratios>1 indicate first flush using Eqn. 3)*					
21 May 96(hydrograph 1)	0.3294	1.0000	1.3236	0.9326	1.1375	1.1321	1.4821
21 May 96(hydrograph 2)	0.3654	1.0000	0.9825	0.9340	1.0041	1.0101	0.9828
18 June 96	0.4862	1.0000	1.2853	1.3398	1.1919	1.1773	1.4603
7 July 96	0.5005	1.0000	1.2843	1.3293	1.3233	1.2478	1.3712
8 August 96	0.6001	1.0000	1.1128	1.0133	1.0429	1.0326	1.0178
17 October 96	0.4447	1.0000	1.6404	1.4684	1.5788	1.4527	no data
25 November 96 (hydrograph 1)	0.4494	1.0000	1.1248	1.0182	1.0461	1.0712	1.0113
25 November 96(hydrograph 2)	0.5211	1.0000	1.0908	1.0246	1.0543	1.0723	1.0067
16 December 96(hydrograph 1)	0.4794	1.0000	1.0492	1.0246	1.2991	1.2042	1.0050
16 December 96(hydrograph 2)	0.3977	1.0000	0.6533	0.6712	1.1099	1.1267	1.0369
12 June 97	0.5071	1.0000	1.0453	1.0210	1.1756	1.1106	1.0960

All solid indices and particle counts from the two intermediate flow rate events produced a first flush. The first flush from the long duration 17 October event was significantly stronger for all solid indices as compared to the very short duration, but more intense 12 June event. Particle counts were not available for the 17 October event.

Particle Size Distributions

PSDs were determined for the total mass of solids collected. Event PSDs and a site mean PSD are plotted in Figure 2.9.8, with PSD statistics summarized in Table 2.9.4. PSD data previously reported for five 1995 events are also summarized (Sansalone and Buchberger, 1997). Figure 2.9.8 indicates differences in gradations but similar PSD trends. Variation in PSD indices are shown in Table 2.9.4. Results indicate the greatest relative variance occurred for the d_{10} size.

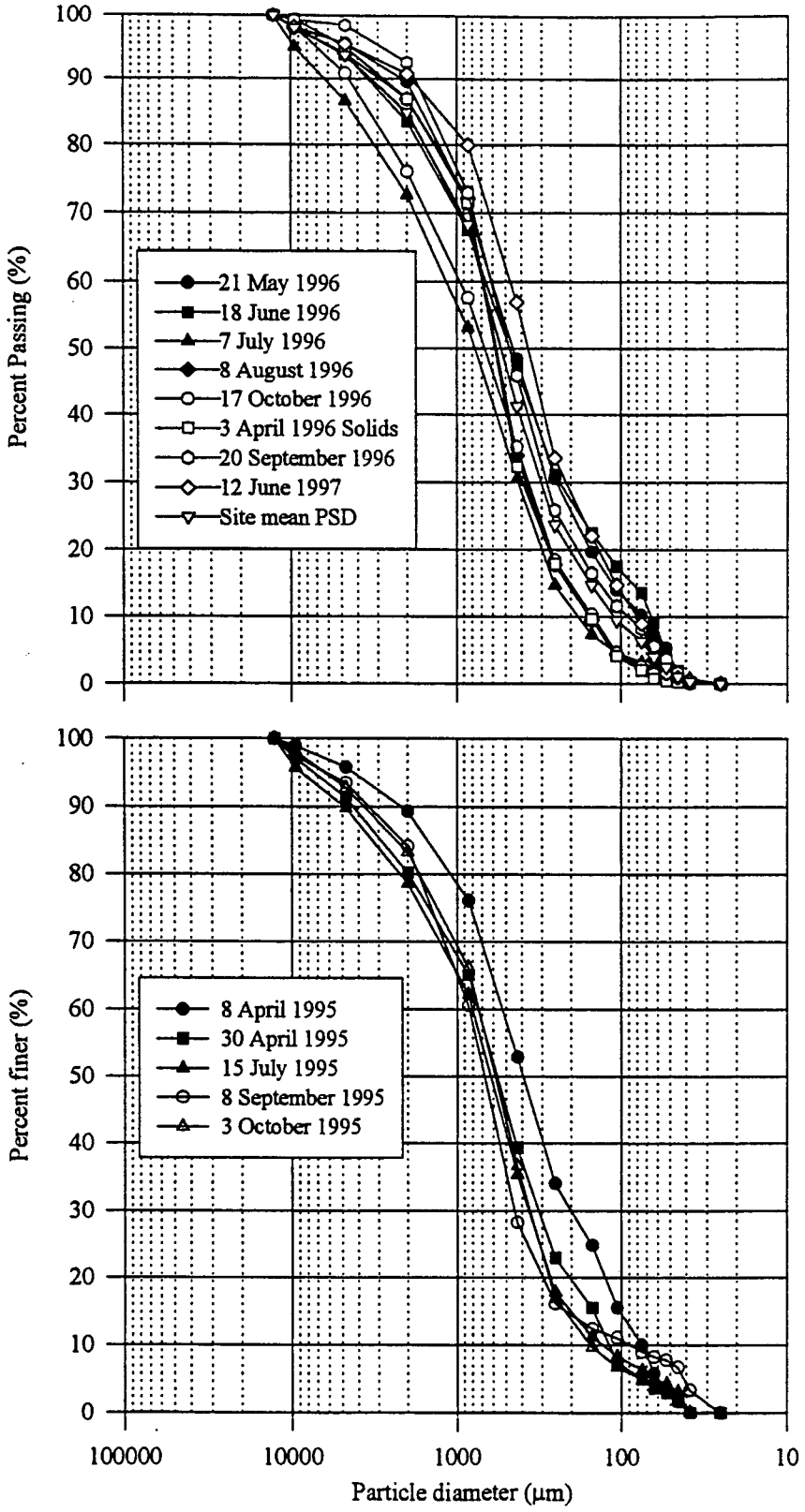

Figure 2.9.8 Particle size distributions (PSD) for each event.

Table 2.9.4. Particle size distribution (PSD) and particle counting indices.

Event date (19##)	d_{60} (mm)	d_{50} (mm)	d_{30} (mm)	d_{10} (mm)	C_u	C_c	d_{50} (mm)	Total counts
	Mechanical sieve PSD indices (for particle dia. > 25 mm)						Particle Counter (for dia. < 25 mm)	
3 April 96	690	590	395	160	4.3	1.4	no data	no data
21 May 96	705	450	250	65	10.8	1.4	4.3	$1.9x10^{11}$
18 June 96	680	465	245	75	9.1	1.2	4.9	$9.7x10^{11}$
7 July 96	1200	785	415	180	6.7	0.8	11.2	$1.5x10^{11}$
8 August 96	695	585	380	160	4.3	1.3	11.8	$1.2x10^{13}$
28 September 96	710	470	280	90	7.9	1.2	no data	no data
17 October 96	950	690	375	155	6.1	1.0	no data	no data
25 November 96	no data	no data	no data	no data	no data	no data	4.1	$2.2x10^{11}$
16 December 96	no data	no data	no data	no data	no data	no data	4.0	$1.9x10^{11}$
12 June 97	480	370	220	80	6.0	1.3	4.7	$7.9x10^{10}$
8 April	510	400	200	77	6.6	1.0	4.1	no data
30 April	690	570	230	110	6.5	0.7	4.8	no data
15 July	795	605	350	130	6.1	1.2	no data	no data
8 September	850	670	450	83	10.2	2.9	no data	no data
3 October	700	570	370	150	4.7	1.3	no data	no data

Specific Surface Area Distributions

Measured SSA results were plotted as a function of nominal particle size as shown in Figure 2.9.9. Results indicate a generally increasing trend in SSA with decreasing particle size. SSA trends for the 18 June and 7 July events are approximately monotonic. SSA results for other events also show a monotonically increasing trend until the 53 - 45 mm range where for smaller sizes there was either no increase in SSA or a decrease in SSA. Contrasted with these measured SSA results are computed SSA values based on a assumption of spherical particles with a specific gravity of 2.65 g/m^3. These calculations plotted in the lower right plot of Figure 2.9.9, show a monotonically increasing SSA trend with decreasing size. Spherical particle SSA values were multiplied by a factor of 1000 to plot them on the same scale as the actual measured SSA values.

Total Surface Area Distributions

To determine surface area distributions, Equation 2.6.10 was applied to each event using the SSA and PSD data. For comparison, surface area distribution was also computed using the site mean PSD and the assumption of spherical particles. Resulting surface area distributions are plotted in Figure 2.9.11. The 425 to 850 mm range has the highest surface area for all events. This is also the range where the d_{50} values are located. The shape of all surface area distributions are similar. Below 100 mm the surface area contribution is relatively small. The site mean surface area is significantly underestimated using the assumption of spherical particles. However, the pattern for the surface area distribution as a function of particle diameter is the same. Figure 2.9.11 - 2.9.17 also compare Zn, Cd, Pb, Fe and Cu mass to PSDs, SSA and total surface area.

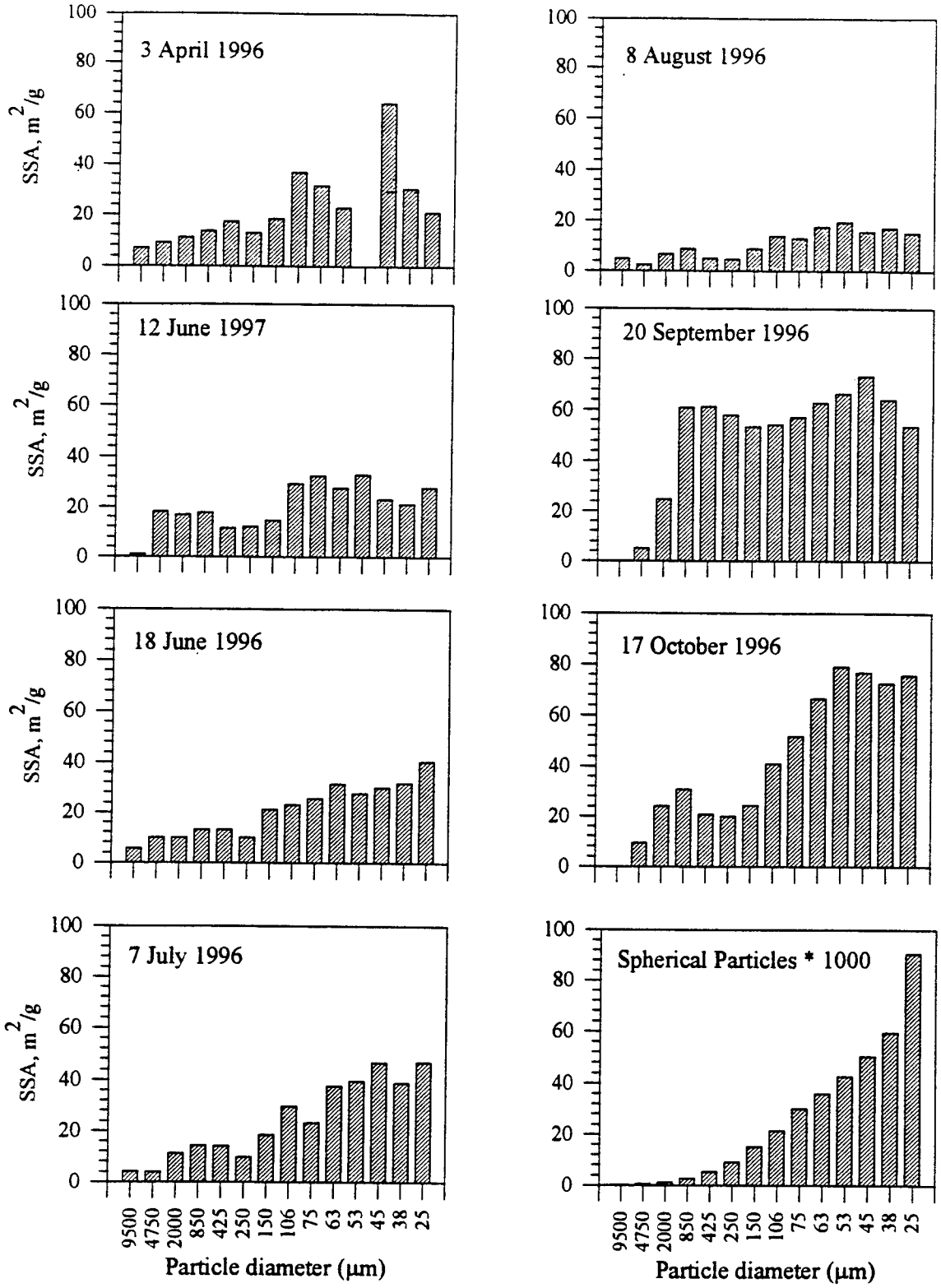

Figure 2.9.9 Distribution of solids specific surface area across particle size ranges.

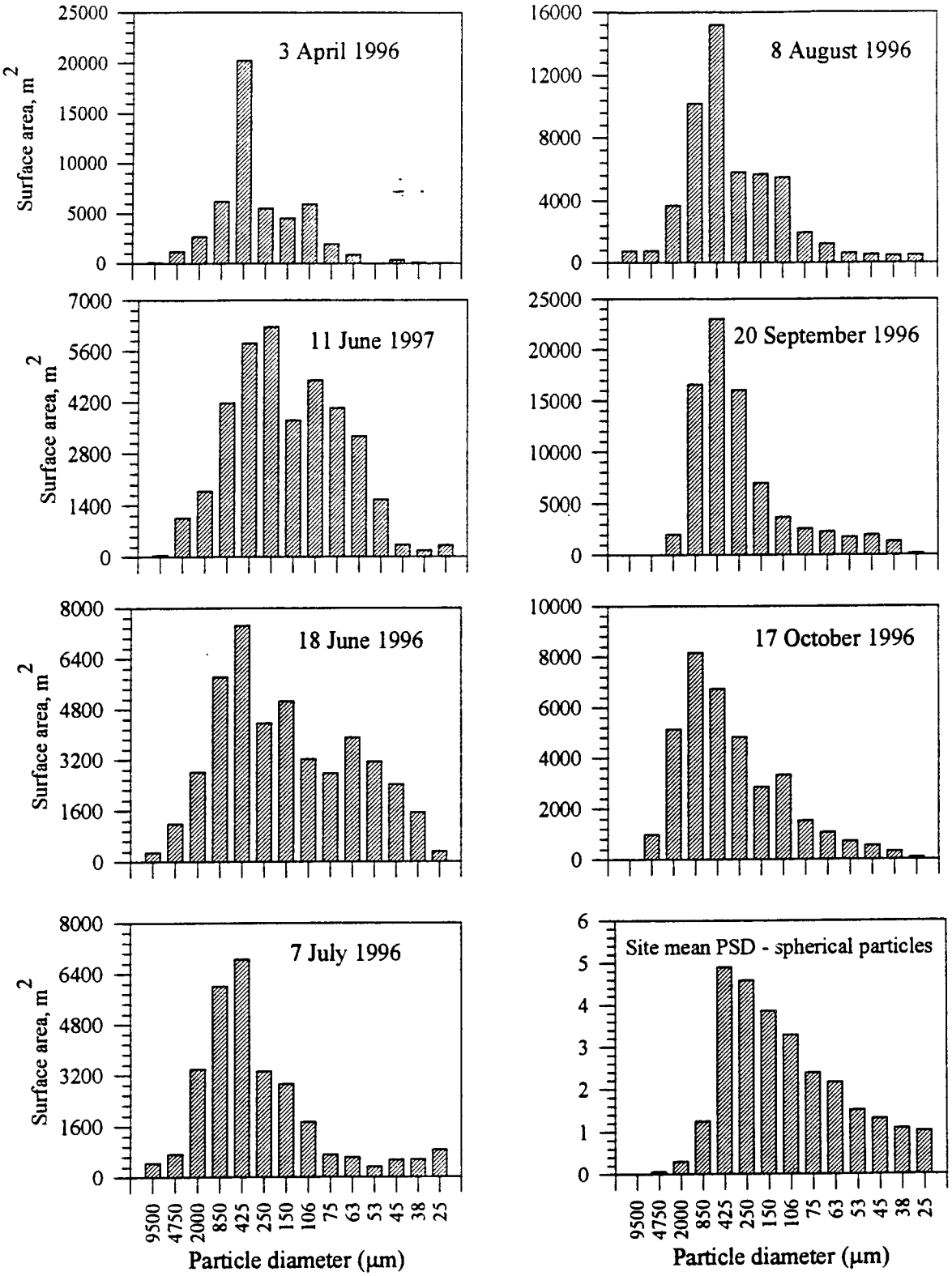

Figure 2.9.10 Distribution of total surface areas across particle size ranges.

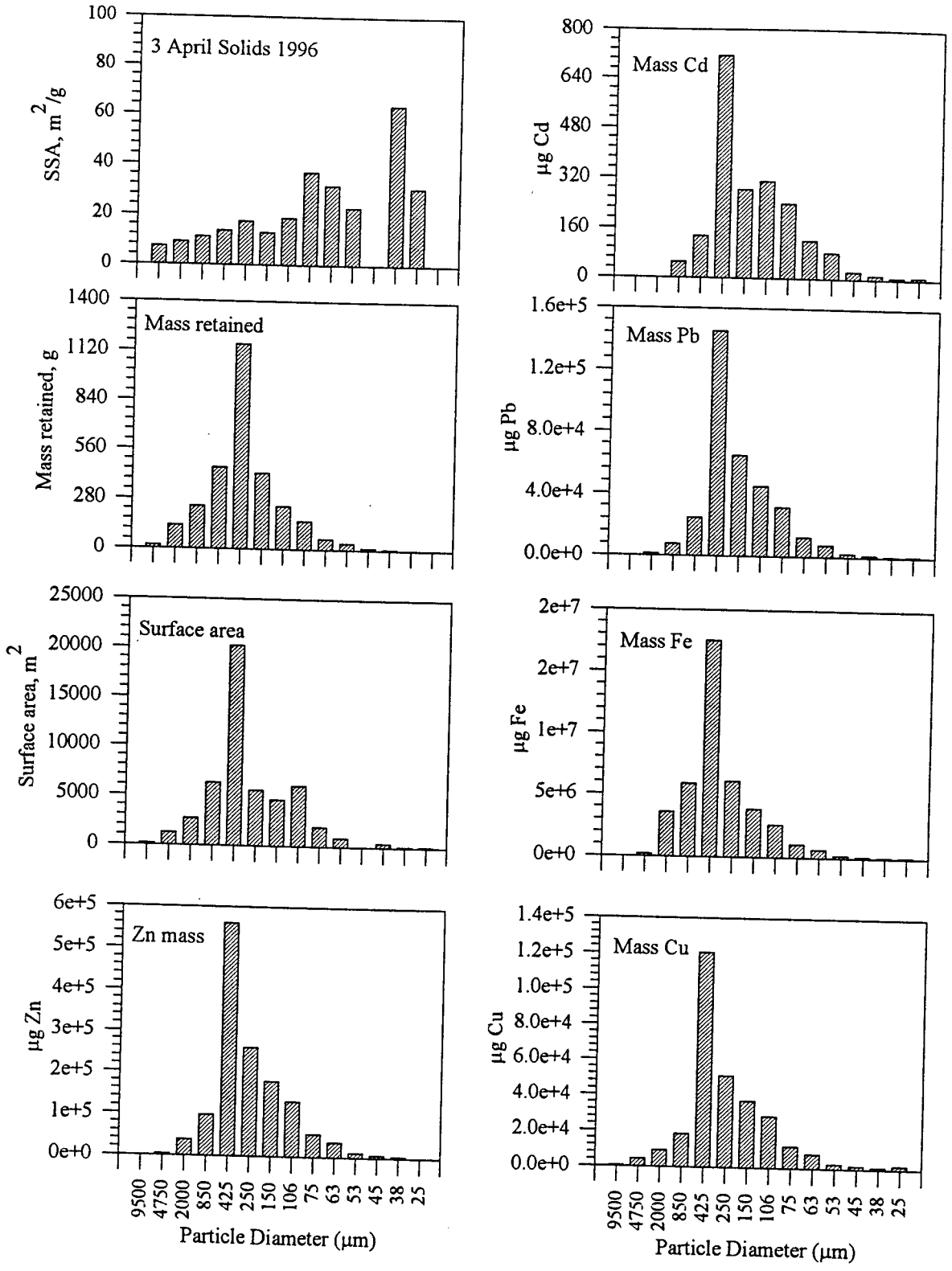

Figure 2.9.11 Particle analysis for 3 April 1996 runoff solids (Note vertical scale differences).

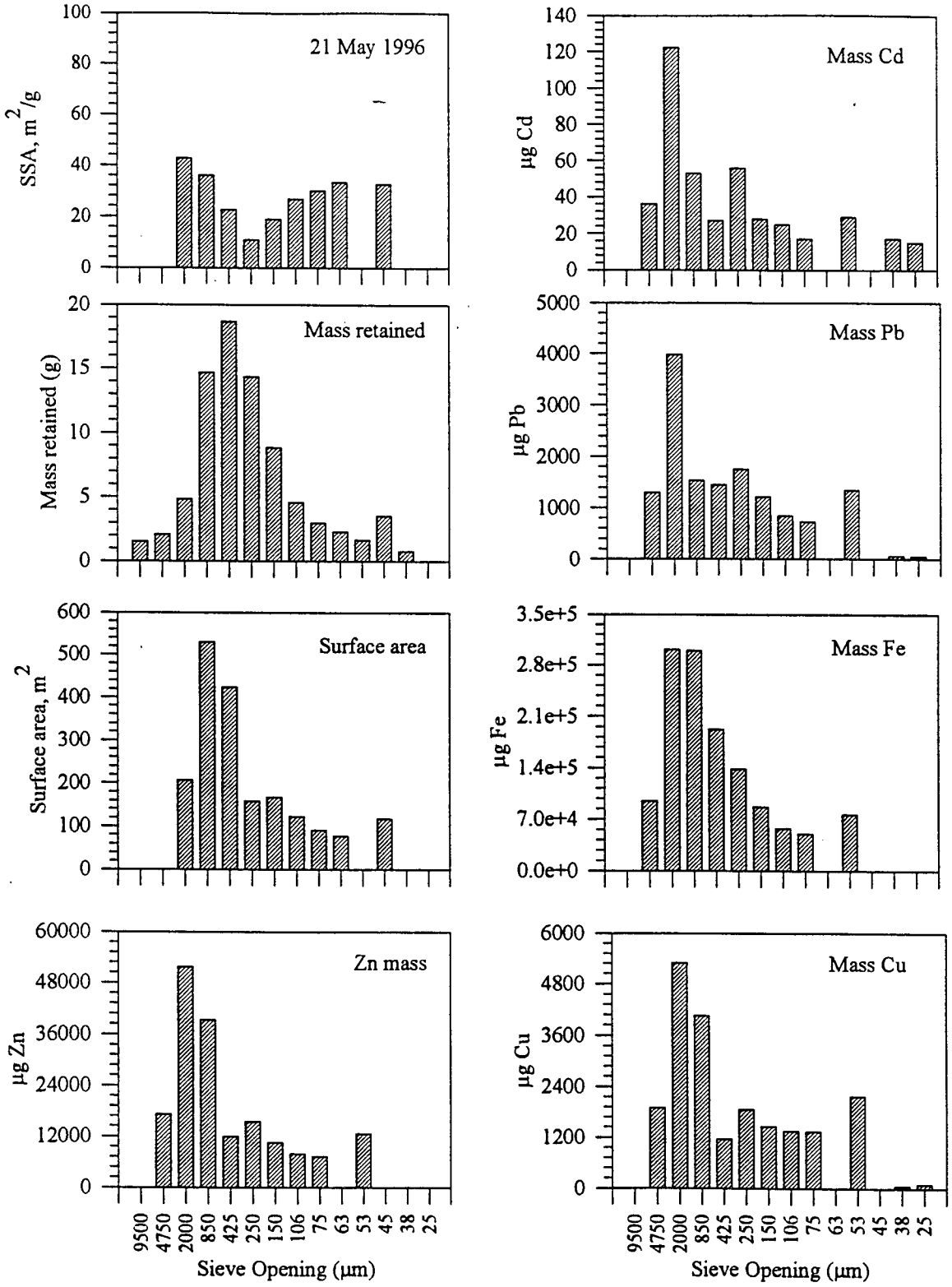

Figure 2.9.12 Particle analysis for 21 May 1996 runoff solids (Note vertical scale differences).

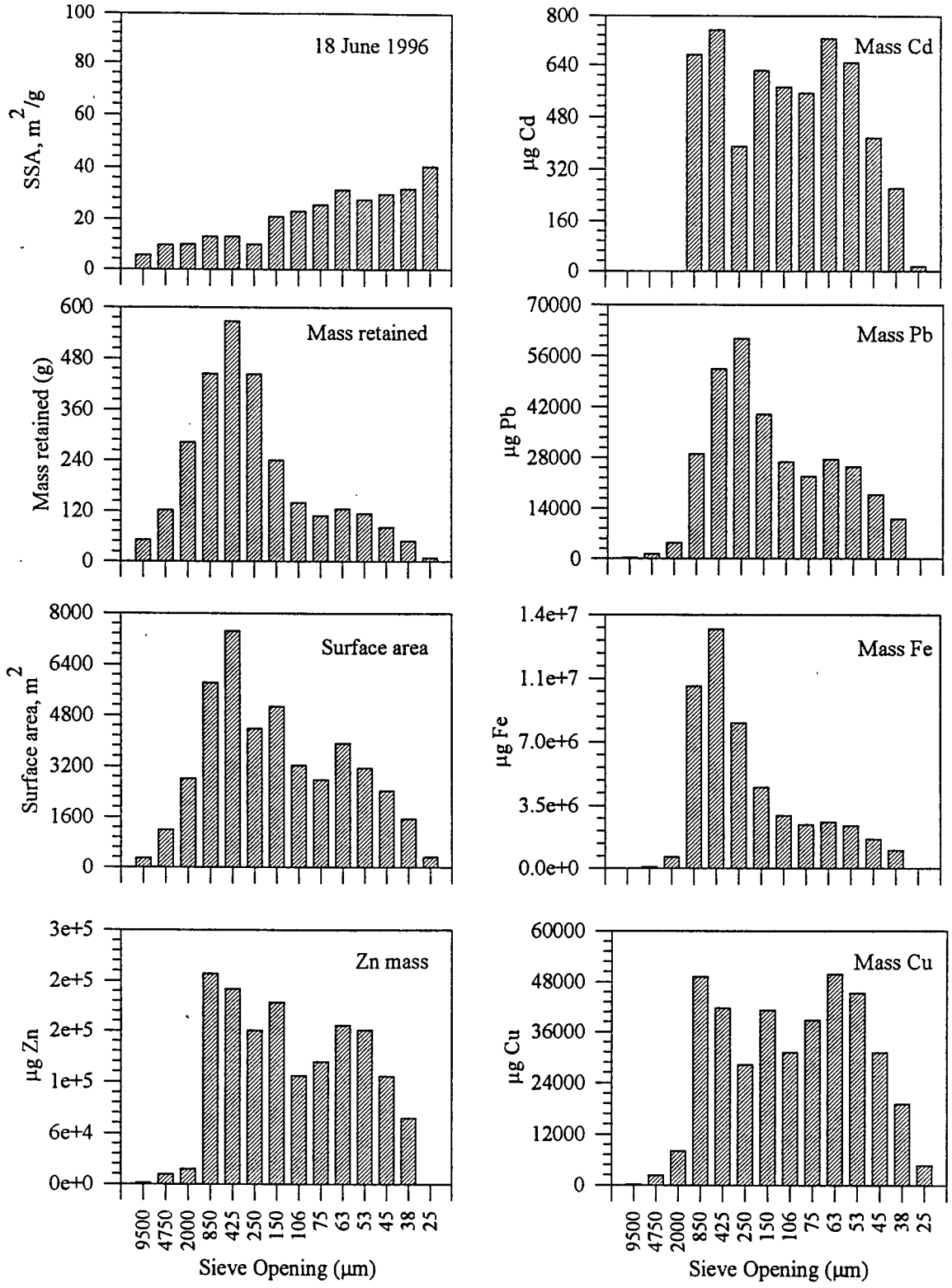

Figure 2.9.13 Particle analysis for 18 June 1996 runoff solids (Note vertical scale differences).

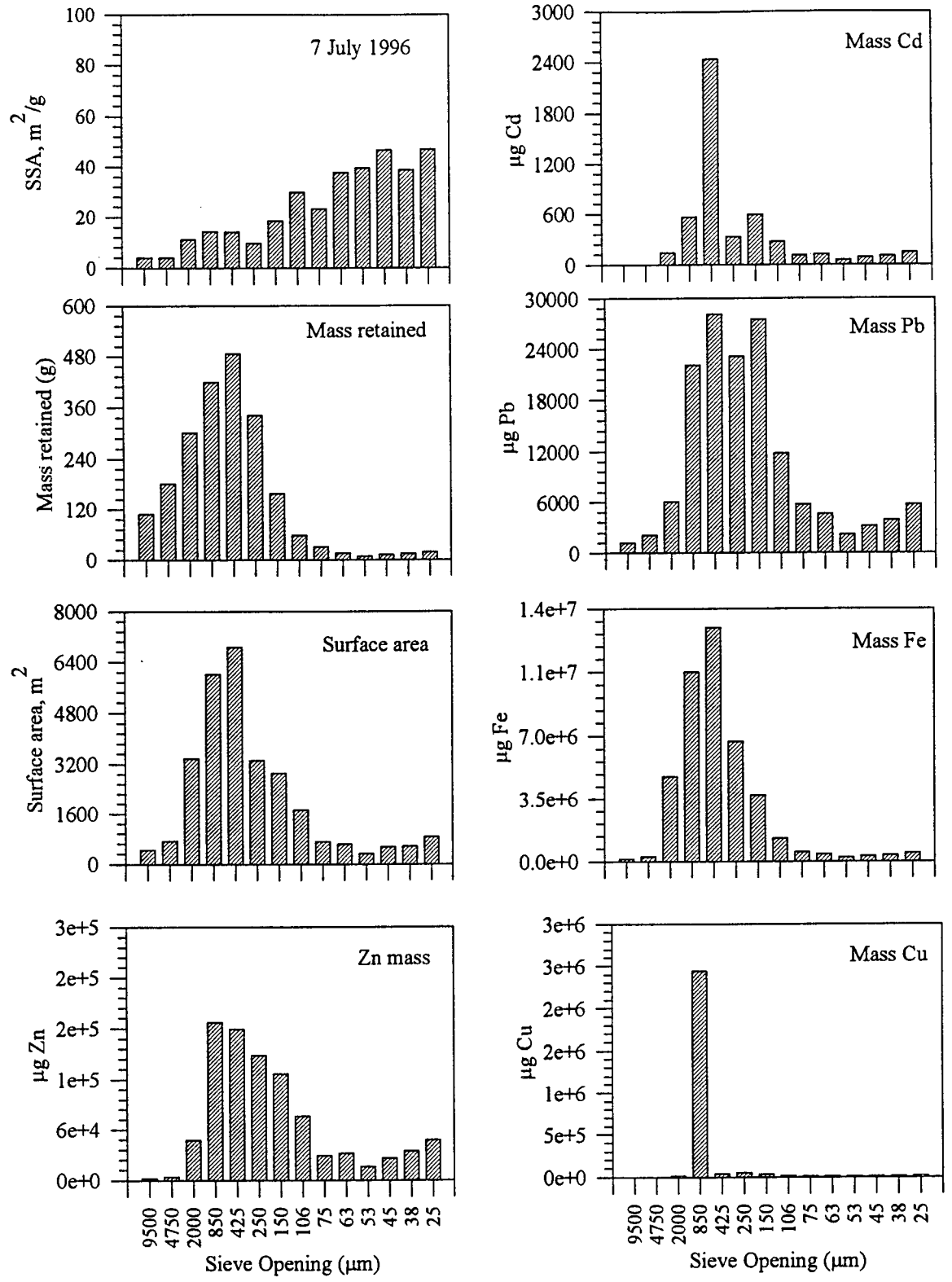

Figure 2.9.14 Particle analysis for 7 July 1996 runoff solids (Note vertical scale differences).

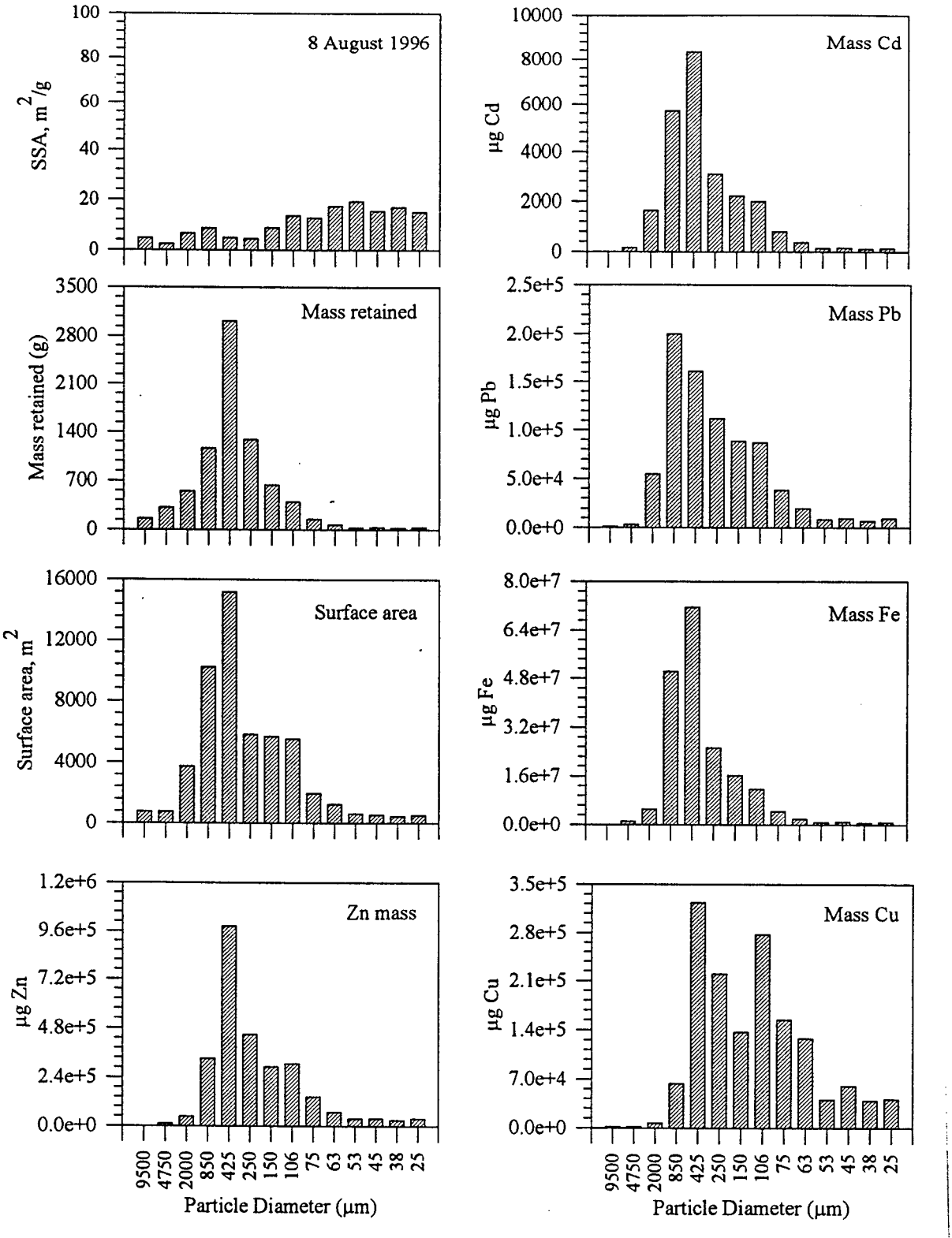

Figure 2.9.15 Particle analysis for 8 August 1996 runoff solids (Note vertical scale differences).

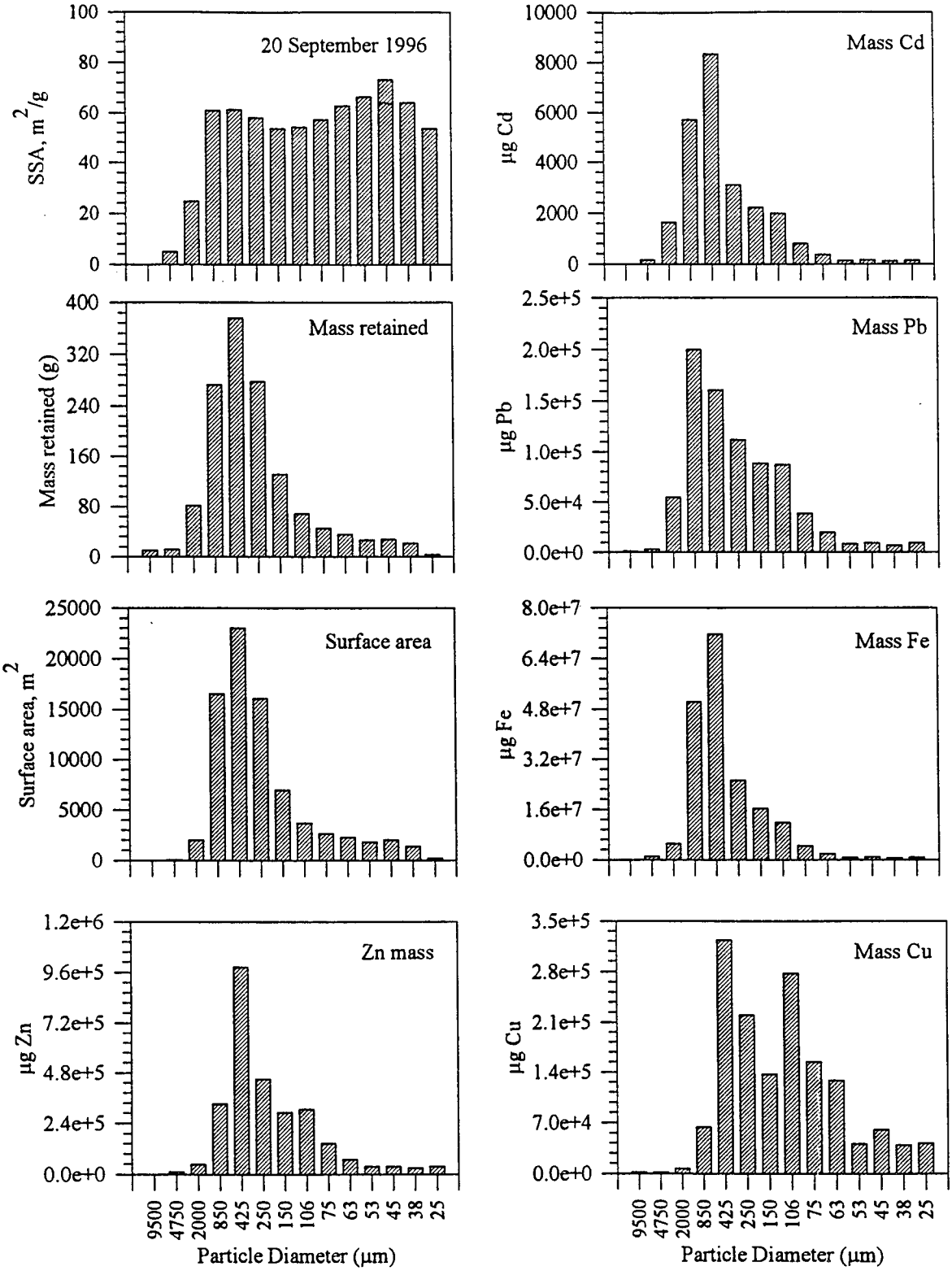

Figure 2.9.16 Particle analysis for 20 Sept. 1996 runoff solids (Note vertical scale differences).

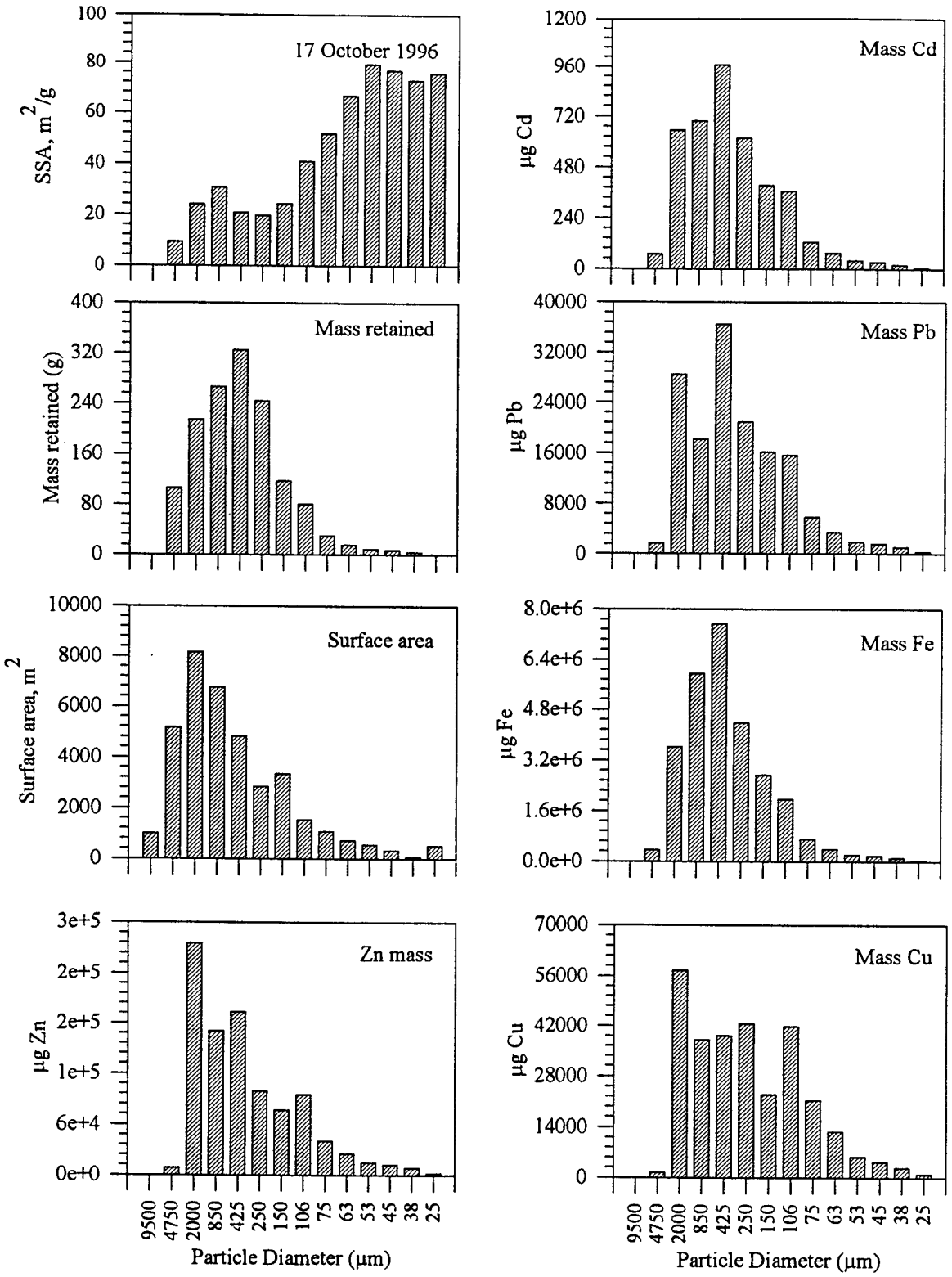

Figure 2.9.17 Particle analysis for 17 Oct. 1996 runoff solids (Note vertical scale differences).

2.10 Discussion and implications of 1996 - 1997 results

This part of the field research focused of lateral pavement sheet flow from a heavily traveled highway in Cincinnati, and focused on the physical characteristics and delivery of solid fractions and particles. Flow rate/duration and traffic intensity were primary variables controlling solids and particle delivery. Particle counting offered insight regarding particle re-supply by traffic during low flow, intermittent events. Particles in the 2 through 8 mm range, are rapidly washed off the pavement during each event. For the low intensity, intermittent events during periods of heavy traffic particle size and counts provide an indication of the equilibrium between particles generated from traffic and particles washed off from the pavement. Such events also have the largest values of flow APRT, which was also a factor in the equilibrium.

A first flush occurred for most events, albeit a weaker first flush for the low flow rate events. The heavy traffic during those events served not only as a source for solids and particles but also may have provided an effective means to entrain and mix particles. This supply and mixing of particles may be partially responsible for the weaker particle first flush results. Particle diameters ranged from a lower detection limit of 2 mm to greater than 10,000 mm. Particle diameters greater than 25 mm are very few in number. In this range, counts decreased to less than 10 particles/mL as compared to the 3 mm particle with greater than 100,000 particles/mL. Particle counting can be a useful characterization tool for sizing and counting particles less than 25 mm while mechanical sieve analysis can effectively be applied to larger particles.

From a water quality perspective, the geochemical transport and fate of reactive constituents transported in urban roadway drainage is mediated by reactions with solid surfaces of large SSA. SSA tends to increase with decreasing particle size. This increasing trend is not consistently monotonic in contrast to SSA for spherical particles. Stormwater particle SSA were approximately three orders of magnitude greater than SSA for spherical particles and constant specific gravity. The large difference may be attributed to a number of factors. With all other factors held constant, spherical particles yield the minimum surface area for a given particle mass. When viewed under a microscope, actual stormwater particles were highly irregular, with angular, cylindrical or blocky shapes. When viewed under a stereomicroscope, pore openings and a pattern of porosity can be observed, increasing the surface area. Digestion and analysis of these particles indicate high levels of iron, manganese and aluminum. Oxides of these metals have high SSA. In addition, organic carbon on the particle surface can significantly increase SSA.

This field effort measured hydrologic and solid loadings typical of heavily traveled urban roadways for assessment of receiving water quantity and quality impacts. Results can be used for bench scale development of in-situ treatment strategies and hydrologic design of the prototype treatment devices. Solid fractions and particle count results are required when selecting and designing treatment strategies such as infiltration systems or settling basins. For example, hydrograph loadings combined with PSDs and particle counting data can be used to assess the potential trapping efficiency of a settling basin as well as provide guidance for the design of hydraulic structures to convey flows. PSDs and solids loadings combined with hydraulic loadings provide data for applicability of in-situ adsorptive-infiltration strategies.

DEVELOPMENT AND CHARACTERIZATION OF SORBENT MEDIA

3.1 Introduction

A number of sorbent media are available for the transfer of dissolved or entrained particulate-bound metal elements from the liquid phase onto or into the surface of the porous media. For the water and wastewater industries two of the most common media are granular activated carbon (GAC) and filter sand. GAC has been used as a sorbent for dissolved metal element contaminants (Corapcioglu & Huang, 1987). In water and wastewater treatment processes GAC can be successfully regenerated (Reed et al., 1995).

Filter sand has a long history as an effective media to remove particulate-bound contaminants from water and wastewater (Yao et al, 1971). Although filter sand has been used most effectively as a media to remove particulate-bound contaminants, it has also been applied as a sorbent for dissolved contaminants in groundwater (Igarashi and Mahara, 1994). Like GAC, filter sand can be successfully regenerated through back-washing at both the laboratory and operational-scale (Sontheimer et al, 1988)

Another sorbent media, of very recent origin, is iron-oxide coated sand (OCS). The synthetic form of this material has been made by coating silica sand with a thin layer of iron-oxide. OCS has been shown to be an effective sorbent media for metal elements (Benjamin & Sletten, 1993). OCS has also been shown to be effective as a filtration media for removing entrained particles in water and wastewater (Stenkamp & Benjamin, 1994). OCS can also be effectively regenerated as both a sorbent and filter media (Benjamin & Sletten, 1993). The primary attributes the iron-oxide coating provides for the sorption of metal elements as compared to silica sand are the increase in surface area and the amphoteric surface charge. The primary attribute the silica sand substrate provides is a hard durable and relatively acid-resistant surface for the coating. Therefore an understanding of the process chemistry involved in the formation and transformation of iron oxide solutions for coatings is critical.

The main focus of this chapter will be on the development and characterization of iron-oxide minerals and iron-oxide coated sand. From a number of sorbent media alternatives, OCS was chosen as the media having the greatest overall potential from sorption, filtration and strength considerations. GAC and silica sand will also be characterized since breakthrough performance with respect to OCS was evaluated.

3.2 The natural occurrence of iron oxide minerals

Iron oxides are present in varying amounts in soil from different climatic regions in one or more of their mineral forms and are the most abundant metallic oxide in soil. The various iron oxide minerals are created under the influence of the primary soil forming factors of temperature, moisture, pH and Eh. Once formed these iron oxides can be modified through changes in the soil environment. Iron oxides have strong pigmenting ability even at low concentrations and determine the color of many soils. As an example, Alabama soils are reddish in color because in

warmer humid climates, the strength of the red hematite color even at low concentrations can mask the yellow goethite mineral which is also present, possibly at higher concentrations. In cooler climates, such as the Upper Midwest, temperatures are not as conducive to formation of even small amounts of hematite and therefore the yellowish-brown color of soils is the pigmenting of the iron oxide mineral, goethite. Synthetic, very finely dispersed iron-oxides are used as pigmenting agents in paints.

There are a total of 13 iron oxide minerals, of which there are 8 major iron oxides. These iron oxides differ in composition, the valence state of Fe and in crystalline structure. However all iron oxides contain Fe and O or OH. Table 3.2.1 summarizes the major iron oxide minerals with selected characteristics.

Table 3.2.1 Selected properties and attributes of major iron oxide minerals

Mineral Name	Formula	Structural system	Density (g/cm^3)	SSA (m^2/g)	Color
Hematite	α-Fe_2O_3	Trigonal	5.26	20-30	blood red
Maghemite	γ-Fe_2O_3	Cubic or tetragonal	4.87	80-130	chocolate
Magnetite	Fe_3O_4	Cubic	5.18	~4	black
Goethite	α-FeOOH	Orthorhombic	4.26	20-40	mustard
Lepidocrocite	γ-FeOOH	Orthorhombic	4.09	70-80	orange-brown
Ferrihydrite[1]	$5Fe_2O_3 \cdot 9H_2O$ [2]	Trigonal	3.96	180-300	deep brown
Feroxyhyte	δ`-FeOOH	Hexagonal	4.20	190-210	brown
Akaganeite	β-FeOOH	Tetragonal	3.56	~30	dark mustard

[1]: ferrihydrite & feroxyhyte have the only amorphous or poorly-crystalline structures
low SSA from $Fe(NO_3)_3 9H_2O$ hydrolysis, high SSA from Fe^{3+} precipitation with KOH
[2]: other formulas include : $Fe_5HO_8 \cdot 4H_2O$ and $Fe_6(O_4H_3)_3$
point of zero charge (pzc) for all minerals shown is between pH 7-8
α : hexagonal close packed (more stable than γ)
β : goethite polymorph in presence of high Cl^- levels
γ : cubic close packed
δ` : poorly-ordered ferrimagnetic form of FeOOH

The most common naturally-occurring Fe^{3+} iron oxide is goethite. Hematite is also a naturally-occurring common Fe^{3+} iron oxide. Ferrihydrite is also a naturally-occurring, poorly crystalline Fe^{3+} iron oxide. Ferrihydrite is a typical component of young iron oxides and will eventually transform through an aging process, on a pedogenic time scale, to goethite or hematite. Ferrihydrite is the only iron oxide which is nearly completely soluble in acid ammonium oxalate in the dark.

Goethite is the most thermodynamically stable of these minerals under aerobic conditions. With respect to goethite, lepidocrocite, ferrihydrite and maghemite are less stable. In most soils both goethite and hematite co-exist and the goethite-hematite ratio is a common index. This ratio is affected by the valance of the Fe source, the Fe concentration, pH, Eh, temperature, soil water activity, soil organic matter, and activity of Al in the soil solution. Ferrihydrite is a necessary precursor to hematite and can also act as a source for formation of goethite. Hematite and goethite form through two mutually competitive processes given a source of ferric ions.

3.3 Synthetic preparation of iron oxide minerals

There are two common methods of preparing iron oxides. The first method involves preheating 2000 mL of DI water to 75°C in an oven and then withdrawing the water and adding 20 g of unhydrolyzed crystals of $Fe(NO_3)_3 \cdot 9H_2O$. The solution is stirred rapidly and reheated at 75°C for 10 to 12 minutes. The formation of iron hydroxy polymers will change the solution from a dull gold color to a dark reddish brown. The solution is then dialyzed for three days to produce approximately 5 g of iron oxides. This procedure produces a ferrihydrite of lower SSA, in the range of 180 to 200 m^2/g. A second method involves dissolution of 40 g of $Fe(NO_3)_3 \cdot 9H_2O$ in 500 mL of DI water and addition of approximately 330 mL of 1M KOH until the pH is 7 to 8 while stirring the solution. This procedure produces a ferrihydrite of higher SSA, in the range of 200 to 300 m^2/g. The solution is then centrifuged and dialyzed to produce approximately 10 g of ferrihydrite.

3.4 Preparation of iron-oxide coated sand (OCS)

Although the procedures have been presented to produce iron oxides synthetically, the permanent coating of silica sand with iron oxide is a much more difficult process. The process has three components. The first is preparing an iron oxide solution using procedures similar to those described in Section 3.3 but at a much larger scale. The second component involves immersing the silica sand in the iron oxide solution and heating until dry. The final component involves disaggregating the coated particles and washing the sand. The source of ferric ions is either $Fe(NO_3)_3 \cdot 9H_2O$, (ferric nitrate (FN)) or $FeCl_3$, (ferric chloride (FC)). Both FN and FC are available as reagent-grade salts or commercially in larger quantities as bulk solutions. A variety of procedures have been used to make OCS at laboratory scale quantities, usually less than 1 kg batches.

A number of iron oxide coating procedures were experimented with to produce sand for the column simulations until a durable coating was produced. Many of the initial experiments produced a coating which would readily flake off or completely wash off during rinsing. It was determined that a more careful surface preparation of the silica sand may be required to remove any surface films which may inhibit bonding. Therefore the silica sand (Ottawa 2030) was first soaked and slowly tumbled in 2.2L HDPE containers containing 2% trace-metal grade HNO_3 and 0.1% HF for 24 hours. After tumbling the solution had become fairly turbid. The sand was then rinsed with a DI water until the rinse water ran clear. The sand was re-rinsed a second time in DI water, dried at 110°C, cooled and stored in HDPE buckets. This procedure was used for the sand

to be iron oxide coated and for the silica sand used as control. A summary of the final procedure to coat approximately 25 kg of sand is summarized in Table 3.4.1.

Table 3.4.1 Summary of iron oxide coating procedure used for this research

Iron oxide solution[1]	Drying time @ temperature	Sand (Ottawa 2030)	Base added to solution	OCS color
1.6 M FN in 2000 mL soln.	24 hrs @ 110°C &4, 3 hr. re-dry	6000 g	none added	brown with reddish tint
[1]: Initial bonding coat of ~ 1M FN or FC was applied & dried before 1.6 M FN coating. For each 6000g batch OCS was sieved and then stored for column experiments. OCS particle diameters were not significantly larger than plain silica sand				

There are a number of differences between this procedure and those of previous researchers. First, because of a number of early coating failures the silica sand is cleaned and tumbled in acidic solution, rinsed with DI water, cleaned and tumbled in a very dilute basic solution before a final rinse is made. Second, to promote bonding, an initial scratch coat of ~ 1M FN was applied to the sand. Once this coating was heated until dry, the sand was disaggregated and rinsed in DI water to remove any loose coating. After washing, this sand was reheated until dry and then cooled before the second coat of 1.6 M FN was applied. Third, because of the larger scale of the OCS batch compared to other researchers drying time was longer. It was found that better bonding would occur if base were not added.

Drying was carried out in a 30 cm x 60 cm shallow Pryex glass container which was covered by another Pryex glass container such that volatilized fumes could escape from a gap left between the two containers. Drying times were a matter of judgment since the goal was to volatilize most of the HNO_3 of HCl generated depending whether FN or FC was used. However, drying times were minimized in order not to promote the transformation to hematite due to dehydration, one pathway for the transformation of ferrihydrite to hematite. Researchers indicate that to ensure the thermal transformation from ferrihydrite to hematite does not occur, drying of ferrihydrite from solution should be at 40°C (Schwertmann and Cornell, 1991). For any significant production of OCS, even at 6000 g batches at the laboratory scale, this requires weeks of drying which is impractical at any level of production.

Once drying was complete, the sand was allowed to cool and the coated sand grains were disaggregated. The sand was then sieved through a #10 then a #20 sieve to ensure sand grains were disaggregated. Sand was then stored in HDPE buckets for later use in column simulations. The OCS was not washed until placed in the column. In the column the sand was washed by passing DI water through the column until the effluent ran clear and the effluent pH was between 7 and 8. This also removed any loose OCS coating. Attempts to wash the OCS outside the column were more time-consuming than carrying the procedure out in a column.

Both FN and FC salts are sources of ferric ions. The only observed difficulty with FC was the hydrogscopic nature of the coating unless the coating is fully dry. Benjamin and Sletten used both FC and FN to produce OCS. Therefore at a laboratory scale the difference between FN or FC with respect to an iron oxide product and cost appears to be small. However at the field-scale the difference in economies between the two iron salts is significant. FC salt is one-third the cost of FN salt. FC salt or solution is also a common inorganic coagulant used in water treatment processes and is therefore readily available. Additionally, FC is a by-product from certain metal treatment waste and therefore the use of this FC by-product has the added advantage of waste minimization.

3.5 Characterization of iron oxide coating and OCS

A number of qualitative and quantitative methods are available for the determination of the presence of specific iron oxide minerals. These include color, electron microscopy, crystal shape, x-ray diffraction (XRD), differential thermal analysis (DTA), infra-red spectroscopy (IR), specific surface area (SSA) determination, and Mossbauer spectroscopy. Of these crystal shape, DTA and Mossbauer spectroscopy were not utilized but are equally valid tools for characterization of iron oxide minerals

Color

Color provides one of the most rapid, simplest, albeit qualitative, indications of an iron oxide mineral. Specific iron oxide minerals have distinct colors. The variation of distinct colors of iron oxides have been recognized and used since prehistoric times. For example, the now famous prehistoric cave paintings at Lascaux in southern France reflect the orange-yellowish colors of ochreous goethite deposits used as paint pigments. In northwestern Spain the famous cave paintings of Altamira reflect the reddish color of hematite deposits used as paint pigments (Schwertmann & Cornell, 1991).

Scanning electron microscopy

Crystal dimensions, morphology and topographic information can be measured using scanning electron microscopy (SEM). SEM can also identify the morphology of amorphous mineral forms such as ferrihydrite where techniques such as x-ray diffraction cannot. However prolonged exposure to the electron beam may cause radiation damage to the amorphous forms of iron oxides. SEM will also provide quantitative information about the elemental composition of a surface. In obtaining the electron microscope image the surface of the sample is scanned with a finely focused beam of electrons. Several signals are produced from a surface when scanned with a beam of electrons. These include backscattered, secondary, and Auger electrons; X-ray fluorescence and other photons of various energies. The most common detectors for these signals are scintillation detectors and semiconductor detectors (Skoog and Leary, 1992).

SEM analysis, shown in Figure 3.5.1 through 3.5.4 was provided at magnification of 3500x and 10000x by the Department of Material Science and Engineering at the University of Cincinnati. The upper picture in Figure 3.5.1 shows the planar surface of an Ottawa 2030 sand

particle while the lower picture demonstrates the three-dimensional morphology of the iron-oxide coating. Uncoated planar areas of the silica sand substrate can be observed in this lower picture. Figure 3.5.2 contains two pictures, both at 3500x, of surface morphology from another OCS particle. These pictures reveal the presence of fibrous needles intermixed with plates stacked on end, indicative of feroxyhyte and hematite, respectively. Figure 3.5.3 contains two pictures from another sand grain revealing another variation of the coating morphology. The upper picture, at 3500x, has distinct hexagonal plates protruding from a more poorly-ordered amorphous surface. Further analysis of an amorphous area, at 10000x in the lower picture, reveals poorly-ordered plates and nodules indicative of ferrihydrite. Finally, Figure 3.5.4 contains two pictures from yet another sand grain indicating a greater predominance of platelike morphology. The upper picture, at 3500x, also indicates some amorphous areas of a with a less pronounced profile and some needle and rod-like crystals can also be seen.

X-ray diffraction

X-ray diffraction (XRD) provides information on the identification and purity of an iron oxide mineral. However XRD can be applied to crystalline materials. Crystalline structures have systematic and periodic arrangements of atoms or ions in a three-dimensional array, Crystals are composed of regularly spaced atoms and each crystal contains planes of atoms which are separated by a constant distance. These distances between planes are characteristic of the crystalline species.

X-rays consist of electromagnetic and electrostatic field which oscillate in periodic cycles in planes perpendicular to one another and to their direction of propagation through space. For XRD x-rays on the order of 10^{-3} to 10^{1} nm are generated with high velocity electrons. The bombardment of the electrons at the anode generates the emission of x-ray photons. X-ray photons may be considered as packets of monochromatic electromagnetic waves which are directed in a narrow beam at the sample. The phenomenon of diffraction involves the scattering of these x-rays by atoms of the sample's crystals and the reinforcement of scattered rays in definite directions away from the crystal. Reinforcement of the scattered rays can be related to the distance of separation of atomic planes by application of Bragg's law,

$$n\lambda = 2d[\sin(\theta)] \qquad (3.5.1)$$

X-rays will only be reflected from the crystal if the angle of incidence satisfies the following condition.

$$\sin\theta = \frac{n\lambda}{2d} \qquad (3.5.2)$$

where:
- n = an integer number of wavelengths
- λ = wavelength of radiation (a function of the x-ray tube used)
- θ = angle of incidence
- d = interplanar spacing of the crystal

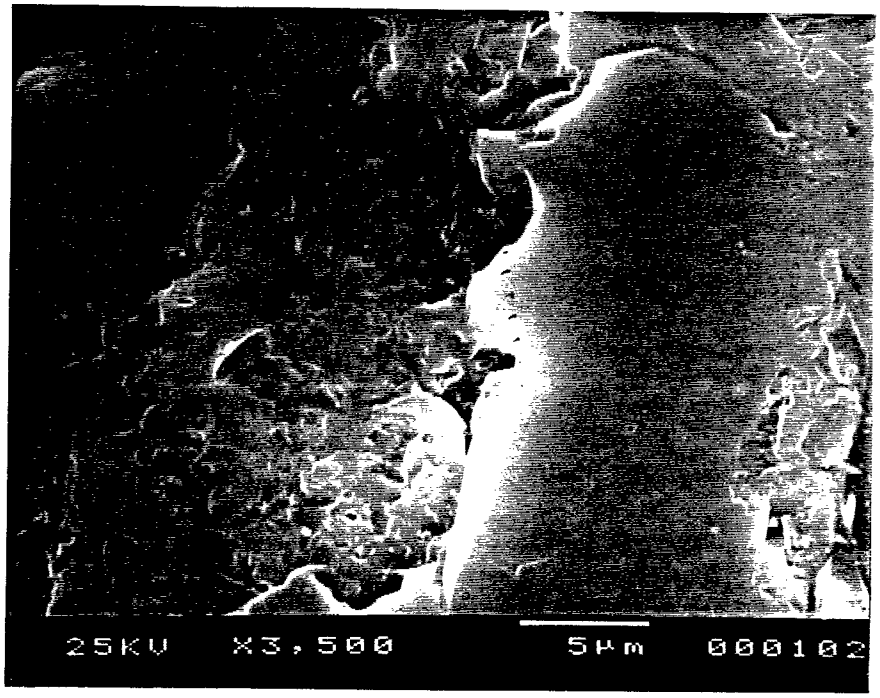

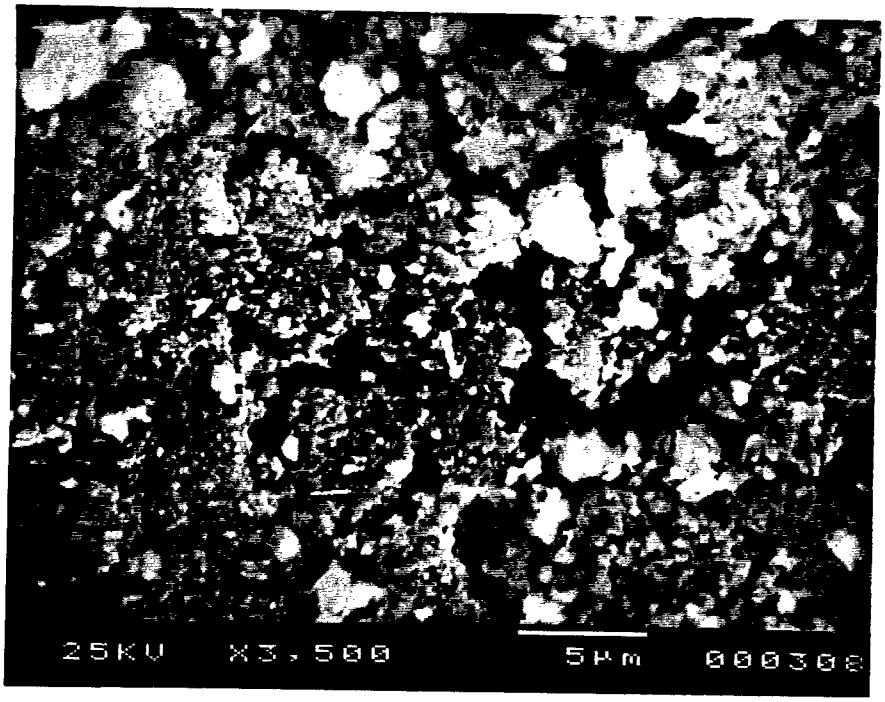

Figure 3.5.1. Scanning electron micrographs of silica sand (upper) and IOCS (lower).

Figure 3.5.2. Scanning electron micrographs of IOCS indicating feroxyhyte and hematite.

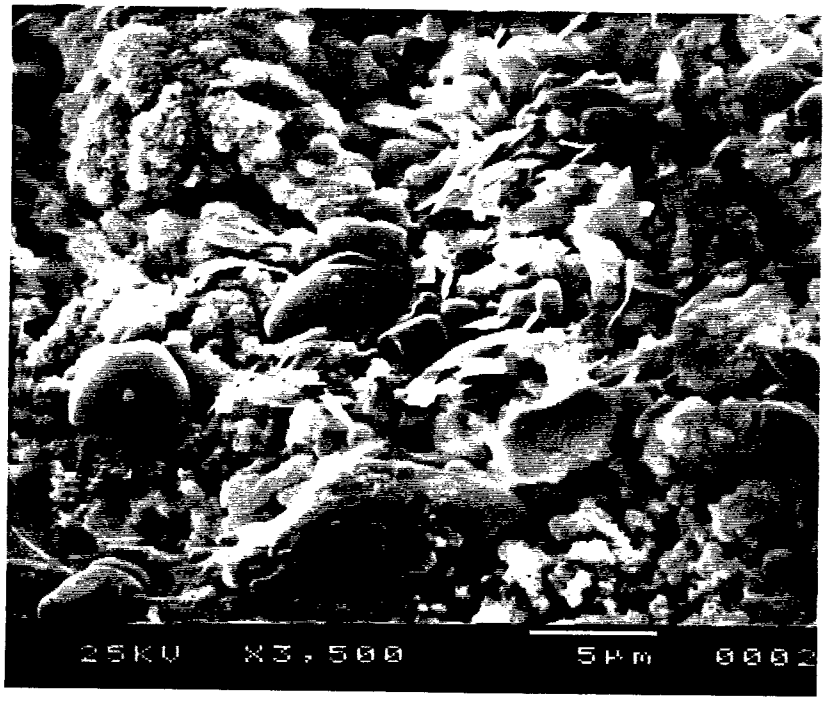

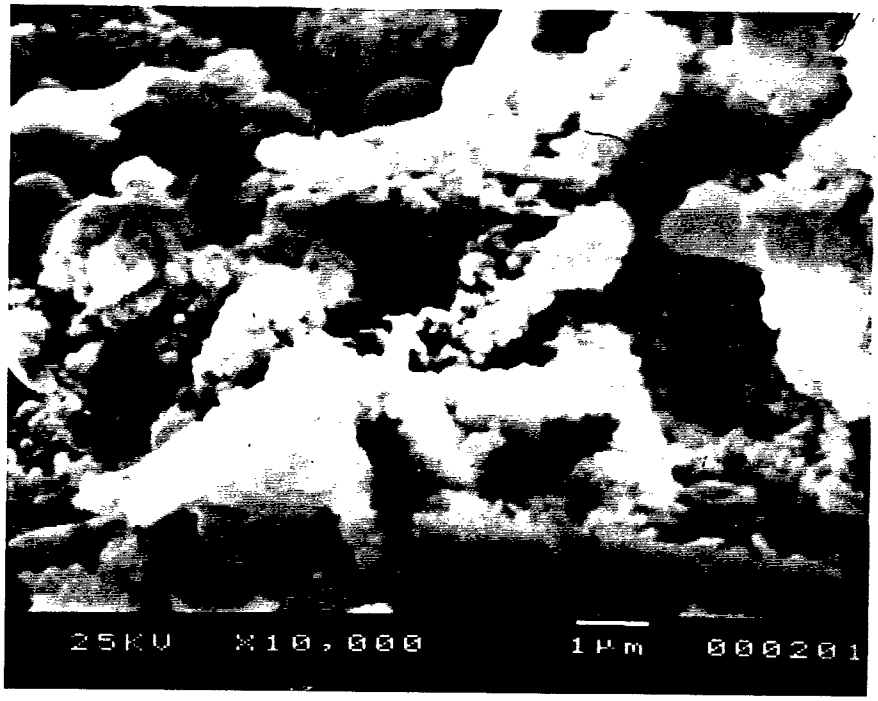

Figure 3.5.3. Scanning electron micrographs of IOCS indicating hematite and ferrihydrite.

Figure 3.5.4. Scanning electron micrographs of IOCS indicating hematite and ferrihydrite.

The angle of incidence is varied by rotating the sample in the path of the primary x-ray beam. A detector, either a Geiger, proportional or scintillation counter is used to intercept and measure the diffracted rays. The detector also moves in such a way as to maintain the angle with the sample which is equal at all positions to the angle of incidence of the incoming x-ray beam. The result of a direct reading XRD will be values of the diffracted measured intensity usually expressed as counts as a function of 2θ. XRD analysis was provided by the Department of Geology at the University of Cincinnati.

Infra-red spectroscopy

In this method, radiation from an infra-red source (wavelength of 2.5 to 50 micrometers) is passed through a iron oxide sample and absorbed as a function of the structure and composition of the iron oxide sample. The wavelength of the radiation is varied by scanning with a monochromater and the degree of absorbance is plotted against the wavelength or wave number to give an IR spectrum.

The total energy of a molecule consists of translational, rotational, vibrational and electronic energies. Transitions among the different types of energy levels occur in different regions of the electromagnetic spectrum. Infra-red radiation is associated with transitions between rotational and vibrational energy levels of the ground state. The oscillation frequency of atoms and molecules about their equilibrium position is 10^{13} to 10^{14} cycles per second. Infra-red radiation has frequencies in this range and therefore promotes transitions in a molecule between rotational and vibrational energy levels of the ground electronic state.

There are two types of commercially available infra-red spectrometers. The first is sequential dispersive spectrometers and the second is multiplex nondispersive interferometer spectrometers, typified by the Fourier transform infra-red spectrometer (FTIR). The FTIR utilizes infrared energy much more efficiently than the first type, making use of all frequencies simultaneously rather than individually. A Perkin-Elmer FTIR was provided by the Department of Material Science and Engineering at the University of Cincinnati so FTIR analysis could be carried out.

Iron oxide samples were prepared by encapsulation in a KBr pellet in the ratio of 0.5 to 2 mg of iron oxide to 300 mg of KBr. Both the iron oxide and KBr were carefully ground and mixed into a uniformly colored powder. The powder was placed in a die having a 13 mm diameter and held under a 10000 kg pressure and under vacuum for 10 to 15 minutes. The final pellet should be transparent. Blanks of pure KBr were also made at the same time and the blank FTIR results were subtracted from the pellets with iron oxide results. Samples were analyzed within 1 hour of pellet preparation. This is a brief summary of a sample preparation method typical of procedures using alkali halide pressed pellets (White and Roth, 1986).

Specific surface area

The method used to determine SSA has previously been described in detail. It is important to emphasize that the choice of the EGME method for iron oxides is because the required dehydration process for the BET method transforms the iron oxide, for example transforming ferrihydrite to hematite. SSA results will yield an indication of the mineral type present. For example if SSA values are in the range of 20 m^2/g the iron oxide is probably either hematite or goethite and certainly not ferrihydrite. Each of these methods have been applied to characterize the eight most common iron oxide minerals presented in Table 3.2.1. From this characterization work selected criteria used for the identification of iron oxide are presented in Table 3.5.1. In many cases more than one criterion is required to identify the predominant iron oxide mineral.

Table 3.5.1 Selected criteria for iron oxides (adopted from Schwertmann & Cornell, 1991).

Mineral Name	Color (Munsell)	Most intense XRD spacings, (nm)	SSA (m^2/g)	Crystal shape	IR bands (cm^{-1})
Hematite	5R-2.5YR	0.270, 0.368, 0.252	20-30	hexagonal plates	345, 470, 540
Maghemite	Chocolate	0.252, 0.295	80-130	cubes	400, 450, 570
Magnetite	Black	0.253, 0.297	~4	cubes	400, 590
Goethite	7.5YR-10YR	0.418, 0.245, 0.269	20-40	elongated needles	890, 797
Lepidocrocite	5YR-7.5YR	0.626, 0.329, 0.247, 0.1937	70-80	lath	1026, 1161, 753
Ferrihydrite[1]	5YR-7.5YR	0.254, 0.224, 0.197,0.173, 0.147	180-300	hexagonal plates	- - - -
Feroxyhyte	5YR-7.5YR	0.254, 0.222, 0.169, 0.147	190-210	fibers, needles	1110, 920, 790, 670
Akaganeite	5YR-7.5YR	0.333, 0.255, 0.747	~30	elongated rods	

[1]: Poorly ordered hexagonal plates for shape.

3.6 Characterization results of OCS

Characterization of OCS was also carried out for OCS media used in columns simulations. The OCS characterized was produced based on the batch procedure provided in Table 3.4.1. Earlier batches were also characterized however because of the instability of the coatings these were not used in column simulations and for brevity they are not discussed. The characterization results for the OCS used in the column simulations are presented in Table 3.6.1.

Table 3.6.1 Characterization results from OCS coatings used for column simulations.

Color observed	Most intense XRD spacings (nm)	OCS SSA (m^2/g)	coating SSA (m^2/g)	Crystal shape (SEM)	IR bands (cm^{-1})
deep brown, some red	0.252, 0.270, 0.170, 0.368, 0.334, 0.149, 0.221, 0.145, 0.184	3.4-9.0	79.8	poorly-ordered and hexagonal plates,	1384, 1121, 1043, 550

These results are compared to criteria presented in Table 3.5.1 and Table 3.2.1. The color results indicate the presence of ferrihydrite from the brown color and some hematite from the red tint. ***Color analysis indicates the presence of ferrihydrite and to some degree hematite.*** The SEM analysis was used to identify the presence of amorphous ferrihydrite. ***SEM analysis indicates the presence of mainly ferrihydrite with some hematite present as indicated by the poorly-ordered plate morphology and hexagonal plates visible from the scans.*** XRD analysis was used to distinguish between the crystalline minerals of iron oxide present, although amorphous ferrihydrite and feroxyhyte can also be detected. XRD d-spacings are in order from most intense to least intense in Table 3.6.1. All of the d-spacing for hematite are present. The 0.170, 0.149 and 0.145 d-spacings are indicative of ferrihydrite. The 0.334 spacing is indicative of akaganeite. The 0.221 spacing is indicative of feroxyhyte. The 0.184 d-spacing indicates lepidocrocite. XRD results are plotted in Figure 3.6.1. ***XRD analysis indicates the potential presence of hematite, ferrihydrite, feroxyhyte, akaganeite and lepidocrocite.***

IR spectroscopy indicates the presence of NO_3^- at a frequency wavenumber of 1384. A wavenumber of 1121 is indicative of feroxyhyte. A wavenumber of 1046 is probably indicative of lepidocrocite. A wavenumber of 548 is indicative of hematite. No reference wavenumbers were found in the literature for ferrihydrite IR results are plotted in Figure 3.6.2. ***IR analysis indicates the potential presence of hematite, feroxyhyte and lepidocrocite.*** It is difficult to use the results of the SSA analysis for the coating to yield a definitive indication of the iron oxide form present. An SSA value of 79.8 could represent a wide variety of SSA combinations since there are likely several iron oxide forms present. ***SSA analysis is inconclusive in determining the iron oxide forms present.***

Summary of OCS analysis

A synthesis of these results indicates that ferrihydrite is present to the greatest extent with traces of hematite and feroxyhyte also present. SEM analysis was carried out for 12 OCS grains. During the SEM analysis a visual determination of the percentage of amorphous areas of ferrihydrite on each OCS grain was made. This visual classification indicated that approximately 80% of the iron oxide coating was ferrihydrite. XRD and IR analysis indicate the remaining portion is composed of mainly hematite; with feroxyhyte and lepidocrocite present to a lesser extent. Trace amounts of akaganeite were also measured due to residual contamination of laboratory equipment from previous OCS batches made from FC solution.

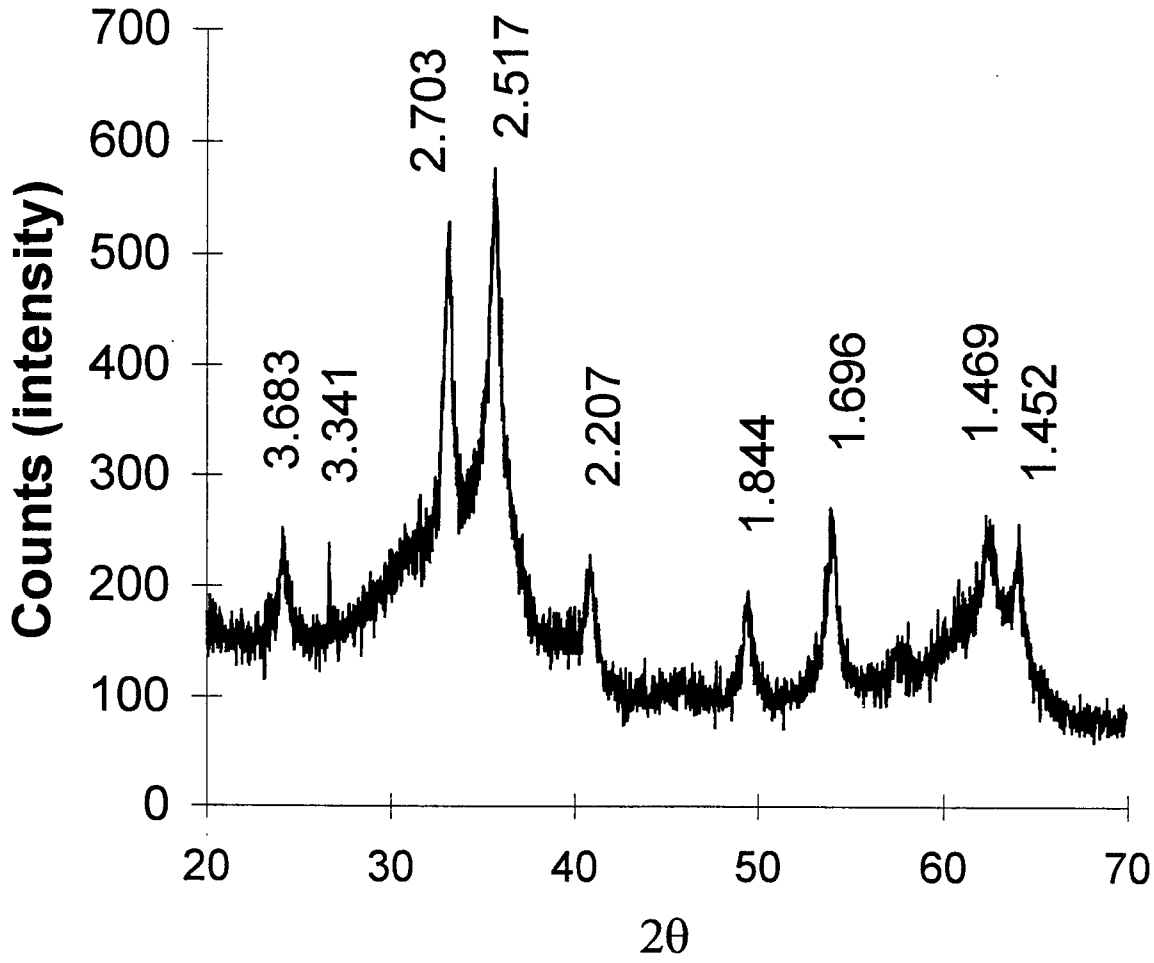

Figure 3.6.1. XRD analysis of IOCS used in column simulations.

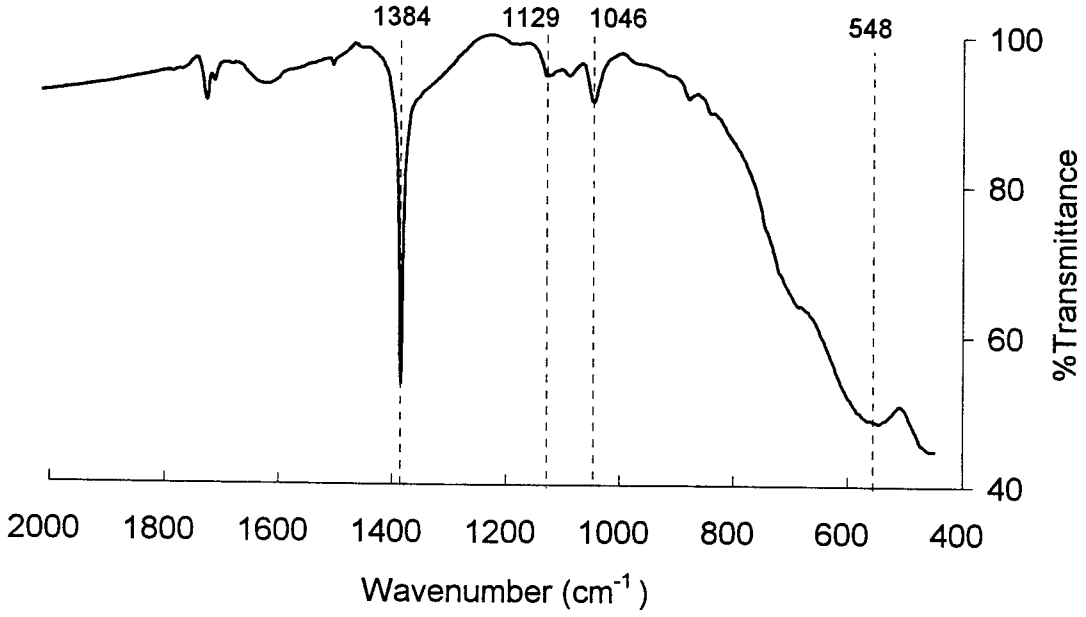

Figure 3.6.2. FTIR analysis of IOCS used in column simulations.

3.7 Characterization of silica sand and GAC media

In addition to OCS, silica sand and GAC were used as porous media in column simulations. Both were used as control media in the column simulations. Silica sand was used in order that the difference between plain silica sand and iron oxide coated silica sand (OCS) could be evaluated. GAC was used as control to evaluate its capacity with respect to OCS.

Ottawa 2030 is a commercially available silica sand. Ottawa 2030 is also a commonly used research product. Other researchers have used this sand for coating with iron oxide (Stenkamp and Benjamin, 1994). This sand is also used as a laboratory-scale surrogate for clean, natural sand deposits requiring stabilization using injection grouting techniques. A chemical analysis of Ottawa 2030 was provided by U.S. Silica, Ottawa, Illinois. Before cleaning, tumbling and washing the sand as previously described, the sand was mechanically sieved through the #20 and #40 sieves. Any material retained on the #20 sieve was discarded and any material passing the #40 was also discarded. On a mass basis, the material discarded represented less than 1% of the batch of sand sieved.

Chemical analysis of Ottawa 2030	
SiO_2	99.800%
Fe_2O_3	0.020%
Al_2O_3	0.050%
TiO_2	0.020%
CaO	<0.010%
MgO	<0.010%
Volatile organics	0.090%

The GAC used was Filtersorb 400 (F 400) from the Calgon Carbon Corporation, Pittsburgh, Pa. No preparation of GAC was carried out. Once the F400 was packed into the column, the column was flushed with DI water until the effluent was clear of any GAC fines. A summary of silica sand and GAC characteristics is presented in Table 3.6.1.

Table 3.7.1 GAC and silica sand porous media characteristics

	Particle Size (mm)	Specific gravity [1] (g/cm^3)	SSA [2] (m^2/g)	Internal pore volume (cm^3/g)	pH at PZC
Silica sand (Ottawa 2030)	0.42-0.84	2.63 (2.65 reported)	0.04-0.10	~0	(2-3)[3]
GAC (F 400)	0.55-0.75	1.8	1120-1250	0.85-0.95	(10.2-10.4)[4]

[1]: ASTM method D 421
[2]: EGME method
[3]: McBride, 1986
[4]: Sontheimer et al., 1988; Corapcioglu and Huang, 1987

BENCH-SCALE COLUMN SIMULATIONS

4.1 Introduction

In order to experimentally simulate the behavior of a PET subject to stormwater loadings containing metal elements, bench-scale column experiments were carried out. These column experiments were designed to evaluate the breakthrough behavior and capacity of OCS, silica sand and GAC. Initially, using DI water and the metal elements of Zn, Cd, Cu and Pb each run separately, breakthrough was evaluated. Later, combinations of these metals were run in DI water to evaluate competitive breakthrough. Finally, actual stormwater spiked with elevated concentrations of Zn, Cd, Cu, and Pb was run to evaluate particulate-bound and dissolved metal element breakthrough. Bench-scale column design and operation was based on experimental layouts from previous column studies and measured field parameters.

4.2 Background

The geochemical transport and eventual fate of a majority of reactive substances, including metal elements, is controlled by the reaction of these substances with solid surfaces. The solid-liquid interface of these solids, are a reservoir for reactive substances, which are characterized by large surface area to solid volume ratios (Stumm, 1992). The surfaces of natural, synthetic iron oxides and OCS serve as reservoirs for reactive substances, specifically metal elements in these experiments. These surfaces could be solids surfaces in an aqueous suspension or solids surfaces which are part of a fixed porous matrix. Examples of the former include oceans, rivers, lakes and experimental systems such as CSTRs, while examples of the latter include soils, porous rocks and experimental systems such as media-packed columns. The focus of this chapter is the OCS surface as a reservoir for Zn, Cd, Pb and Cu in a surrounding aqueous solution.

Surface complexation types

Iron oxide surfaces can be conceptualized as a surface of inorganic polymers having extending structures containing surface functional groups. In the presence of water these oxide surfaces are generally covered with surface hydroxyl groups, protons and coordinated water molecules. These surface functional groups provide a variety of interactions with the metal elements and ligands in the surrounding solution through the formation of coordinative bonds. These interactions are collectively categorized as surface coordination or surface complexation. There are three basic metal element sorption complexation types at an oxide-water interface (Stumm, 1992):

(1) Outer-sphere complexes
(2) Inner-sphere complexes
(3) Surface precipitates

Outer-sphere complexes bond the metal ion in solution, through coordinated water molecules, to the oxide surface in a monolayer. Inner sphere complexes bond metal ions in solution, directly to the oxide surface in a monolayer. Inner sphere complexes are developed when a largely covalent bond is formed between the metal ion and the electron donating surface oxygen ion (Stumm, 1992). Inner sphere complexes can be monodentate or bidentate surface complexes. Surface

precipitates bond directly to the oxide surface and surrounding complexed metal ions in multiple layers extending from the oxide surface.

Complexation reactions

The formation of surface complexes of metal ions (cations) by hydrated iron oxides involves the coordination of the metal ions with surface hydroxyl oxygen atoms. This coordination also involves the release of protons from the hydroxyl surface. These protons are reversibly bound and the partitioning between the surface and aqueous solution is primarily controlled by solution pH. However, sorption of other species including metal elements can also influence the surface proton and hydroxyl ion condition by altering the interfacial charge and potential. For a number of iron oxide minerals including ferrihydrite the surface proton density has been measured at 1.0 ± 0.1 protons per surface site over a pH range extending ± 3 units from the point of zero charge (Benjamin & Leckie, 1981).

Experimental studies of adsorption stoichiometry have indicated that more than one proton is released to solution per metal ion adsorbed. A number of bonding reactions have been postulated to explain these results (Benjamin & Leckie, 1981; Stumm, 1992).

$$2\text{S-OH} + \text{Me}^{2+} \leftrightarrow (\text{S-O})_2\text{Me} + 2\text{H}^+ \quad (4.2.1)$$

$$\text{S-OH} + \text{Me}^{2+} + \text{H}_2\text{O} \leftrightarrow \text{S-OMeOH} + 2\text{H}^+ \quad (4.2.2)$$

$$\text{Me}^{2+} + \text{S-OH}_x \leftrightarrow \text{S-OMe} + x\text{H}^+ \quad (4.2.3)$$

$$\text{Me}^{2+} + \text{H}_2\text{O} + \text{S-OH}_y \leftrightarrow \text{S-OMeOH} + (y+1)\text{H}^+ \quad (4.2.4)$$

$$\text{S-OH} + \text{Me}^{2+} \leftrightarrow \text{S-OMe}^+ + \text{H}^+ \quad (4.2.5)$$

$$(\text{S-OH})_2 + \text{Me}^{2+} + \text{H}_2\text{O} \leftrightarrow (\text{S-O})_2\text{-MeOH} + 3\text{H}^+ \quad (4.2.6)$$

where:

S:	oxide surface
S-OH:	hydroxyl group bonded to oxide surface
Me^{2+}:	metal ion (Zn^{2+}, Cd^{2+}, Pb^{2+}, Cu^{2+})
$(S\text{-}O)_2Me$:	bidentate surface complex
S-OMe:	monodentate surface complex

Reaction (4.2.1) indicates a bidentate bonding where the metal ion is bonded to 2 hydroxyl sites and consequently 2 protons are released. Reaction (4.2.2) is a simultaneous sorption and hydrolysis reaction where the metal ion is bonded to a single hydroxyl site. Because of the hydrolysis a total of two protons are released by this reaction. Both of these reactions assume that all oxides surface sites where bonding can occur are similar; their energies, acidities and bonding affinities are identical.

Reactions (4.2.3) and (4.2.4) represent reactions where the release of more or less than 1 proton per metal ion sorbed may be explained by preferential sorption of the metal ion to sites of differing acidity or proton density than the "average" site. These oxides surfaces have a variety of site types, each of differing affinities for metal ions and protons. These differing affinities may also result in a preference for one metal ion over another under competitive conditions.

Reaction (4.2.5) indicates monodentate bonding where the metal ion is bonded to a single hydroxyl sites and consequently 1 proton is released. Reaction (4.2.6) involves multiple hydrolysis and multidentate bonding resulting in the release of 3 protons.

To verify these postulated reactions, the number of protons released when metal ions are sorbed to ferrihydrite have been measured for Zn, Cd, Pb and Cu (Benjamin & Leckie, 1981). For Cd, Pb and Cu between 1.5 and 2.0 protons are released on average for each metal ion sorbed. However, for Zn, 3.2 protons were released for each Zn ion sorbed. This indicates there may be a difference in the reaction by which Zn is sorbed as compared to Cd, Pb or Cu. Zn sorption may follow the reaction shown in (4.2.6) while Cd, Pb and Cu may follow reactions shown in (4.2.3) or (4.2.4).

Influence of pH on sorption

The sorption of a metal ion to the hydrous iron oxide surface including ferrihydrite is strongly pH dependent. For cations, sorption increases with pH and the fraction of a cation sorbed increases from 0 to 1 over a narrow pH range, usually 2 pH units. This range varies depending on the metal element. For Pb^{2+} the pH range is form 3 to 5.5, for Cu^{2+} the range is from 4 to 6.5, for Cd^{2+} the pH range is from 5 to 7.5 and for Zn^{2+} the pH range is from 5.5 to 7.5. For all of these metal elements the lower pH values represents 0% sorbed while the upper pH value represents 100% sorbed. Because the onset of metal ion sorption and the beginning of metal hydroxide precipitation is often not separated by a wide pH margin, the sorption-nucleation-precipitation sequence is rarely resolved into discrete processes as evidenced by clear changes in the sorption curves (McBride, 1994). Sorption of anions is greatest at low pH and decreases gradually as pH increases (Dzombak & Morel, 1990). The net surface charge of the hydrous iron oxide is strongly pH dependent.

Oxides and hydroxides of Fe, Al, Mn and Si possess little or no permanent surface charge, excepting cases of isomorphic substitution, and generate cation and anion exchange capacity (CEC and AEC) through surface protons and hydroxyl ions. These mineral surfaces are amphoteric and both protons and hydroxyl ions coexist at the oxide surface in relative populations determined by solution pH. An electrically neutral surface would be one where an equal population of protons and hydroxyl ions exist. This amphoteric behavior leads to the definition of the point of zero charge (PZC). The PZC in its most simple definition is the pH at which the net surface charge is zero. Alternately, the PZC is the pH at which the surface negative charge (CEC) equals the surface positive charge (AEC) (McBride, 1994).

Therefore for iron oxides which have a PZC between 7 and 8, a solution pH of 8 or greater would indicate the predominance of surface bonding sites would be negatively charged and available as metal ion (cation) bonding sites. On the other hand, a solution pH of less than 7 would indicate the predominance of surface bonding sites would be positively charged and not available as metal ion bonding sites. The bonding of metal ions to the oxide surface will alter the PZC. Sorbed metal ions will increase the surface positive charge and shift the PZC higher, limiting further sorption of metal ions at the same solution pH. Likewise, sorbed anions will increase the surface negative charge and shift the PZC lower.

Competitive sorption of metal elements

Under conditions where a number of metal elements are present in solution the competitive order of sorption has been explained using covalent theory, electrostatics or the tendency of a metal element to undergo hydrolysis followed by sorption. Electronegativity is an important factor in determining which metal element will complex to an iron oxide surface with the highest preference. The more electronegative metal elements would form the strongest covalent bonds with the oxygen atoms of the surface hydroxy groups. According to covalent theory, for divalent metal ions, the predicted order of bonding preference would be (McBride, 1994):

$$Cu > Ni > Co > Pb > Cd > Zn > Mg > Sr \qquad (4.2.7)$$

However, on the basis of electrostatics, the bonding preference would be for the metals with the greatest charge-to-radius ratio. This would produce a different order of preference for this group of divalent metals (McBride, 1994):

$$Ni > Mg > Cu > Co > Zn > Cd > Sr > Pb \qquad (4.2.8)$$

Electrostatics would also predict that trivalent metal ions such as Cr^{3+} would have a greater bonding preference to all divalent metal ions. Based on the tendency to hydrolyze, the bonding preference of selected metal ions to iron oxides would be (McKenzie, 1980):

$$Pb > Cu > Zn > Co > Ni > Cd > Mn \qquad (4.2.9)$$

The reaction of hydrolysis and sorption would be of the same form as either reaction (4.2.4) or (4.2.6).

4.3 Previous Studies

Bench-scale column experiments are utilized to experimentally simulate the fate and transport of contaminants in both natural and engineered systems. Bench-scale columns experiments for engineered systems are used to assess potential behavior of the prototype system under a variety of simulated conditions and the potential capacity of the system for specific contaminants.

A review of the recent literature has documented the viability of bench-scale column experiments for simulating the mobility of contaminants in natural systems such as groundwater. The fate and transport of orthophosphate in groundwater was experimentally simulated using column experiments (Isenbeck-Schroter et al., 1993). Acrylic columns of 44 mm diameter and 500 mm length were packed with aquifer sand and injected with actual orthophosphate-contaminated groundwater. Results of this study indicated that simulated transport of orthophosphate was retarded by both sorption and precipitation for the simulated geochemical conditions and aquifer sand.

The fate and transport of arsenate and arsenite in acidic groundwater was simulated using column experiments (Isenbeck-Schroter et al. 1994). Acrylic columns of 50 mm diameter and 250 mm length were packed with silica sand and injected with arsenic contaminated water composed to simulate the groundwater geochemistry. Results of this study indicated that arsenite breakthrough was much more rapid than arsenate and therefore posed a greater risk for groundwater contamination exposure.

The fate and transport of Cd and Cu in groundwater was simulated using column experiments (Hamer et al., 1994). Acrylic columns of 50 mm diameter and 460 mm length were packed with silica sand and calcite and injected with Cd and Cu contaminated water composed to simulate the groundwater geochemistry. Results of the study indicate Cd mobility was retarded by sorption and recrystallation towards a CdCa-carbonate while Cu mobility was retarded by sorption and precipitation.

A review of the literature has also documented the viability of bench-scale column experiments for simulating the immobilization and eventual breakthrough of contaminants in engineered systems. The immobilization of Pb and Pb-complexes by GAC was experimentally simulated using 29 mm diameter by 381 mm acrylic columns (Reed et al., 1994). The columns were injected with a synthetic wastewater of pH 4 and 5.4 containing either Pb or Pb-complexes, at a flow rate of 40 mL/min, with an empty bed contact time (EBCT) of 1.5 minutes. Results indicated that Pb immobilization was significant due to both adsorption and precipitation while Pb-complex immobilization was considerably weaker.

The immobilization of Pb, Cu, Ni and Cd and ammonia complexes of these metals by OCS (iron-oxide coated Ottawa 2030 sand) packed columns was experimentally simulated using 20 mm diameter by 150 mm acrylic columns with a porosity of 0.33 (Edwards and Benjamin, 1989). The columns with an EBCT of 5 minutes were injected with a synthetic wastewater containing a single metal or metal-complex for a pH range from 8 to 10. Uncoated Ottawa 2030 silica sand was used as experimental control. Results indicated that OCS was significantly more effective than silica sand for immobilizing Pb, Cu, Ni and Cd as well as ammonia complexes of these metals.

The feasibility of treatment of metal-bearing wastewater from a Superfund site containing Pb, Cu and Cd was experimentally simulated using 18 mm diameter by 880 mm acrylic columns packed with OCS with EBCT ranging from 1 to 4 minutes (Benjamin and Sletten, 1993). The columns were injected with simulated and actual metal-bearing wastewater. Both individual metals and individual metal-complexes were injected into the columns as well as actual metal bearing wastewater. pH values varied from 6.0 to 9.0. For all individual uncomplexed metals, results indicated that as the pH increased from 6.0 to 9.0, the number of pore volumes required for breakthrough increased from 300 to over 1600, for a given EBCT. For the case of uncomplexed Pb, Cu and Cd, mainly particulate-bound, run simultaneously each at 5000 ug/L, a pH of 9.0 and EBCT of 2 minutes, breakthrough was essentially simultaneous for all metals around 700 pore volumes. In a similar case, except with metal concentrations of 500 ug/L, the Cd breakthrough curve could be observed to occur before Pb or Cu, around 7000 pore volumes. The run was terminated at 7000 pore volumes although Pb and Cu breakthrough were less than 50% of influent values.

Cu and Cd ammonia complexes were also effectively immobilized by the OCS. When run simultaneously at 5000 ug/L, a pH of 10.0 and EBCT of 2 minutes, both Cd and Cu breakthrough occurred at 1200 pore volumes. In comparison, EDTA-complexed Pb, Cd and Cu run simultaneously at 5000 ug/L, a pH of 10.0 and EBCT of 2 minutes, breakthrough occurred within 100 pore volumes. In this study OCS packed columns were successfully regenerated by

circulating a pH 2.0 solution through the column for 2 hours. The OCS columns were subsequently pH re-conditioned and ready for operation again.

4.4 Experimental column configuration

The main component of the experimental configuration was two acrylic columns run simultaneously in parallel. A schematic diagram of the experimental setup is illustrated in Figure 4.4.1. Each column had a diameter of 38.1 mm (ID) and 612 mm length. Each column was packed with porous media for the full 612 mm length. The column diameter of 38.1 mm ID (1.5") was based on maintaining a column diameter to media diameter ratio (D/d) greater than 50 (Lang, et. al., 1993). Other researchers suggest that D/d ratios as low as 12 may be used without introducing significant influence on axial velocity profiles and wall skin friction in laboratory columns (Chellam and Wiesner,1993). The GAC media used in this study had an effective size range from 0.55 to 0.75 mm while the silica sand (Ottawa 2030) had a size range from .425 mm to .85 mm. Minimizing column diameter was important in reducing the amount of influent which had to be prepared or stormwater which had to be transported to the laboratory.

Influent feed to the columns was supplied by use of a variable-flow digital drive, peristaltic pump heads and pump controller. This drive and pump configuration was capable of delivering flow rates of 0.006 to 2300 mL/minute with a digital drive control of 0.1% however the tubing restricted the actual flow rates to between 10 and 1000 mL/minute. Peristaltic pump feed lines were 4.8 mm ID flexible Viton tubing and transported influent feed from a 20 L continuously-stirred tank (CST) to the columns. Once the pumps and controller were calibrated, column runs were initiated, terminated and monitored through a computer interface to the controller.

Effluent manifold lines from each columns were 4.0 mm ID Teflon PFA (perfluoroalkoxy). Peristaltic effluent sampling pumps were tapped into each column manifold line through 4.8 mm ID flexible Viton tubing. The effluent sampling pumps were fixed-flow pump drives and sampled at a flow rate of 50 mL/minute. Effluent sampling pumps were controlled by microprocessor-based pump controllers. There was a total of 8 sampling pumps each with two peristaltic pump heads in parallel. Sampling of both columns was simultaneous. Pump controllers were programmed to sample both columns every three hours. The sampling duration was 2 minutes. Effluent sample bottles were 125 mL wide-mouth straight-sided Teflon PFA. Each sample bottle lid was fitted with a Teflon hose-barb to accept the effluent pump tubing. Influent samples were withdrawn directly from the CST by either manual turning on a sampling pump or connecting this pump to the controllers.

After sampling, effluent discharges from each column were directed into fixed-bed reactor tanks to remove any metal elements which had broken through the columns. These 10 L upflow tanks contained a 10 cm layer of crushed limestone and NaOH pellets covered by a 15 cm layer of GAC and topped by a 15 cm layer of OCS. Effluent from these tanks was sampled and analyzed as columns approached breakthrough to ensure metal elements were not discharged to the drains.

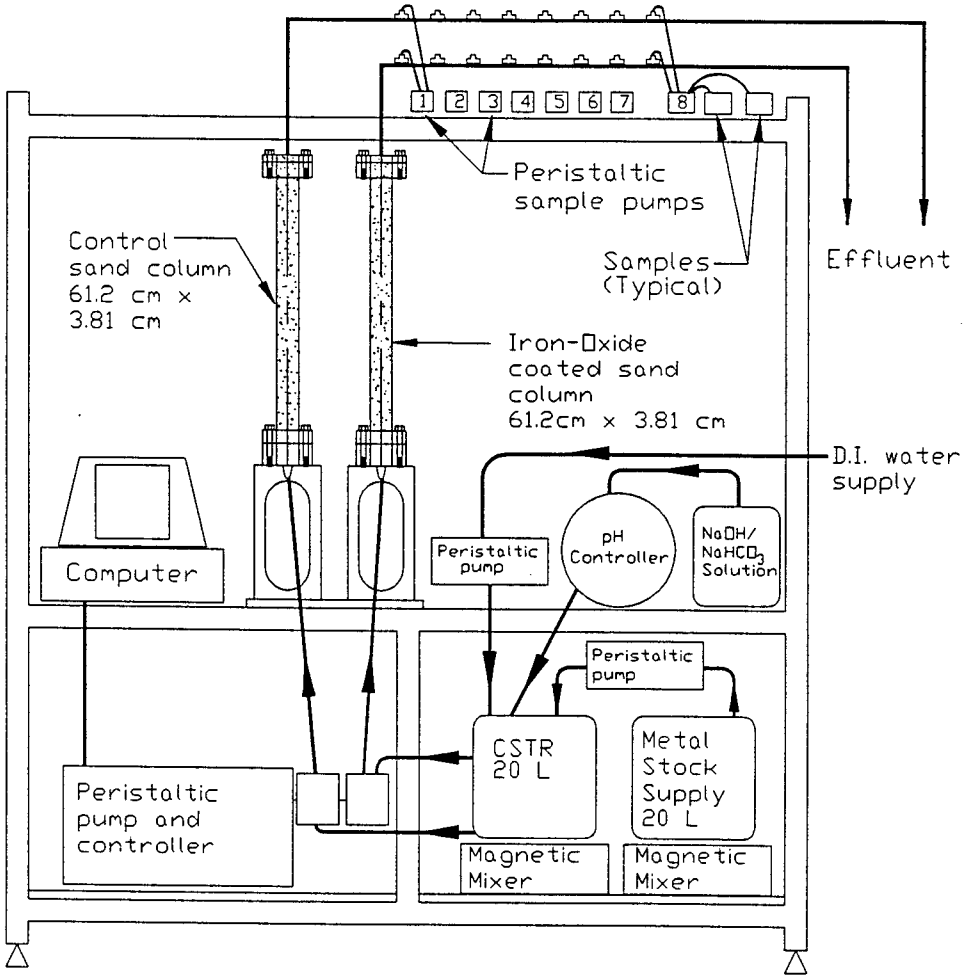

Figure 4.4.1 Schematic of bench scale column experimental configuration (NTS).

The CST was supplied by either DI water or stormwater, metal stock solution and pH and buffer solution. The CST was a 20 L fluorinated HDPE carboy. The liquid volume was fixed between 10 to 12 L and kept completely mixed by a magnetic stirrer and a 7.6 cm stir bar. CST sampling, pH measurement and influent intake were made at the mid-depth of CST liquid volume. Metal stock solution was supplied to the CST by use of a variable-flow analog drive and peristaltic pump head through 1.6 mm ID flexible Viton tubing. This drive and pump configuration was capable of delivering flow rates of 0.006 to 380 mL/minute with an analog drive control of 0.1%, however the small tubing restricted flow rates to between 1.3 to 130 mL/min. DI water or stormwater was supplied to the CST by use of a variable-flow analog drive and peristaltic pump head through 4.8 mm ID flexible Viton tubing. This drive and pump configuration was capable of delivering flow rates of 0.006 to 2300 mL/minute with an analog drive control of 0.1%, however the tubing restricted flow rates to between 10 to 1000 mL/min. DI water or stormwater was stored in separate 210 L polypropylene closed-dome tanks.

pH in the CST was moderated by a pH controller. The resolution of the controller was 0.1 pH units with an accuracy of ± 0.1 pH units. The controller integrated a variable-flow metering pump and proportional output programming to allow pH solution pumping to decrease proportionally until the pH set point is reached. The reservoir was a stirred 2L glass beaker.

4.5 Influent DI water and stormwater

All experimental column simulations utilized a synthetic stormwater spiked with metal elements with the exception of one simulation which utilized actual stormwater generated from a rainfall-runoff event. DI water from the Rhodes Hall DI system was polished using two ion-exchange cartridges in series, followed by a GAC adsorber cartridge with a 0.45 um in-line filter. This DI water was then pumped on demand into a 210 L polypropylene storage tank for use as influent DI water. Approximately every 1000 L cartridges were exhausted, as observed by color change, and replaced. Table 4.5.1 presents characteristics of the polished DI water.

Table 4.5.1
Characteristics of polished DI water used in column experiments

Conductivity (uS/cm)	TDS [ppm]	TOC [mg/L]	Chlorine [mg/L]	pH	ORP (mV)	Ca, Mg, Na, Fe, Mn, Al, Ni, Cr, Zn, Cu, Cd, Pb
1 - 2	< 1	- - - -	0.2-0.4	6.7-6.9	+300-350	below ICP-AES MDL

To simulate the performance of the PET subject to actual stormwater loadings, column runs were performed using urban roadway stormwater transported from the experimental site. Stormwater from an 18 June 1996 rainfall-runoff event was collected in a 2000 L holding tank at the experimental site on I-75. At the end of the event, 1500 L of the stormwater was transported in a HDPE tank to the Environmental Hydrology laboratory for use as influent for column runs. A mechanical paddle stirrer kept the stormwater influent mixed until the column runs were terminated. The water quality characteristics of the 1500 L of well-mixed stormwater are presented in Table 4.5.2. The measurements were made at the beginning of the column run on 18

June 1996. It should be noted that the dissolved values presented are lower than dissolved EMC values for rainfall-runoff events at the experimental site. This is attributed to the high pH in the runoff as well adsorption loss to the HDPE field tank, transport tank and laboratory tank.

Table 4.5.2
Water quality characteristics of stormwater influent at beginning of column run

pH	ORP (mV)	Temp. (°C)	Cond. (mS/cm)	Alkalinity mg $CaCO_3$/L	TSS [mg/L]	VSS [mg/L]	TDS [mg/L]	VDS [mg/L]
7.28	+236	23.2	31	20	137	47	93	40

Metal element concentrations of stormwater influent at beginning of column run

	Zn	Cd	Cu	Pb	Ni	Mn	Fe	Cr	Al	Mg	Ca	Na
dissolved	523	<2	30	23	12	121	35	36	268	1469	15369	8727
particulate	748	17	183	355	114	24	999	3	2738	2346	27429	12541
All values represent the arithmetic mean of 3 replicates in [ug/L]												

4.6 Metal stock solution

Based on rainfall-runoff, snowmelt characterization and USEPA-OEPA discharge criteria Zn, Cu, Cd and Pb were metal elements chosen for the experimental column simulations. Influent metal stock solution was prepared from Certified A.C.S. grade metal salts for each of these metal elements and maintained completely mixed at a pH of 2.5 to 3 in the 20L fluorinated HDPE metal stock reservoir during each column run. Depending on the influent concentration desired, metal stock was prepared at 25, 125 or 250 mg/L. Metal stock solutions were injected into the 20L CST and mixed with either DI water or actual stormwater depending on the column run. Table 4.6.1 presents characteristics of the metal salts used and the prepared metal stock solutions.

Table 4.6.1
Characteristics of metal salts and metal stock solutions used in column experiments

	Zinc Chloride Anhydrous	Cupric Chloride	Cadmium Chloride Anhydrous	Lead Nitrate Anhydrous
Formula [1]	$ZnCl_2$	$CuCl_2 \cdot 2H_2O$	$CdCl_2$	$Pb(NO_3)_2$
Formula weight	136.28	170.48	183.31	331.20
Acidification [2]	HCl	HCl	HCl	HNO_3
Metal stock pH	2.5 - 3.0	2.2 - 2.5	2.5 - 3.0	2.0 - 2.3
Conc. [mg/L]	250	25, 125	25	25, 125
1: Metal salts are Certified ACS grade				
2: Acids are Trace-metal grade				

4.7 Flow rates and flow regime

The influent flow rate to both columns was 50 mL/minute for all experimental runs Flow was volumetrically calibrated daily and any measured variance was less than ± 2 mL/minute. Metal stock inflow to the CST was calibrated for either 2.0 or 4.0 mL/minute and influent DI water flow to the CST was calibrated to 98 or 96 mL/minute, respectively. Flow rates were calibrated twice a day and CST liquid volume was kept between 10 and 12 L. The flow regime was characterized by the Reynolds number as defined in equation 4.7.1. These numbers are tabulated in Table 4.7.1 .

$$\mathrm{Re}_d = \frac{\rho_w V d_{50}}{\mu} \tag{4.7.1}$$

Table 4.7.1
Reynolds numbers and EBCT for flow rate and porous media

	Silica sand (Ottawa 2030)	OCS	GAC (F-400)	BSPET
Flow rate (cm^3/min)	50	50	50	50
$V_{superficial}$ (cm/min.)	4.39	4.39	4.39	4.39
media d_{50} (mm)	0.5	0.5	.65	.5
porosity	0.35	0.37	0.73	.39
Re_d	3.6	3.6	4.7	3.6
Flow regime	turbulent	turbulent	turbulent	turbulent
EBCT (min.)	4.4	4.5	8.1	4.6
T : temperature = 20 °C μ : dynamic viscosity = 1.009×10^{-2} g/(cm-sec) ρ_w : density of water = 0.998 g/cm^3 spherical particles				

The flow rate of 50 mL/minute was determined using the peak flow from the measured washoff hydrographs at the experimental site, the pavement drainage area and the design infiltration surface area of a field-scale PET. The conversion from measured LPF in the field to a bench-scale column was calculated as follows. Applying the 15 L/min-m design inflow with a design PET width of 0.3048 m (1.0') equates to a lateral pavement sheet flow loading rate of 49.2 L/min-m^2. The bench-scale columns had a cross-sectional area of 11.4 cm^2. The equivalent loading rate at laboratory bench-scale, using a column cross-sectional area of 11.4 cm^2, required an equivalent loading rate at laboratory scale of 56 mL/minute. A loading rate of 50 mL/minute was used for all bench-scale column runs.

The decision to utilize a peak flow typical of a hydrograph from a moderately high intensity rainfall-runoff event will under-estimate PET breakthrough capacity. This has been shown at the bench-scale level for OCS columns for separate runs of Cd and Cu at influent

concentrations of 500 ug/L (Benjamin and Sletten, 1993). Other bench-scale results using columns packed with GAC and wastewater influent improved breakthrough capacity when hydraulic loading rates were lowered from 4 gpm/ft^2 to 2 gpm/ft^2 (Reed, et. al, 1996)

4.8 Experimental column run matrix

Column runs were carried out with a single metal element and later with a combination of metal elements. Individual metal elements runs were conducted to assess individual metal element breakthrough as a baseline comparison to multiple metal element competitive breakthrough. Metal element concentrations utilized in each run were chosen based on the following criteria.

Metal element concentration criteria

1. Concentration of Zn were based on runoff characterization data.
2. Concentration of Pb was based on snow washoff characterization data.
3. Concentration of Pb was also kept sufficiently above ICP-AES MDL
4. Concentration of Cu was based on snow washoff characterization data.
5. Concentration of Pb and Cu helped facilitate breakthrough in a reasonable time.
6. Concentration of Pb and Cu allowed comparison to recently published OCS work
7. Concentration of Cd, an order of magnitude higher than "first-flush" levels, permitted measurement of Cd sufficiently above ICP-AES detection limits.

The experimental matrix incorporated Zn, Cu, Cd and Pb run individually and in combination using a DI water matrix. For the stormwater matrix, the metal elements were run only as a combination. Each set of runs was carried out at two pH levels. A pH level of 6.5 was utilized as representative of measured pH washoff values obtained at the I-75 site. Experimental runs conducted at pH 6.5 were intended to simulate the PET performance without the pH elevation provided by the porous cementatious infiltration surface of the PET. A second set of experimental runs, conducted at pH 8.0, were intended to simulate the PET performance with the pH elevation provided by the porous cementatious infiltration surface.

The experimental matrix incorporated four porous media packing configurations. The first column configuration utilized uncoated silica sand (Ottawa 2030), packed for the entire column length, as experimental control. The second utilized iron-oxide coated sand (OCS) packed for the entire column length. The third utilized 8 cm of crushed cementatious porous pavement aggregate at the influent end with the balance of the 61.2 cm length packed with OCS and was designated BSPET. Flow infiltrating through the cementatious porous pavement block will increase in pH and alkalinity. The alkalinity increase produced by calcium hydroxide is capable of neutralizing influent acidity (Shively, et al, 1986). The porous pavement from which the aggregate was taken had an unconfined compressive strength of 2000 psi, indicating a relatively low cement content. The fourth configuration utilized GAC (F 400) packed for the entire column length. The experimental matrix is summarized in Table 4.8.1. EMC values measured at the experimental site are provided at the bottom of Table 4.8.1 for comparison.

Table 4.8.1
Experimental matrix for column runs

Runs	Influent						Column media			
	Cd [ug/L]	Cu [ug/L]	Pb [ug/L]	Zn [ug/L]	pH	Solute matrix	Silica sand	OCS	GAC	BSPET
Cd65-1	1000	----	----	----	6.5	DI water			----	----
Cd80-1	1000	----	----	----	8.0	DI water				----
Cu65-5	----	5000	----	----	6.5	DI water			----	----
Cu80-5	----	5000	----	----	8.0	DI water				----
Pb65-5	----	----	5000	----	6.5	DI water			----	----
Pb80-5	----	----	5000	----	8.0	DI water			----	----
Zn65-10	----	----	----	10000	6.5	DI water			----	----
Zn80-10	----	----	----	10000	8.0	DI water				----
Zpcc65-5	5000	5000	5000	5000	6.5	DI water				----
Zpcc80-5	5000	5000	5000	5000	8.0	DI water				----
Zpcc65-1	1000	1000	1000	10000	6.5	DI water	----	----		
Zpcc65-s	1000	1000	1000	10000	6.5	runoff				
site EMCs	12	135	68	4340	6.4	runoff	----	----	----	----

4.9 Experimental column run results

The results of the column runs are presented in terms of breakthrough curves. Column run results are presented in the order in which they appear in Table 4.8.1. Since pH is a major variable influencing the breakthrough behavior of each media, pH plots are presented with each breakthrough curve. Equally as important to metal element behavior is oxidation-reduction potential (ORP) measured as Eh. For all runs Eh values remained in a range between +100 to +300 mV. Eh values were tabulated along with pH values but not plotted.

Data points are shown on those plots where their inclusion does not impair the ability to compare and contrast data sets plotted on the same graph. Breakthrough curves are plotted as the ratio of measured effluent concentration to influent concentration as a function of pore volumes. The vertical concentration scale is consistent for all plots however pore volume scales varied because of variation in breakthrough performance.

To compare OCS capacities a breakthrough criterion of $C/C_0 \geq 0.90$ was chosen. 90 percent breakthrough was chosen because the slope of most breakthrough curves were still steep enough and monotonic that a clear determination of this point could be made.

4.10 Single metal element runs in DI water

Run Cd65-1 :

The single metal element solute in this run was Cd at a constant influent concentration of 1000 ug/L. The influent pH was held constant at 6.5. One column contained silica sand as a control media while the other column contained IOCS. For a DI water matrix with no solids, and no sulfur at a pH of 6.5 and Eh of +200 mV ± 50 mV, Cd is mainly present as Cd^{2+} (Brookins, 1988).

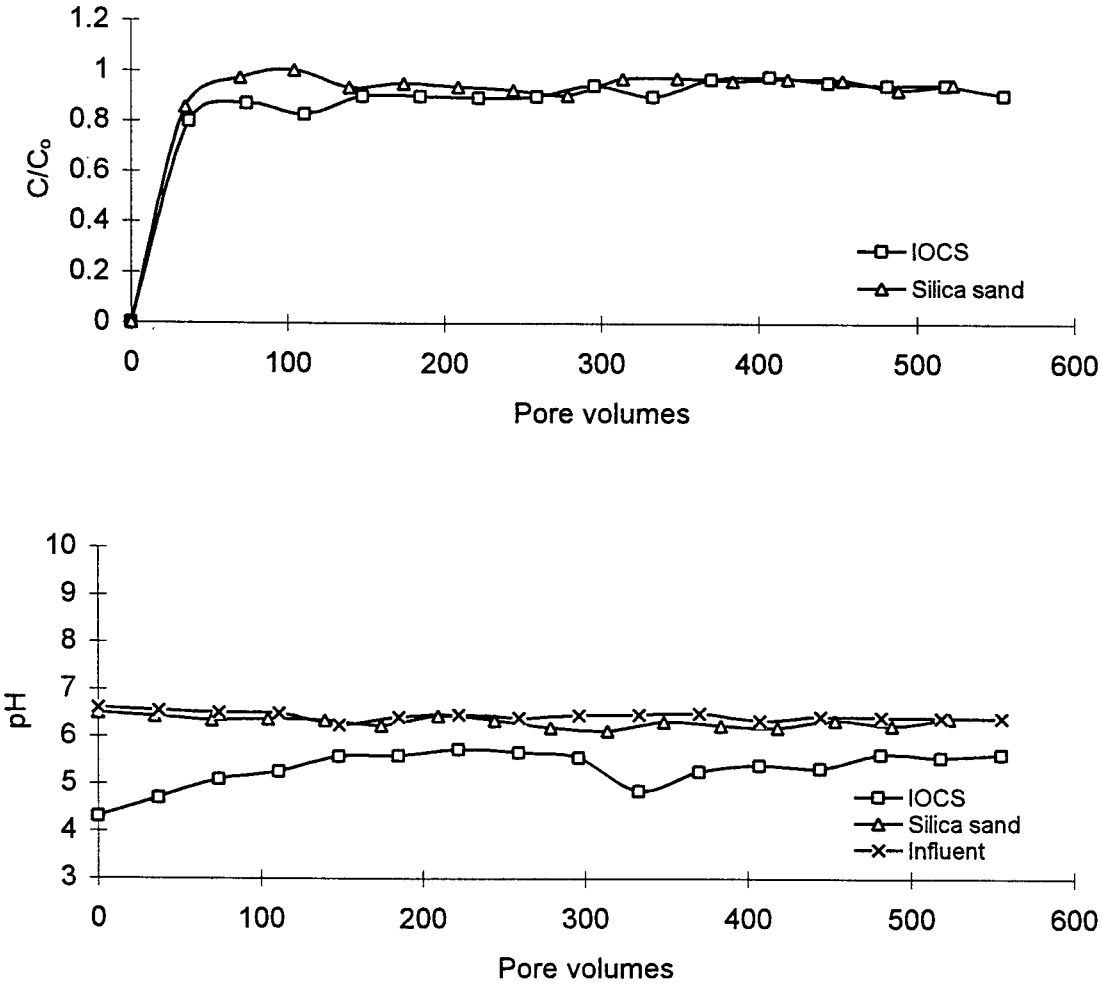

Figure 4.10.1 Breakthrough curves for Cd influent @ 1000 µg/L (DI @ pH 6.5).

The breakthrough curves presented in the upper plot of Figure 4.10.1 indicate the capacity of OCS at a pH of 6.5 is not significantly greater than silica sand used as control. Although OCS effluent concentrations were discernibly lower than silica sand up to 150 pore volumes, beyond 150 pore volumes the breakthrough behavior was identical for both. From 150 to 300 pore volumes C/C_0 remained approximately at 90% for both media. Beyond 300 pore volumes influent and effluent concentrations were essentially identical.

The pH profile is shown in the lower plot of Figure 4.10.1. The effluent pH from the silica sand column was equal to the influent concentration for the entire run. However, the effluent pH for the OCS column was clearly lower for the entire run. There are two potential explanations for this pH lowering. As breakthrough is approached the sorption of cations on iron oxides results in the release of protons. Proton exchange stoichiometries between 1.5 and 2.0 H^+ per M^{2+} sorbed have been measured (Dzombak & Morel, 1990). This phenomenon may partially explain the lower pH trend. Additionally, the surface acidity of the OCS may not have been fully neutralized as indicated by the consistently lower pH profile after breakthrough.

At a pH of 6.5 with an influent concentration of 1000 ug/L breakthrough occurred within 50 pore volumes (12.2L of influent) for silica sand and 148 pore volumes (38.2 L of influent) for OCS. However, at this pH, the capacity of both media was relatively small.

Run Cd80-1 :

This experimental run was the companion to Run Cd65-1. The single metal element solute in this run was Cd at a constant influent concentration of 1000 ug/L. The influent pH was held constant at 8.0. One column contained silica sand as a control media while the other column contained OCS. A column of GAC was also run for comparison to OCS. For a DI water matrix with no solids, at a pH of 8.0 and Eh of +200 mV ± 50 mV, Cd is mainly present as Cd^{2+} (Brookins, 1988).

The breakthrough curves presented in the upper plot of Figure 4.10.2 indicate the capacity of OCS at a pH of 8.0 is significantly greater than silica sand used as control and also much greater than GAC. Silica sand breakthrough at pH of 8.0 was not significantly different than silica sand breakthrough at pH = 6.5; 55 pore volumes compared to 50 pore volumes, respectively. For both silica sand and GAC the slopes of the breakthrough curves were steep and relatively uniform until approximately 90% of breakthrough was reached. The intensity of the GAC breakthrough was not as great as for silica sand.

In contrast, OCS 90% breakthrough occurred at 1900 pore volumes. The initiation of breakthrough for OCS was retarded for approximately 1500 pore volumes at which point only 20% of breakthrough had occurred. Breakthrough occurred more rapidly beyond 1500 pore volumes although the rate of breakthrough was less than GAC.

The pH profile is shown in the lower plot of Figure 4.10.2. The effluent pH from the silica sand column followed the influent pH profile initially. However by breakthrough the silica 2030 sand effluent pH had decreased approximately one-half of a pH unit compared to the test influent

levels. This batch of IOCS was more rigorously neutralized initially and therefore the pH lowering may be attributed to proton exchange. The pH of the GAC is erratic but remained above 9 for the entire run. The brief but periodic pH swings cannot be explained.

At a pH of 8.0 with an influent concentration of 1000 ug/L breakthrough occurred at 55 pore volumes (13.3 L) for silica sand, 115 pore volumes (58.5 L) for GAC and 1900 pore volumes (490.5 L) for IOCS. At a pH of 8.0 the capacity of IOCS was significantly enhanced than at a pH of 6.5 and significantly outperformed silica sand and GAC.

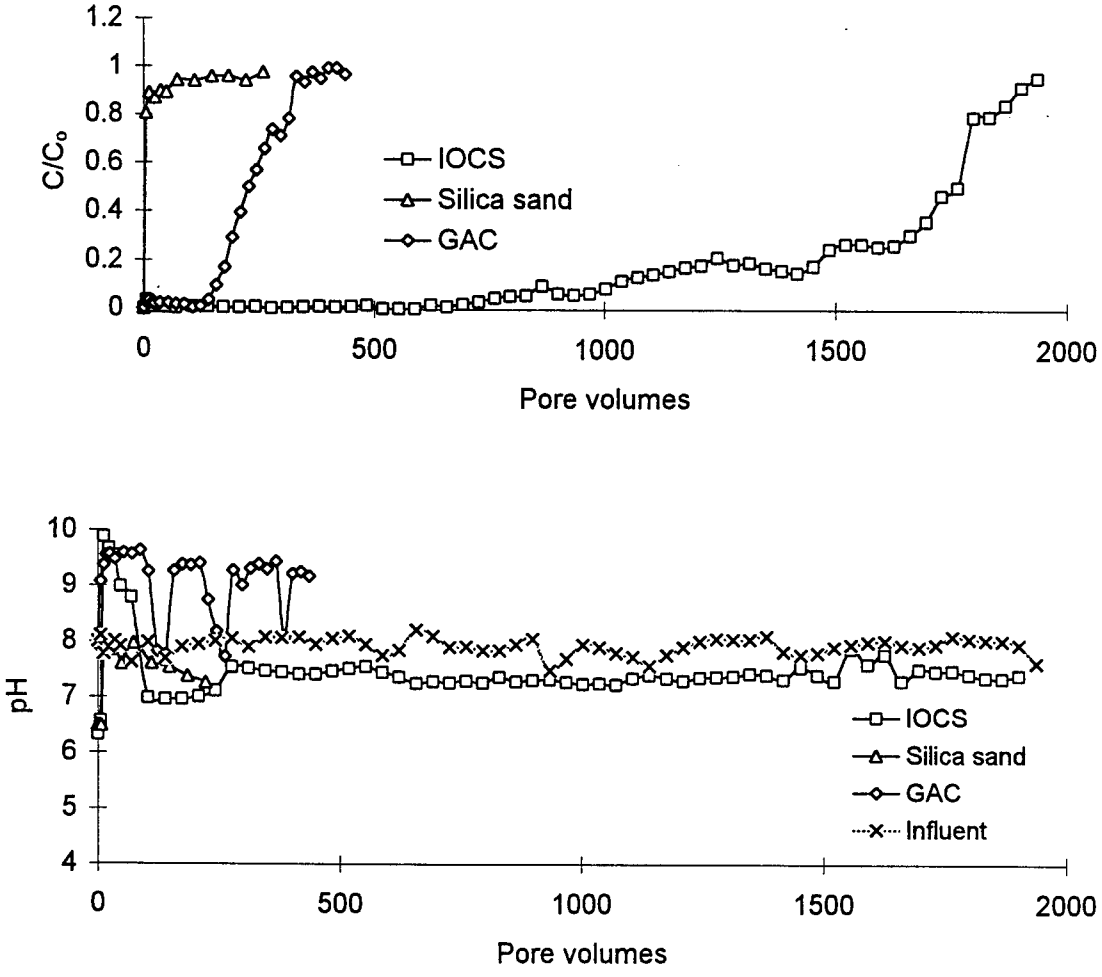

Figure 4.10.2 Breakthrough curves for Cd influent @ 1000 µg/L (DI @ pH 8.0).

Run Cu65-5:

The single metal element solute in this run was Cu at a constant influent concentration of 5000 ug/L. The influent pH was held constant at 6.5. One column contained silica sand as a control media while the other column contained OCS. For a DI water matrix with no solids, at a pH of 6.5 and mean Eh of +374 mV (range of 220 to 569 mV), Cu is mainly present as Cu^{2+} although some tenorite (CuO) can be present as the pH approaches 7.0 (Brookins, 1988).

The breakthrough curves presented in the upper plot of Figure 4.10.3 indicate the capacity of OCS is significantly greater than silica sand. Cu breakthrough for the silica sand column occurred within 37 pore volumes while OCS breakthrough occurred at 510 pore volumes. The slope of the silica sand breakthrough curve was significantly steeper than that of the OCS. The OCS exhibited a "s-shaped" type of adsorption curve. Beyond their respective breakthrough points effluent concentration remained relatively stable.

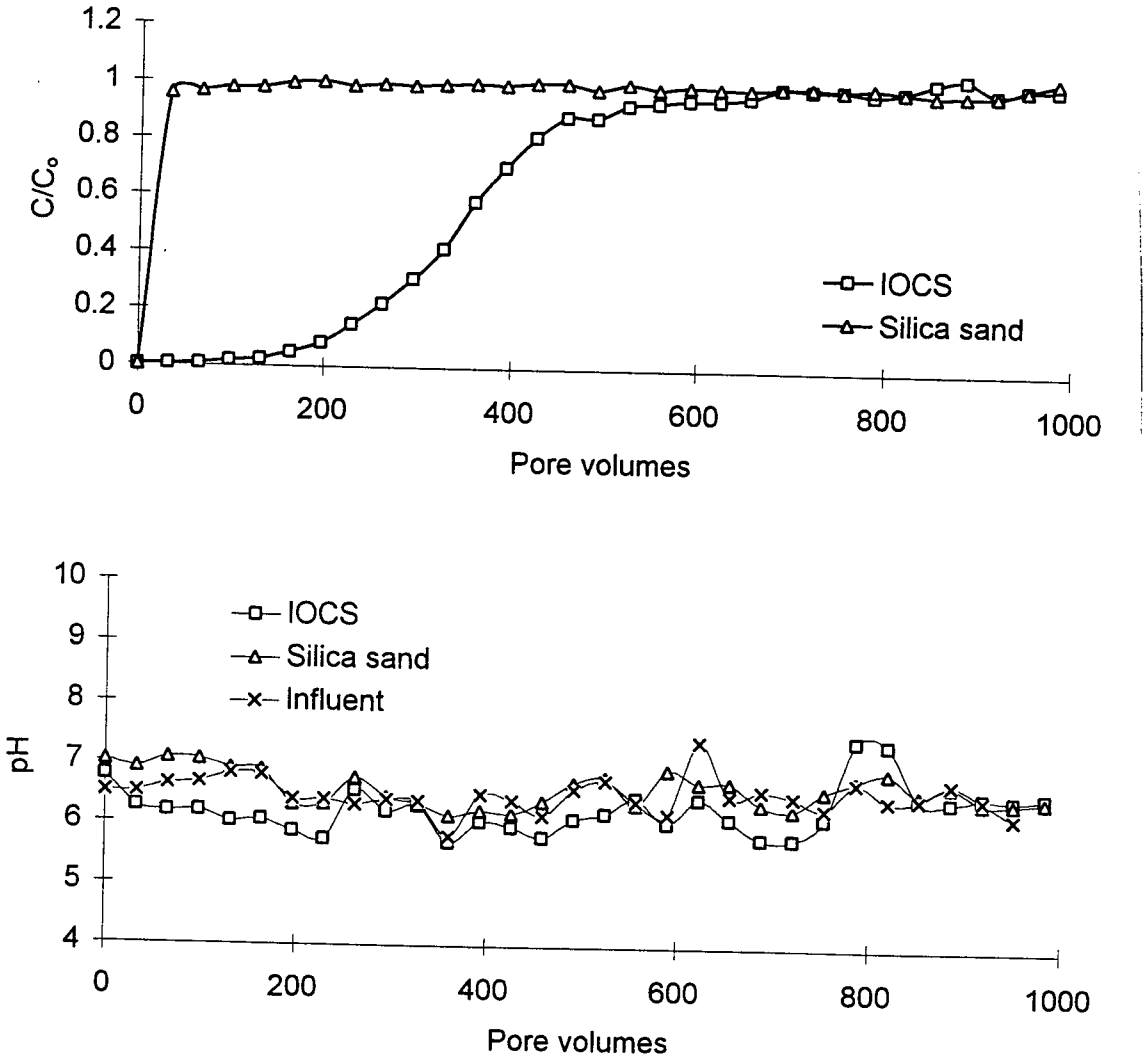

Figure 4.10.3 Breakthrough curves for Cu influent @ 5000 µg/L (DI @ pH 6.5).

The pH profile is shown in the lower plot of Figure 4.10.3. The effluent pH profile from the silica sand column followed the influent pH profile. The OCS effluent pH profile generally remained below influent pH levels except after breakthrough. After breakthrough pH values of the OCS effluent rose to influent pH values

At a pH of 6.5 with an influent concentration of 5000 ug/L breakthrough occurred at 37 pore volumes (8.9 L) for silica sand and 510 pore volumes (131.7 L) for OCS. The OCS significantly outperformed silica sand at a pH of 6.5.

Run Cu80-5:

This experimental run was the companion to Run Cu65-5. The single metal element solute in this run was Cu at a constant influent concentration of 5000 ug/L. The influent pH was held constant at 8.0. One column contained silica sand as a control media while the other column contained OCS. A column of GAC was also run for comparison to OCS. For a DI water matrix with no solids, at a pH of 8.0 and Eh of +203 mV (range of +171 to 229 mV), Cu is mainly present as $CuCO_3^0$ (carbonatocopper-II) and CuO although some Cu_2O (cuprite) can be present in the lower range of Eh values (Brookins, 1988), (Snoeyink & Jenkins, 1980).

The breakthrough curves presented in the upper plot of Figure 4.10.4 indicate the capacity of OCS at a pH of 8.0 is significantly greater than silica sand used as control. Note that because of the increased capacity at a pH of 8.0 the pore volume scale extends to 3000. A column of GAC was also run for comparison, however the results are not representative of other column run results using GAC. Silica sand breakthrough at pH of 8.0 was greater than silica sand breakthrough at pH = 6.5; 95 pore volumes compared to 37 pore volumes, respectively. The slope of the silica sand breakthrough curve was steep, however at and beyond breakthrough effluent behavior was erratic. At 500 pore volumes GAC began to breakthrough, however before reaching 40% breakthrough effluent the trend reversed and effluent values generally began decreasing to about 1500 pore volumes.

In contrast, OCS breakthrough occurred at 3000 pore volumes. The initiation of breakthrough for OCS was retarded for approximately 1000 pore volumes at which point only 5% of breakthrough had occurred. Breakthrough occurred at a constant but steeper rate until 2000 pore volumes and then flattened out until breakthrough.

The pH profile is shown in the lower plot of Figure 4.10.4. The influent pH profile was slightly higher than the influent pH for the duration of the silica sand column run. Influent pH values were consistently low, between 7.5 and 8.0 instead of the target value of 8.0. GAC effluent pH values were initially above 9.0 but gradually decreased to influent levels. OCS effluent pH values remained at or above influent pH values.

At a pH of 8.0 with an influent concentration of 5000 ug/L breakthrough occurred at 95 pore volumes (23.1 L) for silica sand and 3021 pore volumes (779.8 L) for OCS. GAC had not broken through by 1701 pore volumes (864.4 L) although breakthrough behavior was erratic. At

a pH of 8.0 the capacity of OCS was significantly enhanced than at a pH of 6.5 and significantly outperformed silica sand.

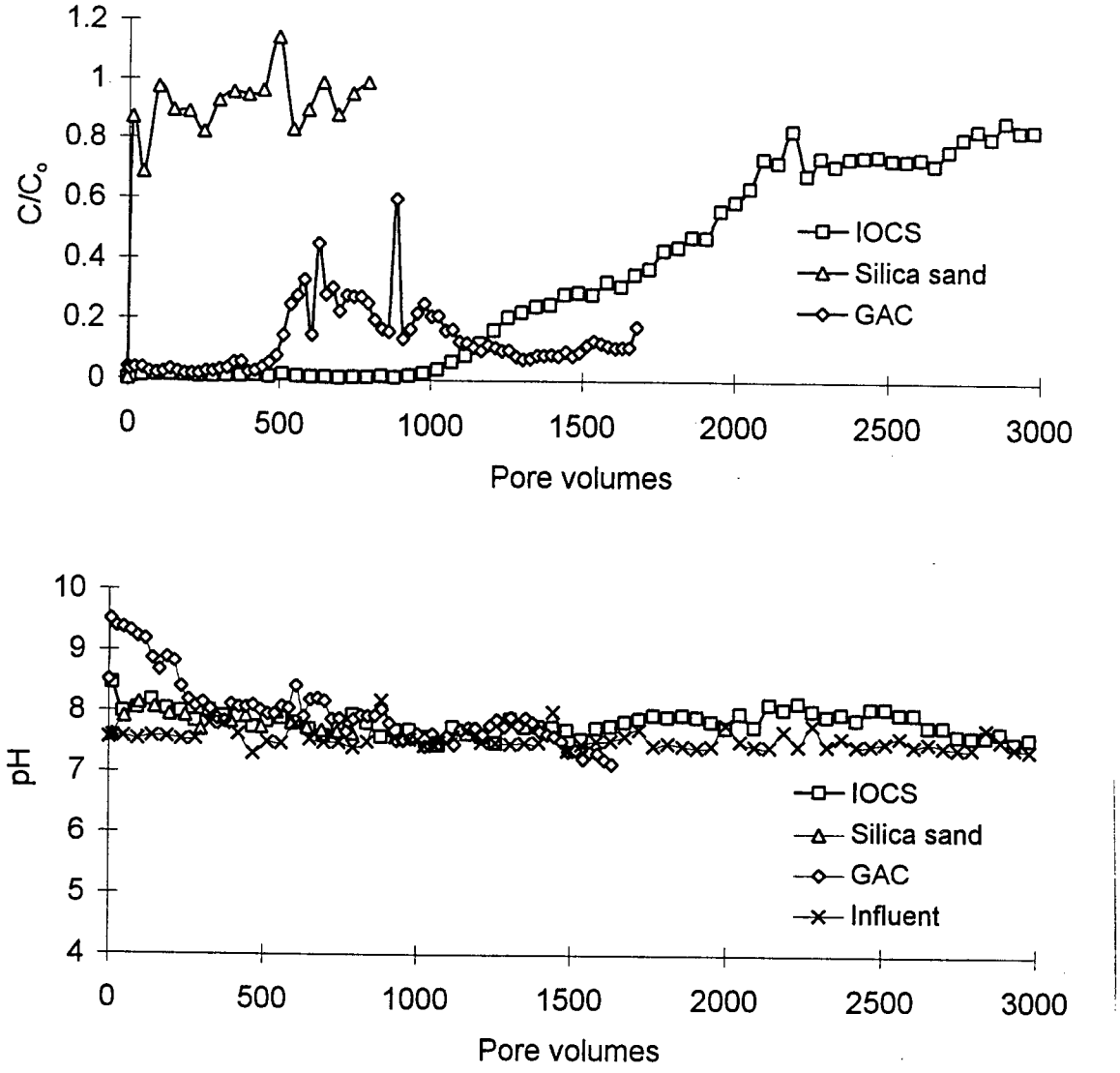

Figure 4.10.4 Breakthrough curves for Cu influent @ 5000 µg/L (DI @ pH 8.0).

Run Pb65-5:

The single metal element solute in this run was Pb at a constant influent concentration of 5000 ug/L. The influent pH was held constant at 6.5. One column contained silica sand as a control media while the other column contained OCS. For a DI water matrix with no solids, and no sulfur, at a pH of 6.5 and mean Eh of +212 mV (σ of 5.4), Pb is mainly present as $PbCO_3$ (cerussite) (Krauskopf & Bird, 1995).

The breakthrough curves presented in the upper plot of Figure 4.10.5 indicate the capacity of OCS is significantly greater than silica sand. Pb breakthrough for the silica sand column occurred within 290 pore volumes while OCS breakthrough was negligible through the entire run

of 1200 pore volumes. The slope of the silica sand breakthrough curve was less steep than for Cd and Cu at the same pH. Beyond the breakthrough point of silica sand the effluent concentration remained moderately stable.

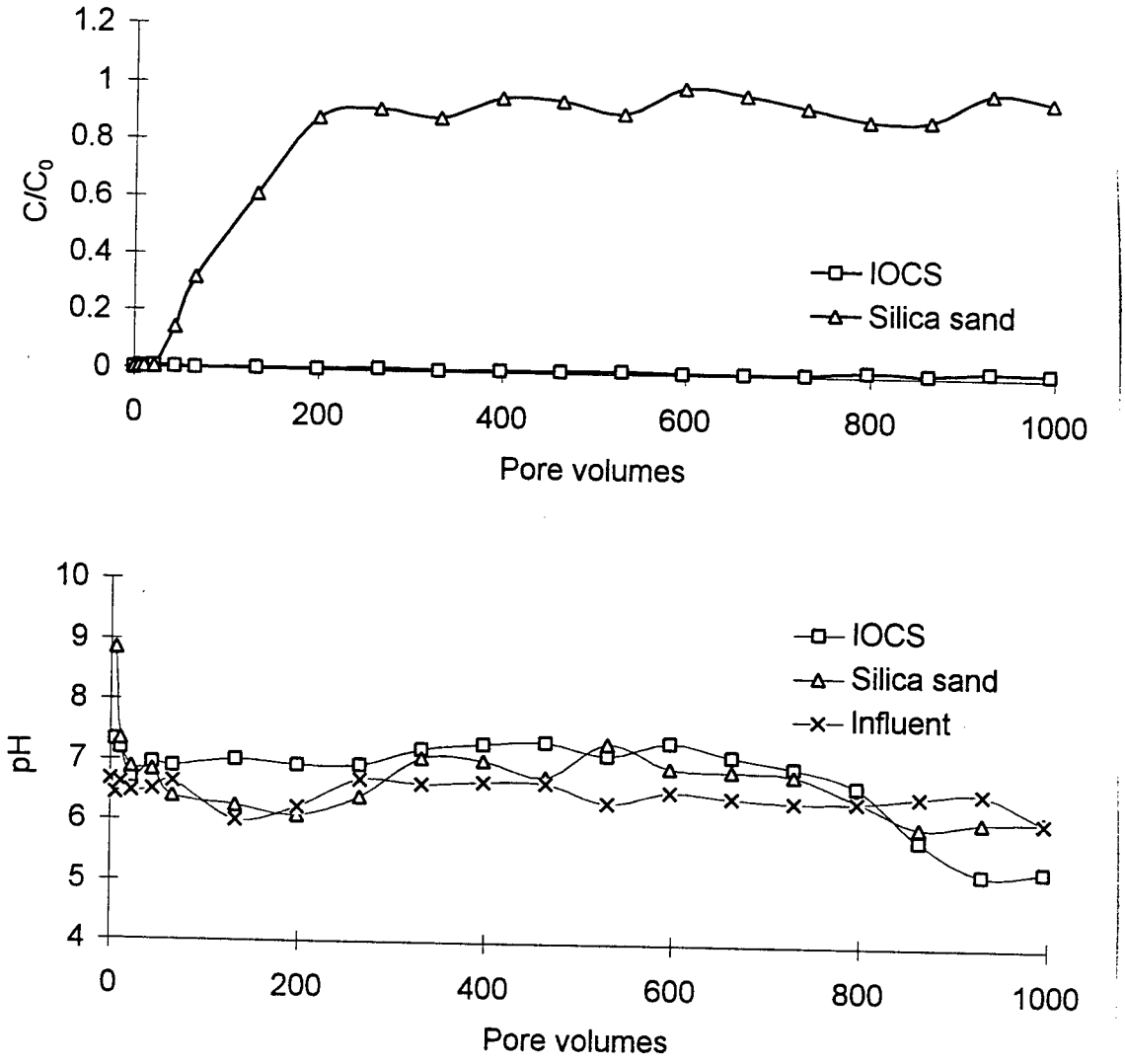

Figure 4.10.5 Breakthrough curves for Pb influent @ 5000 µg/L (DI @ pH 6.5).

The pH profile is shown in the lower plot of Figure 4.10.5. After equilibrating in the initial 50 pore volumes the effluent pH profile from the silica sand column varied above and below the influent pH profile within 0.5 pH units. The OCS effluent pH profile generally remained above the pH levels except beyond 800 pore volumes when OCS effluent pH levels dropped to 1 pH unit below influent levels.

Run Pb80-5:

This experimental run was the companion to Run Pb65-5. The single metal element solute in this run was Pb at a constant influent concentration of 5000 ug/L. The influent pH was held constant at 8.0. One column contained silica sand as a control media while the other column contained OCS. A column of GAC was also run for comparison to OCS. For a DI water matrix with no solids, at a pH of 8.0 and Eh of +182 mV (σ of 5.7), Pb is present as $PbCO_3$ (Krauskopf & Bird, 1995).

The breakthrough curves presented in the upper plot of Figure 4.10.6 indicate the capacity of OCS at a pH of 8.0 is significantly greater than silica sand used as control. Note that because of the increased capacity at a pH of 8.0 the pore volume scale extends to 3000 as was the case for Cu at a pH of 8.0. Silica sand breakthrough at pH of 8.0 was greater than silica sand breakthrough at pH = 6.5; 590 pore volumes compared to 290 pore volumes, respectively. The slope of the silica sand breakthrough curve was more gradual than at a pH of 6.5 and exhibited an "s-shaped" profile up to the point of breakthrough. Beyond breakthrough the effluent behavior was erratic. OCS breakthrough was negligible for the entire 3150 pore volumes.

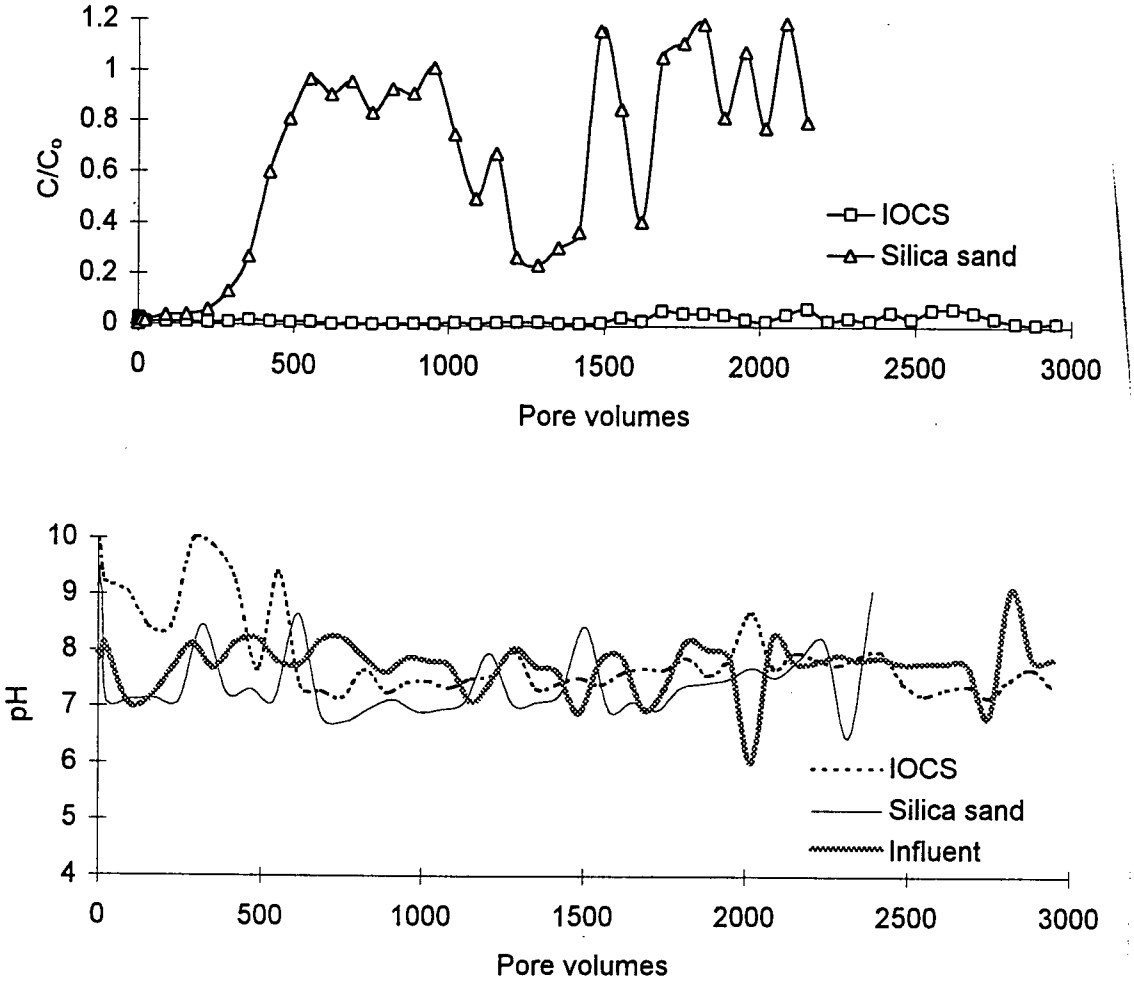

Figure 4.10.6 Breakthrough curves for Pb influent @ 5000 µg/L (DI @ pH 8.0).

The pH profile is shown in the lower plot of Figure 4.10.6. The influent pH profile was more erratic as compared to other runs. Silica sand pH values were generally lower than the influent pH profile except for sporadic but short pH spikes above influent levels. OCS effluent pH values were initially high and required 500 pore volumes for equilibration. Between 500 and 3000 pore volumes OCS effluent pH followed influent pH levels.

At a pH of 8.0 with an influent concentration of 5000 ug/L breakthrough occurred at 590 pore volumes (143.5 L) for silica sand and was still negligible at 3150 pore volumes (813.2 L) for OCS. At a pH of 8.0 the capacity of OCS could be expected to be significantly enhanced as compared to a pH of 6.5, however breakthrough was not observed in either run. At a pH of 8.0 the OCS significantly outperformed silica sand. The relatively erratic behavior of the silica sand beyond initial breakthrough may suggest that at a pH of 8.0, Pb as $PbCO_3$ may be immobilized as a surface precipitate. The precipitate can continue to form on the surface with a consequential reduction in effluent concentration until it is scoured into the effluent after which the process may repeat itself.

Run Zn65-10:

The single metal element solute in this run was Zn at a constant influent concentration of 10,000 ug/L. Influent pH was held constant at 6.5. One column contained silica sand as a control media while the other column contained OCS. In DI a water matrix with no solids, and no sulfur, at a pH of 6.5 and Eh of +324 mV (σ of 5.2), Zn is mainly present as Zn^{2+} (Brookins, 1988).

The breakthrough curves presented in the upper plot of Figure 4.10.7 indicate the capacity of OCS is significantly greater than silica sand. Zn breakthrough for the silica sand column occurred within 36 pore volumes while OCS breakthrough occurred within 290 pore volumes. The slope of the silica sand breakthrough curve was steep, similar to that of Cd for silica sand at the same pH. Beyond the breakthrough point of silica sand the effluent concentration remained stable. The slope of the breakthrough curve for OCS was relatively gradual with effluent concentration remaining stable after breakthrough. Beyond 250 pore volumes the breakthrough curve flattened out for OCS.

The pH profile is shown in the lower plot of Figure 4.10.7. The effluent pH profile from the silica sand column followed the influent pH profile up to 300 pore volumes. Beyond this point, even though the influent pH dropped by over 0.5 pH units the silica sand effluent pH remained constant. The OCS effluent pH profile remained below the influent pH levels up to 200 pore volumes. Beyond 200 pore volumes OCS effluent pH remained constant although the influent pH dropped beyond 300 pore volumes.

At a pH of 6.5 with an influent concentration of 10,000 ug/L breakthrough occurred at 36 pore volumes (8.8 L) for silica sand and breakthrough occurred within 290 pore volumes (74.9 L) for OCS. The OCS outperformed silica sand at a pH of 6.5.

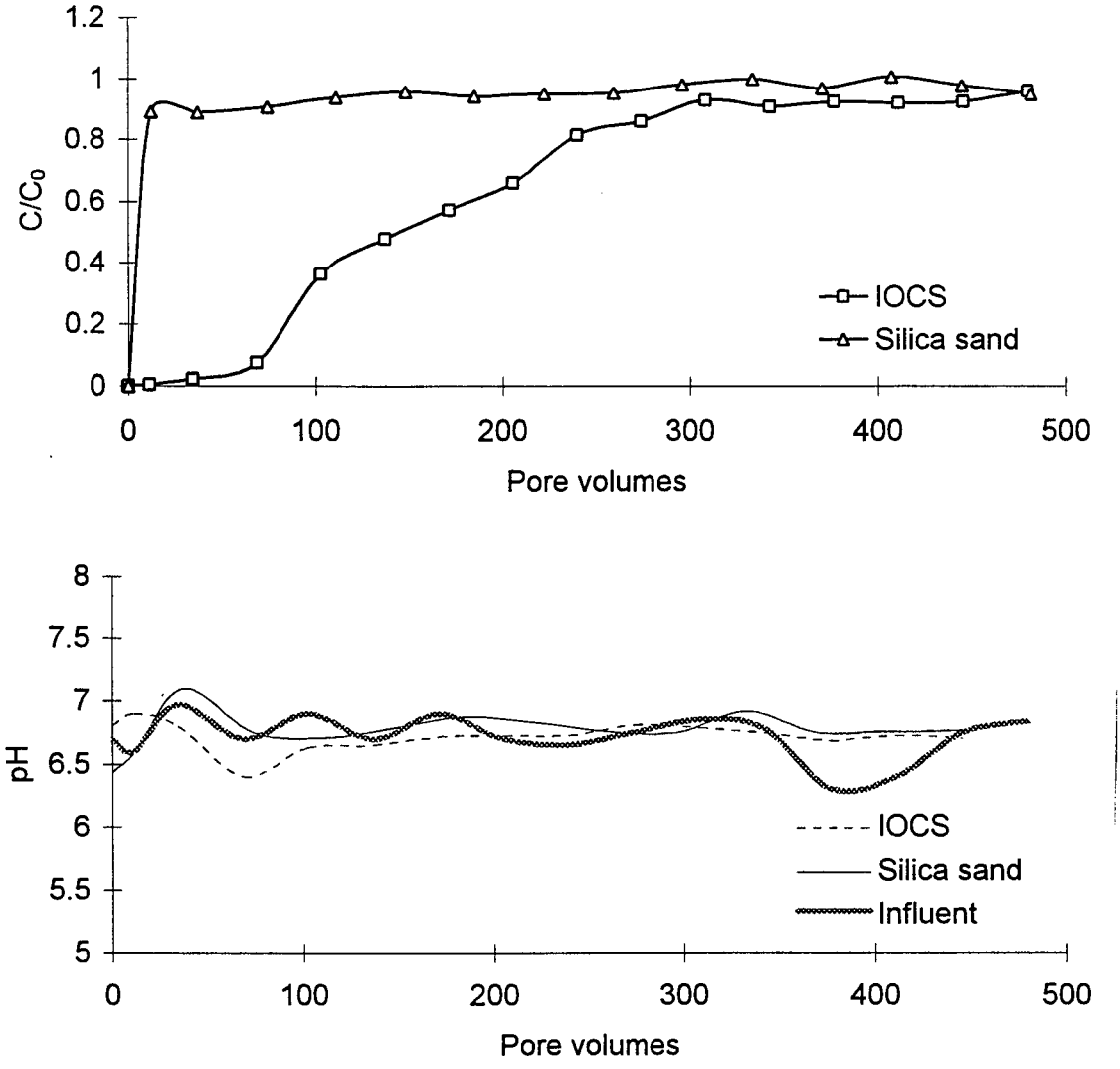

Figure 4.10.7 Breakthrough curves for Zn influent @ 10,000 µg/L (DI @ pH 6.5).

Run Zn80-10:

This experimental run was the companion to Run Zn65-5. The single metal element solute in this run was Zn at a constant influent concentration of 10,000 ug/L. The influent pH was held constant at 8.0. One column contained silica sand as a control media while the other column contained OCS. A column of GAC was also run for comparison to OCS. For a DI water matrix with no solids, at a pH of 8.0 and Eh of +214 mV (σ of 4.8), Zn is present as Zn^{2+}, $ZnCO_3^0$ (smithsonite) and ZnO (zincite) (Brookins, 1988).

The breakthrough curves presented in the upper plot of Figure 4.10.8 indicate the capacity of OCS at a pH of 8.0 is significantly greater than silica sand used as control. Note that because of the increased capacity at a pH of 8.0 the pore volume scale extends to 2000. A column of GAC was also run for comparison. Silica sand breakthrough at pH of 8.0 was only slightly greater than silica sand breakthrough at pH = 6.5; 42 pore volumes compared to 36 pore volumes, respectively. The slope of the silica sand breakthrough curve was steep. Beyond breakthrough effluent behavior remained relatively stable. GAC breakthrough occurred within 390 pore volumes.

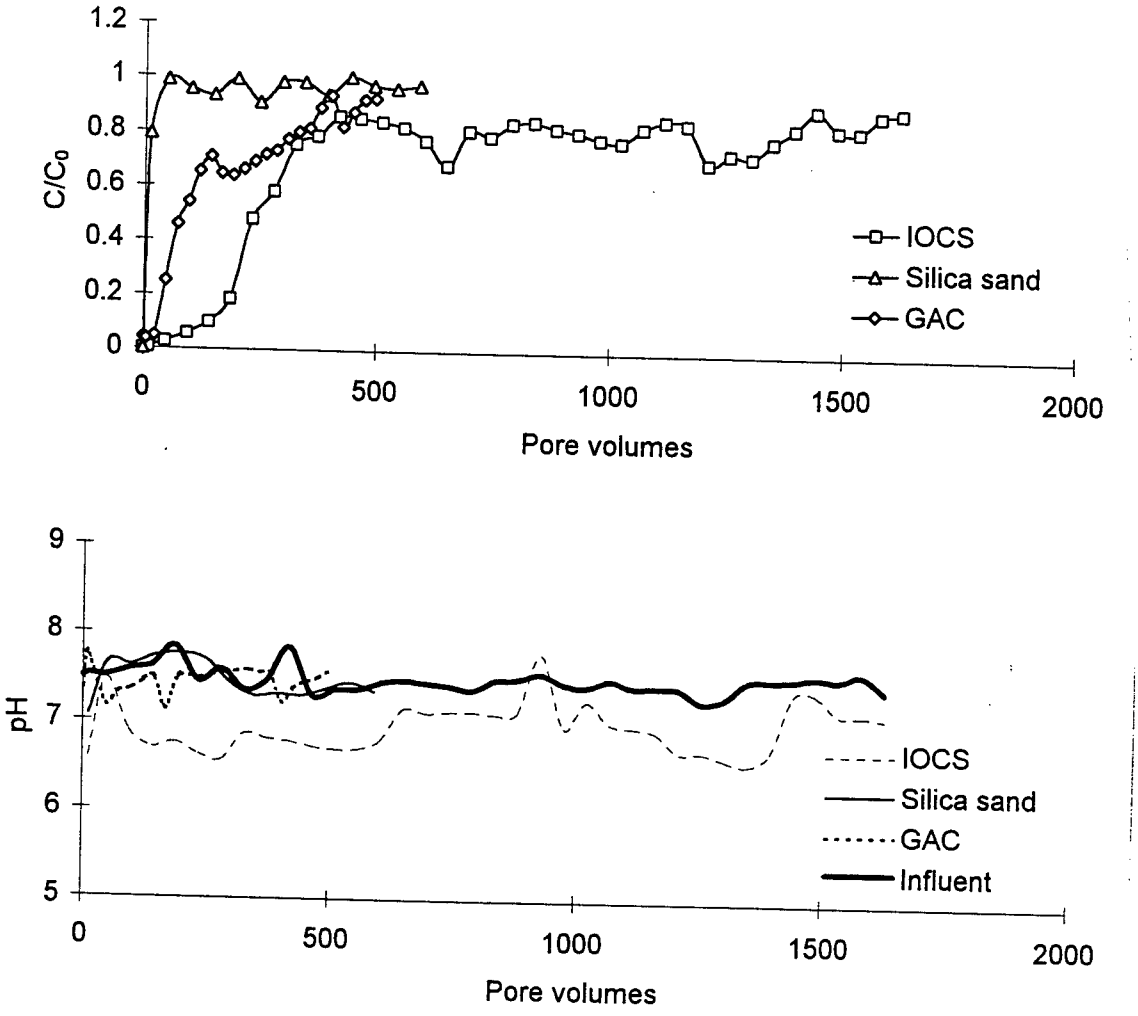

Figure 4.10.8 Breakthrough curves for Zn influent @ 10,000 µg/L (DI @ pH 8.0).

In contrast, OCS breakthrough occurred at 1441 pore volumes. The initiation of breakthrough for OCS occurred relatively rapidly and the breakthrough curve slope was similar to the breakthrough curve slope at pH of 6.5. Beyond 80% breakthrough (400 pore volumes) the increase in breakthrough was erratic up to 1441 pore volumes.

The pH profile is shown in the lower plot of Figure 4.10.8. After initial equilibration , the silica sand effluent pH profile followed the general trend of the influent pH. The OCS effluent pH was lower than the influent pH values for the entire run. As with run Cd65-1, the surface acidity of the OCS may not have been fully neutralized as indicated by the consistently lower pH profile after breakthrough. GAC effluent pH values were relatively constant in the range of 7.5 although occasional but short pH drops occurred.

At a nominal pH of 8.0 with an influent concentration of 10,000 ug/L breakthrough occurred at 42 pore volumes (10.2 L) for silica sand and 1441 pore volumes (372 L) for OCS. GAC breakthrough occurred within 390 pore volumes (198.2 L). At a pH of 8.0 the OCS capacity OCS was greater than at pH of 6.5 and outperformed silica sand.

4.11 Combination metal element runs in DI water

Results for each of these runs are presented as separate breakthrough plots for each media. A comparison can then be made of the competitive breakthrough of each metal element for each media. For each run the pore volume axis is kept at a fixed scale so a direct comparison can be made between the performance of each media.

Zpcc65-5

The metal elements in this run were Zn, Pb, Cd and Cu each at a constant influent concentration of 5000 ug/L. The influent pH was held constant at 6.5. One column contained silica sand as a control media while the other column contained OCS. A column of GAC and a BSPET column were also run. The DI water matrix contained no solids and the Eh was +256mV (σ of 44.2). The objective for this experiment was to characterize breakthrough behavior of various media, especially OCS, at the pH of stormwater. Metal elements were at equal concentration to assess the competitive breakthrough of each metal element.

The breakthrough curves presented in the upper plot of Figure 4.11.1 for silica sand indicate the breakthrough capacity is negligible for all metal elements. The breakthrough of Cd and Zn are the most rapid and breakthrough behavior is essentially identical. The actual order of breakthrough capacity is Pb (4.9 L) $\approx$ Cu (4.4 L) > Zn (1.5 L) $\approx$ Cd (1.2 L) Above a breakthrough of 80% the breakthrough of Pb and Cu is more gradual than for Zn and Cd. After an initial pH of 7, silica sand effluent equilibrates to influent pH levels and tracks influent pH values after a 150 pore volumes.

The breakthrough curves presented in the middle plot for GAC indicate a distinct variation in metal element breakthrough compared to silica sand at a pH of 6.5. The GAC acts as a chromatograph, eluting each metal element separately. The capacity of GAC at breakthrough has the following order Cu (259.1 L) > Pb (213.4 L) > Zn (81.3) > Cd (25.4 L). GAC capacity is greater than silica sand for all metal elements. Once breakthrough has occurred, effluent concentration remained relatively stable until the run was terminated. The slopes of the breakthrough curves had the following order Cd > Pb > Zn > Cu. The effluent pH of GAC was initially at pH 8, decreasing over time, but remaining above influent pH levels for the entire run.

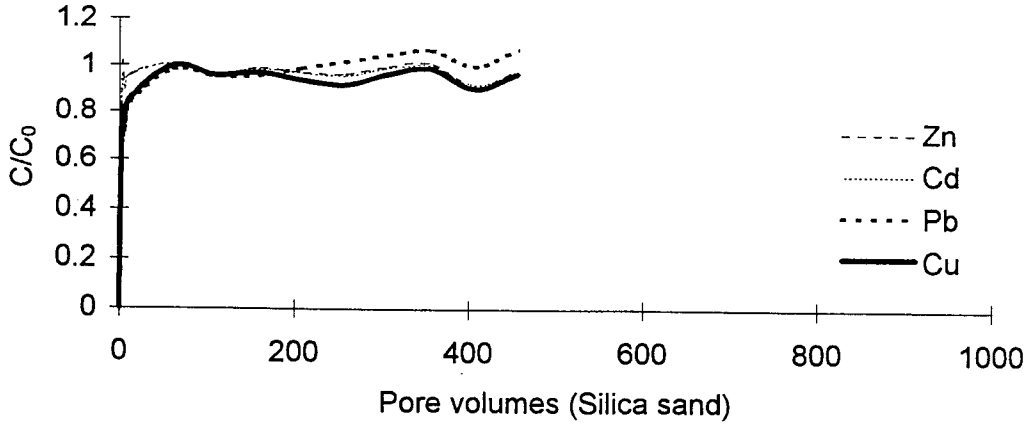

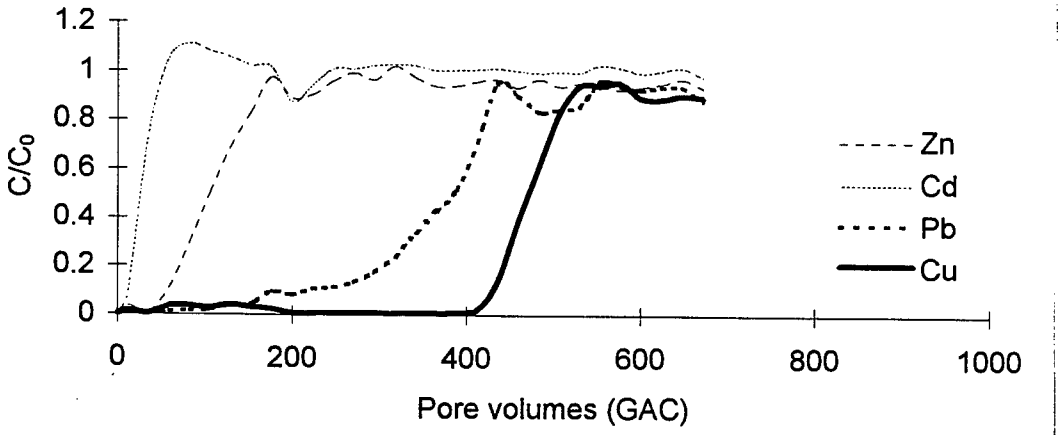

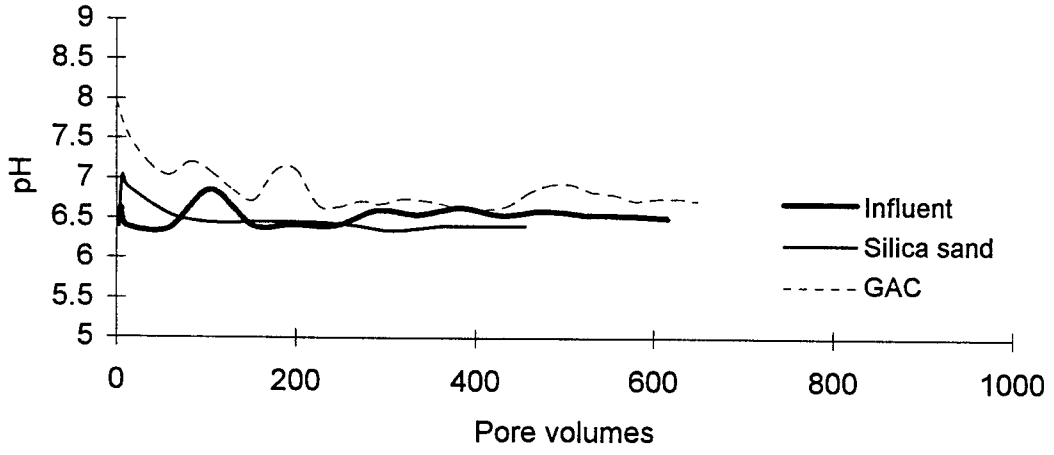

Figure 4.11.1 Breakthrough curves for Zn, Cd, Cu, and Pb influent @ 5,000 µg/L (DI water @ pH 6.5) (Silica sand and GAC)

OCS breakthrough curves are presented in the upper plot of Figure 4.11.2. OCS capacity is greater than silica sand but less than GAC. Breakthrough for Cd and Zn were essentially identical; Cu and Pb behavior were distinct. OCS capacity has the order: Pb (144.5 L) > Cu (110.9 L) > Zn (15.2) > Cd (14.2 L). Although these capacities are greater than silica sand, they

are less than GAC. The breakthrough curve slopes had the order Cd ≈ Zn > Cu > Pb. The OCS pH effluent profile is presented in the lower plot. After initial equilibration, effluent pH remained below influent levels except between 400 and 600 pore volumes.

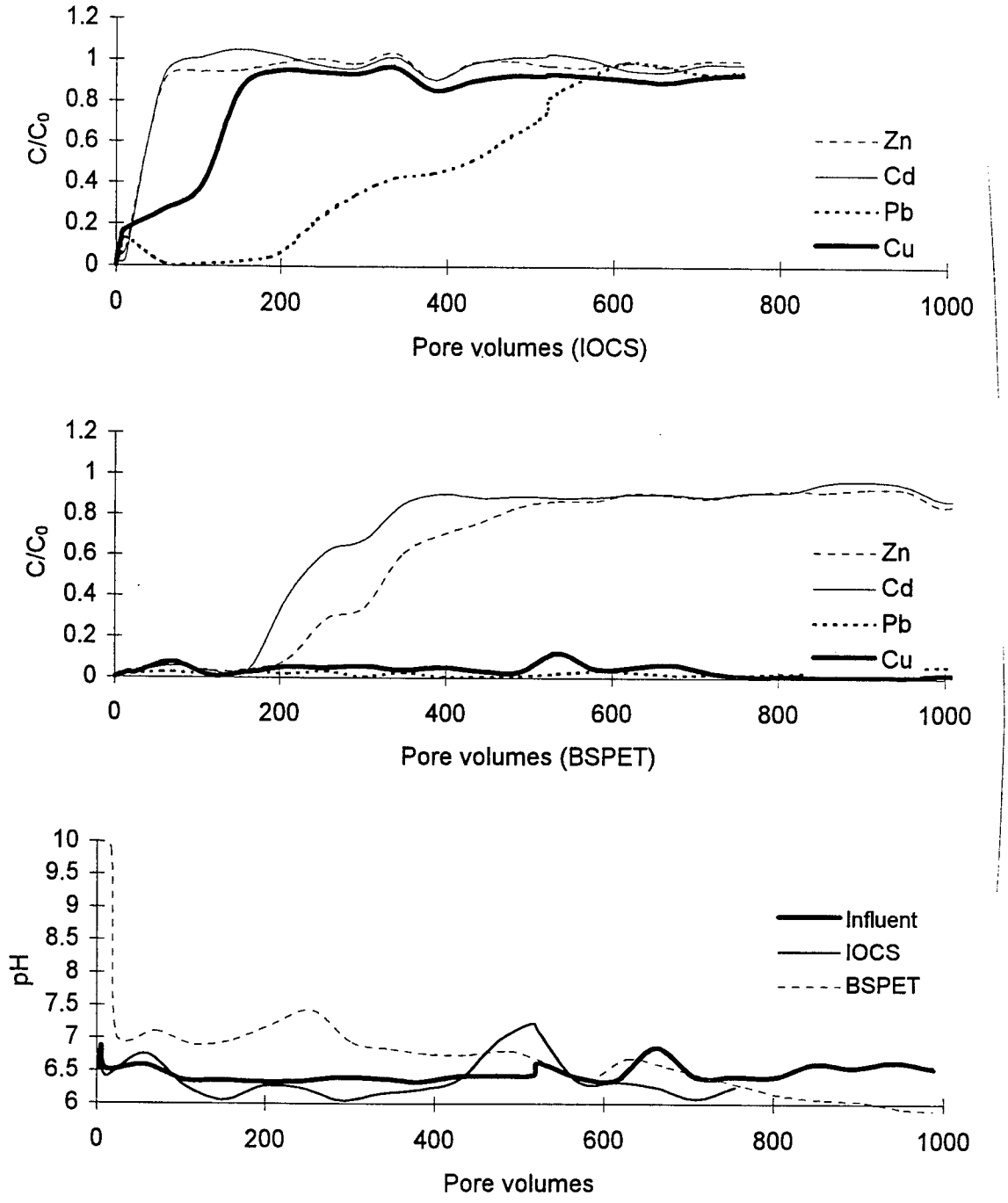

Figure 4.11.2 Breakthrough curves for Zn, Cd, Cu, and Pb influent @ 5,000 µg/L (DI water @ pH 6.5) (BSPET and OCS)

The breakthrough curves for the BSPET are presented in the middle plot of Figure 4.11.2. The breakthrough capacity of the BSPET is greater than silica sand, OCS and GAC for all metal elements. The replacement of 8 cm of OCS with crushed cementatious aggregate resulted in distinctly different behavior. A comparison of the upper two plots of Figure 4.11.2 clearly demonstrates the influence of the crushed cementatious aggregate. The capacity for both Zn and Cd have significantly increased over OCS and after 1000 pore volumes both Cu and Pb were at less than 10% breakthrough. The capacity of the BSPET at breakthrough has the following order Cu (>> 441L) ≅ Pb (>> 441L) > Zn (172.7L) > Cd (108.6 L). Once breakthrough has occurred, effluent concentration remained relatively stable until the run was terminated. The slopes of the breakthrough curves had the following order Cd > Zn >> Pb ≈ Cu. The initial effluent pH of the BSPET was high , remained above 7 for 400 pore volumes, and remained above influent pH for the entire run. Although the cement content of the 8 cm of aggregate was low it was sufficient to elevate the effluent pH for 110 L and strongly influence the breakthrough behavior of the iron-oxide coated sand in the BSPET.

Zpcc80-5

This experimental run was the companion to Zpcc65-5. The metal elements in this run were Zn, Pb, Cd and Cu each at a constant influent concentration of 5000 ug/L. The influent pH was held constant at 8.0. One column contained silica sand as a control media while the other column contained OCS. A column of GAC was also run. A BSPET was not required for this experiment. The DI water matrix contained no solids and the Eh was +216mV (σ of 58.4). The objective for this experiment was to characterize breakthrough behavior or various media, especially OCS, at a raised pH level due to the influence of the cementatious porous pavement on infiltrating stormwater. As with run Zpcc65-5 metal elements were at equal concentration to assess the competitive breakthrough of each metal element at a pH of 8.0. It was hypothesized that this run would serve as the bench-scale model for the ideal performance of the prototype PET for dissolved metal elements. Note that the pore volume scale extends to 2000 for all media.

The breakthrough curves presented in the third plot of Figure 4.11.3 for silica sand indicate the breakthrough capacity is negligible for all metal elements. It can be discerned that the breakthrough capacity for Cu is greater than Pb which is greater than Cd and Zn. The breakthrough of Cd and Zn are the most rapid and breakthrough behavior is essentially identical. The actual order of breakthrough capacity is Cu (71.9 L) > Pb (25.5L) > Zn (0.7L) ≈ Cd (0.7L). The capacity of the silica sand at pH of 8.0 was similar to the capacity at pH of 6.5 for Zn and Cd and significantly greater for Cu and Pb as compared to capacities at pH of 6.5. Silica sand effluent remained below influent pH levels until termination of the silica sand run. The breakthrough curves presented in the second plot for GAC indicate a distinct variation in metal element breakthroughs. Although the column run was terminated before Pb breakthrough the GAC again acts as a chromatograph, eluting each metal element separately. The capacity of GAC at breakthrough has the following order Pb (>> 398.4L) > Cu (≈398.4L) > Zn (249.1L) > Cd (158.6L). GAC capacity is significantly greater than silica sand for all metal elements. The slopes of the breakthrough curves had the following order Zn > Cu > Cd. The effluent pH of GAC was initially at pH 10, decreasing over time and dropping below influent pH levels by 400 pore volumes.

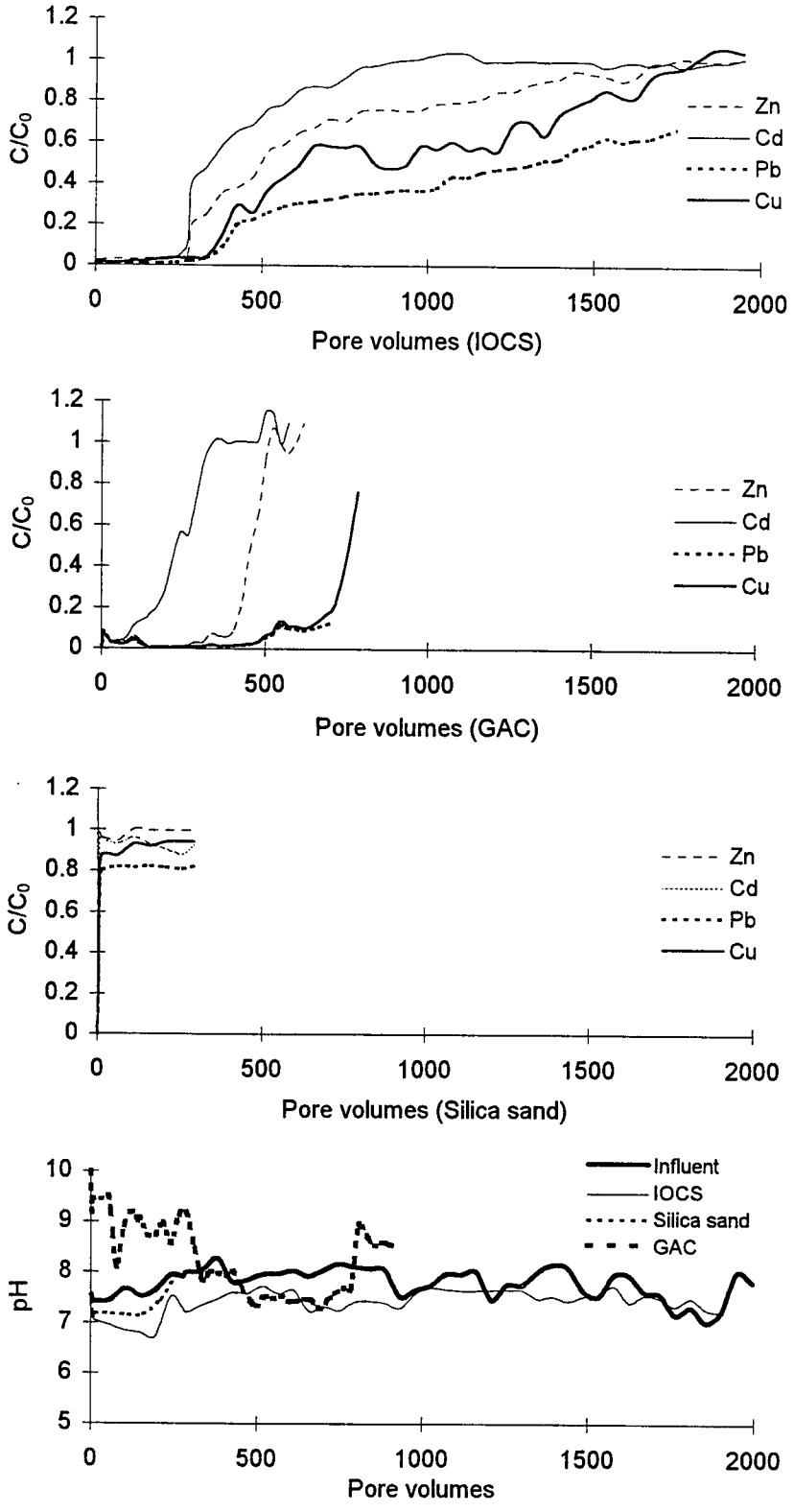

Figure 4.11.3 Breakthrough curves for Zn, Cd, Cu, and Pb influent @ 5,000 µg/L (DI water @ pH 8.0)

The breakthrough curves for OCS are presented in the upper plot of Figure 4.11.3. The breakthrough capacity of OCS is greater than silica sand at a pH of 8.0 for all metal elements and significantly greater than OCS at a pH of 6.5. Beyond 300 pore volumes breakthrough behavior is distinct for each metal element. The capacity of OCS at breakthrough has the following order Pb (>502.8L) > Cu (428.5L) > Zn (345.9) > Cd (191.1L). These capacities are greater than GAC at a pH of 8.0. Once breakthrough has occurred, effluent concentration remained relatively stable until the run was terminated. The slopes of the breakthrough curves had the following order Cd ≥ Zn > Pb > Cu. The OCS effluent pH profile is shown in the lower plot. The effluent pH remained below influent levels except at the end of the run beyond 1700 pore volumes. The results of the OCS run at pH of 8.0 indicate that pH elevation from 6.5 to 8.0 does significantly increase the breakthrough capacity of the OCS. These experimental results demonstrate the importance of developing a cementatious porous pavement block to elevate the pH of infiltrating stormwater throughout the design life of the PET.

Zpcc65-1

The metal elements in this run were Zn, Pb, Cd and Cu. Zn had and influent concentration of 10000 ug/L while Pb, Cd and Cu had influent concentrations of 1000 ug/L. The influent pH was held constant at 6.5. One column contained GAC while the other column was a BSPET configuration. The DI water matrix contained no solids and the Eh was +256mV (σ of 44.2). The objective for this experiment was to characterize breakthrough behavior of the BSPET column configuration with an influent pH of 6.5 for a DI water matrix for comparison to a companion run with stormwater. A column of GAC was used in this experiment as control. OCS and silica sand were not run because previous runs had established that their breakthrough capacity at a pH of 6.5 was consistent and relatively small.

The breakthrough curves presented in the upper plot of Figure 4.11.4 for the BSPET indicates the breakthrough of Zn and Cd was suppressed up to approximately 300 pore volumes. This breakthrough suppression appears to be correlated to the increase in pH provided by the porous pavement aggregate as shown in the lower plot of Figure 4.11.4. capacity is negligible for all metal elements. The order of breakthrough capacity is Cu (>> 987.5L) ≈ Pb (987.5L) >> Zn (458.9L) > Cd (261.2L). Although the influent concentration of Cd was an order of magnitude lower than Zn the capacity of Cd was still lower than for Zn. Up to 400 pore volumes the porous pavement aggregate provided pH elevation for the iron-oxide coated sand. However the BSPET profile indicates that the OCS had not been fully neutralized and a percentage of the pH elevating capacity was utilized in neutralizing the pH of the iron-oxide coated sand. The sudden pH drop for the BSPET effluent at 700 pore volumes cannot be explained. The pH of the BSPET effluent remained consistently above the influent pH for the balance of the run beyond 700 pore volumes.

The breakthrough curves presented in the middle plot for GAC indicate a distinct variation in individual metal element breakthrough. The capacity of GAC at breakthrough has the following order Cu (470.1L) ≈ Pb (467.5L) > Zn (177.9) >> Cd (34.6L). The slopes of the breakthrough curves had the following order Cd > Pb > Zn > Cu. The effluent pH of GAC was initially above pH 8, decreasing over time, but remaining above influent pH levels for the entire run. The breakthrough capacity of GAC was less than the BSPET for all metal elements.

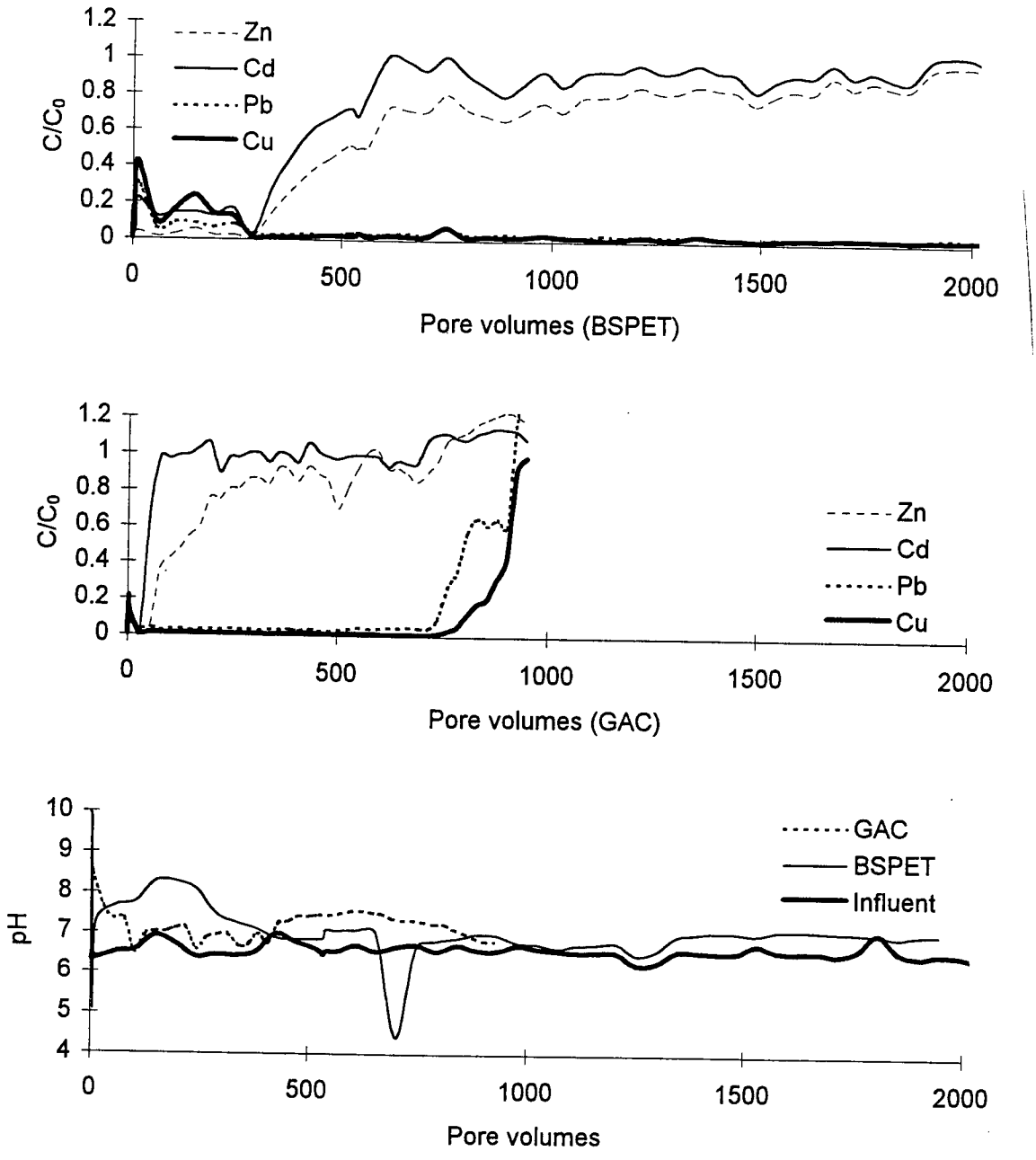

Figure 4.11.4 Breakthrough curves for Zn influent @ 10,000 μg/L and Cd, Cu, and Pb influent @ 1,000 μg/L each. (DI water @ pH 6.5)

4.12 Combination metal element runs in stormwater

Results for each of these runs are presented as separate dissolved and particulate-bound fractions breakthrough plots for each media. A comparison can then be made of the competitive breakthrough of each metal. For each run the pore volume axis is kept at a fixed scale so a direct comparison can be made between the performance of each media.

Zpcc65-S:

The stormwater was spiked with the metal elements of Zn, Pb, Cd and Cu. Zn was added at a constant influent concentration of 10000 ug/L. Pb, Cd and Cu were added at a constant influent concentration of 1000 ug/L. The influent pH was held constant at 6.5. One column contained silica sand as a control media while the other column contained OCS. A column of GAC and a BSPET column were also run. The stormwater matrix contained solids and the Eh was +196.3mV (σ of 44.2). Table 4.6.1 presents a summary of the water quality characteristics including solids for the stormwater matrix. The objective was to characterize breakthrough behavior of the media, especially OCS and the BSPET configuration using a stormwater matrix.

Silica sand

The breakthrough curves for the dissolved fraction are presented in the upper plot of Figure 4.12.1 for silica sand. The breakthrough capacity is negligible for all metal elements. From the plot it can be discerned that the breakthrough capacity for Cu and Pb is slightly greater than for Cd and Zn. The breakthrough of Cd and Zn are the most rapid and breakthrough behavior is essentially identical. The actual order of breakthrough capacity is Cu (12.2L) $\approx$ Pb (11.6L) > Zn (1.2 L) $\approx$ Cd (1.2 L). The silica sand effluent pH followed the influent pH profile.

The breakthrough curves for the particulate-bound fraction are presented in the middle plot of Figure 4.12.1 for silica sand. Note the scale change for the vertical axis. Particulate-bound metal element breakthrough has C/C_0 values which are greater than 1.0 especially for Cd and Zn. This phenomena may have several explanations. The first is that there may be a building up of particulate matter on the media surface which is sloughed off causing spikes in particulate-bound effluent concentrations. The second explanation is that the spiked metal elements in the influent are contacting this build-up of filtered particulate matter and are in part adsorbed, thereby enriching the metal element concentration of these particles

The capacity is negligible for all metal elements although Cu and Pb do not achieve breakthrough until 640 pore volumes. The breakthrough of Cd and Zn are the most rapid and breakthrough behavior is essentially identical. The actual order of breakthrough capacity is Pb (155.9L) $\approx$ Cu (155.6L) >> Zn (0.5L) $\approx$ Cd (0.5L).

OCS

The breakthrough curves for the dissolved fraction are presented in the upper plot of Figure 4.12.2 for OCS. Breakthrough capacity is small for Zn and Cd but breakthrough does not

occur for Cu and Pb. The actual order of breakthrough capacity is Cu (>194.9L) ≈ Pb (>194.9L) >> Zn (154.9) > Cd (61.9L). These capacities are significantly greater than the capacities for silica sand. The OCS effluent pH profile followed the influent pH for the entire run.

The breakthrough curves for the particulate-bound fraction are presented in the middle plot of Figure 4.12.2 for OCS. Note the scale change for the vertical axis. Breakthrough capacity for Cd and Zn was small compared to Cu and Zn The actual order of breakthrough capacity is Cu (>194.9L) ≈ Pb (194.9L) >> Zn (90.3L) > Cd (59.4L). At 400 and 700 pore volumes there is an increase in particulate-bound effluent concentration for both Zn and Cd resulting in C/C_0 approaching 2.0. This effect is not as pronounced for Cu and Pb.

BSPET

The breakthrough curves for the dissolved fraction are presented in the upper plot of Figure 4.12.3 for the BSPET configuration. Breakthrough capacity has been increased for Zn and Cd as compared to OCS and breakthrough does not occur for Cu and Pb. The actual order of breakthrough capacity is Cu (>340.2L) ≈ Pb (>340.2L) > Zn (314.2) > Cd (182.9L). The initiation of Zn and Cd breakthrough was significantly retarded by the replacement of 8 cm of OCS with cementatious porous pavement aggregate, as compared to OCS results. The BSPET effluent pH profile remained above the influent pH profile except for a brief period beyond 800 pore volumes. From 100 through 300 pore volumes the pH elevation due to the porous pavement aggregate was clearly evident. The breakthrough capacity was significantly increased for all metal elements due to the inclusion of the porous pavement aggregate.

The breakthrough curves for the particulate-bound fraction are presented in the middle plot of Figure 4.12.3. Note the scale change for the vertical axis. Breakthrough capacity for Cd and Zn was smaller than Cu and Zn The actual order of breakthrough capacity is Pb (166.4L) ≈ Cu (165.1L) > Zn (121.0L) > Cd (99.1L). At 600 pore volumes the particulate-bound effluent concentration for Cd, Zn and Cu suddenly increase to several times above the influent concentration. Beyond 600 pore volumes breakthrough of Cd, Zn and Cu become erratic. BSPET breakthrough capacity is controlled by the particulate-bound fraction.

GAC

The breakthrough curves for the dissolved fraction are presented in the upper plot of Figure 4.12.4 for GAC. Breakthrough capacity was small for Cd and Zn as compared to Cu and Pb. Neither Cu or Pb were above 5% of breakthrough when the run was terminated. The actual order of breakthrough capacity is Cu (>>338.9L) ≈ Pb (>>338.9L) > Zn (193.1) > Cd (70.1L). The GAC effluent pH profile remained significantly above the influent pH for the entire run.

The breakthrough curves for the particulate-bound fraction are presented in the middle plot of Figure 4.12.4 for GAC. Note the scale change for the vertical axis. Breakthrough capacity for Cd and Zn was small compared to Cu and Zn The actual order of breakthrough capacity is Pb (168.5L) ≈ Cu (167.7L) > Zn (0.5L) ≈ Cd (0.5L). The particulate-bound effluent

concentration is particularly erratic for Zn and Cd. GAC breakthrough capacity is controlled by the metal element particulate-bound fraction.

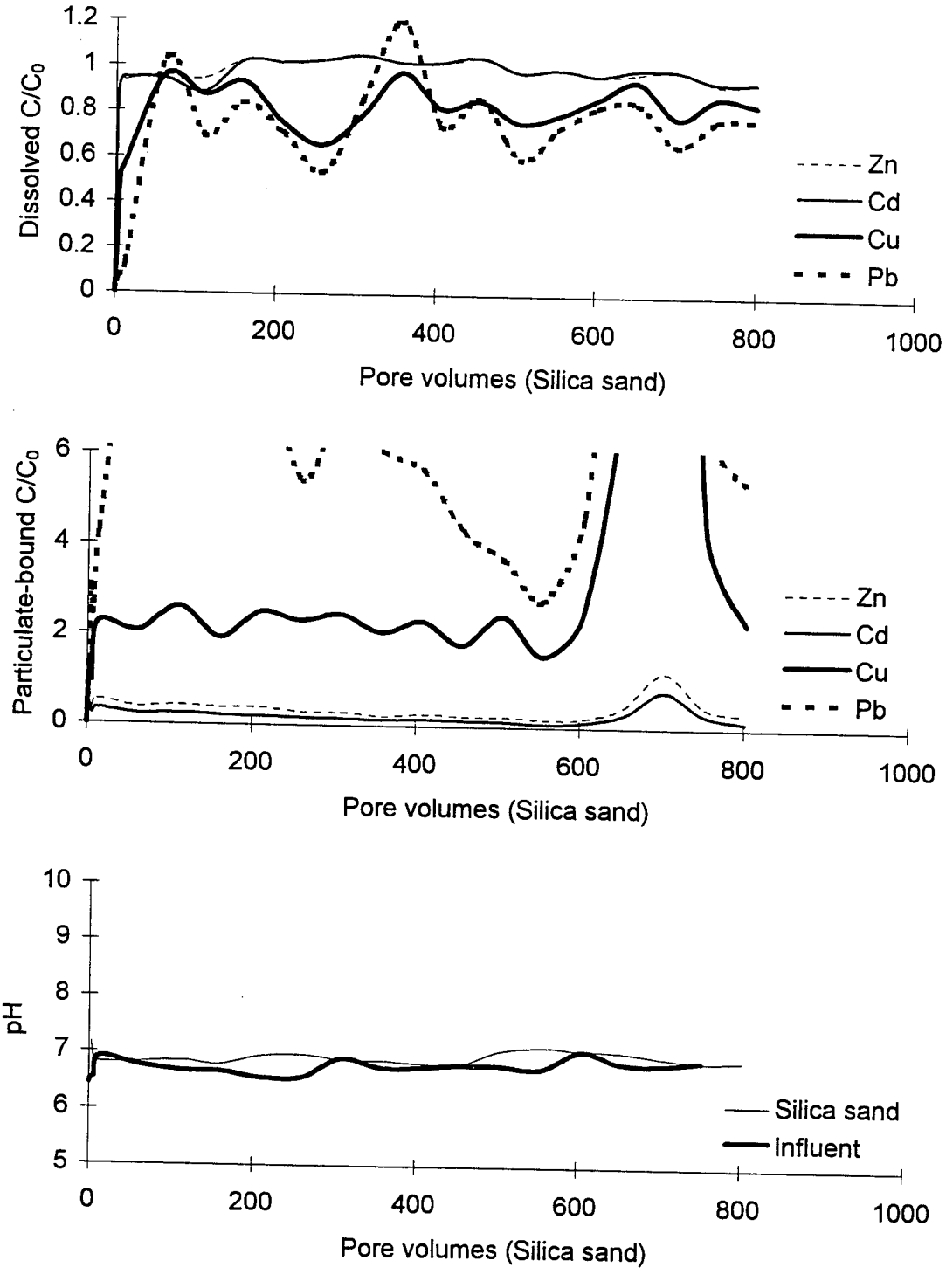

Figure 4.12.1 Breakthrough curves for Zn influent @ 10,000 µg/L and Cd, Cu, and Pb influent @ 1,000 µg/L each. (18 June 1996 stormwater) (Silica sand)

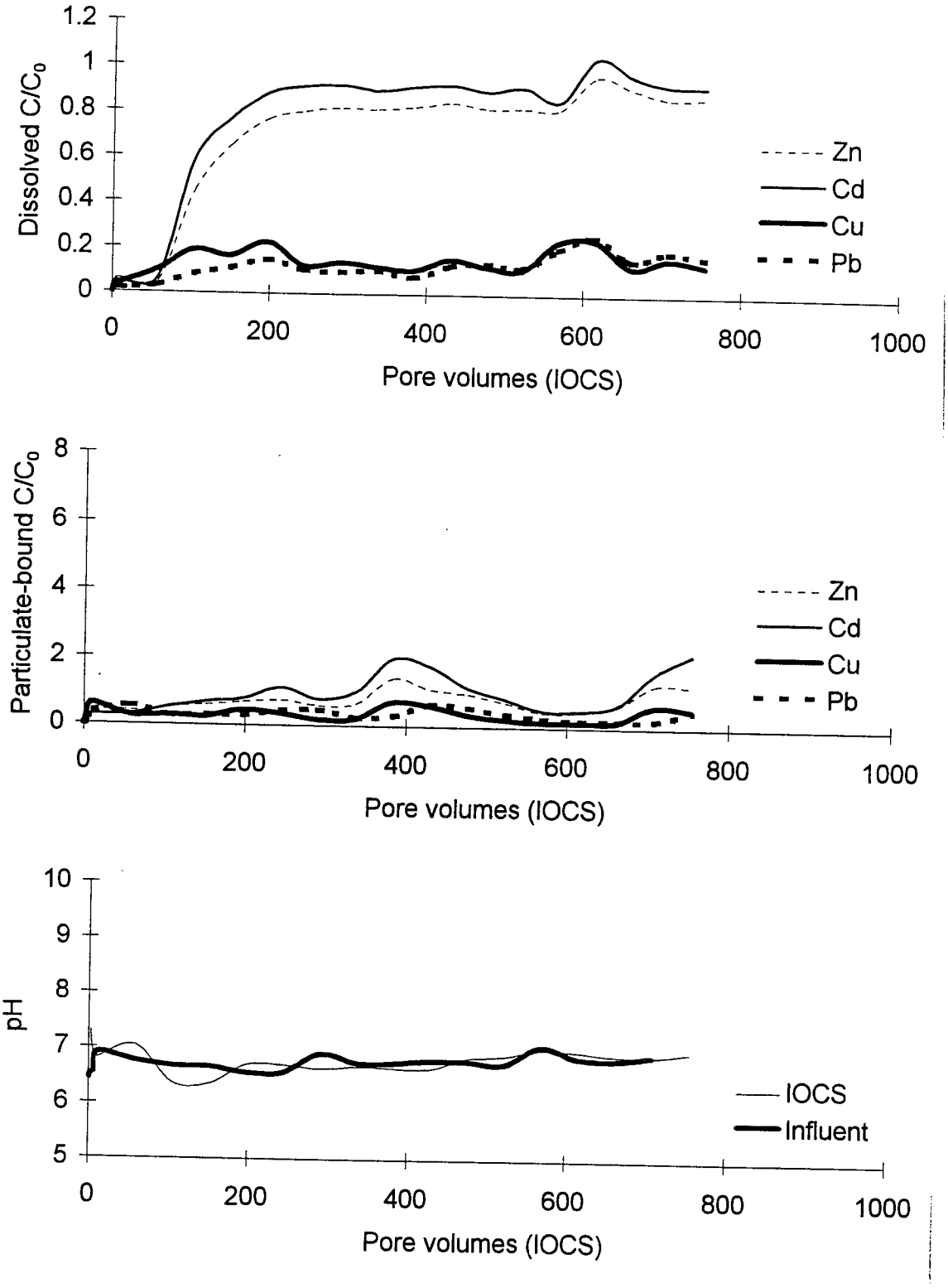

Figure 4.12.2 Breakthrough curves for Zn influent @ 10,000 µg/L and Cd, Cu, and Pb influent @ 1,000 µg/L each. (18 June 1996 stormwater) (IOCS).

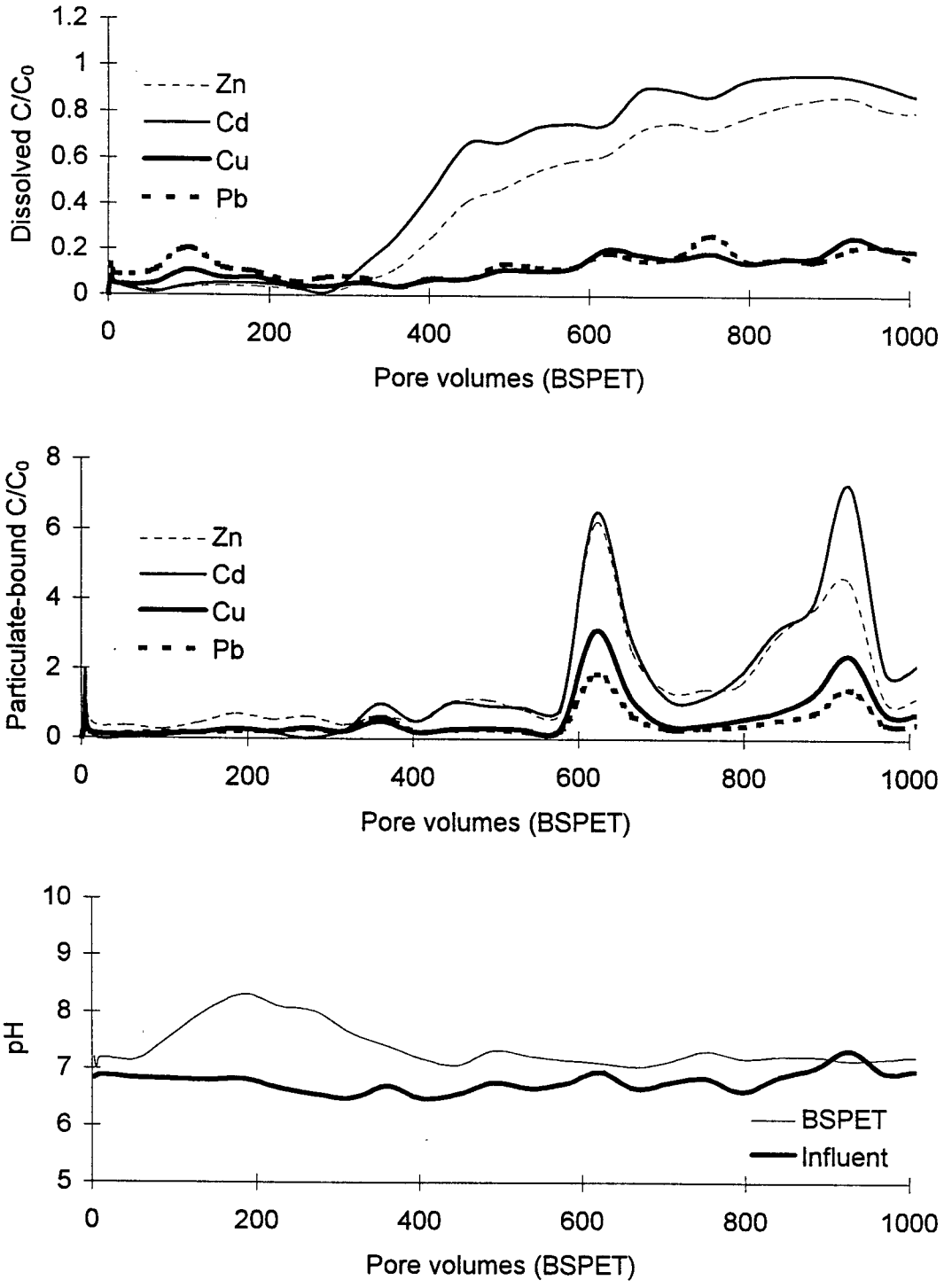

Figure 4.12.3 Breakthrough curves for Zn influent @ 10,000 µg/L and Cd, Cu, and Pb influent @ 1,000 µg/L each. (18 June 1996 stormwater) (BSPET).

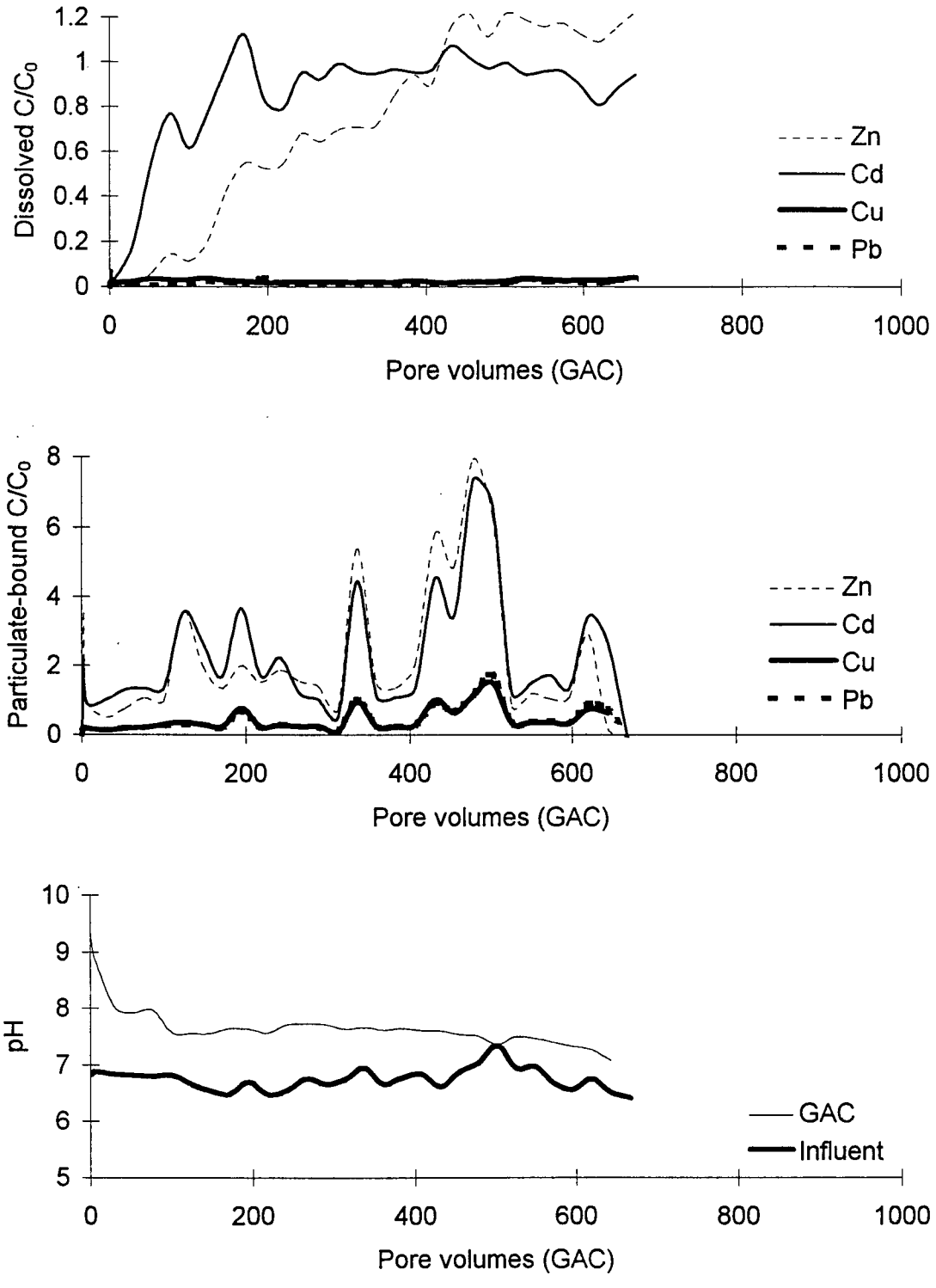

Figure 4.12.4 Breakthrough curves for Zn influent @ 10,000 µg/L and Cd, Cu, and Pb influent @ 1,000 µg/L each. (18 June 1996 stormwater) (GAC).

A mass balance was carried out for each of these runs and plotted as the ratio of the effluent mass divided by the influent mass. The mass balance was plotted for the total mass, and the dissolved and particulate-bound fractions. Mass balances were computed to ensure stormwater fractionation results as plotted in Figures 4.12.1-4 were accurate for the particulate-bound breakthrough. These mass balance results are plotted in 4.12.5-8.

4.13 Comparison of metal element capacity at breakthrough.

The mass of each metal element sorbed at $C/C_0 = 0.90$ are summarized in Table 4.13.1 for individual metal element runs and Table 4.13.2 for combined metal element runs. The results are summarized as mg of metal element sorbed per dry kg of porous media.

Individual metal elements in DI water

The capacity of silica sand, OCS and GAC for column runs utilizing individual metal elements in a DI water matrix are presented in Table 4.13.1. Several results stand out. First, the sorption capacity of OCS compared to plain silica sand is significantly greater for all metal elements. Second, pH has a significant influence on OCS capacity for all metal elements. As the pH is raised from 6.5 to 8.0 the capacity of the OCS is significantly greater. For OCS with a PZC between 7 and 8, this would be expected since a solution pH of 8 or greater would indicate the predominance of surface bonding sites would be negatively charged and available as metal ion bonding sites. At an influent pH of 6.5 the predominance of surface bonding sites would be positively charged and not available as metal ion bonding sites.

Table 4.13.1
Metal element mass sorbed per dry mass of media at $C/C_0 = 0.90$ breakthrough
(individual metal element in DI water)

		mass sorbed per dry mass at $C/C_0 = 0.90$			
Run	Metal Element	Silica sand (mg/kg)	OCS (mg/kg)	GAC (mg/kg)	BSPET (mg/kg)
Cd65-1	Cd	1.0	6.8	- - - -	- - - -
Cd80-1	Cd	1.3	317.1	302.6	- - - -
Cu65-5	Cu	1.3	357.5	- - - -	- - - -
Cu80-5	Cu	13.4	1920.8	10433.2	- - - -
Pb65-5	Pb	96.7	1176.7	- - - -	- - - -
Pb80-5	Pb	350.8	3181.7	- - - -	- - - -
Zn65-10	Zn	2.9	335.8	- - - -	- - - -
Zn80-10	Zn	5.0	992.5	2792.3	- - - -
1 silica sand pore volume mass(mg) =			1200		
1 OCS pore volume mass(mg) =			1200		
1 GAC pore volume mass(mg) =			351		

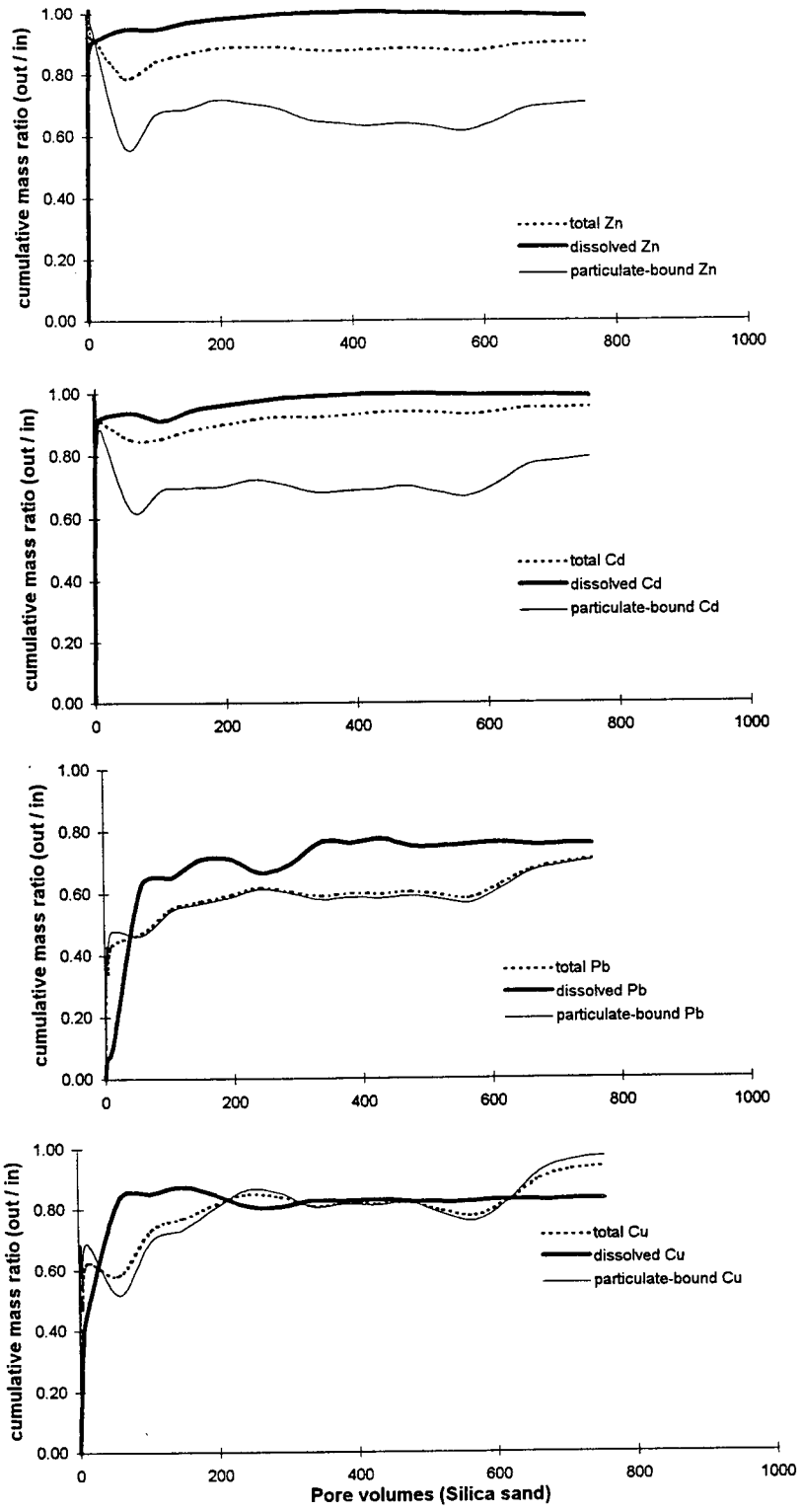

Figure 4.12.5 Column run cumulative mass balance using 18 June 1996 stormwater. (silica sand)

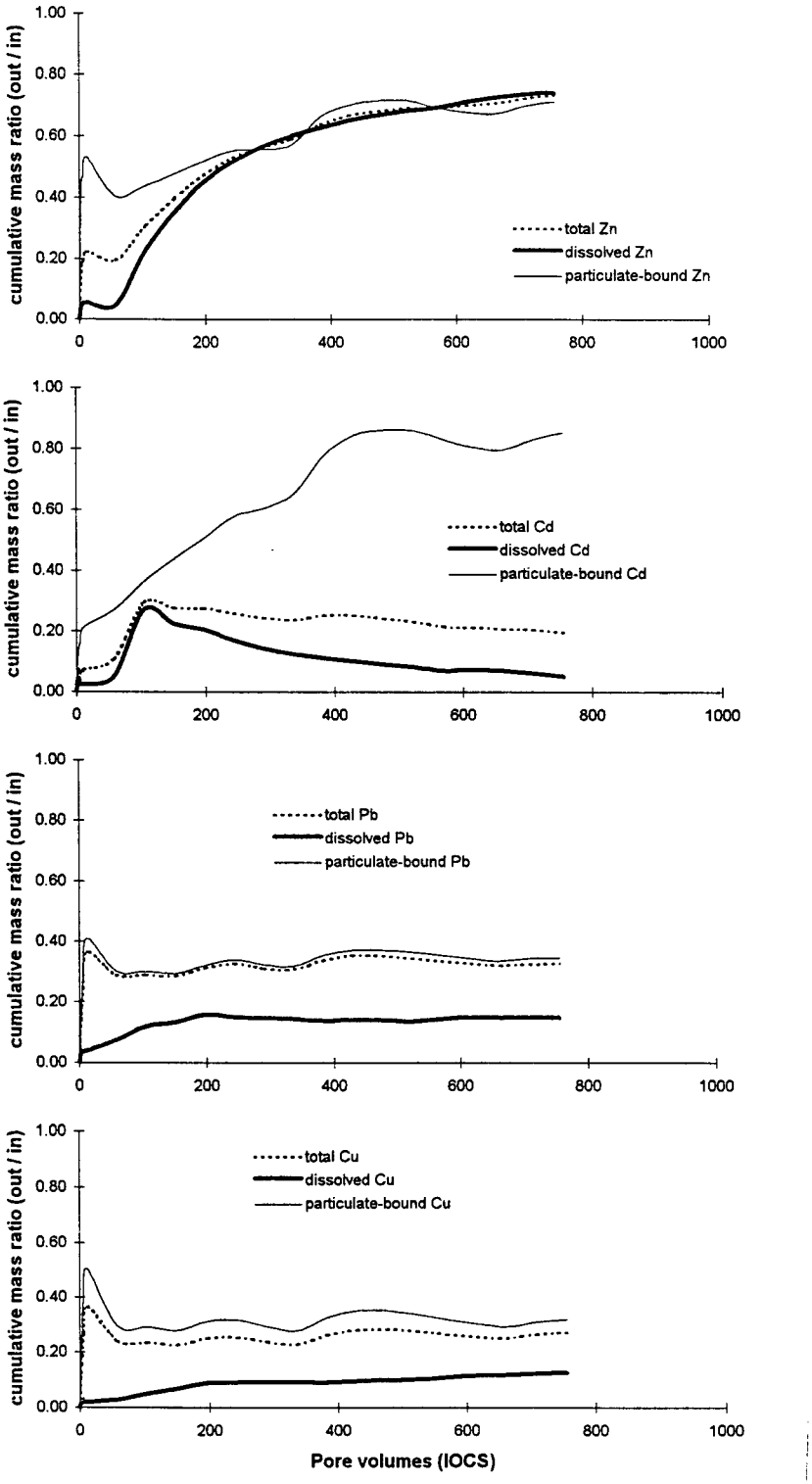

Figure 4.12.6 Column run cumulative mass balance using 18 June 1996 stormwater. (IOCS)

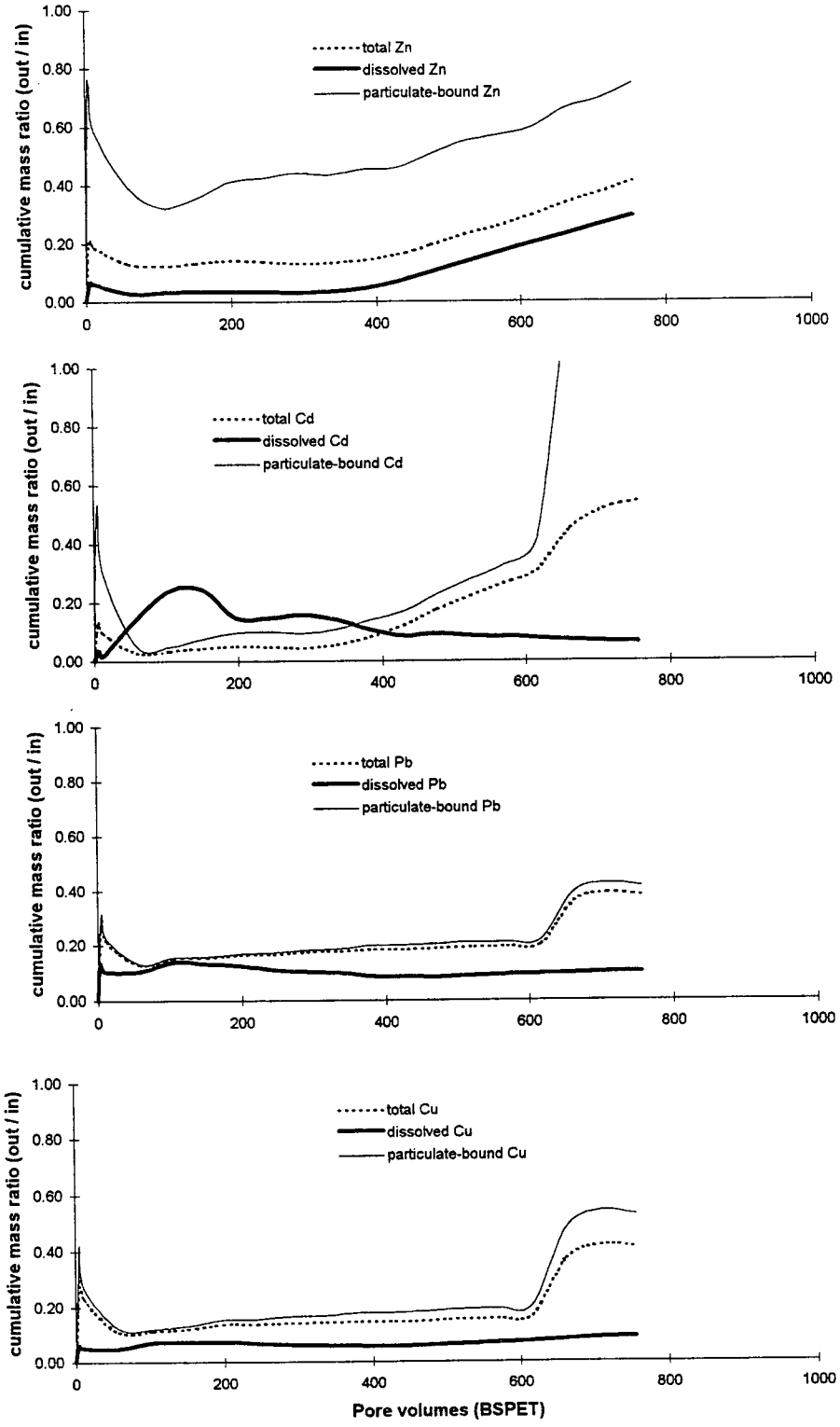

Figure 4.12.7 Column run cumulative mass balance using 18 June 1996 stormwater. (BSPET)

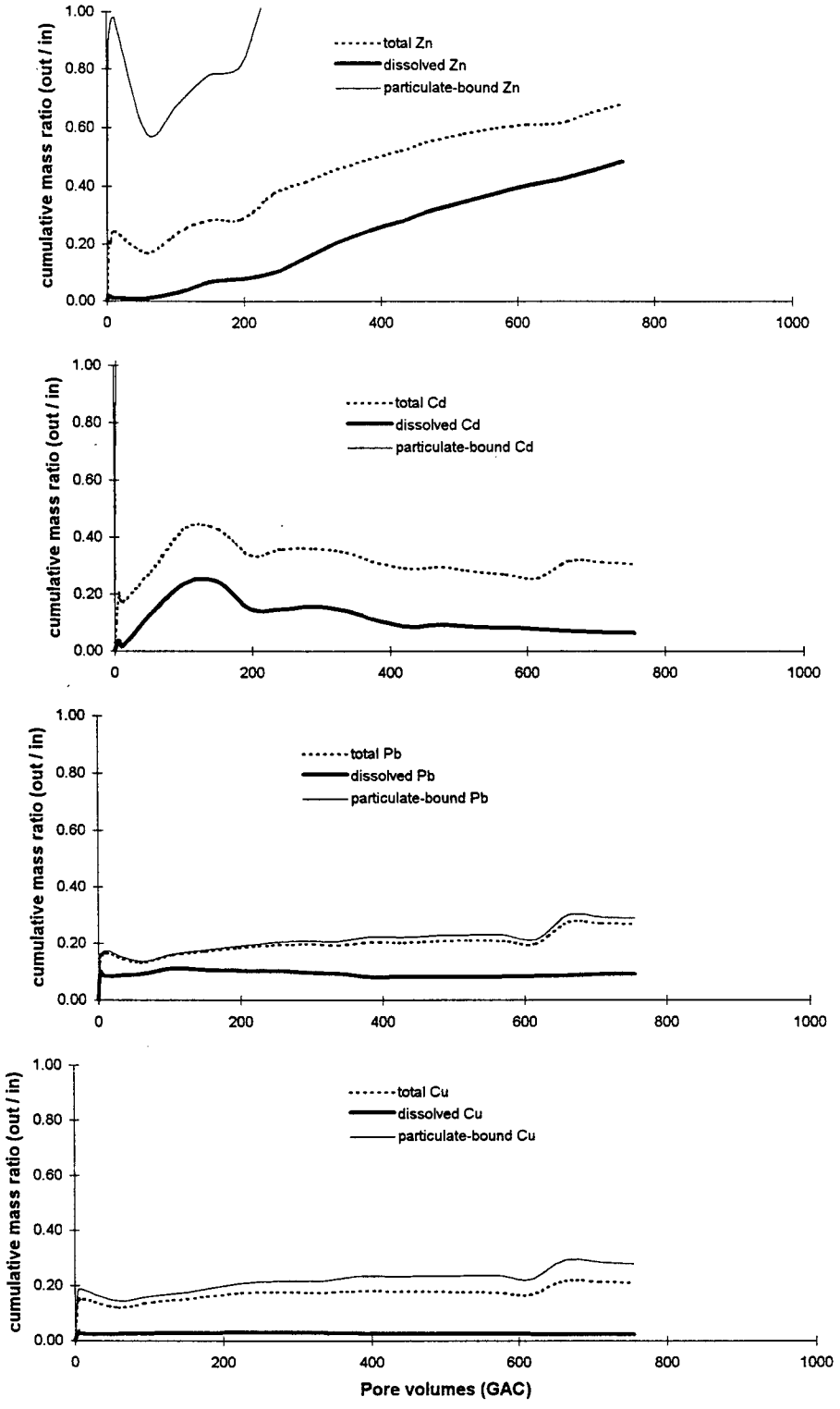

Figure 4.12.8 Column run cumulative mass balance using 18 June 1996 stormwater. (GAC)

Table 4.13.2
Metal element mass sorbed per dry mass of media at $C/C_0 = 0.90$ breakthrough
(combined metal elements in DI water & combined metal elements in stormwater runs)

		Mass sorbed per dry mass at $C/C_0 = 0.90$			
Run	Metal	Silica sand	OCS	GAC	BSPET
Zpcc65-5	Zn	1.0	23.0	105.0	551.0
	Cd	1.0	15.0	125.0	303
	Cu	3.2	116.0	1420.0	> 1970.0
	Pb	5.2	438.0	1070.0	> 1843.0
Zpcc80-5	Zn	1.0	781.0	1250.0	- - - -
	Cd	1.0	490.0	684.0	- - - -
	Cu	16.0	1170.0	2085.0	- - - -
	Pb	63.0	1480.0	1952.0	- - - -
Zpcc65-1	Zn	- - - -	- - - -	730.0	1838.0
	Cd	- - - -	- - - -	15.4	95.0
	Cu	- - - -	- - - -	428.0	878.0
	Pb	- - - -	- - - -	405.0	898.0
		dissolved fraction			
Zpcc65-S	Zn	1.9	1870.0	5046.0	11836.0
	Cd	0.2	42.0	56.0	522.0
	Cu	2.5	> 838	> 2077.0	> 2045.0
	Pb	4.0	> 670	> 3248.0	> 2785.0
		particulate-bound fraction			
Zpcc65-S	Zn	5.0	591.0	5.0	633.0
	Cd	0.3	14.0	0.2	33.0
	Cu	22.0	> 2090.0	4838	1202.0
	Pb	98.0	> 4333.0	1971.0	2965.0
1 silica sand pore volume mass (mg) =		1200			
1 OCS pore volume mass (mg) =		1185			
1 GAC pore volume mass (mg) =		351			
1 BSPET pore volume mass (mg) =		1168			

OCS has the greatest capacity for Pb followed by Cu then by Zn and finally by Cd. At a pH of 6.5 all metal elements except Pb exist predominately as divalent ions. Therefore at this pH the selective affinity of the OCS could possibly be explained by surface hydroxyl sites having preferential affinities for one metal ion, Cu, as compared to Zn or Cd. The large affinity for Pb can be explained by precipitation of Pb at a pH of 6.5, a sorption mechanism not present for the other metals. At a pH of 8.0 only Zn and Cd remain as divalent ions while Pb and Cu will precipitate. It is difficult to draw any conclusions regarding the influence of influent metal element concentration since Cd was run at 1 mg/L, while Cu and Pb were run at 5 mg/L and Zn was run at 10 mg/L.

Combined metal elements in DI water

The capacity of silica sand, OCS, GAC and BSPET configurations for column runs utilizing combined metal elements in a DI water matrix are presented in Table 4.13.2. Again, a number of results stand out. First, the sorption capacity of OCS compared to plain silica sand is significantly greater for all metal elements while the capacity of the BSPET is significantly greater than the OCS. Second, pH has a significant influence on OCS capacity for all metal elements. As the pH is raised from 6.5 to 8.0 the capacity of the OCS is significantly greater.

For run zpcc65-5 and zpcc80-5, Zn, Cd, Pb and Cu were run simultaneously at 5 mg/L. At both pH levels OCS had the greatest capacity for Pb followed by Cu and finally by Cd; the same order measured for individual metal elements in DI water. Since these metal elements were run simultaneously at the same influent concentration, these runs can provide an indication that iron oxide surface hydroxyl sites have a preference for Cu over Zn and finally over Cd. Because Pb will precipitate at both pH levels it is difficult to conclude that iron oxide has the strongest preference for Pb. This order of preference is the same order as that presented in Equation (4.2.9) based on the tendency of a metal element to hydrolyze and undergo sorption.

The BSPET results for zpcc65-5 demonstrate the influence of pH elevation on the capacity of the OCS. Breakthrough capacity was never achieved for Cu and Pb for the duration of the run. When comparing these results to those of zpcc80-5 several comparisons can be made. The BSPET capacity for Zn and Cd was lower, probably because the pH elevation capacity provide by the porous pavement dropped to below 7.5. Second the BSPET capacity for Cu and Pb was greater, possibly due to precipitation of Cu and Pb onto the porous pavement.

Finally, a BSPET run (zpcc65-1) was carried out using metal element concentrations that would also be run for the spiked stormwater; Zn at 10 mg/L and Cd, Pb and Cu at 1 mg/L. As with all BSPET runs, the influent pH for this run was 6.5 and the porous pavement aggregate provided the pH elevation capacity. This run was intended to provide a comparison of BSPET capacity for metal elements in a DI water matrix as compared to the stormwater matrix. However the results can also be compared to run zpcc80-5 and zpcc65-5. A comparison indicates that because of the relative increase of Zn influent concentration compared to Cd, Pb and Cu the iron oxide capacity for Zn has increased at the expense of decreased capacity for Cd, Pb and Cu. Clearly, the relative concentration of metal elements under competitive sorption conditions in assessing the performance of OCS. It may be difficult to accurately compare the overall capacity of both BSPET runs. There appears to be at least an 18% difference in total capacity between the two, however this could an artifact of the porous pavement aggregate used or the different batches of OCS.

Combined metal elements in stormwater

The capacity of silica sand, OCS, GAC and BSPET configurations for column runs utilizing combined metal elements in stormwater are presented for the dissolved and particulate-bound fractions in Table 4.13.2. The stormwater was spiked with 10 mg/L of Zn and 1 mg/L of

Cd, Pb and Cu. For the dissolved fraction of Pb and Cu, breakthrough did not occur for the OCS, BSPET or GAC configurations.

For the dissolved fraction, at a pH of 6.5, the OCS capacity for Zn has significantly increased as compared to previous combined metal element runs in a DI matrix. There appear to be at least two reasons for this. First, some of the increased capacity comes from the decreased capacity of Cu, Pb and Cd due to the increase in Zn concentration. Second, the increase in dissolved capacity for Zn may be an result of partitioning to and enrichment of the filtered solids by dissolved Zn. This dissolved behavior for Zn can be seen for OCS, GAC and BSPET configurations. Because of this partitioning and enriching it is difficult to make a direct comparison these stormwater runs and previous DI water matrix runs. The porous pavement pH elevation capacity improved the BSPET capacity for all dissolved metal elements. Some portion of this improvement for Cu and Pb is likely due to the precipitation of Cu and Pb on the porous pavement aggregate and partitioning to and enrichment of filtered solids appears to occur. However, enrichment does not occur to the same extent of Zn.

For the particulate-bound fraction, at a pH of 6.5, OCS capacity at breakthrough for Zn and Cd has significantly decreased compared to the dissolved fractions of Zn and Cd. This is also the case for the GAC and BSPET configurations. Previous runs did not include particulates so the only comparison which can be made to other runs is that the capacity is reduced by more rapid particulate-bound breakthrough. The BSPET configuration improved the capacity for Zn and Cd, possibly indicating some capacity of the porous pavement aggregate for Cd and to a lesser extent Zn. The higher capacity of the OCS configuration for Cu and Pb compared to the BSPET configuration is difficult to explain.

Comparison to other studies of OCS capacity

Benjamin and Sletten (1993) utilized OCS to immobilize dissolved and particulate-bound metal elements from a metal-bearing waste stream. They developed breakthrough curves for solutions of single metal elements and combined metal elements. However the results were presented in terms of total metal elements and the dissolved and particulate-bound fractions were not separated. For individual metal elements, run at a constant influent concentration of 0.5 mg/L, OCS capacity was determined. Unfortunately, Benjamin and Sletten claim to report capacities at $C/C_0 = 0.5$ and 1.0, however only one set of values is reported and no indication was provided as to which C/C_0 this was. For Cu @ pH 8.0 the total capacity ranged between 342 and 563 mg/kg, for Cd @ pH 8.0 the total capacity was 168 mg/kg and for Pb @ pH of 6.5 the total capacity was 102 mg/kg.

Benjamin and Sletten also ran experiments with a combination of 5 mg/L of Pb, Cd and Cu metal elements, although they reported that influent concentrations fluctuated between 3 and 7 mg/L. As with the individual metal elements the results were presented in terms of total metal elements and the dissolved and particulate-bound fractions were not separated. Breakthrough was nearly identical for all metal element run at a pH of 9.0. The total capacity (dissolved and particulate-bound) was approximately 1870 mg/kg of OCS at pH 9.0 for each metal element. Benjamin and Sletten carried out other experiments on individual metal elements and combined metal elements however capacities were not reported.

A direct comparison of the results of Benjamin and Sletten to those presented herein is difficult to make for the individual metal elements since there was no particulate-bound fraction for the DI matrix runs. It can be seen that with particulates present, breakthrough is reduced for Cu, Pb and Cd when compared to capacities for these metals in only dissolved form. Comparing the 5 mg/L combined Cu, Pb and Cd capacities to the OCS capacities using stormwater a better comparison may be drawn. For zpcc65-S the particulate-bound OCS capacity for Cu (> 2090 mg/kg) and Pb (> 4333 mg/kg) was greater than 1870 mg/kg but significantly less for Cd (14 mg/kg).

There appear to be several reasons for these differences. First, the stormwater run contained 10 mg/L of Zn and only 1 mg/L of Cu, Pb and Cd at a influent pH of 6.5. This relatively high level of Zn, typical of urban highway runoff, controlled the performance of the OCS and apparently the OCS capacity for other dissolved metals such as Cd. At a pH of 6.5, less than the PZC of 7 to 8 for iron oxides, the iron oxide surface had less capacity than at a pH of 9.0. Second, the chemical and physical nature of the particulate matter from the Benjamin and Sletten work with Superfund metal-bearing waste was probably quite different than the particulate matter transported in highway runoff. However, for both individual and combined metal elements in a DI matrix and in stormwater, the OCS presented in this research has a greater capacity than OCS produced by Benjamin and Sletten.

4.14 Conclusions

Bench-scale column experimental simulations were utilized to determine the breakthrough capacity of several media. Simulations were carried out for individual metal elements in a DI water matrix with no solids at a pH of 6.5 and 8.0. Simulations were also carried out for a combination of Zn, Cd, Cu and Pb in a DI water matrix with no solids at a pH of 6.5 and 8.0. Finally a simulation using actual stormwater containing solids was carried out. The media evaluated were silica sand (Ottawa 2030) used as control, OCS (iron-oxide coated Ottawa 2030), a BSPET configuration (an OCS column with 8 cm of porous pavement aggregate) and GAC (F-400). The influent flow rate was held constant at 50 mL/minute for all runs and this rate was established from the hydrology of the experimental site on I-75.

The capacity of the silica sand was negligible for Zn, Cd, Cu and Pb at both a pH of 6.5 and 8.0. This was expected and is the reason silica sand was used as control. Once coated with iron-oxide, the metal element capacity of the sand as OCS was significantly improved. Additionally, the performance of the OCS was significantly increased when the influent pH was raised from 6.5 to 8.0. This result held for individual metal runs as well as combined metal runs. For all runs the breakthrough capacity was smallest for Cd followed by Zn with breakthrough capacity greatest for Cu and Pb especially at the higher pH.

Breakthrough results demonstrated that the replacement of 8 cm of a 61 cm OCS column with porous pavement aggregate results in an increase in breakthrough capacity as compared to OCS at a pH of 6.5. The porous pavement is capable of raising influent pH sufficiently to make

the OCS an effective sorbent. The ability of the porous pavement to elevate stormwater alkalinity and provide surficial solids straining are important for the functioning of the PET.

Finally, the performance of each media was also evaluated with stormwater spiked with the metal elements of Zn, Cd, Cu and Pb. Breakthrough capacity was evaluated for the dissolved and particulate-bound fractions separately. The BSPET configuration provided a significant improvement in breakthrough capacity for the dissolved fraction of each metal, as compared to OCS. The BSPET configuration provided improved particulate-bound capacity for Zn and Cd but approximately a 15 percent decrease for Cu and Pb as compared to OCS. The reason for this decrease is not readily apparent except that at a higher pH both Cu and Pb are more particulate-bound. Therefore the influent at a pH of 6.5 will have less particulate-bound mass as compared to the effluent which has passed through the porous pavement aggregate. The resulting pH increase results in a greater change in partitioning for Cu and Pb as compared to Zn and Cd.

The results indicate that the critical design objectives of the PET are the porous pavement surface for straining influent solids at the surface of the porous pavement and controlling solids at the OCS interface and at the underdrain from the PET. Solids control to reduce particulate-bound breakthrough can be achieved with a geosynthetic filter at the porous pavement-OCS interface and a geosynthetic filter wrap surrounding the outfall underdrain.

PROTOTYPE PET DESIGN AND CAPACITY BASED ON COLUMN EXPERIMENTS

5.1 Introduction

To be effective throughout its intended design life, the components of a PET must perform a number of specific functions. These functions are summarized in Table 5.1.1. and illustrated in Figure 5.1.1. A schematic diagram of a PET is shown in Figure 1.2.1.

Table 5.1.1
Specific functions of PET components

	PET components				
Function	Porous pavm.	OCS	geosynthetics	underdrain	soil
Infiltration	■				
Straining surficial solids	■				
Structural capacity	■				
Sorbing dissolved metals		■			
Filtering infiltrated solids		■			
Straining infiltrated solids			■		
Underdrainage				■	
Exfiltration					■

As presented in this chapter, the primary focus for the PET design is metal element capacity, although other PET components and functions are considered. In order to estimate the PET design life for metal element capacity, data from both the experimental site and columns simulations were used. The experimental site provided data on metal element and solid EMCs, partitioning, pH, and lateral pavement sheet flow while the column simulations provided data on OCS metal element breakthrough capacity. From Table 5.1.1, infiltration and pH elevation will be presented in detail in this chapter while sorbing dissolved metals and filtration of infiltrated particulate-bound metal elements results have been addressed through column runs presented in Chapter 4. Results from the column run using spiked stormwater indicate breakthrough capacity of a bench scale PET column (BSPET) is controlled by the breakthrough of Zn, specifically particulate-bound Zn. The breakthrough curves for the BSPET are presented in Figure 4.12.3.

The bench scale column breakthrough capacity of the PET is controlled by Zn because the total concentration of Zn used was an order of magnitude greater than Pb, Cu or Cd. This order of magnitude difference, with Zn predominating over concentrations of Pb, Cu and Cd, is typical of results measured at the I-75 experimental site and other urban highway sites.

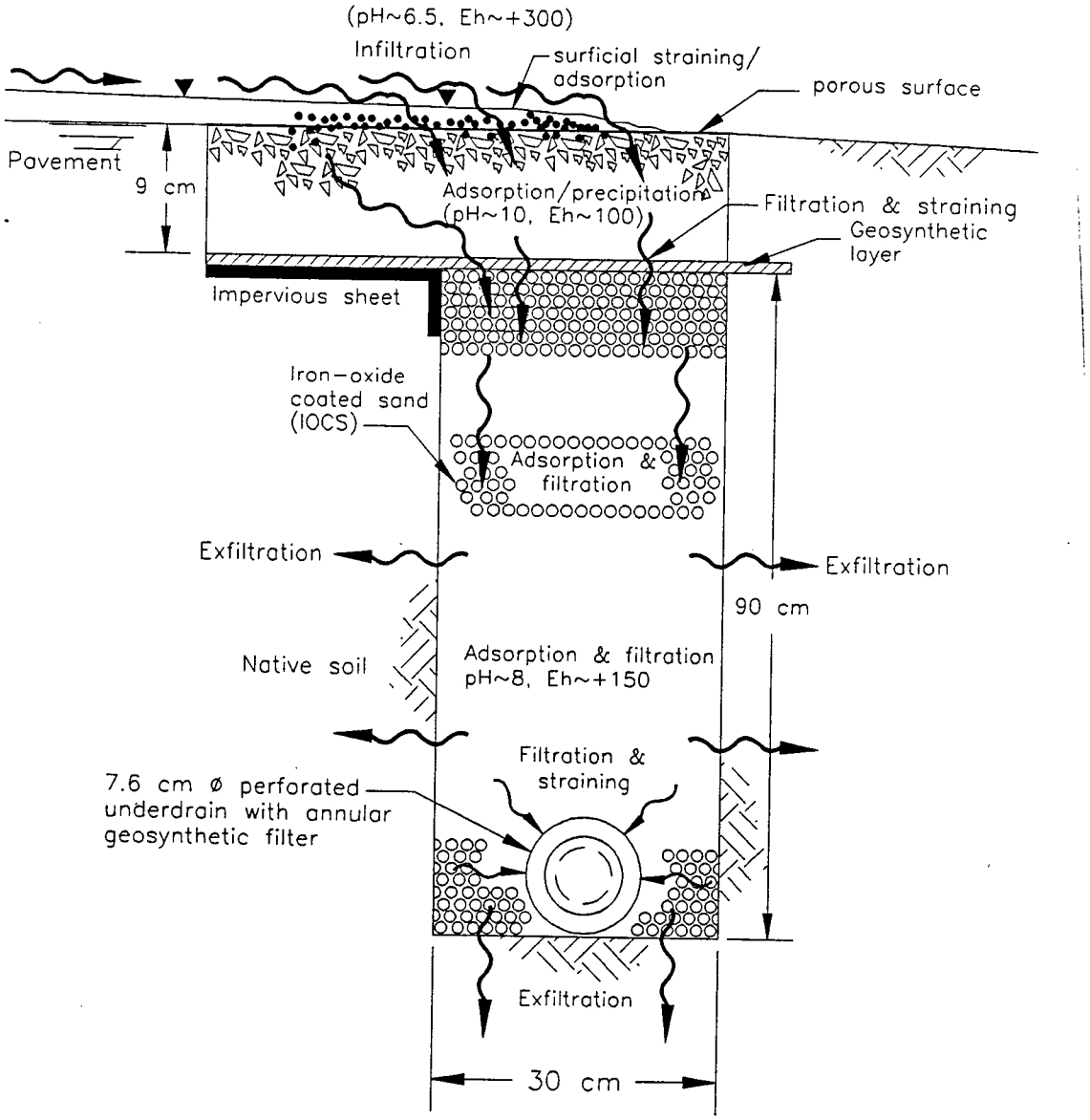

Figure 5.1.1. Physico-chemical mechanisms influencing solute/solid immobilization and flow components in the PET.

5.2 Design standard

In order to apply bench scale breakthrough results the level of breakthrough must be chosen. Several options were considered when choosing what level of breakthrough or design capacity to apply to a prototype PET. The criteria are:

1. $C/C_0 = 0.90$; applying a safety factor of 3 to a prototype PET.
2. $C/C_0 = 0.50$; with no safety factor.
3. metal element effluent ≥ metal element discharge standard.
4. Cumulative metal element mass loading = 50% of PET metal element capacity.

Criterion 1 was used when applying breakthrough results to a prototype PET capacity. Using this criterion breakthrough results could be applied directly to a prototype PET and the factor of safety applied to the PET capacity. This criterion is reasonable since the OCS has a fixed capacity under given flow conditions, pH, aqueous matrix and relative proportions of metal elements. By using $C/C_0 = 0.50$, criterion 2 is different from 1 in that a safety factor is applied to the breakthrough results instead of the prototype PET capacity. Criterion 2 was not applied. Criterion 3 can be a viable criterion if the duration of a discharge violation is established. Such a criterion would be applied over the entire discharge event as an EMC discharge standard. For Cd and Pb rainfall runoff concentrations it would be difficult to apply column simulations of unspiked stormwater to a prototype PET using Criterion 3. For Cd and Pb, rainfall runoff concentrations, if used as column influent, would be an order of magnitude or less of the ICP-AES detection limits and effluent concentrations would be less than detection limits until breakthrough. Criterion 3 was not applied. Criterion 4 is essentially the same concept as Criterion 1 or 2 but based on mass not metal element discharge levels. **Criterion 1, using a level of breakthrough at C/C_0 = 0.90 was chosen.**

5.3 Design functions of the porous pavement

Infiltration capacity

By design, the approach flow to a PET occurs as a thin sheet of lateral pavement runoff. The PET is not intended to be loaded by concentrated flow. Lateral pavement sheet flow hydrographs from the I-75 experimental site were presented in Figure 2.7.1.

A lateral peak flow (LPF) of 15 L/min-m was chosen as the design inflow for the bench-scale columns. This flow was determined from the experimental site hydrologic data. This peak flow is typical of moderate intensity (65 mm/hr) rainfall event hydrograph peaks as occurred during the 3 October 1995 event. Using the APRT of 3.3 minutes for this event (Table 2.7.1) to compute an intensity, a rainfall return period of approximately 1 year was required to match the 65 mm/hr intensity. The LPF of 15 L/min-m exceeds the events of 30 April, 15 July and 8 September but is less than the very high intensity short duration peak (100 mm/hr) of 8 April 1995. Since the column experiments were carried out during the first half of 1996, data from the 1995 events was utilized.

In order to evaluate the infiltration capacity of porous pavement 20.3 cm x 40.6 cm x 8.9 cm paver blocks were manufactured by a regional block manufacturer. Measured infiltrated flow rate per unit area was approximately twice the rate of 50 mL/minute used for the column simulations. 6.9 cm diameter x 9.2 cm long specimens were cored from the block and placed in a falling head permeameter. The block must have the hydraulic capacity to infiltrate 49.2 L/min-m^2 (15 L/min-m^2 for a 0.305 m wide PET) unless some amount of flow by-pass may be tolerated. The measured hydraulic conductivity of porous pavement, manufactured for the experimental field site, is presented in Table 5.2.1. Each precast block is 61 cm x 61 cm x 10 cm thick. Although the actual trench containing OCS is 0.30 meters wide, the porous pavement block is 0.601 meters wide. An impermeable sheet is placed under this 0.30 meters in front of the OCS trench so that

all infiltrated flow is transported to the trench.

Based on these data, the blocks for the prototype were specified to have a greater hydraulic conductivity. In the actual prototype PET, joint flow between blocks will provide a greater overall hydraulic conductivity. Preferential joint flow has been observed for the prototype PET during the 17-18 October rainfall runoff event.

pH elevation capacity

The efficacy of the pavement aggregate to elevate pH was tested in the laboratory. DI water at a nominal pH of 6.5 was used as the permeating liquid. Three consecutive effluent samples were collected from each core and analyzed for pH, ORP and alkalinity. The results are summarized in Table 6.2.1. The aggregate from crushing these cores was passed through the #10 sieve and the aggregate retained on the #10 sieve was used in the BSPET column simulations.

Table 5.3.1
Measured effluent pH, ORP and alkalinity for porous pavement cores.

Core[1]	pH		ORP (mV)		Alkalinity (mg/L as $CaCO_3$)		Hydraulic Conductivity[2] (cm/sec)	
	mean	σ	mean	σ	Mean	σ	Mean	σ
DI water effluent								
No. 1	11.96	0.29	+100 ± 10	- - - -	677	103	0.00531	0.00031
No. 2	11.95	0.19	+100 ± 10	- - - -	585	26	0.00550	0.00010
No. 3	11.88	0.037	+100 ± 10	- - - -	564	49	0.00534	0.00032
DI water influent								
DI water	6.3	0.071	+305	13.5	- - - -	- - - -	- - - -	- - - -

[1]: 3 consecutive effluent volumes of 240 mL ± 10 mL were analyzed for each core
[2]: Hydraulic conductivity evaluated using falling head permeameter
Nominal unconfined compressive strength of block was 2000 psi (per manufacturer)
Influent was DI water at pH = 6.3

The purpose of the increased width of the porous pavement is twofold. First, the bench-scale column results demonstrated the ability of elevating the pH to 8.0 or greater. The increased width provides an additional infiltration/straining surface area. Second, while the increased width provides greater infiltration surface it also reduces the surface loading rate from 49.2 to 24.6 L/min-m^2. This width is particularly beneficial for low intensity rainfall with long APRT which result in higher dissolved metal element fractions. Runoff will infiltrate at the leading edge of the porous pavement, and travel diagonally towards the PET trench, thereby increasing flow length and travel time in the pavement. This phenomenon has been observed for a low intensity, long duration event occurring on 17-18 October 1996.

Straining surficial solids

There are two components of the PET which are critical to the control and discharge of solids. The first component is the porous pavement block which serves as initial control preventing solids from entering the PET. The porous pavement block is capable of straining larger suspended solids before these solids enter the PET. The porous pavement aggregate is pea gravel and sand having gradations presented in Figure 5.3.1. This coarse aggregate gradation combined with a low water-cement ratio can produce a porous pavement block capable of significant infiltration while also providing a surface where which solid straining can occur.

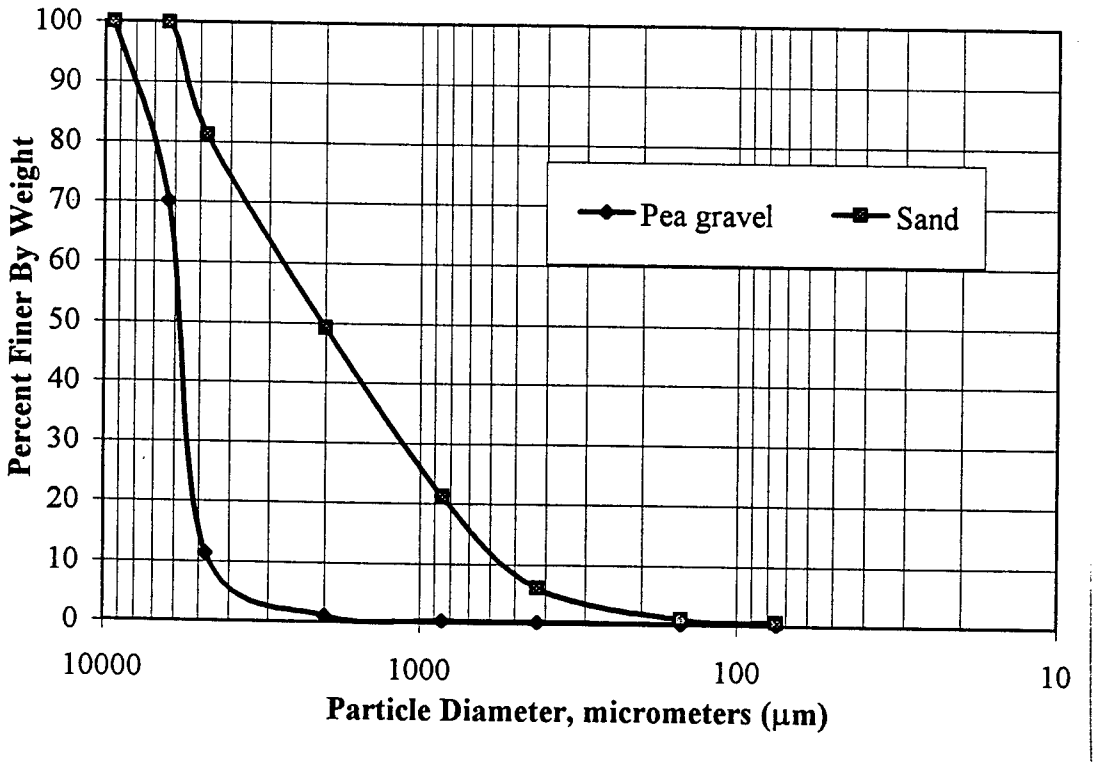

Figure 5.3.1. Porous pavement aggregate and sand gradations.

Solids in pavement runoff have a wide particle size distribution. PSDs have been measured range in size from less than 1 μm to greater than 10,000 μm. The PET is not designed to function as a depth filter for these solids. The porous pavement block is designed to strain solids at the surface of the block. A schematic mechanism for surficial straining is shown in Figure 6.2.2. Using the criteria presented in Figure 5.3.2 and a 0.60 mm uniform particle size for IOCS, solids greater than 30 μm should be strained at the porous pavement surface. Typically less than 5% of the particles by weight, for the rainfall runoff PSDs presented in Figure 2.9.8 are finer than 30 μm. The surficial straining is important for two reasons. First, the PET does not have the capacity to function as a deep bed filter for particles in the 30 to 60 μm range since it is not feasible to backwash the PET. Second, when the solids are strained at the surface, proven practices for porous pavement such as dry or wet vacuuming are reasonable to apply on a regular maintenance schedule (Niemczynowicz, 1990).

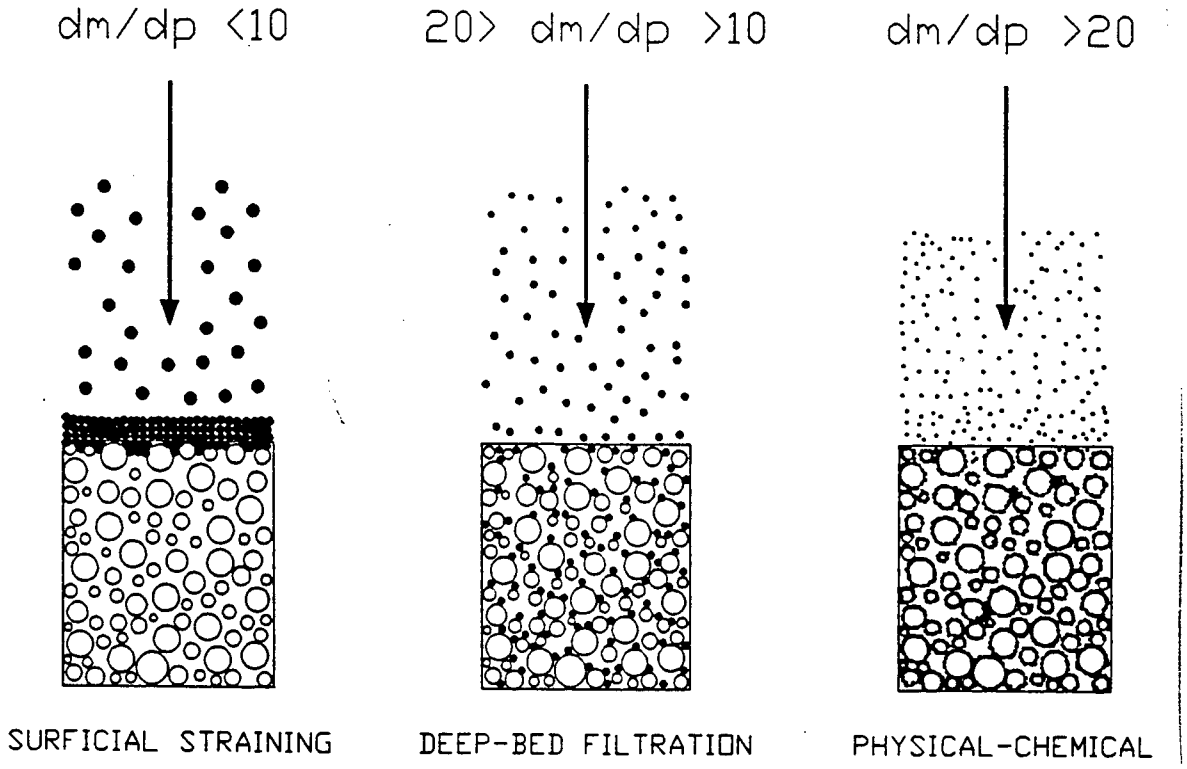

Figure 5.3.2 Filtration mechanisms of porous pavement and OCS.

Structural capacity

Although the PET is located outside of the traveled pavement, it will experience occasional wheel loads. Therefore the porous pavement and OCS backfill must be designed to transfer imposed wheel loads to surrounding soil without excessive deformation or structural distress. Unconfined compressive strength (UCC) is typically used as an index for structural performance of pavement materials. The standard concrete blocks provided by the regional manufacturer had a nominal UCC of 1406 kPa which was increased for the prototype PET to 3515 kPa for the purpose of pH elevation and durability.

Sorbing dissolved metals

The pavement may have some capacity to sorb and precipitate dissolved metal elements. This capacity has not been evaluated.

5.4 Design for OCS metal element breakthrough capacity

As shown in Table 5.1.1 the OCS component of the PET has two functions, one to adsorb dissolved metal elements and also to filter particulate-bound metal elements. The design life of a PET in terms of metal element capacity is primarily dependent on the performance of the OCS for adsorption and filtration. Bench scale column experiments using spiked stormwater from the I-75

experimental site were carried out to evaluate metal element capacity. A methodology, summarized in Figure 5.4.1, applies OCS bench scale breakthrough capacity coupled with loadings typical of an urban highway site for a prototype PET design. Additional explanation is provided below.

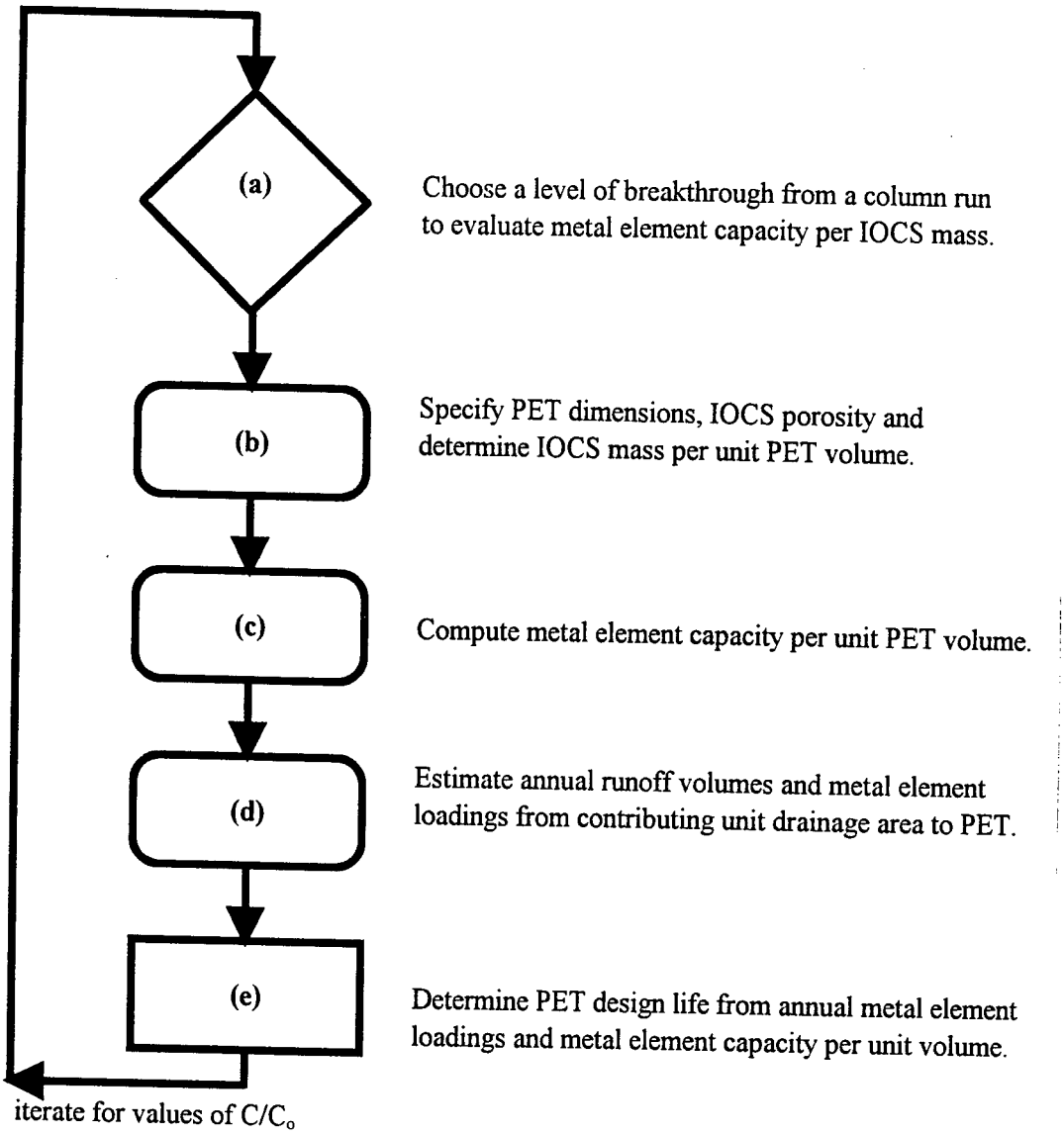

Figure 5.4.1. Flowchart for PET design life analysis based on metal element capacity.

(a) From the column runs, zpcc65-S represents OCS capacities using a stormwater matrix spiked with metal elements and are more representative of actual PET capacity. The BSPET results from run Zpcc65-S may under-estimate actual PET capacity because only the pea gravel aggregate from the porous pavement was used in the BSPET configuration since the porous pavement core diameter was too large to fit the BSPET column. The pea gravel aggregate does not provide the alkalinity which would occur if the influent had contacted the entire pavement matrix.

(b) A range for standard PET dimensions can be specified based on various site and loading constraints. For example, as an underdrain replacement, a standard PET dimension would be 100 cm deep by 30 cm wide. An iteration procedure could be used to develop a range of dimensions as a function of breakthrough level, design life or other constraints. OCS mass is computed from the PET dimensions, the porosity and specific gravity of the OCS. OCS mass per unit PET volume is determined.

(c) The OCS mass per unit PET volume is multiplied by the metal element capacity per OCS mass at the chosen breakthrough level.

(d) Using rainfall-runoff data from the experimental site measured rainfall depths were converted to expected runoff volumes assuming no abstractions. The measured runoff volume was divided by the precipitation to yield a runoff volume coefficient between 0 and 1.0 (Bedient & Huber, 1988). A site specific average runoff volume coefficient was computed using runoff volume results from the measured rainfall-runoff events. A single runoff volume coefficient was applied as a site average. This coefficient will be applied to annual average rainfall depth for the Greater Cincinnati area. Using the runoff volume coefficient and annual average rainfall depth an annual runoff volume can be computed.

From water quality characterization of runoff collected at a site the EMC for the dissolved and particulate-bound fractions of metal elements is determined. By multiplying the EMC by the total runoff volume for each event the dissolved and particulate-bound mass transported by each event could be determined. From each event the dissolved and particulate-bound metal element EMCs will be averaged to yield a single site average EMC for each fraction of each metal element. These site average EMC values will be multiplied by the average annual runoff volume to calculate an annual metal element mass for both dissolved and particulate-bound fractions.

(e) The metal element capacity per unit PET volume of each metal element fraction was divided by the calculated annual mass loadings for each metal element fraction to yield an ultimate capacity per unit PET volume. A factor of safety can be chosen to account for future increases in metal element loadings, deviation in PET behavior and flow variations as compared to the bench-scale column simulations.

5.5 Design for geosynthetic control of solids discharge

Control of solids at the porous pavement-OCS interface

Finer solids can pass through the connected porous pavement voids or though the joint between porous pavement blocks. A geosynthetic layer at the porous pavement-OCS interface is used to control these solids before they reach the OCS. This layer of geosynthetic is a simple, inexpensive component which augments the solids control of the porous pavement and prevents solids from clogging the OCS. Using the criteria presented in Figure 5.3.2 and a 0.6 mm OCS diameter the geosynthetic would be designed to trap solids greater than 30 μm. The prototype PET has a geosynthetic layer located at the porous pavement-OCS interface.

Control of infiltrated solids

A second component of the PET for control of solids, to prevent discharge particulate-bound metal element discharge from the underdrain, is a properly designed geosynthetic filter around the underdrain. Results from the column simulation utilizing stormwater indicated that metal element breakthrough was controlled by movement of particulate-bound metal elements. Additionally, particulate-bound breakthrough curves indicated that some particles which were initially filtered were then sloughed off and enriched by influent metal elements. As a result, future PET designs and the prototype PET has a geosynthetic sock surrounding the underdrain.

Underdrain design

The underdrain is intended to function as the primary conveyance for the infiltrated runoff. The underdrain is a continuous, perforated pipe located at the bottom of the PET. The diameter of the underdrain is 7.6 cm. This diameter is capable of conveying all infiltrated flow to existing drainage structures or to surface flows. The underdrain is designed under the assumption of minimal native soil exfiltration.

5.6 Results

The methodology described in Section 5.4 was applied to evaluate the design life of the PET for dissolved and particulate-bound metal elements for a typical roadway site.

The chosen column simulation was Zpcc65-S using spiked stormwater. The incremental mass sorbed per dry mass of OCS was continually summed until breakthrough.. The lower portion of Table 5.9.2 summarizes these results in terms of total metal element mass sorbed at breakthrough per dry mass of OCS for run Zpcc65-S.

PET dimensions were specified based on the replacement of an existing underdrain by a PET. Assuming a OCS porosity of 0.35 and OCS specific gravity of 2.73, the dry bulk density of OCS is 1.8 g OCS per cm^3 (1786 kg/m^3) of trench. From the I-75 site an average runoff volume coefficient was determined.

Table 5.6.1
Experimental site hydrologic data used for a site specific average runoff coefficient

Rainfall event	Measured Runoff (L)	Measured rain depth (mm)	LEMF (L/min-m)	Rainfall duration (min.)	Traffic intensity	Average runoff coefficient
08 Apr. 95	5439	25.0	1.2	295	light	0.73
30 Apr. 95	211	1.0	0.1	109	very light	0.70
15 Jul. 95	41	0.4	0.2	16	moderate	0.34
08 Sep. 95	401	4.0	0.1	202	very heavy	0.33
03 Oct. 95	1260	8.5	0.2	393	very heavy	0.49
21 May 96	199	1.02	0.1	125	moderate	0.65
18 Jun. 96	2779	9.39	2.6	70	light	0.98
07 Jul. 96	9644	33.53	11.5	56	light	0.96
Site specific average runoff coefficient :						**0.65**
Drainage area = 15m x 20 m Average daily traffic (north and southbound lanes) = 150,000 vehicles						

The average annual rainfall in the Greater Cincinnati area is 1020 mm per year. *Assuming no abstractions*, this rainfall depth would equate to an expected annual runoff volume of 1020 L/m^2 drainage area for the PET. Application of the site specific runoff volume coefficient results in an average annual runoff volume of 663 L/m^2 of pavement drainage area to be infiltrated per meter length of PET.

Site EMC data from 1995 events were utilized to compute EMC values for the dissolved and particulate-bound fractions of Zn, Cd, Cu and Pb. Results are summarized in Table 5.6.2.

Table 5.6.2
Experimental site rainfall-runoff EMC values used for site specific EMC values.

	Dissolved EMCs (ug/L)				**particulate-bound EMCs (ug/L)**			
Rainfall Event	Zn	Cd	Cu	Pb	Zn	Cd	Cu	Pb
08 Apr 95	250.5	2.8	13.4	12.9	208.5	2.6	29.2	48.6
30 Apr 95	1327.1	18.4	44.0	14.2	171.0	3.4	26.1	17.1
15 Jul 95	13756.0	19.5	224.3	14.6	641.6	2.4	90.3	29.3
08 Sep 95	3049.2	2.2	102.7	15.7	561.9	2.8	63.6	72.6
03 Oct 95	1069.8	3.2	28.9	24.4	618.2	2.7	54.4	90.1
site EMC	3890.5	9.2	82.7	16.4	440.2	2.8	52.7	51.5

The EMC values from Table 5.5.2 are converted to mass loadings for the dissolved and particulate-bound fractions of each metal element by multiplying site EMC values from bottom of Table 5.5.2 by the average annual runoff volume of 663 L per m^2 of pavement drainage area. Snow loadings were not considered since this material is plowed from the pavement and would reside beyond the PET's porous pavement block. The annual metal mass loadings per unit area of pavement are summarized in Table 5.6.3.

Table 5.6.3
Annual metal element mass loadings per m^2 of pavement drainage area.

	annual dissolved mass loadings (mg/m^2)				**annual particulate-bound mass loadings (mg/m^2)**			
Metal	Zn	Cd	Cu	Pb	Zn	Cd	Cu	Pb
site average	2582	6.1	54.8	10.9	291.8	1.86	34.9	34.1

The PET capacity can be determined for a typical urban roadway condition assuming similar hydrologic and metal element loading conditions.

5.7 Example of PET design life calculations

This example is based on standard design criteria for urban roadway layout and hydrologic/metal element loading for conditions similar to the experimental site.

Site data

ADT	= 150,000
Pavement type	= Asphalt (some cracking)
Pavement drainage area (m^2/m of PET length)	= 15 (3 lanes + paved berm)
Pavement slope towards PET	= 2.0%
Average runoff volume coefficient	= 0.65
Average annual rainfall (mm)	= 1020
Average annual runoff volume (L/m^2 pavement area)	= 663

PET data

PET location (as an underdrain replacement)	= outer edge of paved berm
Porous pavement width x thickness (cm)	= 60 x 10
Porous pavement UCC (psi)	= 5000
PET width x depth (cm)	= 30 x 76
OCS specific gravity (g/cm^3)	= 2.73
OCS bulk density (g/cm^3)	= 1.8 (1786 kg/m^3)

Metal element loading data

Average annual site EMCs	= Table 5.6.2
Average annual metal element loadings	= Table 5.6.3

OCS capacity from bench scale results

Level of breakthrough (%)	= 90
OCS capacity (mg/kg of OCS)	= Table 4.13.2
Factor of safety for design life	= 3

PET design life results

From the data and application of the methodology presented in Figure 5.4.1 metal element loadings were determined and summarized in Table 5.7.1:

Table 5.7.1
Annual metal element mass loadings for typical urban roadway site ($15m^2/m$).

	annual dissolved mass loadings (mg)				annual particulate-bound mass loadings (mg)			
Metal	Zn	Cd	Cu	Pb	Zn	Cd	Cu	Pb
site average	38730	92	822	164	4377	28	524	512

OCS capacities were determined and are summarized in Table 5.7.2:

Table 5.7.2
Metal element mass capacity of design example PET.

	Prototype PET metal element mass capacity (grams) [1]				
Run	Zn	Cd	Cu	Pb	fractionation
Zpcc65-S	4083	180	>>705	>>961	dissolved
Zpcc65-S	219	12	1023	414	particulate-bound
[1]: based on 414 kg/m of OCS $15m^2/m$ PET drainage area					

The results summarized in Table 5.7.2 represent 90% OCS capacities for the given PET configuration and site drainage area. These ultimate or unfactored capacities are divided by the annual mass loadings of Table 5.5.3 to yield unfactored design life values for each metal element fraction. A factor of safety of 3 has been chosen for the factored design life. This factor accounts for uncertainties in metal element loading, capacities of OCS coating and pH elevation by the porous pavement. The unfactored and factored design life based on each metal element fraction are presented in Table 5.5.6

Table 5.7.3
Ultimate and factored PET design life for specific metal element fractions

	Factored design life (years)				Ultimate design life (years)			
Fraction	Zn	Cd	Cu	Pb	Zn	Cd	Cu	Pb
dissolved	35	652	286	1953	105	1956	858	5859
particulate-bound	17	143	651	270	50	428	1952	809

Depending on the level of breakthrough chosen, a design life range for a targeted metal element can be obtained. This range is shown for Zn, the breakthrough-controlling metal element, in Figure 6.7.1.

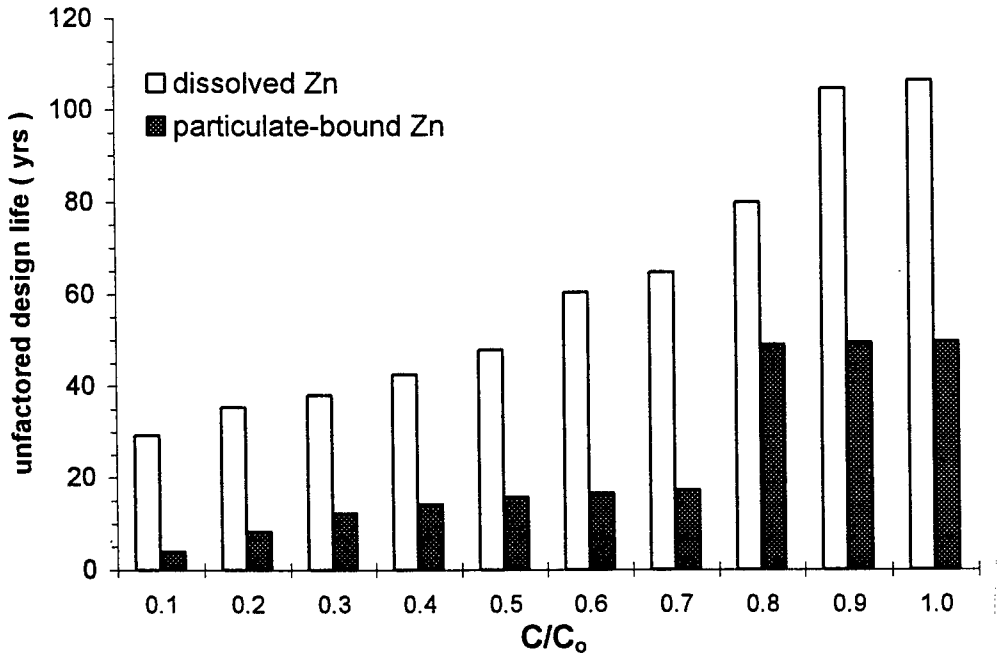

Figure 5.7.4 PET design life as controlled by breakthrough of particulate-bound Zn.

5.8 Conclusions

The critical design elements of a PET are sufficient hydrologic loading capacity, sufficient breakthrough capacity for targeted metal elements and capability to surficially strain solids at the porous pavement surface and filter finer infiltrated solids which would be otherwise discharged through the PET underdrain Column simulations were carried out to assess the capacity of IOCS to immobilize Zn, Cd, Cu and Pb. Column simulations using stormwater spiked with Zn, Cd, Cu and Pb were considered most representative for evaluating the capacity of a prototype PET. A methodology was presented to evaluate the potential capacity of a prototype PET from application of column simulation results. Hydrologic parameters and loadings as well as metal element fraction loadings, all derived from the experimental site were used to estimate annual loadings to a prototype PET.

Results from application of this methodology to a PET design at the experimental site suggest that the design life of a PET in terms of metal element breakthrough is controlled by breakthrough of particulate-bound metal elements. Results indicate that the factored design life of a PET is approximately 15 to 20 years dictated by breakthrough of particulate-bound Zn. This result underscores the importance of solids control by surficial straining and the use of a geosynthetic liner at the block-OCS interface. Additionally, with respect to particulate-bound metal element discharges from the underdrain, the use of a geosynthetic liner around the underdrain would augment particle retention and therefore extend the design life of the PET.

This conclusion assumes that the design life is based on setting a discharge criterion at 90% breakthrough for a particular metal element fraction. Levels of Cd, Cu and Pb were one to two orders of magnitude higher than typical rainfall runoff EMCs. Lowering influent levels of Cd, Cu and Pb would have provided addition OCS capacity for dissolved Zn and possibly provided additional competitive adsorption sites for Zn which enriched filtered solids.

A 15 year PET design life is comparable to the service life of the typical asphalt pavement on urban highways. One alternative to rejuvenate PET capacity would be to replace the OCS. This could be accomplished using the same OCS on-site. Using a mobile process the OCS would be excavated, washed at a low pH and replaced back in the PET as clean OCS. The PET design would allows in-situ backwashing only under conditions where soil hydraulic conductivity was very low, as in clayey soils.

FULL-SCALE PROTOTYPE PET PERFORMANCE AT EXPERIMENTAL SITE

6.1 Introduction

A number of researchers have investigated various aspects of urban roadway stormwater infiltration. Swedish researchers have shown that asphaltic porous pavement, a type of infiltration device, effectively removes a wide range of constituents transported in highway runoff. The Swedish porous pavement, known as the Swedish Unit Superstructure, was developed as both a water quantity and quality control device. Simulations using 30 years of exposure to "stormwater rain" indicated the Unit Superstructure performed effectively. The simulation results indicated negligible clogging and these results were confirmed during tests of in-situ porous pavement (Niemczynowicz, 1989).

The practice of stormwater infiltration has also led to concerns related to degradation of surrounding soils and receiving groundwater. In a recent study, the influence of natural organic matter (NOM) on facilitated metal element transport was experimentally simulated using large-scale soil columns (Igloria et al., 1997). For this study, results indicated that the presence of NOM did not enhance metal element transport. For stormwater infiltration through porous pavement, large solids are strained at the surface while finer particles can be infiltrated through the porous pavement structure. Street cleaning techniques such as spraying high-pressure water on the porous pavement and vacuuming will effectively remove solids from the porous pavement (Colandini, 1995).

6.2 Materials and Methods

The primary focus of the PET design was metal element immobilization and capacity, although other PET functions were also considered. In order to evaluate the prototype PET, data from the experimental site were required.

Experimental Facility

In early 1995 the highway stormwater collection and sampling system was constructed. In late summer of 1996 the prototype PET was constructed at the experimental site, after bench scale testing of the PET had been completed. The experimental facility and PET were designed to intercept only lateral pavement sheet flow from across the four lanes, exit lane and shoulder. Since the catchment lies in a flat vertical sag there was no concentrated longitudinal gutter flow, or flows from outside the pavement catchment area.

The PET was installed north of an existing experimental runoff sampling structure located in Cincinnati, Ohio, along Interstate 75, in the center grassed median approximately 750 feet north of the Western Hills Viaduct Overpass. Figure 6.2.1 shows the location of the PET. The preexisting sampling structure is used to establish water quality parameters of the runoff before infiltration through the PET. A cross-section of the installed PETs is shown in Figure 6.2.2. While most BMPs attempt specifically to control runoff quantity with runoff quality improvement a secondary effect, the PET is a BMP that manages highway runoff for both quantity and quality.

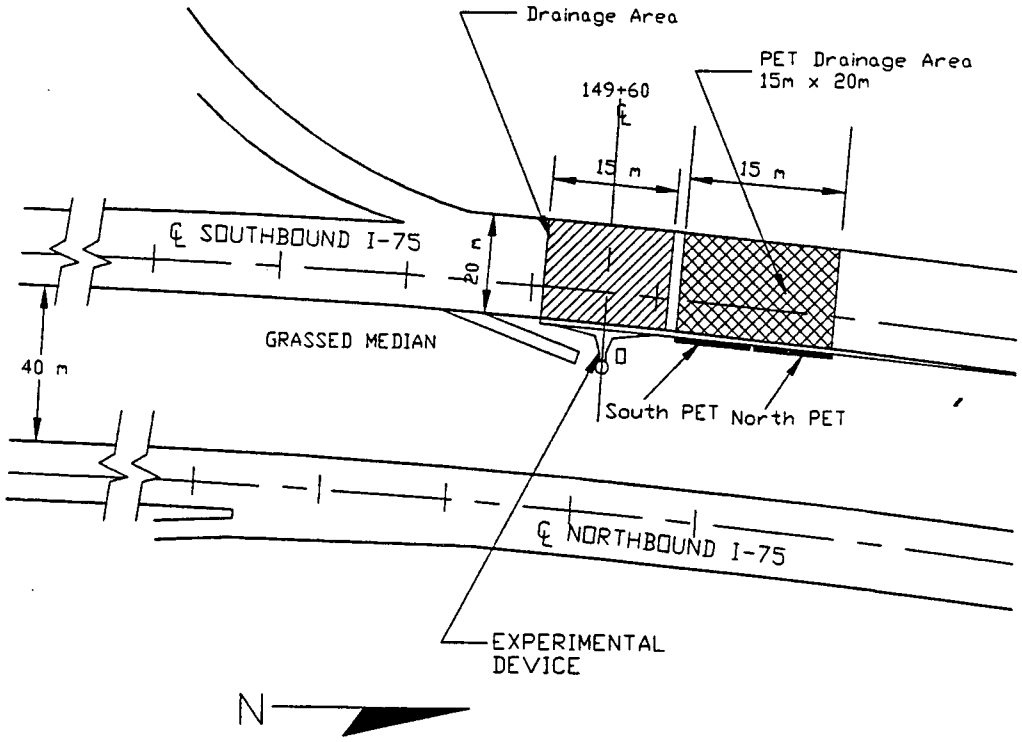

Figure 6.2.1. Location of prototype PET at experimental site on I-75. (NTS)

At the experimental I-75 site, the PET was constructed in two halves, designated North PET and South PET. The South PET was lined with a Typar 3401 geotextile to prevent contamination of the IOCS by the native soil and allow exfiltration to the native soil. The North PET was lined with 12 mil polyethylene liner, eliminating exfiltration and was therefore used to carry out water balances.

The PET was constructed in two phases. The first phase involved making the OCS from filter sand, ferric chloride and sodium hydroxide. The clean filter sand has an effective size between 0.80 and 1.2 mm. This clean silica sand allowed adequate oxide coverage and sufficient hydraulic conductivity. Laboratory trials were conducted until sufficient sand iron oxide coverage was achieved. The gradation of the filter sand is shown in Figure 6.2.3. The filter sand was supplied by R.W. Sidley Inc. of Painesville, Ohio. Filter sand was chosen because it is economically feasible and produced in Ohio. The field batch ingredients for coating the sand are presented in Table 6.2.1.

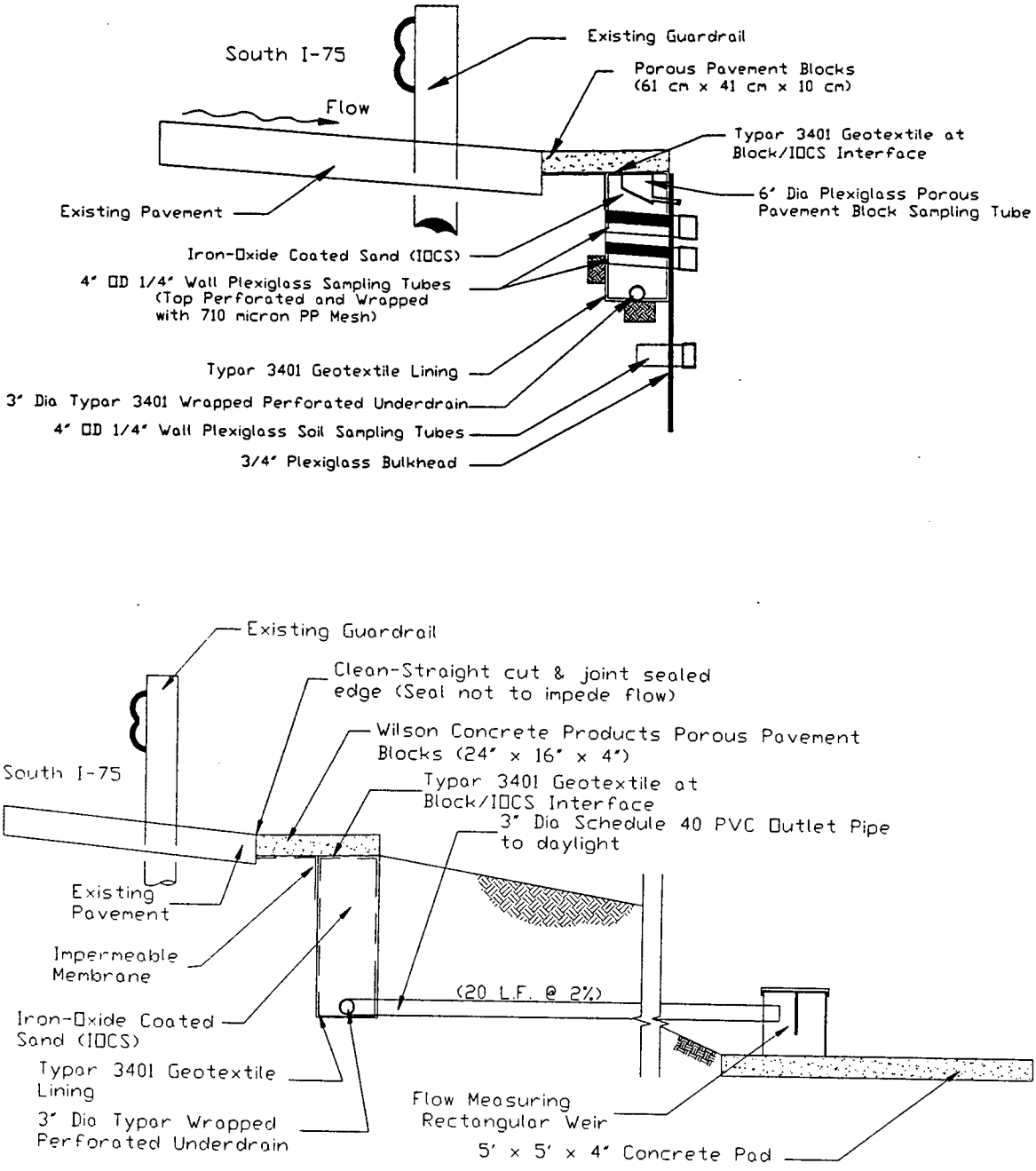

Figure 6.2.2. Cross-section through installed prototype PET at I-75 experimental site.

Table 6.2.1 - Mix design employed for IOCS.

Field Batch	Quantity
Filter Sand	454 kg
Ferric Chloride Solution, 3.5N	216 L
Sodium Hydroxide Solution	5L

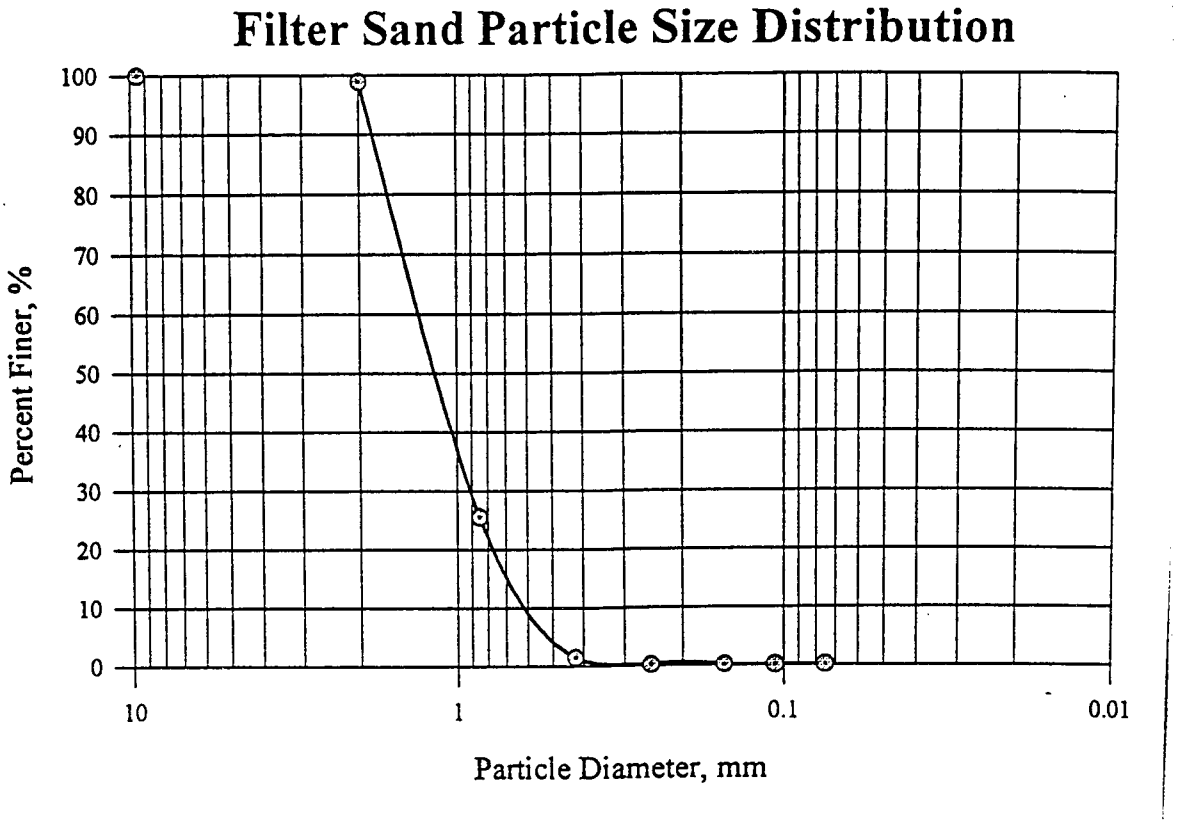

Figure 6.2.3 Gradation curve for filter sand used to make IOCS

Field Production of IOCS

Making the IOCS consisted of two stages. The first stage was to attach the iron oxide to the surface of the sand particles. Attachment of the iron was accomplished by heating a mixture of ferric chloride and filter sand to evaporate the liquid and thus adhere iron to the sand surface. The second step neutralized the pH of the very acidic IOCS with sodium hydroxide. The mix design employed for the IOCS is presented in Table 6.2.1.

Attaching the iron to the surface of the filter sand proved to be a formidable experimental task. The first procedure to attach the iron to the sand surface involved heating the ferric chloride/sand slurry in a small concrete mixer while directing a gas-fired torpedo heater into the mixer. The concrete mixer kept the slurry rotating while the space heater dried the slurry. Rotating the mixture allowed sufficient air flow to accelerate drying at the same time releasing the hydrochloric gas formed by heating. This method proved useful in making small batches of OCS but the time required to make a batch was still too long. For the large amount of sand needed, a faster method to produce sand needed to be invented.

This procedure was scaled up using a larger gas powered concrete mixer and a propane pavement torch. The sand/ferric chloride mixture was placed in the mixer and stirred. Heat was applied via the pavement torch to evaporate the liquid and attach the iron to the sand surface. The larger mixer produced larger batches of sand. The propane heater provided significantly more heat to dry the sand quicker. This method proved feasible to produce the 8000 kg of OCS necessary for the experimental PET.

For each batch, approximately 40 kg of filter sand was placed in the concrete mixer with an excess of ferric chloride. The amount of ferric chloride solution put into the mixture was enough to just cover the filter sand. The mixture was stirred vigorously and heat applied by the pavement torch. The pavement torch was directed into the mouth of the concrete mixer. The slurry was continuously stirred by the concrete mixture until the sand was completely dry. Typical drying time for each batch was 3-4 hours. Once dry, the sand was poured from the concrete mixer into a backhoe bucket and placed in a tandem dump truck for cooling. The sand was then ready for washing.

Complete drying was essential to ensure the iron coating would not be removed by the washing process. If the sand is not completely dry, the iron coating washes off easily when subjected to washing with water. In the first attempt at attaching the iron to the filter sand, the sand was not completely dry. As a result, the coating was dislodged when the sand was put in the sodium hydroxide solution. Thus, the entire 9 tons of sand had to be recoated. In making the second coating, the OCS was thoroughly dry and the coating remained in place when the sand was washed.

With the sand thoroughly dried and cooled, washing was performed. Similar to attaching the iron to the sand, washing was an experimental process. The initial specification for pH neutralization involved the use of a closed circuit system in which wash water would be pumped between two 200 L drums, one filled with OCS. The contractor, however, felt this process was not feasible and developed an alternate plan. The OCS was placed in 55 gallon drums and allowed to soak for a period of 24 hours. This soaking procedure utilized a sodium hydroxide solution by dissolving 5 kg of NaOH pellets in 200 L of tap water.

Washing was deemed complete when the wash water ran clear and no iron oxide coating could be observed coming off in solution or being abraded off. This method of washing produced varied results. In some instances the pH would be raised and in others it would not.

The inability to completely stir the OCS/sodium hydroxide mixture was probably the cause. In addition, this method neutralized a limited amount of sand as dictated by the number of 200 L drums available. As a result, another method was devised.

Since the sand was placed in a tandem dump truck for cooling, the contractor decided to neutralize the entire truckload at once. This reduced handling of the OCS. The dump truck full of OCS was parked facing down a slope and the wash water was poured into the truck bed on top of the OCS. The idea was to create a bathtub effect to wash the sand. The truck bed did leak but the level of the solution was kept above the depth of the sand with continual addition of NaOH solution. Leakage of the truck bed proved beneficial due to the continual addition of new solution to replace loss. The new wash procedure was more capable of cleaning the OCS while the used solution was removed from the system. This method of washing is similar to the original proposed closed circuit system by continual movement of wash solution through the OCS. The OCS was checked at several depths in the truck bed to ensure complete washing of the sand and coating. With the sand completely washed, construction of the PETs commenced. Using this procedure, 8000 kg of OCS, the largest known quantity of such material, was produced.

Field Installation of the PETs

Once the OCS production was completed, the PET was constructed. First, the pavement edge was saw cut utilizing a gas-powered abrasive saw. A saw cut edge was necessary for the porous pavement blocks to be fit against and placed level with the pavement edge. Once the pavement was cut, the one foot wide trenches for the two, 7.5 m long PETs were excavated one foot away from the pavement edge. Each trench sloped longitudinally from 46 cm deep to 76 cm deep in the linear 7.5 m. This yields a 4% slope.

With the trenches open, the water quality sampling structure was installed at the midpoint of each trench. The water quality sampling structure was implemented to sample the runoff at depths of one foot and 46 cm from within the sand. Figures 6.2.4 shows the water quality sampling structure details. The water quality sampling structure consists of a 1.2 m x 1.2 m x 1.9 cm (3/4 inch) plexiglass bulkhead installed along the edge of the PET with plexiglass sampling tubes inserted into the OCS. The bulkhead acts as the edge of the trench and is set flush with the trench surface. Thus, the bulkhead extends two feet below the bottom of the trench at the centerline. At 30 cm below the trench bottom plexiglass sampling ports were installed for future sampling of the clay below the trench to evaluate metal movement as exfiltration occurs. The clear plexiglass permits visual access to the entire trench depth. Pressure treated timber bulkheads were attached to the plexiglass bulkhead to prevent water loss from the trench. The pressure treated bulkheads were attached to the plexiglass bulkhead with caulked angle iron supports and caulked bolts. The u-shaped system was set into place as a single unit. Compacted backfill around the water quality sampling structure proceeded with the addition of bentonite clay to ensure a watertight structure.

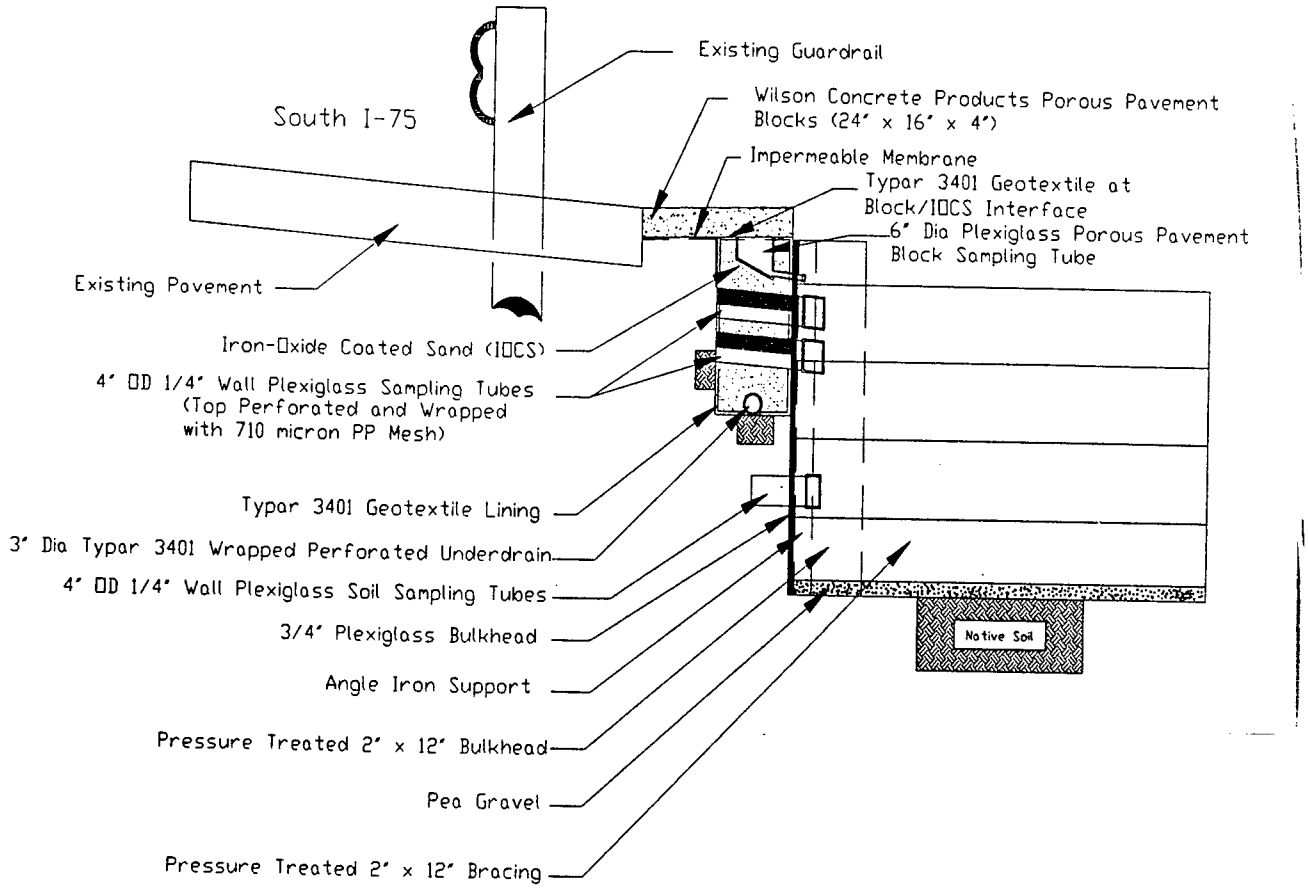

Figure 6.2.4. Cross-section of the PET including the sampling structure. (NTS)

A pressure treated timber bracing system was installed to provide access to, and permit backfilling around, the water quality sampling structure. The bracing system supports the plexiglass bulkhead against the OCS within the trench and provides access to the plexiglass sampling tubes. To prevent someone from falling into the opening left by the bracing system, a pressure treated cover was placed over the opening. The cover removes easily for sampling. A gravel covered underdrain was placed in the bottom of the opening to prevent water storage during a rain event. The underdrain was sloped to the existing median swale.

The plexiglass sampling tubes were installed as the OCS was placed in the trench. For the geotextile-lined South PET trench, the geotextile was cut in an x-shaped fashion to permit tube insertion into the OCS. To assure the plastic-lined North PET would remain watertight, the plexiglass sampling tubes protruded through the lining with a watertight connection. The excess

lining was heavily caulked and attached to the solid portion of the plexiglass sampling tubes with a hose clamp. The entire connection was then taped with polypropylene tape. Since the plexiglass bulkhead is clear, any leakage from the connection would be noticed.

With the water quality sampling structure in place, each trench was lined with its respective liner. A geotextile wrapped underdrain was then installed in each trench and attached to a PVC outlet pipe with a watertight seal. The PVC pipes were sloped at 2% to daylight. In the plastic lined trench, the excess lining due to the opening was wrapped around the PVC pipe and attached in the same manner as the plexiglass sampling tubes to ensure watertightness. With both underdrains in place, the trenches were filled with OCS.

The plexiglass sampling tubes that extend through the plexiglass into the OCS were formed by milling slots in 10.2 cm diameter, 0.63 cm wall plexiglass tubes. The tube slots were wrapped with a polypropylene mesh with an opening of 0.71 mm to prevent OCS loss into the tubes. The mesh opening will still allow water to flow freely into the tubes.

Each trench was filled with OCS placed in loosely with a backhoe in 25 cm lifts. Originally the OCS was to be plate compacted in six inch lifts, but due to confined space the sand was placed loosely and hand compacted with a plate tamper. Hand compaction proceeded to the top 15 cm of the trench at which point a vibratory plate compactor could be utilized. Further compaction of the OCS was provided by a heavy rain that occurred before trench closure.

The final step in trench construction was the installation of the porous pavement blocks. The 61 cm x 41 cm x 10 cm pavers were installed on top of the compacted OCS with an adverse slope of 0.63 cm (1/4 inch) over the 61 cm length toward the pavement edge. The adverse slope was incorporated to mitigate runoff overtopping the blocks during high intensity rain events. The joint between the porous pavement blocks and the saw cut pavement edge was caulked. Between adjacent blocks, the joints were tightly fitted without any sealant.

After the construction of the PETs was complete, the porous pavement blocks were covered with plastic to prevent particle accumulation and water infiltration. This ensured baseline parameters when the PETs were put in use.

Construction and Calibration of Flow Measuring Weirs

In order to determine the flow rate from each PET, the PVC outlet pipe flows into a rectangular sharp-crested weir. The sharp-crested weir is composed of a polypropylene tank with one side removed and replaced with an aluminum rectangular sharp-crested weir. Figure 6.2.5 shows the weir configuration. An adjustable diffuser plate was placed in the tank to provide quiescent flow over the weir. The aluminum sharp-crested weirs were milled from 0.63 cm aluminum stock. Figure 6.2.6 shows the specification for weir milling. For each PET, the flow measuring weir has two aluminum weir plates; a plate with an 0.63 cm (1/4 inch) opening to measure low flow and one with a 1.3 cm (1/2 inch) opening to measure the high flow.

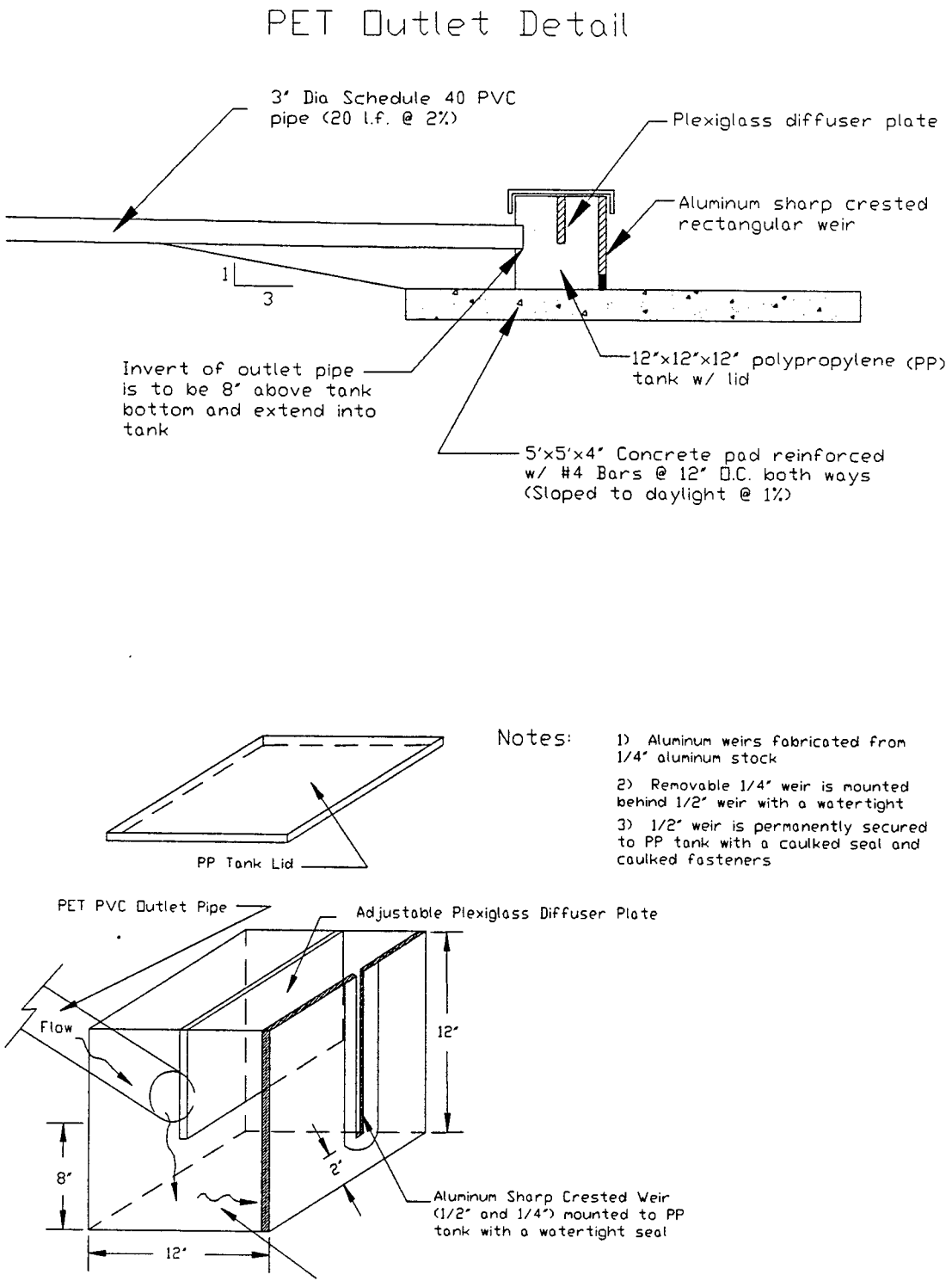

Figure 6.2.5. PET outlet configuration and weir detail.

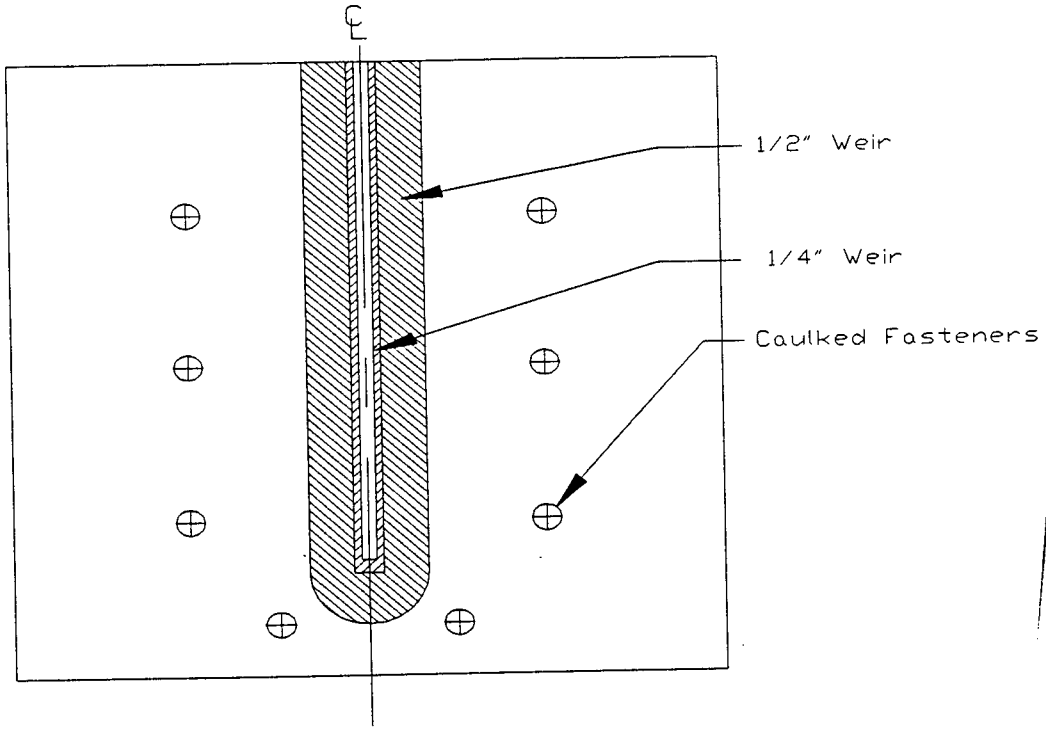

Front View of Weir

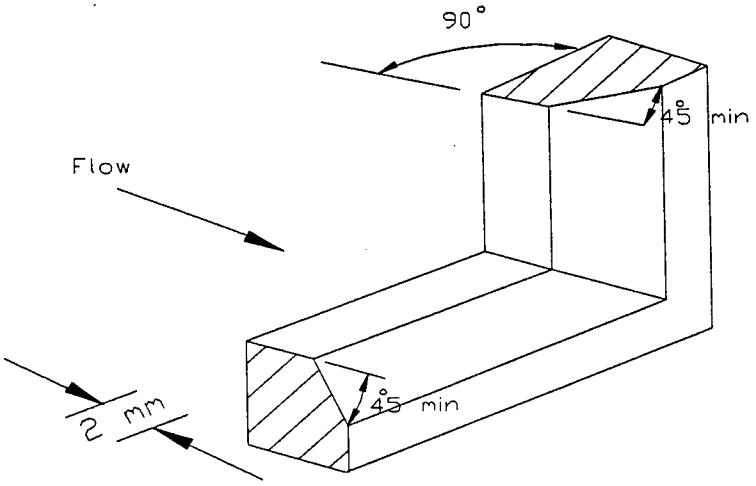

Enlarged View of Crest and Side
of Rectangular Sharp-Crested Weir

Notes: 1) Aluminum Weirs fabricated from 1/4" Aluminum stock
2) Removable 1/4" weir is mounted behind 1/2" weir with a watertight seal
3) 1/2" weir is permanently secured to PP tank with a caulked seal and caulked fasteners

Figure 6.2.6. Aluminum weir milling specifications

The 1/4 inch weir is removable and mounted directly behind the 1/2 inch weir. Between the two weir plates is a rubber gasket to prevent water loss between the plates. Weir calibration was performed in the laboratory to develop the equation for each weir. For each weir size head increments were marked on the front of the plate. The head increments were correlated to a specific flow rate at that level. Correlation was performed by measuring the amount of water flowing through the weir in a specific time at each head level. These values were plotted on a log-log scale to determine the equation for each weir. The flow rate, Q, is related to the head level by the following equation. Table 6.2.2 shows β and r^2 values for weir calibration.

$$Q = H^{\beta}$$

where: Q = flow rate, gal/min
H = weir level, inches
β = laboratory determined weir constant

Table 6.2.2. Weir Calibration Results

Weir	β	r^2
North PET	1.4911	0.997
South PET	1.3838	0.994

Evaluation of the porous pavement

The mix design for the porous pavement is presented in Table 6.2.3. The grain size distribution of the pea gravel and sand used in the mix was presented in Figure 5.3.1. The porous pavement was constructed using a computer controlled hydraulic compression to press the mix into the block form. A hydraulic press exerting up to 35 kN (4 tons) of force was used to place the concrete in the form. The porous pavement was were cured with 90% humidity for one week to promote adequate cement hydration.

Table 6.2.3. Mix Designs for Paver Blocks

Component	Cement (Type II)	Sand	Pea Gravel
	109 kg (240 lbs)	381 kg (840 lbs)	381 kg (840 lbs)

Each batch of porous pavement was sampled at random to determine the strength and infiltration capacity. From each block, 7 cm (2.75 in.) outside diameter cores were drilled. The infiltration capacity of the porous pavement blocks was evaluated by the falling head permeability test for soils. Each core was wrapped with an impermeable membrane to determine hydraulic conductivity of the block. Flow was introduced from the bottom of the sample to ensure complete saturation. Two trials were taken for each core resulting in ten hydraulic conductivity values for each porous pavement mix design. As shown in Table 6.2.4, Batch 3 has the greatest hydraulic conductivity.

Since the PET block may be subject to occasional traffic loads, block strength is essential. The unconfined compression strength of the blocks was evaluated according to ASTM C-39. Two of the five cores from each mix design were tested to determine the unconfined compression strength. Since the length to diameter ratio of the cores was less than 1.8, the strength was reduced by applying the appropriate correction factor as designated in ASTM C-39. Stress-strain plots for one core from each batch are presented in Figure 6.2.8.

Table 6.2.4. Properties of the Porous Pavement Blocks

Mix Design	Unit Weight	Average Hydraulic Conductivity (cm/sec)	Average Unconfined Compressive Strength
Batch 1 (single sample)	14.8 kN/m^3 (93.9 pcf)	0.0091	37,500 kPa (5440 psi)
Batch 2 (single sample)	14.1 kN/m^3 (89.6 pcf)	0.0098	27,700 kPa (4020 psi)
Batch 3 (single sample)	14.6 kN/m^3 (93.0 pcf)	0.0090	33,600 (4880 psi)

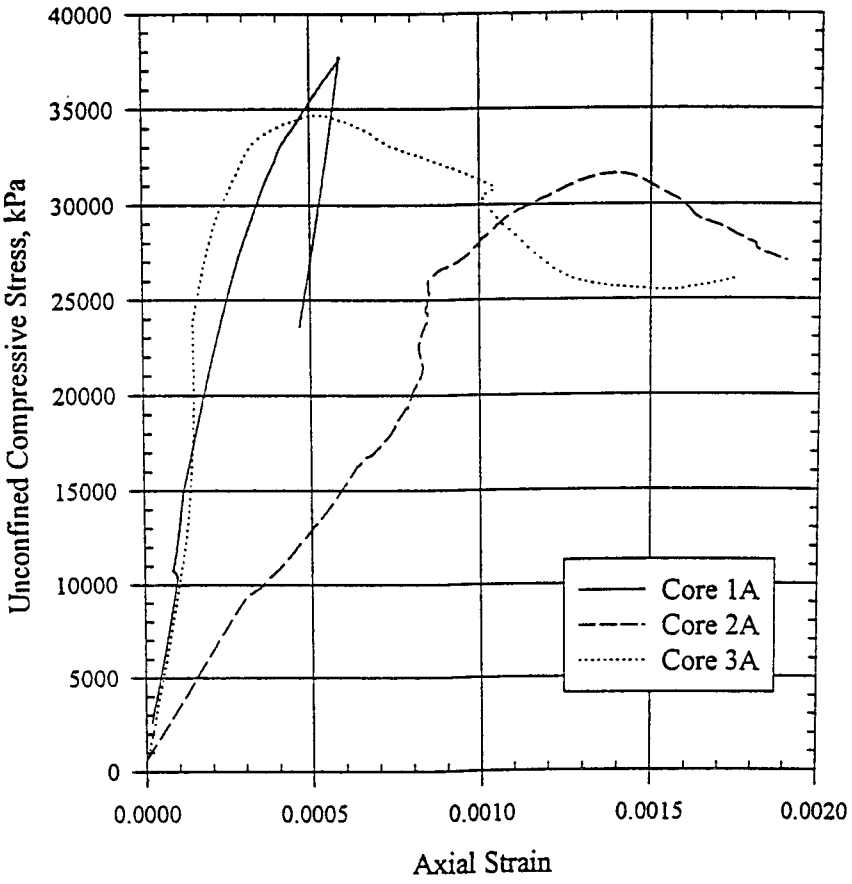

Figure 6.2.8. Stress strain plot from porous pavement unconfined compression tests

Sampling and hydrologic data collection

Runoff influent to the PET was sampled from an adjacent 15 m long instrumented facility attached directly to the sawcut edge of the pavement. One liter samples were obtained at two minute intervals using an automated 24 bottle sampler with polypropylene bottles for the first 50 minutes and thereafter at intervals ranging from 10 minutes to 30 minutes. One liter PET effluent samples were obtained manually at regular intervals for the duration of PET discharge. Sampling and instrumentation details were presented in Chapter 2 . Hydrologic and water quality data were collected during three rainfall-runoff events. Samples were analyzed for metals, solids pH, alkalinity and conductivity for all events.

Metal element fractionation

The dissolved fraction is defined as metal elements of an unacidified sample that pass through a 0.45 micrometer membrane filter (APHA, 1992). Once filtered, the 50 ml dissolved fraction was immediately acidified with 2.5 ml of trace-metal HNO_3. The particulate-bound metal element fraction, retained in the membrane filter, was subsequently digested using a microwave-assisted procedure based on SW-846 Method 3015 (USEPA, 1990). Metal element analyses were conducted on a Perkin-Elmer Optima 3000 Inductively Coupled Plasma Spectrometer.

To measure the performance of the in-situ prototype PET, removal efficiency based on runoff influent and PET effluent mass was computed for each rainfall runoff event characterized. The PET was operational by September of 1996 and the PET performance was evaluated through June of 1997. Removal efficiency was defined as:

$$\beta = \left[\frac{M_{in} - M_{out}}{M_{in}}\right] * 10 \qquad (6.2.2)$$

where β = removal efficiency (%)
M_{in} = influent mass (µg or mg)
M_{out} = influent mass (µg or mg)

6.3 Prototype PET performance

Bench scale results provided a preliminary indication that dissolved or particulate-bound breakthrough may not occur for at least 15 years based on rainfall runoff loadings from highways in the urban Cincinnati area. Therefore to measure the performance of the in-situ prototype PET, removal efficiency based on runoff influent and PET effluent mass was computed for each rainfall runoff event characterized. The PET was operational by September of 1996 and the PET performance was evaluated over the next ten months for four specific events. Hydrologic, water quality results and removal efficiency for solids and metal elements are presented in Table 6.3.1 through 6.3.6. Result are presented for the South PET in these tables. Total particulate-bound

and dissolved metal element mass as well as event mean concentrations for TSS and selected water quality parameters are also summarized. Hydrologic data indicating previous dry period, rainfall duration and runoff depth are presented in Table 2.9.1

Event total influent and effluent flow volumes are summarized along with event mean pH and alkalinity in Table 6.3.1. For each event a simple volume balance was carried out for flows to determine the volume of flow exfiltrated to the soil. These results, presented in percent, are summarized in Table 6.3.1.

Table 6.3.1. Event mean pH, alkalinity and total influent and effluent flow volumes.

Event date (1996-97)	Event mean pH	Event mean Alkalinity (mg/L)	Inflow volume (L)	Event mean pH	Event mean alkalinity (mg/L)	Outflow volume (L)	Volume exfiltrated to soil (%)
	INFLUENT RUNOFF			PET EFFLUENT			
17 October 96	7.10	18	801	7.12	26	547	32.9
25 November 96	7.56	44	108	8.45	80	71	16.4
16 December 96	7.54	36	134	8.48	73	132	24.6
12 June 97	6.70	130	232	7.85	630	192	17.3

Solids characterized as total suspended solids (TSS), total mass and EMCs are summarized for influent and effluent in Table 6.3.2. From the TSS mass, removal efficiencies were computed. For comparison, influent and effluent EMCs are also presented for TSS.

Table 6.3.2. Total suspended solids (TSS) mass, EMCs and removal efficiency for the PET.

Event date (1996-97)	TSS mass (g)	TSS EMC (mg/L)	TSS mass (g)	TSS EMC (mg/L)	Removal efficiency (%)
	INFLUENT RUNOFF		PET EFFLUENT		
17 October	401	107	36	65	91.1
25 November	40	177	4	51	90.9
16 December	38	141	1	9	96.9
12 June 97	33	72	10	55	69.7

Metal element mass characterization for both influent and effluent are summarized in Table 6.3.3 through 6.3.6 for Zn, Cd, Pb and Cu. Results are separated into the dissolved and particulate-bound fractions. Removal efficiencies based on dissolved and particulate-bound mass for each of these fractions are also tabulated. As with TSS, the removal efficiencies are event removal efficiencies.

Table 6.3.3. Zinc mass (mg) and removal efficiency for the prototype PET.

Event date (1996-97)	Influent Zn mass (mg)	Effluent Zn mass (mg)	Removal efficiency (%)	Influent Zn mass (mg)	Effluent Zn mass (mg)	Removal efficiency (%)
	Dissolved fraction			Particulate-bound fraction		
17 October 96	6517	16	99.7	314	11	96.5
25 November 96	141	3	97.9	21	3	88.1
16 December 96	198	3	98.7	25	2	91.4
12 June 97	288	7.5	97.4	10	2	80.0

Table 6.3.4. Cadmium mass (mg) and removal efficiency for the prototype PET.

Event date (1996-97)	Influent Cd mass (mg)	Effluent Cd mass (mg)	Removal efficiency (%)	Influent Cd mass (mg)	Effluent Cd mass (mg)	Removal efficiency (%)
	Dissolved fraction			Particulate-bound fraction		
17 October 96	7.45	0.22	97.0	0.94	0.144	84.6
25 November 96	0.52	0.11	78.9	0.09	0.018	80.0
16 December 96	0.19	0.04	80.3	0.05	0.004	91.3
12 June 97	1.13	0.13	88.4	0.089	0.025	71.4

Table 6.3.5. Lead mass (mg) and removal efficiency for the prototype PET.

Event date (1996-97)	Influent Pb mass (mg)	Effluent Pb mass (mg)	Removal efficiency (%)	Influent Pb mass (mg)	Effluent Pb mass (mg)	Removal efficiency (%)
	Dissolved fraction			Particulate-bound fraction		
17 October 96	107	8.1	92.5	25.2	0.9	96.2
25 November 96	3.3	0.9	72.8	1.9	0.3	84.4
16 December 96	10.6	2.9	72.3	2.9	0.3	89.6
12 June 97	2.4	0.69	71.4	0.82	0.10	87.8

Table 6.3.6. Copper mass (mg) and removal efficiency for the prototype PET.

Event date (1996-97)	Influent Cu mass (mg)	Effluent Cu mass (mg)	Removal efficiency (%)	Influent Cu mass (mg)	Effluent Cu mass (mg)	Removal efficiency (%)
	Dissolved fraction			Particulate-bound fraction		
17 October 96	140	3	97.1	36.2	1.7	95.2
25 November 96	8	1	83.6	2.5	0.5	79.9
16 December 96	7	0.7	89.1	2.9	0.3	91.4
12 June 97	15.4	1.5	90.5	1.9	0.3	84.2

6.4 Conclusions

Results from bench scale PET column experiments indicated that the critical design elements of a PET were sufficient hydrologic loading capacity, sufficient breakthrough capacity for targeted metal elements and capability to filter finer infiltrated solids which would be otherwise discharged through the PET underdrain. Column simulations were carried out to assess the capacity of OCS to immobilize Zn, Cd, Cu and Pb. Column simulations using stormwater were considered most representative for evaluating the capacity of a prototype PET. A methodology to evaluate the potential capacity of a prototype PET from application of column simulation results was developed. Hydrologic parameters and loadings as well as metal element fraction loadings, all derived from the experimental site were used to estimate annual loadings to a prototype PET. Results from application of this methodology to a PET design at the experimental site suggest that the design life of a PET in terms of metal element breakthrough is controlled by breakthrough of particulate-bound metal elements. Results indicate that the design life of a PET is approximately 10 years dictated by breakthrough of particulate-bound Zn. The bench scale performance of the PET columns underscored the importance of solids control through the use of a geosynthetic liner around the underdrain, extending the life of the PET. Bench scale results also indicate the PET has several critical components. The upper surface of porous pavement must intercept and infiltrating pavement flows while straining solids at the pavement surface. The body of the trench filled with oxide coated sand media must function to sorb as well as filter metal elements in the percolating runoff.

The performance of the prototype PET, installed at the I-75 experimental site and subject to lateral pavement sheet flow, has been summarized through computed event removal efficiencies of TSS and metal elements. In addition, event flow volumes exfiltrated to surrounding soils were determined. Exfiltration results indicate that even for clayey silts, depending on the length of the previous dry period and rainfall/runoff duration, a significant portion of the flow volume can be exfiltrated to surrounding soils. Such performance indicates the PET is capable of functioning as a water quantity control strategy. Removal efficiencies for TSS indicate that the PET is effective in trapping TSS, mainly at the porous pavement surface. Removal efficiencies for metal elements are generally excellent except for dissolved Pb and Cd which had event removal efficiencies between 70 and 80 percent. Such removal efficiencies are low based on extrapolation of bench scale results and an anticipated 10 year design life to breakthrough for any metal element fraction. The installation of the geosynthetic liner around the PET underdrain along with staining by the porous pavement appears to be effective in controlling particulate-bound breakthrough. Continued field performance will be evaluated and the PET design improved accordingly. Both the bench scale and prototype PET have demonstrated proof of concept for the PET as a water quantity/quality upgrade to the current practice of underdrainage along roadways.

REFERENCES

Adamson, A.W. (1991) Physical Chemistry of Surfaces, 5th ed., John Wiley & Sons, New York. pp. 763.

American Public Health Association. (1992) "Standard Methods for the Examination of Water and Wastewater", 18th edition, ed. Greenberg, A, Clesceri, L, Eaton, A, Washington D.C., pg. 3-1.

American Society for Testing and Materials, Designation D 421-85 (1993), Standard Practice for Dry Preparation of Soil Samples for Particle-Size Analysis and Determination of Soil Constants, Annual Book of Standards, Vol. 04.08, pp. 8-9.

American Society for Testing and Materials, Designation D 422-63 (1990), Standard Test Method for Particle-Size Analysis of Soil, Annual Book of Standard, Vol 04.08, pp 10-16.

American Sigma. (1994) "Operations Manual,", P.O. Box 820, Medina, New York, 14103.

Amrhein C., Strong J. (1990).The Effect of Deicing Chemicals on Major Ion and Trace Metal Chemistry in Roadside Soils, in The Environmental Impact of Highway Deicing, Institute of Ecology Publication #33, Univ. California-Davis, September pp. 120-139.

Armstrong, L.J., (1994). "Contribution of heavy metals to storm water from automotive disc brake pad wear". Report for Santa Clara Valley Nonpoint Source Pollution Control Program, Woodward-Clyde Consultants. pp. 1-37.

Ball, D., Hamilton, R., Harrison, R. (1991). "The Influence of Highway-Related Pollutants on Environmental Quality.", R. Hamilton & R. Harrison, eds., Highway Pollution., Elsevier Science Publishing Company, Inc., New York, NY., 1-47.

Beckwith, P.R., Ellis, J.B., Revitt, D.M. (1990) "Applications of magnetic measurements to sediment tracing in urban highway environments." The Science of the Total Environment, 93 pp. 449-463.

Bedient, P.B., and Huber, W.C., (1988) "Hydrology and Floodplain Analysis" Addison-Wesley Publishing Company, New York, pp. 650.

Benjamin, M. and Leckie J. (1981) Multiple-Site Adsorption of Cd, Cu, Zn, and Pb on Amorphous Iron Oxyhydroxide, Journal of Colloid and Interface Science, Vol 79, No 1, Jan pp. 209-221.

Benjamin, M. and Sletten, R. (1993) Metal Treatment at Superfund Sites by Adsorptive Filtration, EPA/540/R-93/515, Risk Reduction Engineering Laboratory, Cincinnati, OH, USEPA.

Bennett, T.E. (1992). "Surface Characterization of Iron-Oxide-Coated Sand Media." Master of Science Thesis, University of Washington, Department of Civil Engineering, pp. 113.

Bourcier, D.R., and R.P.Sharma. (1980) Heavy metals and their relationship to solids in urban runoff. International Journal of Environment Analytical Chemistry. Vol. 7 , pp. 273-283.

Bowles, J.E. (1992), Engineering Properties of Soils and Their Measurement, Fourth Edition, McGraw Hill Inc.

Brookins, D.G. (1988). "Eh-pH Diagrams for Geochemistry.", Springer-Verlag, Berlin, 129 pp.

Buchberger, S.G., Sanders, T.G.(1982), A Kinematic Model For Pollutant Concentrations During The Rising Hydrograph, in, Modeling Components of Hydrologic Cycle, Water Resources Publications, Littleton, Colorado.

Calgon Carbon Corporation, (1995) F400 Specification Sheet, P.O. Box 717, Pittsburgh, Pennsylvania, 15230-0717.

Carter, D.L., Mortland M.M , and Kemper, W.D.(1986), Specific Surface.in Methods of Soil Analysis, Part 1 - Physical and Mineralogical Methods, American Society of Agronomy - Soil Science Society of America, Madison.

Carter, D.L., Heilman, M.D. and C.L. Gonzalez (1965), Ethylene Glycol Monoethyl Ether for determining surface area of silicate minerals. Soil Science ,pp. 356-360.

Chellam, S., and Wiesner M.R. (1993). "Slip flow through porous media with permeable boundries: implications for the dimensional scaling of packed beds." Water Environmental Research, 65, 744-749.

Chui, T., Mar, B. and Horner, R. (1982). "Pollutant Loading Model for Highway Runoff." Journal of the Environmental Engineering Division, Proceedings of the American Society of Civil Engineers, Vol. 108, No. EE6, December, 1193-1210.

Colandini, V., Legret, M., Brosseaud, Y., and Balades, J. (1995). "Metallic pollution in clogging materials of urban porous pavements." *Water Science and Technology*, Vol. 32, No. 1, pp. 57-62.

Corapcioglu M.O. and Huang C.P. (1987). "The adsorption of heavy metals onto hydrous activated carbon." Water Research, Vol. (21). No 9. pp. 1031-1044.

Dannecker, W., Au, M. , Stechmann, H. (1990) "Substance load in rainwater runoff from different streets in Hamburg" The Science of The Total Environment, (93) pp. 385-392.

Das, Braja M. (1992), Principles of Geotechnical Engineering, Third Edition, PWS Publishing Company

Dixon J. and Weed S. (1989) Minerals in the Soil Environments, Soil Science Society of America, Madison, WI, pp. 1264.

Domenico P, and Schwartz F.(1990), Physical and Chemical Hydrogeology, John Wiley & Sons Inc, New York, pp. 824.

Douglas B., McDaniel D., Alexander J. (1994) Concepts and Models of Inorganic Chemistry, John Wiley & Sons, New York, pp. 928.

Driscoll, E., Shelley, P., Strecker, E. (1990a). "Pollutant Loadings and Impacts from Highway Stormwater Runoff, Volume IV: Research Data Appendix.", FHWA-RD-88-009, Federal Highway Administration, U.S. Department of Transportation., Washington D.C., 1-139.

Driscoll, E.D., P.E. Shelley, and E.W. Strecker. (1990b) Pollutant Loadings and Impacts from Highway Stormwater Runoff, Volume III: Analytical Investigation and Research Report, FHWA-RD-88-008. FHWA, U.S. Department of Transportation

Dzombak, D.A., and Morel, F.M. (1990). "Surface Complexation Modeling - Hydrous Ferric Oxide.", John Wiley and Sons, Inc., New York, 289 pp.

Edwards, M., and Benjamin, M.M. (1989). "Adsorptive filtration using coated sand: a new approach to treatment of metal-bearing wastes." Journal of Water Pollution Control Federation, Vol. 61, 1523-1533.

Ellis, J.B., Revitt, D.M., Harrop, D.O., Beckwith, P.R..(1987) "The contribution of highway surfaces to urban stormwater sediments and metal loadings" The Science of the Total Environment. (59) pp. 339-349.

Ellis, J., Harrop, D. (1984). "Variations in Solids Loadings to Roadside Gully Pots.", The Science of the Total Environment., Vol. 33, 203-211.

Fetter C.W., Applied Hydrogeology ,(1993) Macmillan Publishing Co, New York, pp. 458.

Gibson, M.J. and Farmer, J.G. (1984). "Chemical partitioning of trace metal contaminants in urban street dirt.", The Science of the Total Environment., Vol. 33, pp. 49-57.

Gjessing, E., Lygren, E., Anderson, S., Berglind, L., Carlberg, G, Efraimsen H., Kallqvist, T., Martinsen, K. (1984) "Acute toxicity and chemical characteristics of moderately polluted runoff from highways." The Science of The Total Environment, 33 pp. 225-232.

Grottker, M. (1987). "Runoff Quality from a Street with Medium Traffic Loading.", The Science of the Total Environment., Vol. 59, 457-466.

Grottker, M. (1990). Pollutant removal by gulley pots in different catchment areas. The Science of the Total Environment. Vol. 93., pp. 515-522.

Hamer, K., von Luhrte, R., and Isenbeck-Schroter, M. (1994). "Transport of Cd and Cu in a zone of calcite dissolution: Column experiments and modeling." in Transport and Reactive Processes in Aquifers, Ed. Dracos & Stauffer, A.Balkema Publishers, Rotterdam., 589 pp.

Hamilton, R.S., Revitt, D.M. and R.S. Warren.(1984) Levels and physico-chemical associations of Cd, Cu, Pb and Zn in road sediments. The Science of the Total Environment, Vol. 33, pp. 59-74.

Hamilton, R.S. and R.M. Harrison. (1991) Highway Pollution, Elsevier Science Publishing Company Inc., New York.

Hamilton, R.S., Revitt, D.M., Warren, R.S., Duggan, M.J. (1987) "Metal Mass Balance Studies Within a Small Highway Dominated Catchment" The Science of The Total Environment, (59) pp. 365-368.

Harrison, R. and Wilson, S. (1985). "The Chemical Composition of Highway Drainage Waters I. Major Ions and Selected Trace Metals." The Science of the Total Environment., Vol. 43, 63-77.

Harrison R..M., & Wilson, S.J. (1985). "The Chemical Composition of Highway Drainage Waters I. Major Ions and Selected Trace Metals." The Science of the Total Environment., Vol. 43, 63-77.

Harrison, R.M., Laxen, D.P., Wilson, S, J. (1981) "Chemical Association of Lead, Cadmium, Copper and Zinc in Street Dusts and Roadside Soils." Environmental Science and Technology, (15) 11, pp. 1378-1383.

Helsel, D., Kim, J., Grizzard, T., Randall, C. and Hoehn, R. (1979). "Land Use Influences on metals in storm drainage." Journal of the Water Pollution Control Federation., Vol. 51, No. 4., 709-717.

Huber, W. (1993). "Contaminant Transport in Surface Water", D. R. Maidment, editor, Handbook of Hydrology, McGraw-Hill Inc., New York, NY., 14.1-14.50.

Hvitved-Jacobson, T., Yousef, Y.A. (1991) Highway Runoff Quality, Environmental Impacts and Control. Highway Runoff, Elsevier Science Publishing Co. Inc., New York.

Igarashi, T. and Mahara Y. (1994). "Comparison of measuring methods for strontium adsorption parameters."| "Transport and Reactive Processes in Aquifers, Eds. Dracos and Stauffer, Balkema, Rotterdam, pp. 89-93.

Igloria, R., Hathhorn, W., and Yonge D. "NOM and Trace Metal Attenuation During Storm-Water Infiltration", *Journal of Hydrologic Engineering*, ASCE, Vol. 2, No. 3, pp. 120-127, (1997).

Isenbeck-Schroter, M., Doring, U., Moller, A., Schroter, J. & Matthess, G. (1993). "Experimental approach and simulation of the retention processes limiting orthophosphate transport in groundwater." Journal of Contaminant Hydrology, 14, 143-161.

Isenbeck-Schroter, M., Hamer, K., Reitz, F., Schubert, J., & Schultz H. D. (1994). "Simulation of Arsenic transport in column experiments: Estimation of sorption kinetics of As(III) and As(V) species in simple aquifer systems." in Transport and Reactive Processes in Aquifers, Ed. Dracos & Stauffer, A.A.Balkema Publishers, Rotterdam., 589 pp.

Jeffcoat, H.H., F.A. Kilpatrick, J.B. Atkins, and J.L. Pearman. (1992) Effectiveness of Highway Edgedrains, U.S. Geological Survey Water-Resources Investigations Report 92-4147, FHWA, U.S. Department of Transportation.

Jumikis, A. R. (1967) Introduction to Soil Mechanics, D. Van Norstrand Company, Inc.

Karim Z. "Characteristics of ferrihydrites formed by oxidation of $FeCl_2$ solutions containing different amounts of silica." Clays and Clay Minerals, Vol. 32, No. 3, pp. 181-184.

Kavanaugh, M. and Leckie J. (1980) Particulates in Water, Characterization, Fate, Effects and Removal, Advances in Chemistry Series, 189, American Chemical Society, Washington D.C., pp. 399.

Kerri, K.D., Racin, J.A., Howell, R.B. (1985). "Forcasting Pollutant Loads from Highway Runoff" Transportation Research Record (1017), National Research Council, pp. 39-47.

Kobriger, N.P. and Geinopolos, A. (1984) Sources and migration of highway runoff pollutants - Research Report Volume III. Report, FHWA/RD-84/059. (PB86-227915) FHWA, U.S. Department of Transportation.

Koerner, R.A. (1994). "Designing with Geosynthetics." Addison-Wesley Publishing Company, New York, pp. 704.

Krauskopf, K.B., and Bird, D.K.(1995). "Introduction to Geochemistry." McGraw-Hill, Inc., New York, 3rd Ed., 647 pp.

Lang, J .S., Giron, J.J., Hansen, R., Trussel R.R. and Hodges, W.E. (1993). "Investigating Filter Performance as a Function of the Ratio of Filter Size to Media Size." Journal of the American Water Works Association, 122-130.

Lygren, E., Gjessing, E., and Berglind, L. (1984). "Pollution Transport from a Highway." The Science of the Total Environment., Vol. 33, 147-159.

Malcom, H.R. (1989). Elements of Urban Stormwater Design, North Carolina State University, Raleigh, North Carolina, 1989.

Marcano-Martinez E., McBride, M.B. (1989). Comparison of the Titration and Ion Adsorption Methods for Surface Charge Measurements in Oxisols, Soil Science Society of America Journal, Vol. 53, pp. 1040-1045.

McBride, M. (1994) Environmental Chemistry of Soils Oxford University Press, New York .

McBride, M. (1995) Toxic Metal Accumulation from Agricultural Use of Sludge: Are USEPA Regulations Protective, Journal of Environmental Quality, Vol. 24, Soil Science Society of America, pg. 5-18.

McDowell-Boyer, L.M., J.R. Hunt, and N. Sitar.(1986) Particle Transport Through Porous Media, Water Resources Research, Vol. 22, No. 13. pp. 1901-1921.

McEldowney S., Hardman, D.J. and Waite S. (1993) Pollution: Ecology & Biotreatment. Longman Scientific & Technical, Essex.

Miller, I., J.E. Freund, and R.A. Johnson. (1990) Probability and Statistics for Engineers, Fourth Edition, Prentice-Hall, Inc., Englewood Cliffs, New Jersey.

Monteith H., Bell J., Thompson D., Kemp J., Yendt M., Melcer H. (1993). Modeling the fate of metals in municipal water pollution control plants, Water Environment Research, Volume 65, Number 2, Water Environment Federation pp. 129-137.

Montgomery J.M.(1987), Water Treatment, John Wiley & Sons, New York, pp. 712.

Morrison, G., Revitt, D. & Ellis, J., Svensson, G., Balmer, P. (1984). "Variation of Dissolved and Suspended Solid Heavy Metals Through an Urban Hydrograph." *Environmental Technology Letters.*, Vol. 7, 313-318.

Muschack, W. (1990). "Pollution of Street Run-Off by Traffic and Local Conditions." The Science of the Total Environment., Vol. 93, 419-431.

Nicholson, K.W. and Branson, J.R. (1990) "Factors affecting resuspension by road traffic" The Science of The Total Environment, (93) pp. 349-358.

Niemczynowicz, J., (1989) Swedish Way to Stormwater Enhancement by Source Control. Urban Stormwater Quality Enhancement - Source Control, Retrofitting, and Combined Sewer Technology, Urban Water Resources Research Council, American Society of Engineers, New York, pp. 156-168.

Pratt, C.J., Elliot, G.E., Fulcher, G.A. (1987) "Suspended solids discharge from highway gully pots in residential catchments." The Science of The Total Environment. (59) pp. 355-364. Racin, J., Howell, R., Winters, G. and Shirley, E. (1982). "Estimating Highway Runoff Quality.", California Department of Transportation, FHWA/CA/TL-82/11.

Racin, J.A., R.B. Howell, G.R. Winters, and E.C. Shirley (1982). Estimating Highway Runoff Quality, California Department of Transportation, FHWA/CA/TL-82/11, Sept.

Reed B.E., Robertson, J. and Jamil, M. (1995). "Regeneration of Granular Activated Carbon (GAC) Columns Used for Removal of Lead." Journal of Environmental Engineering, Vol. 121, No. 9. pp. 653-662.

Reed, B.E., and Arunachalam, S. (1996)."Use of Granular Activated Carbon Columns for Lead Removal.", Journal of Environmental Engineering, ASCE, 120 (2), 416-436.

Reed, B.E., Jamil, M. and Thomas, B. (1996). "Effect of pH, empty bed contact time and hydraulic loading rate on lead removal by granular activated carbon columns." Water Environment Research, (68), July/August, 877-882.

Revitt, D.M., Hamilton, R.S., Warren, R.S. (1990) "The Transport of Heavy Metals Within a Small Urban Catchment." The Science of the Total Environment, (93) pp. 359-373.

Roberts, A.H., Ellis, J.B., Whalley, W.B. (1988) "The Progressive Alteration of Fine Sediments along an Urban Storm Drain." Water Resources, (22) 6 pp. 775-781.

Rose A., Bianchi-Mosquera G.(1993)., Adsorption of Cu, Pb, Zn, Co, Ni, and Ag on Goethite and Hematite: A Control on Metal Mobilization from Red Beds in Sratiform Copper Deposits, Economic Geology, Volume 88, pp. 1226-1236.

Sansalone, J.J., Buchberger, S.G. and Koechling, M. (1995). "Correlations between Heavy Metals and Suspended Solids in Highway Runoff - Implications for Control Strategies", Transportation Research Record (1483) Washington, D.C., pp. 112-119.

Sansalone, J.J. and S.G. Buchberger. (1997). "Partitioning and first flush of metals and solids in urban highway runoff.", *J. Envir. Engrg. Div.* ASCE, 123 (2),134-143.

Sansalone, J.J., S.G. Buchberger, J. Koran & Smithson J. "Relationship between particle size distribution and specific surface area of urban roadway solids", *Transportation Research Record*, (accepted), 1997.

Sartor J.D., Boyd G.B. (1972) Water Pollution Aspects of Street Surface Contaminants, USEPA, Washington D.C., EPA-R2-72-081, pg. 236.

Schueler, T. (1987). "Controlling Urban Runoff: A Practical Manual for Planning and Designing Urban BMP" Metropolitan Washington Council of Governments, Washington DC, 1-275.

Schwertmann U. and R.M. Cornell.(1991) Iron oxides in the laboratory. VCH Verlagsgesselschart mbH. Weinheim FRG. pp. 137.

Schwertmann U. and Fisher W.R.. (1973). "Natural amorphous ferric hydroxide." Geoderma, (10) pp. 237-247.

Schwertmann U. and Murad. E. (1983). "Effect of pH on the formation of goethite and hematite from ferrihydrite." Clay and Clay Minerals, Vol. 31, No. 4, pp. 277-284.

Schwertmann U. and Taylor, R.M. (1989). "Iron Oxides." in "Minerals in the Soil Environment", Eds. Dixon J.B. and Weed S.B., Soil Science Society of America, Madison, Wi, pp. 1244. Scoog D.A. and Leary J.J. (1992). "Principles of Instrumental Analysis." 4th Edit. Saunders College Publishing, Fort Worth, pp. 700.

Sherard J., Dunnigan L., Talbot J.(1984a), Basic Properties of Sand and Gravel Filters, Journal of Geotechnical Engineering, American Society of Civil Engineers, Vol. 110, No. 6, pp. 684-700. Sherard J., Dunnigan L., Talbot J.(1984b), Filters for Silts and Clays, Journal of Geotechnical Engineering, American Society of Civil Engineers, Vol. 110, No. 6, pp. 701-718.

Sherard J., Dunnigan L., Talbot J.(1984a), Basic Properties of Sand and Gravel Filters, Journal of Geotechnical Engineering, American Society of Civil Engineers, Vol. 110, No. 6, pp. 684-700.

Shively W., Bishop, P., Gress, D., Brown, T. (1986) "Leaching tests of heavy metals stabilized with Portland cement" Journal of Water Pollution Control Federation, Vol. 58, #3, pp. 234-241.

Soil Survey of Hamilton County. (1982), United States Department of Agriculture. 1-220.

Smith, D.L. and B.N. Lord.(1990) Transportation Research Record 1279, Transportation Research Board, National Research Council, Washington, D.C. pp. 69-74.

Snoeyink, V.L., and Jenkins, D. (1980). "Water Chemistry." John Wiley and Sons, Inc., New York, 463 pp.

Sontheimer H., Crittenden, J. and Summers, R.S. (1988) "Activated Carbon for Water Treatment." DVGW-Forschungsstelle, Karlsruhe, pp. 744.

Sposito G. (1989), The Chemistry of Soils, Oxford University Press, New York pp. 277.

Srianantha kumar, K. and Codner, G.P. (1992) "Factors affecting pollutant washoff decay coefficients in urban catchments." International Symposium on urban Strormwater Management, Sydney. pp. 390-395.

Stahre, P. and Urbonas B. (1990). "Stormwater Detention.", Prentice Hall, Englewood Cliffs, New Jersey, 1-338.

Stenkamp V.S. and Benjamin M.M. (1994). "Effect of iron oxide coating on sand filtration." Journal of the American Water Works Association, Vol. 86, No. 8., pp. 37-50.

Stotz, G. (1987). "Investigations of the Properties of the Surface Water Run-Off from Federal Highways in the FRG.", The Science of the Total Environment., Vol. 59, 329-337.

Stumm, W. (1992) Chemistry of the Solid-Water Interface, John Wiley & Sons, New York.

Thomann, R. and Mueller, J. (1987). "Principles of Surface Water Quality Modeling and Control", Harper & Row, Publishers, Inc., New York, NY., 1-644.

USEPA (1989). National Air Quality and Emissions Trend Report. EPA-450/4-91-003, Office of Air Quality Planning and Standards, Research Triangle Park.

USEPA (1990). Basic Concepts of Contaminant Sorption at Hazardous Waste Sites (Ground Water Issue). EPA/540/4-90/053, NTIS# PB91-191007, Robert S. Kerr Environmental Research Laboratory, Ada, Oklahoma.

USEPA (1990) Test methods for Evaluating Solid Waste, Physical/Chemical Methods, SW-846, 3rd Edit, Final Update. Washington D.C.

United States Geological Survey, (1993) Manmade Organic Compounds in the Surface Waters of the United States - A Review of Current Understanding, USGS Circular 1007, pg. 92.

Ward, N.I. (1990) "Multielement contamination of British Motorway Environments" The Science of the Total Environment, (93) pp. 393-401.

Wanielista, M. and Yousef, Y. (1993). "Stormwater Management.", John Wiley & Sons, Inc., New York, 1-579.

Walpole, R.E. and R.H. Myers. (1989) Probability and Statistics for Engineers and Scientists, Fourth Edition, MacMillan Publishing Company, New York.

Weber W. (1972), Physicochemical Processes for Water Quality Control, John Wiley & Sons Inc., New York, pp. 640.

Weyer, G., D. Grotehusmann, and R. Rohlfing. (1992) Simulation of Pollution from Stormwater Infiltration Using the Mathematical Model LEACHP, Urban Stormwater Infiltration, Proceedings of the Fifth European Scientist Course, The SOCOMA Group of IAHR and IAWQ Joint Committee on Urban Storm Drainage, Department of Environmental Engineering, Technical Univ. of Denmark, Lyngby, pp. 147-165.

White, P.A.,Rasmussen, J.B, Blaise, C. (1994) "Genotoxicity of snow in the Montreal Metropolitan Area." Water, Air and Soil Pollution (83) pp. 315-334.

White J. L. and Roth C.B. (1988)."Infrared Spectroscopy." in Methods of Soil Analysis Part 1, Physical and Mineralogical Methods, 2nd Edit. Ed. Klute, A., Soil Science Society of America, Madison, WI. pp. 1188.

Xanthopoulos, C. and H.H. Hahn. (1990) Pollutants attached to particles from drainage areas. The Science of the Total Environment, Vol. 93., pp. 441-448.

Xanthopoulos, C. and Hahn, H. (1993). "Anthropogenic Pollutant Wash-Off from Street Surfaces.", Proceedings of the Sixth International Conference on Urban Storm Drainage -Volume 1., IAHR and IAWQ Joint Committee on Urban Storm Drainage, 417-422.

Yao, Kuan-Mu, Habibian, M. T. and O'Melia, C.R. (1971). "Water and Waste Water Filtration: Concepts and Applications." "Environmental Science and Technology", Vol. 5, No. 11, pp. 1105-1112.

Yousef, Y. (1985). "Consequential Species of Heavy Metals", Florida Department of Transportation, BMR-85-286 (FL-ER-29-85), Tallahassee, Florida.